

**THE UNIVERSITY OF CALGARY**

**QUALITY MONITORING**

**OF GPS SIGNALS**

**by**

**Andrew Jonathan Jakab**

**A THESIS**

**SUBMITTED TO THE FACULTY OF GRADUATE STUDIES**

**IN PARTIAL FULFILLMENT OF THE REQUIREMENTS FOR THE**

**DEGREE OF MASTER OF SCIENCE**

**DEPARTMENT OF GEOMATICS ENGINEERING**

**CALGARY, ALBERTA**

**JULY, 2001**

**© Andrew Jonathan Jakab 2001**



**National Library  
of Canada**

**Acquisitions and  
Bibliographic Services**

**395 Wellington Street  
Ottawa ON K1A 0N4  
Canada**

**Bibliothèque nationale  
du Canada**

**Acquisitions et  
services bibliographiques**

**395, rue Wellington  
Ottawa ON K1A 0N4  
Canada**

*Your file Votre référence*

*Our file Notre référence*

**The author has granted a non-exclusive licence allowing the National Library of Canada to reproduce, loan, distribute or sell copies of this thesis in microform, paper or electronic formats.**

**The author retains ownership of the copyright in this thesis. Neither the thesis nor substantial extracts from it may be printed or otherwise reproduced without the author's permission.**

**L'auteur a accordé une licence non exclusive permettant à la Bibliothèque nationale du Canada de reproduire, prêter, distribuer ou vendre des copies de cette thèse sous la forme de microfiche/film, de reproduction sur papier ou sur format électronique.**

**L'auteur conserve la propriété du droit d'auteur qui protège cette thèse. Ni la thèse ni des extraits substantiels de celle-ci ne doivent être imprimés ou autrement reproduits sans son autorisation.**

**0-612-65155-X**

**Canada**

## **ABSTRACT**

**With an increased reliance on the Global Positioning System to provide accurate and reliable results, there has also been an equivalent desire to validate the results. This validation comes in the form of a real-time signal quality monitoring scheme that will be able to detect spurious non-standard transmissions of the satellite signal. These faults result in the distortion of the autocorrelation function that then causes differences in code tracking errors in differently designed receivers.**

**This thesis outlines the associated problems with detecting very small distortion of the autocorrelation function. Manufacturing tolerances of componentry, temperature, and multipath signals all contribute to the problem. A means of correcting for all problems, specifically multipath, is presented based on the use of the newly invented 'Multipath Meter', which will correct the autocorrelation function measurements for multipath without masking a signal failure. Radio Frequency interference detection is also presented as part of the SQM scheme.**

## **ACKNOWLEDGEMENTS**

**Thanks to my supervisor, Dr. Gerard Lachapelle, for his input and guidance during my stay at the university.**

**Thanks to all those involved at NovAtel Inc., specifically Tony Murfin and Michael Clayton, for their continued support in my personal development through RTCA and ICAO meetings, as well as course work at the university and the creation of this thesis.**

**Special thanks to the Stanford University crew, STNA, ENAC, and the FAA for their flurry of questions and software requests that kept me on my toes and spurred my interest and knowledge on the subject of signal quality monitoring.**

## TABLE OF CONTENTS

Approval Page	ii
Abstract	iii
Acknowledgements	iv
Table of Contents	v
List of Tables	viii
List of Figures	ix
Notation	xiii
CHAPTER 1 INTRODUCTION	1
1.1 Background	1
1.2 Research Objective	3
1.3 Thesis Outline	4
CHAPTER 2 RECEIVER CHARACTERISTICS	6
2.1 GPS Signal in Space	6
2.2 Code Generators	9
2.3 Code Tracking Loops	11
2.3.1 Correlators and the Correlation Function	13
2.3.2 Discriminators	14
2.3.3 Multi-Correlator Tracking	16
2.3.4 MDE's and MDR's	17
2.4 False Alarms and Miss-Detections	19
2.5 Wide Band Code Range Corrections	20
2.6 Multipath Estimating Delay Lock Loop (MEDLL <sup>®</sup> )	21
2.6.1 PRN Code Types	22
2.6.2 Multipath	24
2.6.3 MEDLL Equations	25
2.6.4 The Multipath Meter	26
CHAPTER 3 SATELLITE FAILURE MODES	29
3.1 Feared Events	29

3.1.1	Digital Failure (Threat Model A)	31
3.1.2	Analogue Failure (Threat Model B)	34
3.1.3	Combination of Failures (Threat Model C)	36
3.1.4	Failure Impact on Tracking	37
3.2	Additional Possible Failure Modes	39
3.2.1	SV 27 Clock Anomaly	40
3.2.2	SV 20 Erratic Clock	40
3.2.3	SV 21 Miss-Modeling by GPS Master Control Station	41
3.2.4	SV 16 Vehicle Instability	41
3.3	Possible Threats	42
3.3.1	Incorrect or Invalid Broadcast PRN Code	42
3.3.2	Excessive or Insufficient Signal Power	43
3.3.3	Spectrum Corruption	43
3.3.4	Erroneous Navigation Data	44
<b>CHAPTER 4 SIGNAL QUALITY MONITORING</b>		<b>45</b>
4.1	Test Setup	47
4.2	Test Results	48
4.2.1	Consistency Within Sample Periods	48
4.2.2	Consistency Between Receiver Resets	50
4.2.3	Consistency Between Receivers	53
4.2.4	Temperature Variations	54
4.2.5	Componentry Differences	57
4.2.6	Overall Accuracy	59
4.2.7	Thresholds of Detection	60
4.2.8	RF Componentry Bias Removal	61
4.3	Automatic Gain Control Operation	63
4.4	Carrier to Noise Calculation	64
4.5	Multipath Meter Parameters	65
4.5.1	Multipath Meter Outputs	66
4.5.2	Residuals from the Multipath Estimation Process	69
4.5.3	Multipath Corrected Correlator Values	70

<b>CHAPTER 5 MALEVOLENT SIGNAL TESTING</b>	<b>76</b>
<b>5.1 Simulation Setup for Code Correlation Failure Generation</b>	<b>76</b>
<b>5.2 Detection Using MDE and MDR Values</b>	<b>77</b>
<b>5.3 Impact of Multipath on the Correlation Function</b>	<b>81</b>
<b>5.4 Analysis of Threat Model A in the Presence of Multipath</b>	<b>83</b>
<b>5.5 Analysis of Threat Model B in the Presence of Multipath</b>	<b>91</b>
<b>5.6 Analysis of Threat Model C in the Presence of Multipath</b>	<b>97</b>
<b>5.7 Conclusions of Simulation Testing</b>	<b>101</b>
<b>CHAPTER 6 INTERFERENCE ENVIRONMENTS</b>	<b>102</b>
<b>6.1 Test Setup for Interference Generation</b>	<b>102</b>
<b>6.2 C/No Interference Detection</b>	<b>103</b>
<b>6.2.1 C/No Testing Results</b>	<b>106</b>
<b>6.2.2 C/No Interference Detection Threshold</b>	<b>114</b>
<b>6.3 AGC Interference Detection</b>	<b>115</b>
<b>6.3.1 AGC Testing Results</b>	<b>115</b>
<b>6.3.2 AGC Interference Detection Threshold</b>	<b>123</b>
<b>6.4 Standard Deviation of the WBC</b>	<b>125</b>
<b>6.4.1 Background <math>\sigma</math>WBC Information</b>	<b>125</b>
<b>6.4.2 WBC Testing Results</b>	<b>129</b>
<b>6.4.3 WBC Testing Conclusions</b>	<b>137</b>
<b>CHAPTER 7 SUMMARY AND CONCLUSIONS</b>	<b>139</b>
<b>REFERENCES</b>	<b>140</b>

## LIST OF TABLES

<b>Table 2-1: PRN Code Types</b>	<b>22</b>
<b>Table 4-1: List of Measured Correlator Spacings in 4.47S16 in C/A Code Chips</b>	<b>46</b>
<b>Table 4-2: List of Hardware Serial Numbers Used in Testing</b>	<b>48</b>
<b>Table 4-3: Normalized Difference in correlation function measurements between receiver resets, UUT5</b>	<b>51</b>
<b>Table 4-4: Normalized Difference in correlation function measurements between receiver resets for all receivers combined</b>	<b>52</b>
<b>Table 5-1: Signal Simulation Parameters</b>	<b>77</b>

## LIST OF FIGURES

Figure 2-1: Satellite's Signal Path	7
Figure 2-2: Bi-Phase Shift Modulation of code onto carrier	8
Figure 2-3: GPS C/A Code Generator	10
Figure 2-4: Normalized Perfect C/A code Auto-Correlation Function	12
Figure 2-5: DLL Discriminator Output for Various Discriminators	15
Figure 2-6: Direct Path and Multipath (Reflected Path) Signals	24
Figure 3-1: Chip Transitions for Digital Signal Failures	31
Figure 3-2: Digital Failure Effects on Correlation Function	32
Figure 3-3: Chip Transitions for Analogue Signal Failures	33
Figure 3-4: Analogue failure effects on correlation ( $\min f_d$ and $\sigma$ )	34
Figure 3-5: Analogue failure effects on C/A code chip ( $\min f_d$ and $\sigma$ )	34
Figure 3-6: Analogue failure effects on correlation ( $\max f_d$ and $\sigma$ )	35
Figure 3-7: Analogue failure effects on C/A code chip ( $\max f_d$ and $\sigma$ )	35
Figure 3-8: Effect on the Correlation Function for a Combination of Failures	36
Figure 4-1: Correlation Function Measurement Consistency Between Resets, UUT5	50
Figure 4-2: Mean Normalized Card-to-Card Variations Between Correlation Function Measurements	53
Figure 4-3: Temperature Profile for the Temperature Variation Testing	55
Figure 4-4: Multiple Normalized Code Correlation Values During Temperature Variations (100-second smoothed)	55
Figure 4-5: Normalized -0.05115 Code Correlation Values During Temperature Variations (100-second smoothed)	56
Figure 4-6: Difference between Normalized Correlation Functions using 16 and 17 MHz bandwidth filters	59

<b>Figure 4-7: Correlation Function Measurement Consistency Between Resets (Using a 100-second smoother), UUT5</b>	<b>61</b>
<b>Figure 4-8: Simulation of D/U Estimate</b>	<b>67</b>
<b>Figure 4-9: Simulation of Delay Estimate</b>	<b>67</b>
<b>Figure 4-10: Simulation of Pseudorange Error</b>	<b>68</b>
<b>Figure 4-11: Simulation of Estimation Residuals</b>	<b>69</b>
<b>Figure 4-12: +0.10 Mean Correlator Value for PRN1</b>	<b>71</b>
<b>Figure 4-13: +0.10 Mean Correlator Value for PRN3</b>	<b>72</b>
<b>Figure 4-14: +0.30 Mean Correlator Value for PRN3</b>	<b>72</b>
<b>Figure 4-15: +0.10 Correlator Standard Deviation for PRN1</b>	<b>74</b>
<b>Figure 4-16: +0.10 Correlator Standard Deviation for PRN3</b>	<b>74</b>
<b>Figure 4-17: +0.30 Correlator Standard Deviation for PRN3</b>	<b>75</b>
<b>Figure 5-1: MDR1 (0.025-0.075), No Evil</b>	<b>78</b>
<b>Figure 5-2: MDR2 (0.025-0.125), No Evil</b>	<b>79</b>
<b>Figure 5-3: MDE1 (+0.025), No Evil</b>	<b>79</b>
<b>Figure 5-4: MDE2 (+0.125), No Evil</b>	<b>80</b>
<b>Figure 5-5: Correlation Function with Multipath</b>	<b>81</b>
<b>Figure 5-6: Correlation Function with Threat Model C</b>	<b>82</b>
<b>Figure 5-7: Correlation Function with Threat Model C and Multipath</b>	<b>82</b>
<b>Figure 5-8: MDR1 (0.025-0.075), Maximum Threat Model A</b>	<b>84</b>
<b>Figure 5-9: MDR2 (0.025-0.125), Maximum Threat Model A</b>	<b>85</b>
<b>Figure 5-10: MDE1 (+0.025), Maximum Threat Model A</b>	<b>85</b>
<b>Figure 5-11: MDE2 (+0.125), Maximum Threat Model A</b>	<b>86</b>
<b>Figure 5-12: D/U for Maximum Threat Model A with Multipath</b>	<b>87</b>
<b>Figure 5-13: Sum squared correlator residuals, Maximum Threat Model A</b>	<b>88</b>
<b>Figure 5-14: MDR1 (0.025-0.075), Minimum Threat Model A</b>	<b>89</b>
<b>Figure 5-15: MDR2 (0.025-0.125), Minimum Threat Model A</b>	<b>89</b>
<b>Figure 5-16: MDE1 (+0.025), Minimum Threat Model A</b>	<b>90</b>
<b>Figure 5-17: MDE2 (+0.125), Minimum Threat Model A</b>	<b>90</b>
<b>Figure 5-18: MDR1 (0.025-0.075), Minimum Threat Model B</b>	<b>92</b>
<b>Figure 5-19: MDR2 (0.025-0.125), Minimum Threat Model B</b>	<b>92</b>

<b>Figure 5-20: MDE1 (+0.025), Minimum Threat Model B</b>	<b>93</b>
<b>Figure 5-21: MDE2 (+0.125), Minimum Threat Model B</b>	<b>93</b>
<b>Figure 5-22: Sum squared correlator residuals, Minimum Threat B</b>	<b>94</b>
<b>Figure 5-23: MDR1 (0.025-0.075), Maximum Threat Model B</b>	<b>95</b>
<b>Figure 5-24: MDR2 (0.025-0.125), Maximum Threat Model B</b>	<b>96</b>
<b>Figure 5-25: MDE1 (+0.025), Maximum Threat Model B</b>	<b>96</b>
<b>Figure 5-26: MDE2 (+0.125), Maximum Threat Model B</b>	<b>97</b>
<b>Figure 5-27: MDR1 (0.025-0.075), Threat Model C</b>	<b>98</b>
<b>Figure 5-28: MDR2 (0.025-0.125), Threat Model C</b>	<b>99</b>
<b>Figure 5-29: MDE1 (+0.025), Threat Model C</b>	<b>99</b>
<b>Figure 5-30: MDE2 (+0.125), Threat Model C</b>	<b>100</b>
<b>Figure 5-31: Sum squared correlator residuals, Threat Model C</b>	<b>100</b>
<b>Figure 6-1: C/No versus Elevation Angle</b>	<b>105</b>
<b>Figure 6-2: C/No for 100 kHz Interferer, centered at L1</b>	<b>107</b>
<b>Figure 6-3: C/No for 50 kHz Interferer, centered at L1</b>	<b>107</b>
<b>Figure 6-4: C/No for 25 kHz Interferer, centered at L1</b>	<b>108</b>
<b>Figure 6-5: C/No for 10 kHz Interferer, centered at L1</b>	<b>108</b>
<b>Figure 6-6: C/No for 5 kHz Interferer, centered at L1</b>	<b>109</b>
<b>Figure 6-7: C/No for 2.5 kHz Interferer, centered at L1</b>	<b>109</b>
<b>Figure 6-8: C/No for 1 kHz Interferer, centered at L1</b>	<b>110</b>
<b>Figure 6-9: C/No for 0.6 kHz Interferer, centered at L1</b>	<b>110</b>
<b>Figure 6-10: C/No for 100 kHz Interferer, centered at L2</b>	<b>111</b>
<b>Figure 6-11: C/No for 50 kHz Interferer, centered at L2</b>	<b>111</b>
<b>Figure 6-12: C/No for 25 kHz Interferer, centered at L2</b>	<b>112</b>
<b>Figure 6-13: C/No for 10 kHz Interferer, centered at L2</b>	<b>112</b>
<b>Figure 6-14: C/No for 5 kHz Interferer, centered at L2</b>	<b>113</b>
<b>Figure 6-15: C/No for 1 kHz Interferer, centered at L2</b>	<b>113</b>
<b>Figure 6-16: AGC Statistic for 100 kHz Interferer, centered at L1</b>	<b>116</b>
<b>Figure 6-17: AGC Statistic for 50 kHz Interferer, centered at L1</b>	<b>116</b>
<b>Figure 6-18: AGC Statistic for 25 kHz Interferer, centered at L1</b>	<b>117</b>
<b>Figure 6-19: AGC Statistic for 10 kHz Interferer, centered at L1</b>	<b>117</b>
<b>Figure 6-20: AGC Statistic for 5 kHz Interferer, centered at L1</b>	<b>118</b>

Figure 6–21: AGC Statistic for 2.5 kHz Interferer, centered at L1	118
Figure 6–22: AGC Statistic for 1 kHz Interferer, centered at L1	119
Figure 6–23: AGC Statistic for 0.6 kHz Interferer, centered at L1	119
Figure 6–24: AGC Statistic for 100 kHz Interferer, centered at L2	120
Figure 6–25: AGC Statistic for 50 kHz Interferer, centered at L2	120
Figure 6–26: AGC Statistic for 25 kHz Interferer, centered at L2	121
Figure 6–27: AGC Statistic for 10 kHz Interferer, centered at L2	121
Figure 6–28: AGC Statistic for 5 kHz Interferer, centered at L2	122
Figure 6–29: AGC Statistic for 2.5 kHz Interferer, centered at L2	122
Figure 6–30: AGC Statistic for 1 kHz Interferer, centered at L2	123
Figure 6–31: $\sigma$ WBC Ratio for different standard deviation sample sizes	128
Figure 6–32: $\sigma$ WBC Ratio for different smoothing lengths	128
Figure 6–33: $\sigma$ WBC Ratio for 100 kHz Interferer, centered at L1	129
Figure 6–34: $\sigma$ WBC Ratio for 50 kHz Interferer, centered at L1	130
Figure 6–35: $\sigma$ WBC Ratio for 25 kHz Interferer, centered at L1	130
Figure 6–36: $\sigma$ WBC Ratio for 10 kHz Interferer, centered at L1	131
Figure 6–37: $\sigma$ WBC Ratio for 5 kHz Interferer, centered at L1	131
Figure 6–38: $\sigma$ WBC Ratio for 2.5 kHz Interferer, centered at L1	132
Figure 6–39: $\sigma$ WBC Ratio for 1 kHz Interferer, centered at L1	132
Figure 6–40: $\sigma$ WBC Ratio for 0.6 kHz Interferer, centered at L1	133
Figure 6–41: $\sigma$ WBC Ratio for 100 kHz Interferer, centered at L2	133
Figure 6–42: $\sigma$ WBC Ratio for 50 kHz Interferer, centered at L2	134
Figure 6–43: $\sigma$ WBC Ratio for 25 kHz Interferer, centered at L2	134
Figure 6–44: $\sigma$ WBC Ratio for 10 kHz Interferer, centered at L2	135
Figure 6–45: $\sigma$ WBC Ratio for 5 kHz Interferer, centered at L2	135
Figure 6–46: $\sigma$ WBC Ratio for 2.5 kHz Interferer, centered at L2	136
Figure 6–47: $\sigma$ WBC Ratio for 1 kHz Interferer, centered at L2	136
Figure 6–48: $\sigma$ WBC Ratio for 0.6 kHz Interferer, centered at L2	137

## NOTATION

### Acronyms

<b>A/D</b>	<b>Analogue to Digital Converter</b>
<b>AGC</b>	<b>Automatic Gain Control</b>
<b>C</b>	<b>Celsius</b>
<b>CW</b>	<b>Continuous Wave</b>
<b>C/A</b>	<b>Coarse Acquisition</b>
<b>C/No</b>	<b>Carrier to Noise Ratio</b>
<b>dB</b>	<b>Decibels</b>
<b>D</b>	<b>Correlator spacing</b>
<b>DLL</b>	<b>Delay Locked Loop</b>
<b>DoD</b>	<b>Department of Defense</b>
<b>D/U</b>	<b>Desired to Undesired signal ratio</b>
<b>E</b>	<b>Early code correlation measurement</b>
<b>E-L</b>	<b>Early-Late code correlation measurement</b>
<b>ELS</b>	<b>Early Late Slope</b>
<b>ENAC</b>	<b>Ecole Nationale de l'Aviation Civile, France</b>
<b>FAA</b>	<b>Federal Aviation Administration, US</b>
<b>FIR</b>	<b>Finite Impulse Response</b>
<b>FOC</b>	<b>Full Operational Capability</b>
<b>G1</b>	<b>First tapped shift feedback register for the C/A code</b>
<b>G2</b>	<b>Second tapped shift feedback register for the C/A code</b>
<b>GPS</b>	<b>Global Positioning System</b>
<b>HPA</b>	<b>High Power Antenna</b>
<b>Hz</b>	<b>Hertz</b>
<b>I</b>	<b>Inphase code correlation measurement</b>
<b>ICD</b>	<b>Interface Control Document</b>
<b>IF</b>	<b>Intermediate Frequency</b>
<b>IPA</b>	<b>Intermediate Power Antenna</b>
<b>I/S</b>	<b>Interferer to Signal Ratio</b>
<b>KHz</b>	<b>kilohertz</b>

<b>L</b>	<b>Late code correlation measurement</b>
<b>LAAS</b>	<b>Local Area Augmentation System</b>
<b>MDE</b>	<b>Minimum Detectable Error</b>
<b>MDR</b>	<b>Minimum Detectable Ratio</b>
<b>MEDLL</b>	<b>Multipath Estimating Delay Locked Loop</b>
<b>MET</b>	<b>Multipath Eliminating Technology</b>
<b>MHz</b>	<b>Megahertz</b>
<b>MLS</b>	<b>Microwave Landing System</b>
<b>MOPS</b>	<b>Minimum Operation Performance Standards</b>
<b>NANU</b>	<b>Notice Advisory to Navigation Users</b>
<b>NAVSTAR</b>	<b>Navigation Satellite Timing and Ranging</b>
<b>NDU</b>	<b>Navigation Data Unit</b>
<b>NF</b>	<b>Noise Floor</b>
<b>OEM</b>	<b>Original Equipment Manufacturer</b>
<b>P</b>	<b>Punctual code correlation measurement</b>
<b>PRN</b>	<b>Pseudorandom Noise Code</b>
<b>Q</b>	<b>Quadrature (or Quadrature) code correlation measurement</b>
<b>RABF</b>	<b>Ray Antenna Beam Former</b>
<b>RF</b>	<b>Radio Frequency</b>
<b>SA</b>	<b>Selective Availability</b>
<b>SFD</b>	<b>Satellite Failure Detection</b>
<b>S/No</b>	<b>Signal to Noise Ratio</b>
<b>SQM</b>	<b>Signal Quality Monitoring</b>
<b>STEL</b>	<b>Stanford Telecom</b>
<b>STNA</b>	<b>Service Technique de la Navigation Aeriennne, France</b>
<b>SV</b>	<b>Space Vehicle</b>
<b>UUT</b>	<b>Unit Under Test</b>
<b>VCO</b>	<b>Voltage Controlled Oscillator</b>
<b>WAAS</b>	<b>Wide Area Augmentation System</b>
<b>WBC</b>	<b>Wide Band Correction</b>
<b>XOR</b>	<b>Exclusive OR (logic operation)</b>
<b>US</b>	<b>United States</b>
<b>USAF</b>	<b>United States Air Force</b>

## Symbols

$A_1$	L1 signal amplitude
$A_2$	L2 signal amplitude
$A(t)$	C/A code correlation amplitude
$a_{\text{direct}}$	Amplitude of the direct path signal
$a_m$	Component signal amplitude
$a_{\text{multipath}}$	Amplitude of the multipath signal
$\cos(f_1 t)$	Unmodulated L1 signal
$\cos(f_2 t)$	Unmodulated L2 signal
$C/A(t)$	C/A code
$C_{\text{res}}$	Correlator residual
$C_{\text{meas}}$	Measured correlator value
$C_{\text{ref}}$	Reference function correlator value
$\Delta$	Code shift of anomalous signal
$e(t)$	Anomalous signal effect
$f_0$	Base frequency for GPS signal generation
$f_1$	L1 frequency
$f_2$	L2 frequency
$f_d$	Ringing frequency of anomalous signal
$I_E$	Early inphase code correlation value
$I_L$	Late inphase code correlation value
$I_P$	Punctual inphase code correlation value
$L1(t)$	Modulated L1 signal
$L2(t)$	Modulated L2 signal
$M$	Number of signals
$N(t)$	Navigation Data
$n(t)$	Noise
$\omega_d$	Natural frequency
$P(t)$	P-code
$p(t)$	Generic code sequence
$Q_E$	Early quadrature code correlation value
$Q_L$	Late quadrature code correlation value

$Q_p$	Punctual quadrature code correlation value
$S$	Sum squared correlator values
$\theta_m$	Component signal phase
$\sin(f_1 t)$	Unmodulated L1 signal
$\sigma$	Dampening factor
$\sigma_{WBC}$	Standard Deviation of the Wide Band Correction
$T$	Accumulation time
$t$	Time
$\tau_m$	Component signal delay
$x$	Correlation location
$^\circ$	Degrees
$  $	Absolute value

## CHAPTER 1

### INTRODUCTION

#### *1.1 Background*

With the modernization of the Global Positioning System (GPS) and the ingenuity of people to determine new uses for receivers, there is an increasing demand on both the receivers and the signal in space to provide repeatable and reliable results. For safety critical systems, such as airplane guidance, automated landing systems, or ground station reference sites for local or wide area augmentation systems, the ability of these systems to provide the integrity and reliability to which the system was designed is of the utmost importance. For these safety critical situations, it would be the demise of GPS, not only in aviation, if the quoted accuracy and reliability of the GPS signal was not met and a catastrophic accident occurred as a result of a signal failure.

Looking back, the GPS signal in space was available for quite some time before the system became fully operational [41]. Only after the US Department of Defence (DoD) could validate the signal integrity, the system could be declared operational. Before this declaration, the signal in space was used with no guarantees from the DoD as to its accuracy, integrity, or availability. Now that full operation capability (FOC) has been reached, monitoring the signal so that it maintains the specified values is essential for safety critical systems using the GPS for navigation.

Prior to FOC, there was one specific event in GPS's history that led to numerous discussions about the integrity and reliability of the system. The event occurred in October 1993 when satellite PRN 19 exhibited some spurious, non-standard behaviour, resulting in differential pseudorange errors of 3 to 8 meters [10], [26]. This behaviour was not represented by any written material in the GPS interface control document [2] and proved to be quite misleading to all receiver models tracking the

signal. It was observed that the signal was in fact causing satellite range measurement distortions in both single point and differential GPS operations. For a system that is already being used for safety critical applications, this problem needs to be addressed and a solution to a possible tragic end needs to be found as soon as possible. This research is especially important for safety of life applications where GPS is used as a sole means of guidance. This sole means of guidance may become a reality for civil aviation in the near future where the integrity and accuracy of the guidance system must be ensured.

An adequate method of detecting this type of failure needs to be developed so that it improves the users confidence in the signal regardless of the environment that the GPS user antenna is in. These environments can spawn great difficulties in the detection of satellite signal failures if there are nearby reflectors generating additional multipath signals [31]. These environments can also significantly decrease the availability of the detection mechanisms as a result of a high false alarm rate. Furthermore, methods of detecting other satellite signal distortions, whether they are satellite based in the form of signal distortions, clock anomalies, unflagged manoeuvres or ground based in the form of multipath or interference, should be included in this signal quality monitoring (SQM) scheme.

In order to understand how these signal failures can introduce such disastrous positioning errors in a GPS receiver, we first need to understand something about the signal structure being broadcast from the GPS satellite and the components of this signal that are used in the determination of the receivers' measurements. Secondly, we need to examine the nature of the failures of the satellite. Additionally, we need to relate the two components of satellite signal anomalies and receiver measurements together and determine methods of detecting such satellite signal errors in a timely manner.

## ***1.2 Research Objective***

**The main focus and goal of this thesis is to provide a mean of detecting satellite signal failures, which are of similar nature to the PRN 19 failure, as well as additional methods of satellite signal quality monitoring. It will be shown that spurious GPS satellite signal failures can be detected by using a multi-correlator approach and that by using inherent receiver functionality additional signal anomalies can also be detected. For correlation domain signal failures, analysis of the impact of multipath signals, when such a satellite failure is present, is also a key component of this thesis. Removal of the multipath signals before attempting to detect satellite failures will be shown to be advantageous while not masking the effects of the inherent failure. This thesis also provides evidence to support the concept that multipath can be distinguished from satellite signal failures.**

**Given the primary objectives, there are a number of issues that need to be addressed during the course of the investigation:**

- 1. The effects of the receiver Radio Frequency (RF) design which will impact the ability of the receiver to determine the presence of a satellite failure.**
- 2. What inherent capabilities are present in the GPS receiver design that allow for additional signal quality monitoring schemes.**
- 3. The nominal accuracy to which we can measure the:**
  - a) Code correlation peak, in order to determine what the threshold of detection for satellite failures, of the PRN 19 type, will be,**
  - b) Carrier to Noise Ratios (C/No), Wide Band Code Range Corrections and Automatic Gain Control (AGC), as a mean to**

determine when interference or other phenomenons are present,

- c) The possible impacts of multipath signals on correlation domain satellite failures, how the receiver will view the combined signal, and how we can distinguish between the two.

### ***1.3 Thesis Outline***

**This thesis consists of 7 enlightening chapters.**

**Chapter 1 includes a brief introduction to the subject as well as encompassing the research objectives and this outline.**

**Chapter 2 outlines a typical GPS receiver's characteristics in terms of code correlation and how it tracks a GPS signal in space. It also includes information on C/No calculation, wide band code range corrections, the code auto-correlation function, and the Multipath Estimating Delay Lock Loop (MEDLL).**

**Chapter 3 reviews the satellite failure modes related to PRN 19 as well as additional failure modes that have been seen in the past on GPS satellites. It highlights the threat models, which we will be attempting to detect with our SQM scheme.**

**Chapter 4 forms the basis of the Signal Quality Monitoring mechanisms proposed by the author. Experimental results of nominal correlation peak measurements and correlation domain measurement variations are included. Different receiver RF designs are investigated to provide information on these variations. Multiple environmental scenarios are investigated to provide a strong emphasis on detection limits. Results of parameter stability, including the use of the MEDLL to improve SQM availability by removing multipath signals are also presented.**

**Chapter 5 shows additional information related to the generation of a correlation domain satellite failure as well as when this failed signal also contributes a multipath signal at the receiver antenna. The chosen SQM scheme is further validated by these experimentations and investigations. The ability to separate the satellite failure from multipath is also shown.**

**Chapter 6 shows details of interference testing for both narrow and wide band interference. Multiple scenarios are included for various bandwidths of interferers, as well as how we can detect the presence of the interferer.**

**Chapter 7 summarizes the research described in the previous chapters. It identifies the key components in the detection of satellite signal quality monitoring.**

## CHAPTER 2

### RECEIVER CHARACTERISTICS

#### *2.1 GPS Signal in Space*

The Global Positioning System (GPS) is a satellite based navigation system that provides a continuous signal to the Earth using 24 active satellites that can be used for navigation and timing. Coverage nominally ranges from a minimum of six to a maximum of twelve satellites in view, depending on the time of day and geographic location of the receiver. The satellites are aptly named NAVigation Satellite Timing and Ranging (NAVSTAR) satellites, for their ability to provide precise time as well as satellite range information to users. These two components are used together to determine the position of the receiver, relative to the known locations of the satellites. These known satellite locations are part of the message that each satellite broadcasts to the Earth.

The space segment of the system, the actual satellites themselves, is comprised of six orbital planes inclined at an angle of 55° from the Equator. Each plane holds four satellites all with a period of approximately twelve hours.

The signal being broadcast from each satellite consists of a number of important components. The signal being broadcast is on two separate frequencies. The first is called L1 and is at a frequency of 1575.42MHz. The second is called L2 and is at a frequency of 1227.6MHz. The L1 and L2 signals have the following signal structure:

$$L1(t) = A_1P(t)N(t)\cos(f_1t) + A_1C/A(t)N(t)\sin(f_1t) \quad (2-1)$$

$$L2(t) = A_2P(t)N(t)\cos(f_2t) \quad (2-2)$$

Where  $A_1, A_2$  = signal amplitude ( $\pm 1$ )  
 $P(t)$  = P-code  
 $C/A(t)$  = C/A code  
 $N(t)$  = Navigation Data  
 $\cos(f_1t), \cos(f_2t)$  and  $\sin(f_1t)$  = unmodulated L1 or L2 signal  
 $L1(t)$  and  $L2(t)$  = modulated L1 or L2 signal

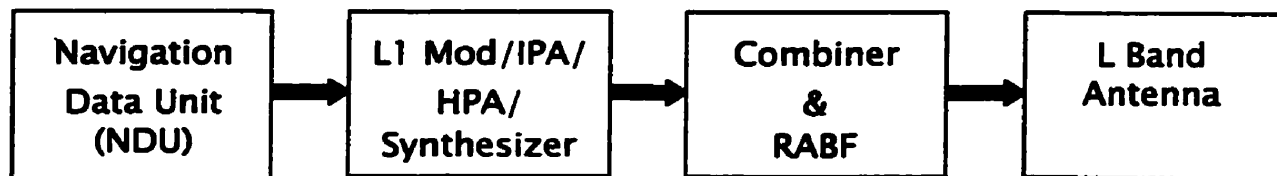


Figure 2-1: Satellite's Signal Path [11]

In equation 2-1 above, the NDU (shown in Figure 2-1) takes the  $\cos$  or  $\sin$  of the  $(f_1t)$  signal and modulates onto it the navigation data  $(N(t))$  and the C/A or P code. This is the block that does the physical multiplication of the signal components together. Once the signal has been created inside the satellite NDU block, the L1 Synthesizer manipulates the signal according to the bandwidth specifications of the signal. There are also additional synthesizers for the P-code on L1 and the P-code on L2. For the L1 signal, the combiner merges the L1 C/A with the L1 P-code signal to form a single message stream. After the signal has completed its generation, it is sent to the L Band antenna for broadcast to the Earth.

"All transmitted signal elements (carriers, codes, and data) are coherently derived from the same on-board frequency source" [2]. This on-board signal frequency is at 1.023MHz, denoted as  $f_0$ . The broadcast L1 signal frequency is  $154*f_0$  and the L2 signal is at  $120*f_0$ .

When the C/A or P code is modulated onto the carrier wave in the NDU, it is done in a manner called bi-phase modulation. This means that on each of the code chip transitions of the signal, from +1 to -1, there is a potential change in phase of the carrier. This 180° phase change in the

carrier is how the code sequence is recovered and correlated to the user receiver generated copy of the same code sequence. An example of this is shown in Figure 2-2 below.

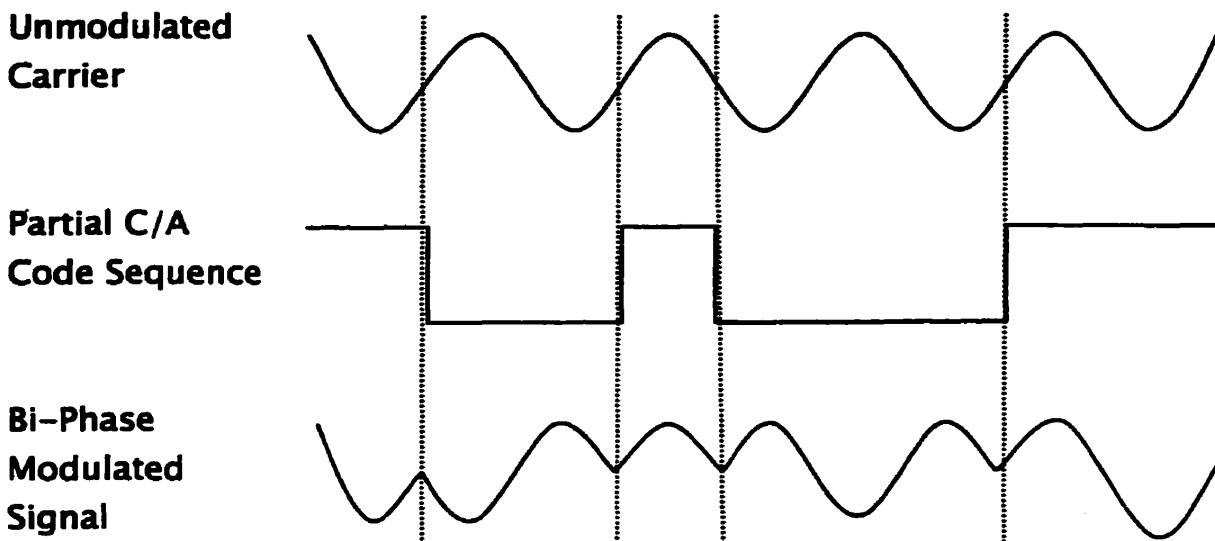


Figure 2-2: Bi-Phase Shift Modulation of code onto carrier

For the scope of this thesis, we will only be concerned with the L1 C/A code portion of the signal. The reason for this has to do with the failure modes of the satellites related to the PRN 19 failure, which will be discussed further in the next chapter. Also, we (as civilian users) do not have direct access to the encrypted P-code signal. As a result, we are currently limited in scope to investigating the L1 C/A code. However, there are some investigations included in this thesis, which deal with the L2 frequency for interference detection (Chapter 6).

## ***2.2 Code Generators***

The code generated at the satellite is identical to the code generated in the GPS receiver. By generating the same code patterns, the satellite signal can be tracked using the receiver-generated copy of this code. This code tracking loop concept will be elaborated on after we understand how to generate the code.

The C/A code length used is 1023 bits long and is generated using what is known as a tapped shift feedback register. To generate the C/A code sequence, a ten-bit register is used. To begin the process of generating the code, a starting value needs to be input into the ten bits, known as the seed value. This kind of register works by shifting all of the bits on each cycle through the code generator. This leaves one bit empty. The value replaced in this location has to be generated from the 'taps' used from the previous state of the register. This single bit is the feedback portion of the code generation. At the same time, the bit that has been shifted off the end of the register is output as the generated code.

We can see in Figure 2-3 that there are two such code generators required to generate the C/A code. The first is designated as the G1 shift register, and the second as G2. For GPS C/A code generation, the G2 register seed value is a constant value of 1. This is the nature of the signal. Therefore, when the feedback is done from all of the required taps of the G2 register, the output bit will always have a constant value as well. Contrary to this, the G1 shift register has different seed values for each PRN code generated. The precise seed values can be found in [2].

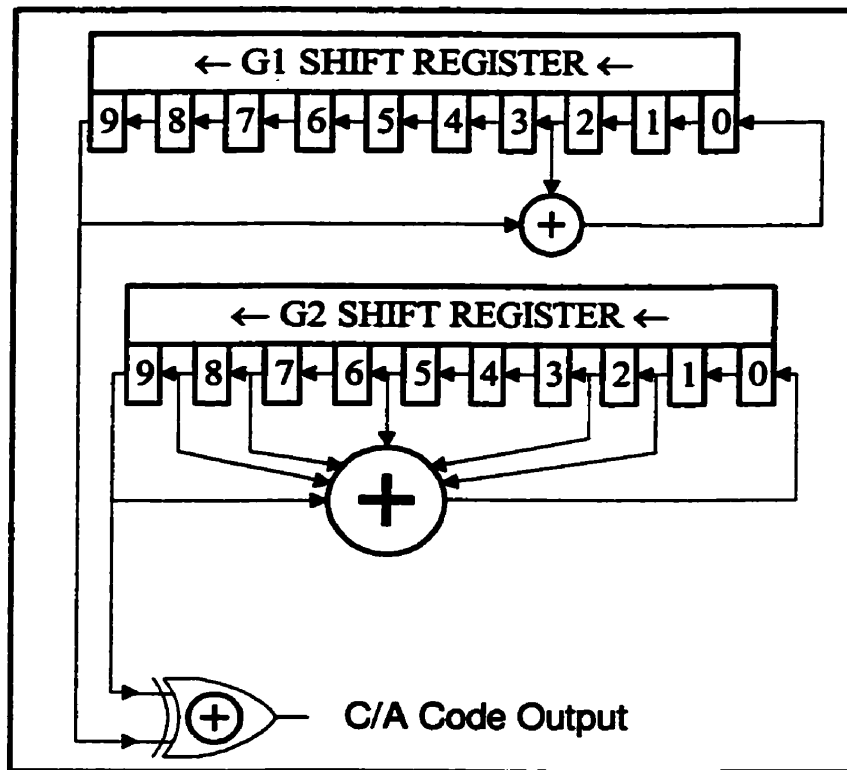


Figure 2-3: GPS C/A Code Generator

The single bit output from the G1 and G2 shift registers is XOR'ed (exclusive logical OR) together to generate the final C/A code output used for code correlation with the incoming satellite code sequence. Keep in mind that the receiver will be correlating the signal at a rate much faster than the bit rate of the C/A code signal. This means that the same C/A code bit will be used numerous times inside the receiver before a new bit is required. The amount of repetition is related to the internal signal-clocking rate of the receiver. Having a higher clocking rate than the actual input signal allows for a much more accurate assessment of where, in time, the incoming satellite code and the receiver generated code should be aligned with respect to one another.

### *2.3 Code Tracking Loops*

The code-tracking loop is the portion of the receiver that keeps the receivers' tracking channel aligned with the incoming code from the satellite. By matching up the receiver-generated code with the internally generated version, an auto-correlation function is generated.

This auto-correlation function, or correlation peak, can be viewed by sliding the local replica of the code in time with respect to the incoming code sequence. When the code sequences are aligned, there is a measured power level. This observed power signifies to the receiver software that there is a signal present at the given alignment. This given alignment is then used as a starting point for the code-tracking loop. The doppler at which the signal was found is also important because it indicates how fast the code is moving. If the doppler estimate is too small or too large, the code matching will not last for a very long period of time because one of the code sequences will be moving out of alignment with respect to the other, and the signal will be lost during the initial stages of acquisition.

Power, in this context, is the sum of the two code sequences multiplied together. It is the nature of the C/A code sequences, that they produce very little power when the two code sequences are not aligned. The sequences must be aligned within fractions of a chip if there is to be measurable power. An example of this is shown in Figure 2-4. Beyond 1 chip away from the perfect alignment, the theoretical correlation value is zero.

From Figure 2-4, we can see that:

$$A(t) = 1, \text{ for } t = 0 \quad (2-3)$$

$$A(t) = 0, \text{ for } |t| > 1 \quad (2-4)$$

$$A(t) = 1 - |t|, \text{ for } |t| < 1 \quad (2-5)$$

Where  $A(t)$  is the amplitude of the normalized signal.

Figure 2-4 has normalized all code samples by the power obtained when the signals are perfectly aligned. For this reason, we see a peak amplitude of 1.

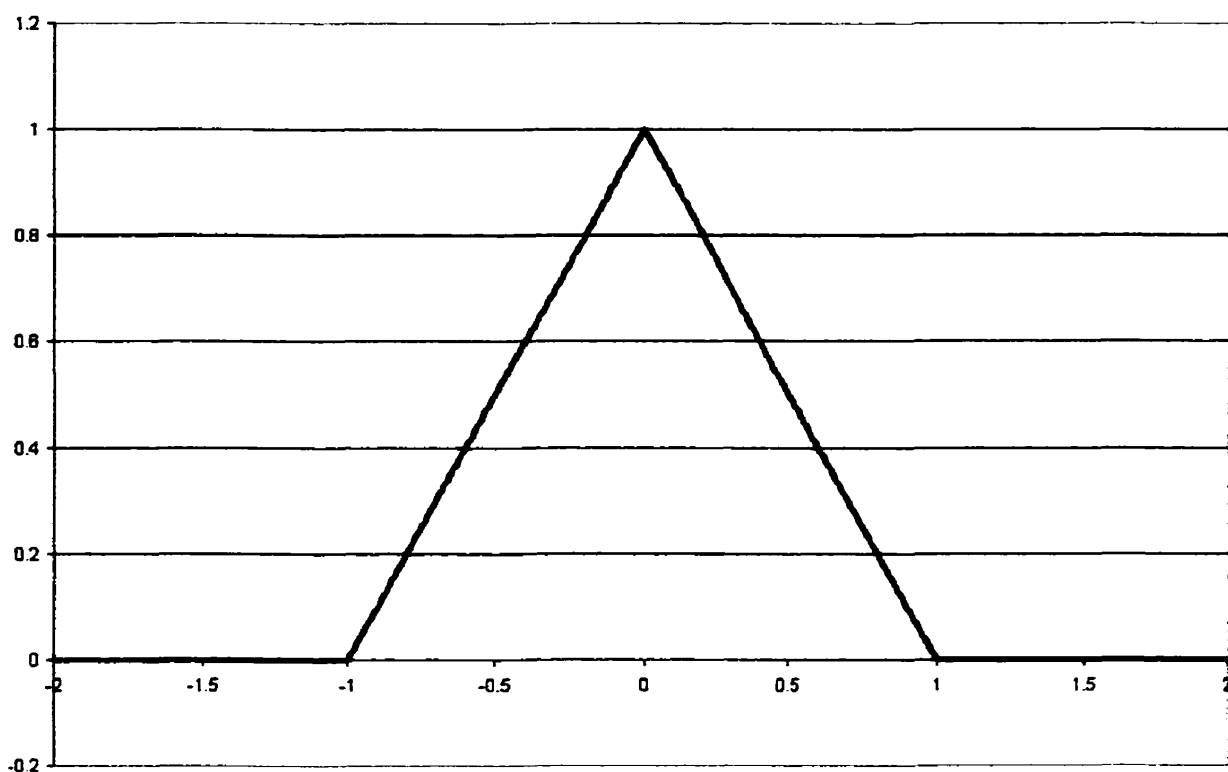


Figure 2-4 Normalized Perfect C/A code Auto-Correlation Function

In reality, these  $A(t)$  values will differ slightly in the  $|t| > 1$  region and will not always be zero. There are a number of different classes of PRN codes, and each will have a different effect at the edge of the correlation peak. These PRN code types are summarized later in Table 2-1.

### 2.3.1 Correlators and the Correlation Function

In order to understand how we correlate data together to generate the correlation function we need to know about the Analogue to Digital Converter (A/D). The A/D is the component of the receiver, which converts the analogue input signal to a digital format that can be further interpreted by the hardware and software. The A/D samples the incoming data in inphase and quadrature components. The quadrature signal measurement is done 90° out of phase, with respect to the inphase component. The signal sampling sequence from the A/D is then in the form ...Q, I, -Q, -I..., where Q represents the quadrature measurement and I the inphase. The A/D and the phase offset between I and Q measurements are done in the hardware of the receiver and is generally not controlled by receiver software.

The alternating inphase and quadrature signal components are separated inside the receiver to generate two independent streams of ...I, -I, I, -I..., and ...Q, -Q, Q, -Q..., each at half the nominal receiver clocking rate. Since only every second sample is used to generate these streams, the clocking rate is half the nominal rate.

These signal streams are correlated together with the receiver generated C/A code sequence. The receiver generated C/A code sequence will be internally advanced and delayed, in order to generate Late and Early correlation samples. A punctual code correlation value is also commonly used in addition to the Early and Late samples.

Two typical schemes for the code-tracking loop involve the following:

1. Early-Late (E-L) and Punctual (P) code correlation samples, or
2. Early (E) and Late (L) code correlation samples.

In the case of the E-L (Early minus Late), P configuration, two correlators are used. One measures the difference between the E and L correlators,

resulting in the E–L sample. The other measures the P. Both correlators correlate the inphase and quadrature samples.

For the second method, the two correlators independently correlate the E and L samples, both giving inphase and quadrature samples.

When correlating the E and L samples separately, the codes go in opposite directions (one positive and the other negative) when the codes are different. This is not the case when using an E–L correlator since the accumulation will only count a difference of 1. Therefore, when differencing the E and L correlators to generate an E–L value in software, the correlation will be twice as large as with the hardware accumulated E–L correlator. When combining or comparing measurements from these two methods of code correlation, this difference in measurements needs to be considered.

### 2.3.2 Discriminators

Discriminators are the way in which the correlation information is used to determine the code tracking error and adjust the code tracking loop. There are a number of different discriminators that can be used [18] to implement the Delay Locked Loop (DLL) including coherent (using both I and Q information) and non-coherent (using only I information).

There are four common discriminator equations, defined below in equations 2–6 through 2–9.

$$\text{Dot-Product Power} \quad (I_E - I_L) * I_P + (Q_E - Q_L) * Q_P \quad (2-6)$$

$$\text{E-L Power} \quad (I_E^2 + Q_E^2) - (I_L^2 + Q_L^2) \quad (2-7)$$

$$\text{E-L Envelope} \quad \sqrt{(I_E^2 + Q_E^2)} - \sqrt{(I_L^2 + Q_L^2)} \quad (2-8)$$

$$\text{Normalized E-L Envelope} \quad \frac{\sqrt{(I_E^2 + Q_E^2)} - \sqrt{(I_L^2 + Q_L^2)}}{\sqrt{(I_E^2 + Q_E^2)} + \sqrt{(I_L^2 + Q_L^2)}} \quad (2-9)$$

Equations 2-6 through 2-9 grow in computational burden, as more and more numerical operations are required to compute the code error. However, with increased computational load comes increased robustness in the code error calculation. This robustness is evident in Figure 2-5 below, which shows the shape of each of these discriminators, as they move across the correlation function from the early to the late side of the curve (assuming 1.0 chip E to L correlator spacing).

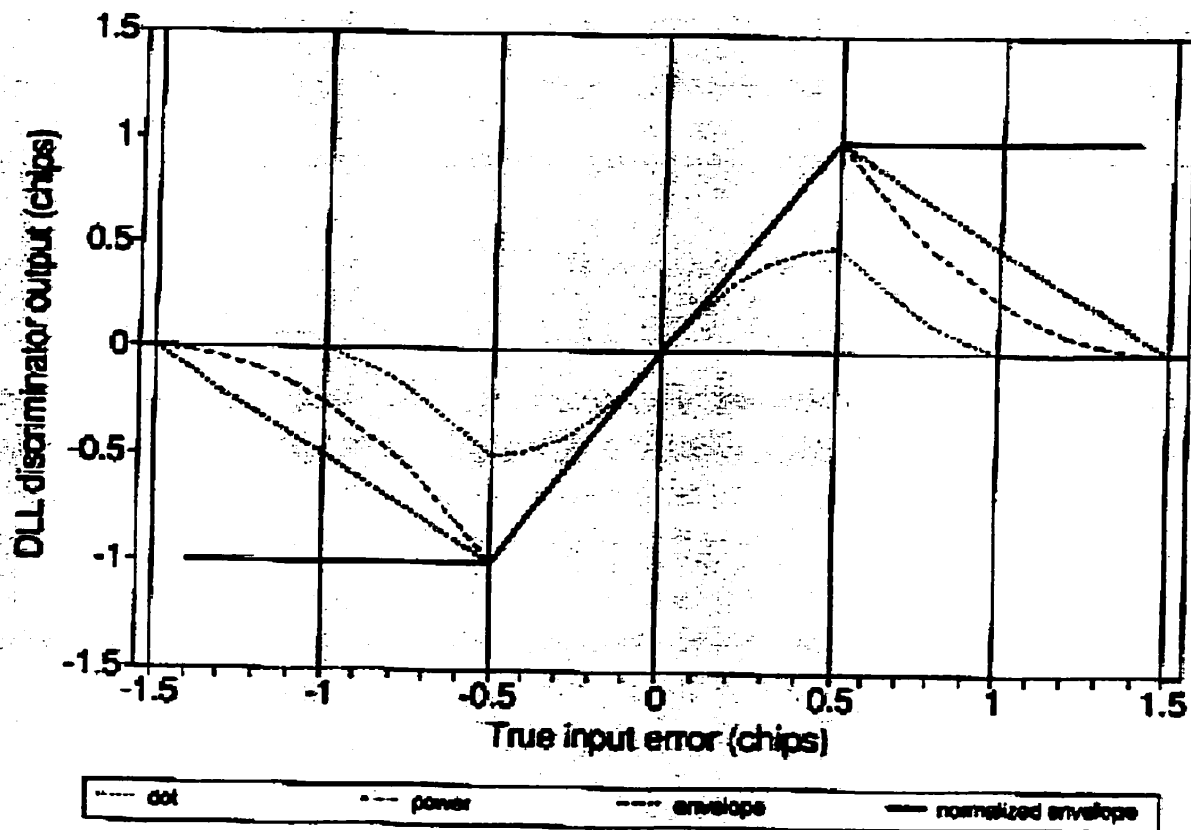


Figure 2-5: DLL Discriminator Output for Various Discriminators [18]

Equation 2-9 is the E-L envelope normalized by the E+L envelope. This discriminator removed any sensitivity due to varying amplitudes of the measured code correlation value.

As the E and L correlators get closer to the correlation peak, the allowable error reduces. This error can be visualized from the region between  $-0.5$  and  $+0.5$  in Figure 2-5, for the 1.0 chip spacing correlators. As the correlators get closer together, this region will reduce proportionally to the amount the correlator spacing is reduced.

### 2.3.3 Multi-Correlator Tracking

There are a number of additional discriminators that can be implemented, all of which attempt to limit the impact of a multipath signals on the code tracking loop. The concept often involves using more than the standard two correlators for tracking, in order to gather more information about the correlation peak. With this additional information, a better estimate of the true tracking position can be made.

One such discriminator is NovAtel's patented Multipath Eliminating Technology (MET<sup>®</sup>) [36]. MET uses an Early Late Slope (ELS) technique to predict the location of the true correlation peak, based on two code correlation values on each side of the P correlator. There are also additional multi-correlator techniques that have been developed including the strobe correlator [51], the double-delta correlator [27], and the Multipath Estimating Delay Lock Loop (MEDLL) [47].

When we have the ability to use additional correlators to determine the shape of the correlation function, we can use that information to reduce the effects of multipath and improve our estimate of the C/A code alignment. We can also use these additional correlators to determine if there has been a failure of the satellite signal itself.

#### 2.3.4 MDE's and MDR's

In order to determine if there is an error in the correlation domain of the broadcast satellite signal, additional correlators must be used in order to gather more information about the shape of the function. Since the use of multiple correlators is required, DLL discriminator techniques such as those mentioned in section 2.3.3 become more attractive to implement. With the additional correlation information available (and being used for signal monitoring) it would be prudent to put this information to use for advanced signal tracking techniques rather than only for SQM.

There are two main concepts that will tell us the nature of the correlation function. The first is the Minimum Detectable Error (MDE) and the second is the Minimum Detectable Ratio (MDR). Both of these concepts relate to the correlation function.

The MDE refers to our ability to detect when a single correlation value is in error. This error can be either above or below what the expected value of the correlation should be given the location of the correlator from the punctual code measurement. We have both a high and low threshold of detection in order to determine when there is an error in the measured signal. It is important to use MDE values at numerous correlator locations in order to improve our ability to detect anomalous signals, since each correlator will only indicate the presence of such an event at its own position. Also, different correlator locations are affected differently by different anomalous waveforms.

The MDR also refers to our ability to detect signal failures. However, with this value we are looking at the variation across the peak of the correlation function. By design, our code-tracking loop is trying to force one of these ratios of E and L correlator values to zero through the use of the DLL. What we are using as a detection mechanism here is the ratio of other non-tracking correlator pairs, also across the peak of the

correlation function. These values are subtracted from the error observed from the tracking pair as a means of removing any inherent tracking offset remaining in the DLL and focusing on the actual signal anomaly, which may or may not be present. These values will help indicate any distortions across different correlation positions rather than a single point with the MDE.

Our detection thresholds for MDE and MDR, sometimes referred to as 'metrics', are dominated by inter-receiver componentry variations, multipath and noise, as seen in Chapter 4. Any distortions due to multipath will be detected in the MDE and/or MDR. It is very important to note that in the correlation domain, it is difficult (but not impossible) to distinguish between multipath and a satellite failure. By using the multiple correlators for signal tracking as well as anomaly detection, we can more easily distinguish between the two, than if we left the tracking and anomaly detection as independent mechanisms.

## ***2.4 False Alarms and Miss-Detections***

With our SQM scheme, there will be times when our algorithms will indicate the presence of a satellite signal failure when in fact none is present. This is known as a false alarm. Contrary to a false alarm is the miss-detection or missed detection of a failure. In this condition, there has been a satellite signal failure and we have not detected it. Both items will have required probabilities that must be met, based on the requirements of the service provider. The service provider is the one that will be using the receiver and its SQM scheme to alert other users as to the suitability of the signals being broadcast from the satellites. The service provider may also send differential corrections to these users as part of their broadcast messages. Balancing the probabilities of false alarm and miss-detection is a difficult task, and should be tackled by the service provider along with the SQM developer at the installation site.

Most installation sites will have multiple ground reference stations within the service area that can be used together as a means of further reducing the false alarm rate. By using the method of majority logic on data received from all reference stations, the false detection of a satellite signal failure due to multipath can be reduced. This reduced probability occurs as a result of only indicating a true failure when more than half of the SQM stations indicates the failure. Multipath is site dependent, but on the other hand all reference stations will observe a satellite failure simultaneously.

The concept of false alarms and miss-detection is applied to satellite signal failures discussed in Chapters 4 and 5, as well as interference detection in Chapter 6.

## ***2.5 Wide Band Code Range Corrections***

**When running the discriminator, we compute a value that corresponds to the code tracking error. This error tells us by how much we need to adjust the position of our tracking in order to remain code-locked on the peak of the correlation function.**

**Often, the DLL has a bandwidth of less than 1 Hz [24]. This means that there is smoothing done on the code error calculated by the discriminator, in order to allow for less noisy operation of the DLL. This means that the correlation values used in the discriminator equations in section 2.3.2 are summed over multiple epochs before running the DLL. In some conditions, we may want to get the discriminator value output to us so that additional calculations and checks can be done on it.**

**The output of the discriminator error is commonly referred to as the wide band code range correction. In theory, by examining how the discriminator is behaving, we can determine if there is any anomaly present on the signal or if the receiver is under the influence of interference. Therefore, theoretically, what we are trying to do is gather information from a noise sequence to determine if something is adversely affecting our tracking loop. Additional investigations into this are shown in Chapter 6.**

## ***2.6 Multipath Estimating Delay Lock Loop (MEDLL<sup>o</sup>)***

**GPS pseudorange and carrier phase measurement are susceptible to systematic errors, which include:**

- 1. Satellite Clock Drift,**
- 2. Satellite Ephemeris Error (orbital prediction),**
- 3. Ionospheric Delay,**
- 4. Tropospheric Delay,**
- 5. Receiver Clock Offset, and**
- 6. Multipath.**

**Items 1 through 4 can be removed through differencing techniques or at least significantly reduced with modelling. The receiver clock offset is usually solved for as an unknown in the position computation of the receiver.**

**Multipath, however, behaves much differently. Multipath is generally not common between receiver locations. As a result, it cannot be removed by differencing techniques. Modelling the multipath source(s) can be quite difficult and impractical [46], but is always still possible.**

**The MEDLL attempts to remove the effect of multipath sources from the input signal inside the receiver using a multi-correlator approach. This significantly reduces the unfavourable impact of multipath signals on the pseudorange and carrier phase measurement accuracy [37].**

**Through an estimation technique based on maximum likelihood estimation [49], the MEDLL estimates the amplitude delay and phase of the multipath source. The method of maximum likelihood estimation allows the MEDLL to use its knowledge of the correlation function distribution in the estimation process. This knowledge is in the form of a reference function, derived for each of the observable PRN code types, which is stored in software.**

### 2.6.1 PRN Code Types

The PRN code types relate to the shape of the correlation function beyond the 1-chip interval around the ideal code alignment. When stated that  $A(t) = 0$ , for  $|t| > 1$  in equation 2-4, this was a generalization. None of the PRN codes will result in this ideal situation but will in fact have slight variations from this ideal. Some of the correlation values produce varying correlation powers at alignments beyond 1-chip from punctual.

When the MEDLL algorithm operates, these different types of PRN codes are instrumental in the accurate estimation of the multipath signal.

The table below summarizes the expected correlation value for each of the GPS PRN codes with varying chip alignments, classifying them into seven groups.

PRN	G2 Delay	Type	Correlation with Chip Lag (C A Code Chips)			
			0	1	2	3
1	5	1	1023	-1	-1	-1
2	6	1	1023	-1	-1	-1
3	7	1	1023	-1	-1	-65
4	8	4	1023	-1	-65	-1
5	17	1	1023	-1	-1	-1
6	18	4	1023	-1	-65	-65
7	139	2	1023	63	-1	-1
8	140	7	1023	-65	63	-1
9	141	1	1023	-1	-1	-1
10	251	5	1023	-1	63	-1
11	252	1	1023	-1	-1	-1
12	254	1	1023	-1	-1	-1
13	255	1	1023	-1	-1	-1
14	256	1	1023	-1	-1	-1
15	257	2	1023	63	-1	-1

PRN	G2 Delay	Type	Correlation with Chip Lag (C A Code Chips)			
			0	1	2	3
16	258	4	1023	-1	-65	-1
17	469	2	1023	63	-1	-65
18	470	5	1023	-1	63	-65
19	471	4	1023	-1	-65	63
20	472	1	1023	-1	-1	63
21	473	2	1023	63	-1	-1
22	474	3	1023	-65	-1	-1
23	509	1	1023	-1	-1	-1
24	512	6	1023	63	-65	-65
25	513	1	1023	-1	-1	-65
26	514	1	1023	-1	-1	-1
27	515	1	1023	-1	-1	-65
28	516	4	1023	-1	-65	-1
29	859	1	1023	-1	-1	-1
30	860	5	1023	-1	63	-65
31	861	1	1023	-1	-1	-1
32	862	1	1023	-1	-1	-1

Table 2-1: PRN Code Types

Note that at 3-chip spacing the effect of the correlation has no impact on the assignment of the PRN type. At a distance of 3-chips away, there is an insignificant impact on the likelihood estimator of MEDLL due to the code correlation. Only those correlation values within two chips are of importance in the multipath estimation process.

In addition, with a variation in correlation values at 1-chip away from the maximum correlation value, there will be marginally different slopes on the sides of the correlation peak, at values less than 1 chip from punctual. The difference between PRNs is significant enough to warrant a unique threshold for detecting distortions on the correlation peak, when determining the threshold values. There could be variations between the

expected and the measured correlation values, in terms of MDE values, based on the PRN code type that may lead to false alarms.

### 2.6.2 Multipath

The term multipath is derived from the fact that a signal transmitted from a GPS satellite can follow a 'multiple' number of propagation 'paths' to the receiving antenna. This is possible because the signal can be reflected back to the antenna off of surrounding objects, including the Earth's surface. Figure 2-6 illustrates this phenomenon for one reflected signal.

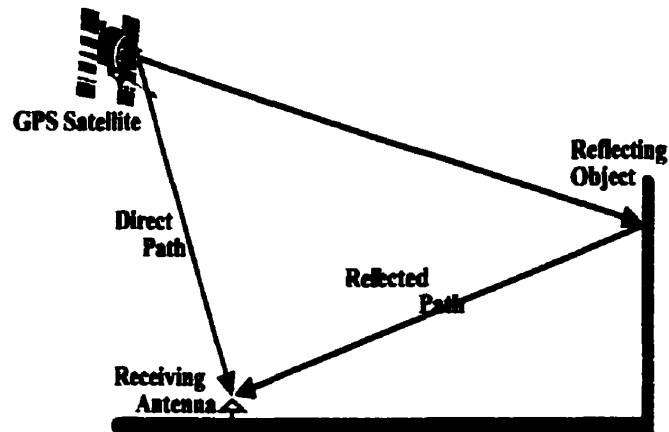


Figure 2-6: Direct Path and Multipath (Reflected Path) Signals

Some important characteristics of multipath are [39]:

- i) The multipath signal will always arrive after the direct path signal because it must travel a longer distance over the propagation path.
- ii) The multipath signal will normally be weaker than the direct path signal since some signal power will be lost from the reflection.
- iii) If the delay of the multipath is less than two PRN code chip lengths, the internally generated receiver signal will partially correlate with it.

Generally, if the delay is greater than 1 chip the correlation power will be negligible.

Multipath signals will adversely affect the correlation function, distorting its shape. This in turn produces a pseudorange error due to the distortion. In the presence of multipath, the DLL does not properly recognize the true peak of the function as the ideal code alignment and is therefore offset resulting in the pseudorange error.

We will further see in Chapter 5 that these assumptions about multipath do not continue to be true in the presence of certain anomalous satellite signals.

### 2.6.3 MEDLL Equations

In the presence of multipath propagation, the received satellite signal can be written as:

$$r(t) = \sum_{m=0}^{M-1} a_m p(t - \tau_m) \cos(\omega t + \theta_m) + n(t) \quad (2-10)$$

Where,

- $M$  = number of signals
- $t$  = time
- $p(t)$  = the code
- $n(t)$  = white noise
- $a_m$  = component signal amplitude
- $\tau_m$  = component signal delay
- $\theta_m$  = component signal phase

For a positioning system like GPS, the parameters of interest are the direct path signal delay and phase. In order to estimate these

parameters, the direct path correlation function needs to be determined. The MEDLL approach involves the decomposition of the correlation function into its direct path and reflected path components.

The MEDLL estimates the amplitude, delay, and phase of each multipath component. Each estimated multipath correlation function component is in turn subtracted from the measured correlation function. The result is an estimate of the direct path correlation function. A standard Dot-Product Power DLL is applied to the direct path component of the correlation function giving a 'multipath free' estimate of the code loop tracking error. This corrected correlation function will also provide us with the multipath corrected correlator values for SQM, used in Chapters 4 and 5.

#### 2.6.4 The Multipath Meter

As an extension of the MEDLL, the Multipath Meter was invented [38]. The Multipath Meter extends the use of the MEDLL by outputting the measured amplitude, delay, and phase of the multipath signal as well as the multipath corrected correlator values [39] used in the estimation process.

By outputting these values, the Multipath Meter gives accurate information about the multipath environment that the receiver is experiencing. Associating the measured quantities with the direction to the satellite can identify reflective surfaces causing the errors. As a result, the overall site statistics (in terms of multipath error) can be assessed using the Multipath Meter.

One of the key concepts related to the multipath meter is the desired to undesired signal ratio (D/U). It is the simple ratio of the desired code correlation amplitude (the measured amplitude corrected for multipath effects), divided by the estimated multipath signal amplitude. This

number is also scaled into a logarithmic value for easier comparisons. When the D/U is high, there is less of an effect due to multipath on the input signal. When the D/U is low, there is a significant impact from multipath. The D/U can be calculated from the following equation:

$$D/U = 20 \cdot \log(a_{direct} / a_{multipath}) \quad (2-11)$$

Where:

$a_{direct}$  = amplitude of the direct path signal, and

$a_{multipath}$  = amplitude of the multipath signal.

In addition, the correlation residuals from the multipath estimation process are available. The residual values are those correlation values that are left over after the removal of the multipath signals. The residuals generally do not follow a trend, like that of a multipath signal, and only represent noise. Analysis of these values can verify the accuracy to which the MEDLL has estimated the multipath signal. If there are multiple multipath signals present, the MEDLL may not accurately estimate them all, and the residuals will increase [16].

Taking the measured correlator values and subtracting off the computed direct path and multipath correlator values give the MEDLL correlator residuals. The direct path and multipath correlator values are calculated using a pre-determined reference correlation function. The correlator residual is represented by,

$$C_{res} = C_{meas} - \sum_{m=0}^{M-1} a_m C_{ref}(x - \tau_m) \cos(\theta_m) \quad (2-12)$$

Where,

$C_{res}$  = correlator residual

$C_{meas}$  = measured correlator value

$C_{ref}$  = reference function correlator value

- M** = number of signals
- $x$**  = correlator position
- $a_m$**  = component signal amplitude
- $\tau_m$**  = component signal delay
- $\theta_m$**  = component signal phase

As previously touched on, another important value that we can use is the multipath corrected correlator values. These values are calculated for all correlator values and are the original correlator values minus the estimated multipath correlation component influence. By removing the impact of the multipath signal before performing any SQM using MDE and MDR values, it will be shown in Chapter 5 that we can detect all tested types of satellite failures in multipath environments where the multipath delay is such that the MEDLL can accurately estimate it for line-of-sight applications. Although in certain environments with very short delay multipath (where the Multipath Meter does not perform well) the failure may also be detectable depending on its characteristics. Removing the multipath effects will not mask the satellite signal failure. Chapter 4 will also validate the improvements in using the multipath corrected correlator values instead of the raw correlator values for the MDE and MDR calculations. When using the measured uncorrected correlator values for SQM there are certain multipath environments, when coupled with satellite signal failures, which result in the non-detection of the signal failure. Removing the multipath effects will result in the detection of satellite failures, regardless of the multipath environment.

All of the estimates from the Multipath Meter are output in real time, which allows for immediate analysis of the data and real time SQM.

## CHAPTER 3

### SATELLITE FAILURE MODES

In terms of satellite failure modes, there are a number of different failures that can result in significant pseudorange errors. These pseudoranges are then used in the computation of the position time solution in the receiver, which can result in large positional discrepancies depending on the internal signal processing mechanisms of the receiver. The ability of the receiver to identify such failures is imperative to its successful operation. This detection method involves monitoring the broadcast signal within the receiver for known failure conditions.

An anomalous signal can be defined as a failure at or near the satellite causing an unannounced degradation of the expected signal accuracy and integrity. The accuracy relates to the results obtained from using the system (i.e. calculation of a position or use any of the data output from a receiver) and the integrity to the ability of the system to consistently provide these results.

#### *3.1 Feared Events*

All of the failure modes presented in this section have a basis in circuit reality. That is to say that the failures can physically occur and be traced back to a specific component, or region of signal generation on the satellite, after the failure has occurred. Once such a satellite signal failure has occurred, it is assumed that the signal will remain in this failed state. There will be no intermittent failure modes of the satellite signal.

There was a single event in GPS's history that has lead to this feared event of a satellite signal failure. It related to a signal failure of GPS PRN 19 that occurred in October of 1993 [10], [26]. Distortions were realized in both differential and single point mode. The US DoD has classified the

underlying cause of the error, and has not made their internal report available to the public. However, research activities within RTCA Inc., whose recommendations are used by the US Federal Aviation Administration (FAA) as the basis for policy, program, and regulatory decisions and by the private sector as the basis for development, investment, and other business decisions, has shed some light on the failure modes. It was determined that failures related to the PRN 19 event can manifest themselves as flat, distorted, or multiple peaks in the correlation domain from a second order step response applied to the C/A code chips broadcast by the satellite [10], [11], [15], [32].

The mathematical model used to represent this second order step response is described as:

$$e(t) = 1 - e^{(-\sigma t)} \left[ \cos(\omega_d t) + \frac{\sigma}{\omega_d} \sin(\omega_d t) \right] \quad (3-1)$$

**Where:**

$\omega_d$  = natural frequency

$\sigma$  = damping factor

$t$  = time

$e(t)$  = anomalous signal effect

### 3.1.1 Digital Failure (Threat Model A)

Digital failures are generated when the chip transitions do not occur at the anticipated times. Either the rising or the falling edge of each chip transition is advanced or delayed in time. Each of these events is mutually exclusive, in that only one of them will ever occur at a time. This is the nature of the failure as it relates to the physical componentry of the satellite. This phenomenon can be seen in Figure 3-1 below:

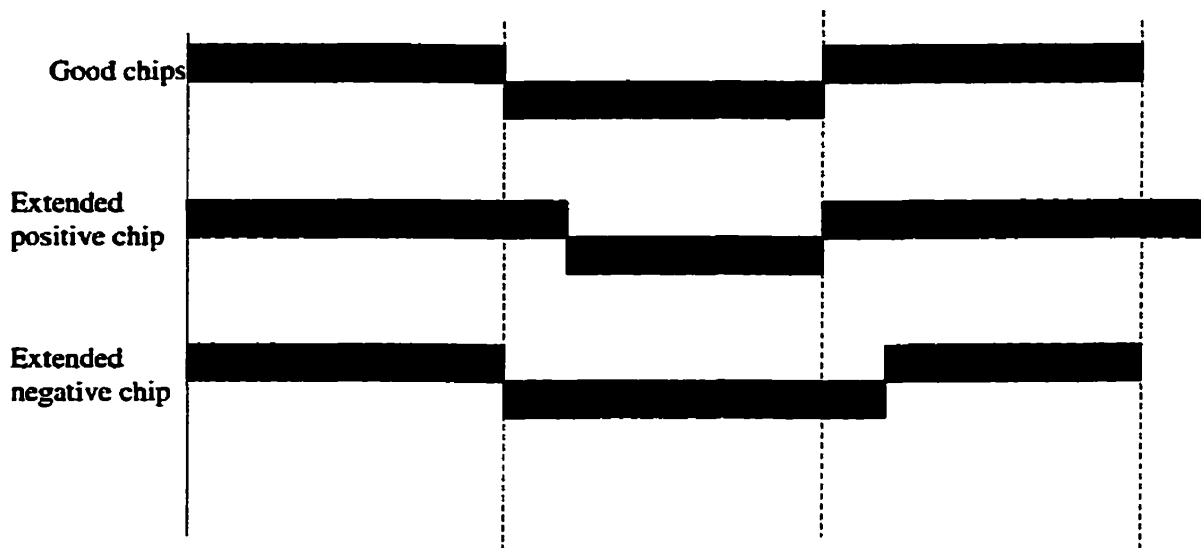


Figure 3-1: Chip Transitions for Digital Signal Failures

The amount of lead or lag in the chip transition is limited to 0.12 chips [28], [43].

This kind of signal failure will generate a flat correlation peak inside the receiver. This effect can be seen in Figure 3-2 for various lengths of C/A code chip distortions. The level of distortion is referred to as  $\Delta$ , and is measured in units of C/A code chips.

We can observe from Figure 3-2 that as we correlate our receiver generated C/A code sample with the incoming satellite code sequence,

whose chip falling edges are increasingly distorted, the length of the flatness of the correlation function increases proportionally.

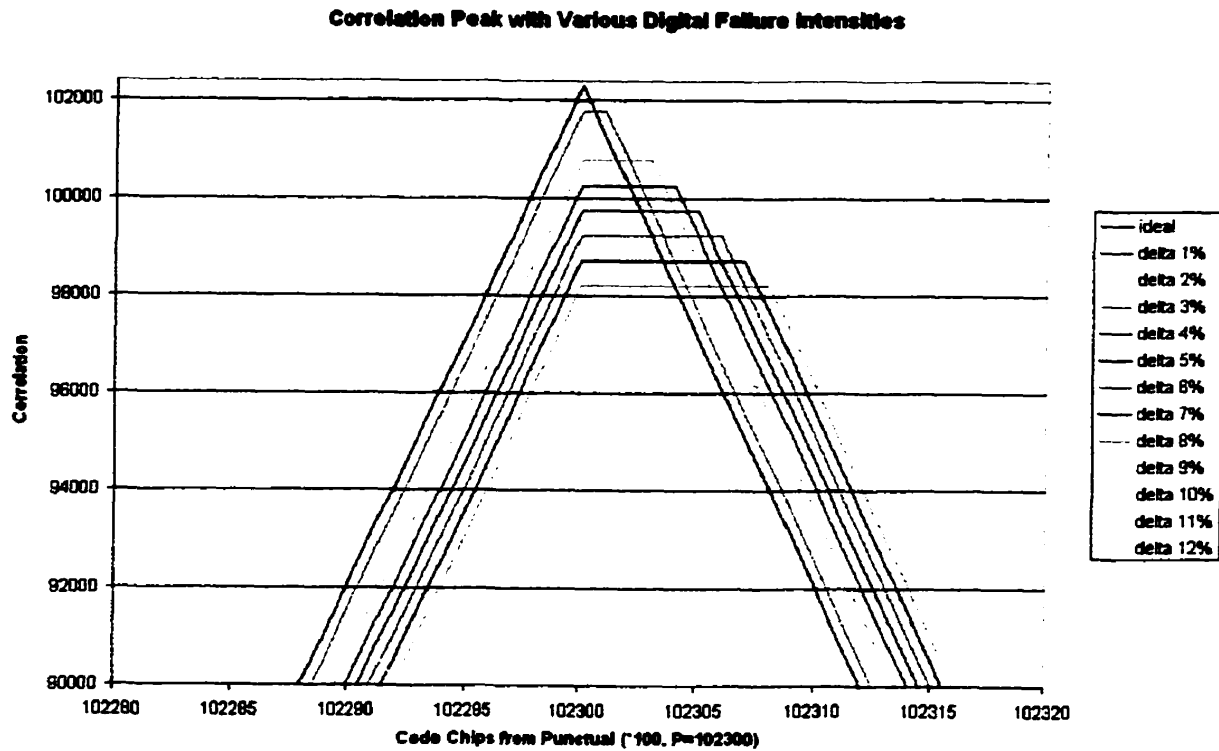


**Figure 3-2: Digital Failures Effect on Correlation Function**

### 3.1.2 Analogue Failure (Threat Model B)

Analogue failures are generated using equation 3-1 and applying the result to the chip transitions of the C/A code. The effect will be applied to each transition, whether it is from -1 to +1 or vice versa. The result is a 'ringing' effect on the transitions of the chips. This effect can be seen below in Figure 3-3:

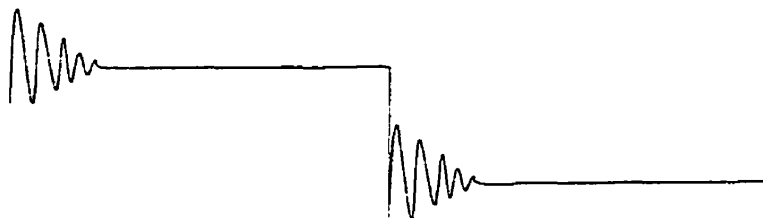


Figure 3-3: Chip Transitions for Analogue Signal Failures

The varying frequency and damping factors described in equation 3-1 are limited by  $4 \leq f_d \leq 17$  and  $0.8 \leq \sigma \leq 8.8$  [28], [43]. Figure 3-4 shows the effect of having an  $f_d$  of 4MHz and a damping factor of 0.8 on the correlation function. These are the minimum values within this threat space. We can see that there is a significant ringing effect on the correlation function that mimics the frequency of the underlying anomalous signal frequency.

Figure 3-5 shows the effect on the C/A code chip. By correlating our perfect (ideal) receiver generated C/A code sequence with this incoming satellite C/A code sequence, we will generate the correlation function shown in Figure 3-4. The black line in Figure 3-5 shows what the non-failed (ideal) C/A code chip should look like. We can compare Figure 3-4 to Figure 2-4 and see that the anomalous signal can introduce significant distortions in the correlation function.

Also, we can see the varying effects for  $f_d = 17\text{MHz}$  and  $\sigma = 8.8$  in Figures 3-6 and 3-7.

Correlation Function for Analogue Failure of  $f_d = 4\text{MHz}$  and  $\sigma = 0.8$

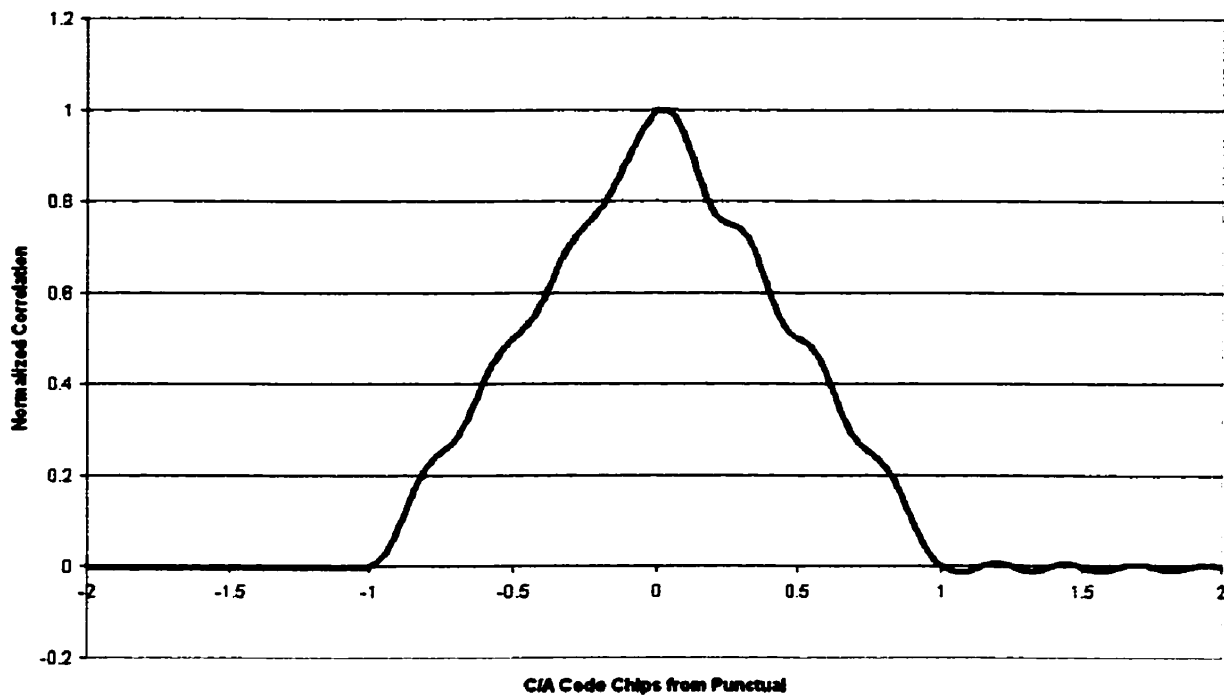


Figure 3-4: Analogue failure effects on correlation (min  $f_d$  and  $\sigma$ )

C/A Code Chip for Analogue Failure of  $f_d = 4\text{MHz}$  and  $\sigma = 0.8$

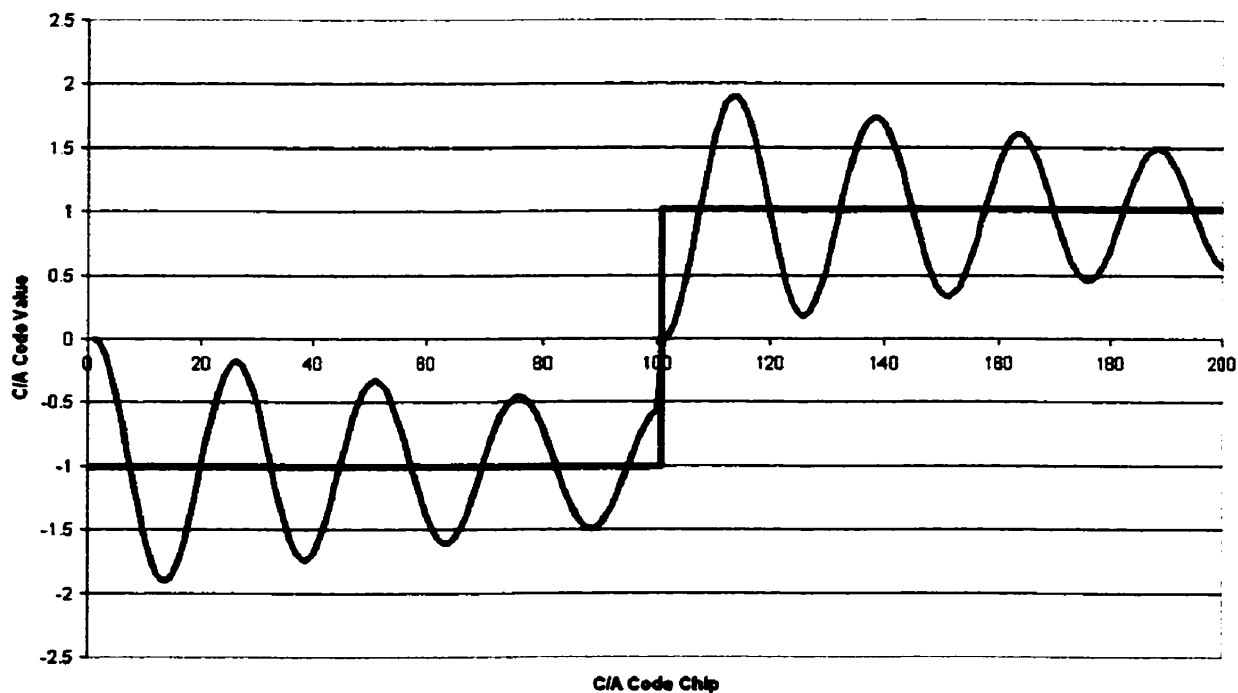
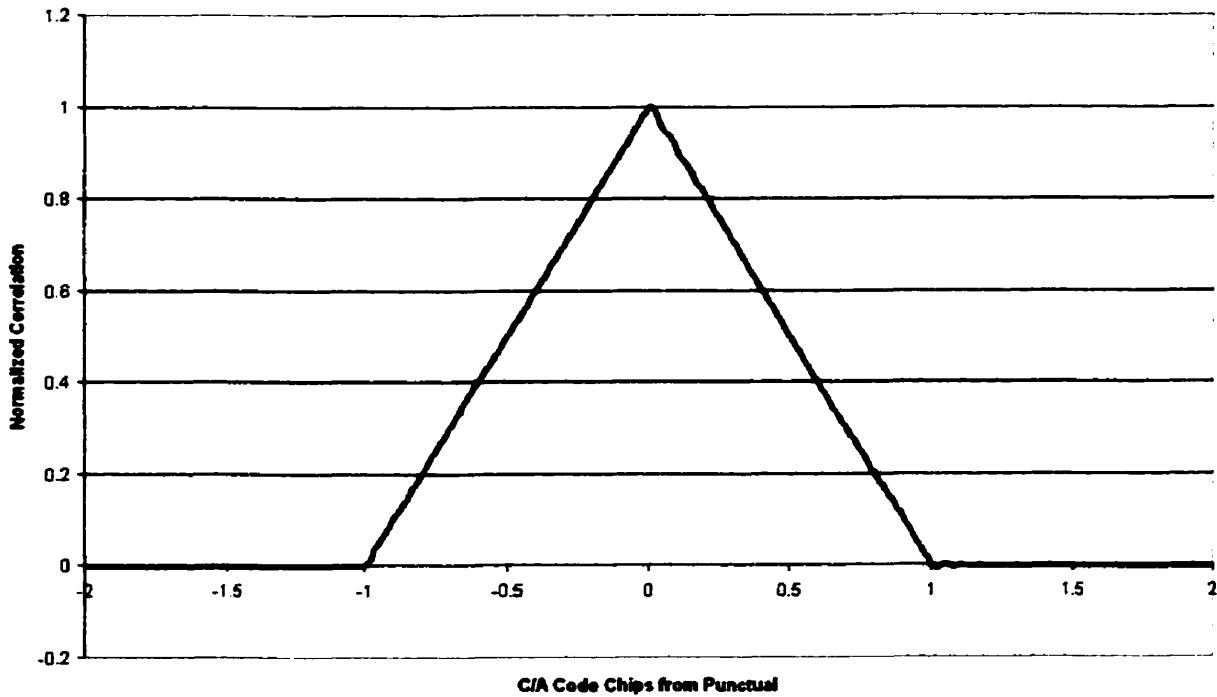


Figure 3-5: Analogue failure effects on C/A code chip (min  $f_d$  and  $\sigma$ )

**Correlation Function for Analogue Failure of  $f_d \approx 17\text{MHz}$  and  $\sigma \approx 8.8$**



**Figure 3-6: Analogue failure effects on correlation (max  $f_d$  and  $\sigma$ )**

**C/A Code Chip for Analogue Failure of  $f_d \approx 17\text{MHz}$  and  $\sigma \approx 8.8$**

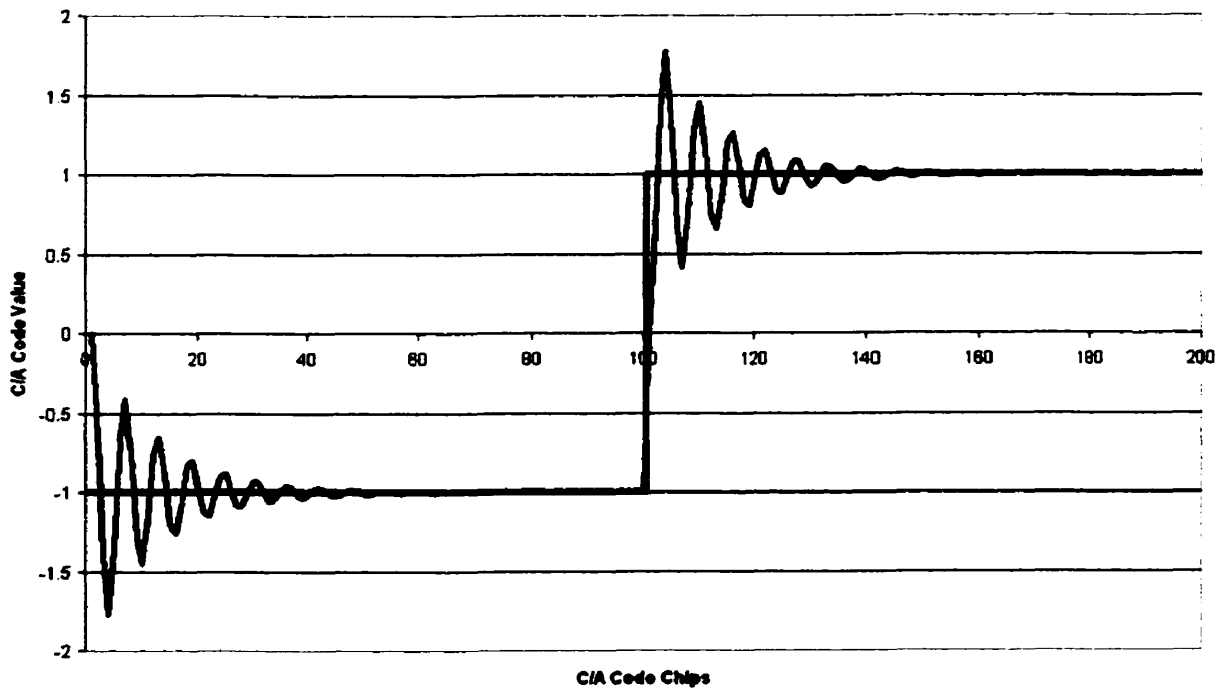


**Figure 3-7: Analogue failure effects on C/A code chip (max  $f_d$  and  $\sigma$ )**

### 3.1.3 Combination of Failures (Threat Model C)

There is also the possibility of having both analogue and digital failures occur at the same time. When this type of failure occurs, the digital failure threat space still remains at 0.12 chips, however the analogue failure threat space has been reduced to  $7.3 \leq f_d \leq 13$  and  $0.8 \leq \sigma \leq 8.8$  [28], [43].

The effects of such a failure mode can introduce multiple peaks into the correlation domain or produce secondary peaks that reoccur at a spacing related to the frequency of the failure. The intensity of the secondary peaks is related to the damping of the analogue failure. One example of this failure mode can be seen in Figure 3-8 with  $\Delta = 0.12$ ,  $f_d = 10.5\text{MHz}$ , and  $\sigma = 4.8$ . These values were chosen to demonstrate the occurrence of multiple peaks.

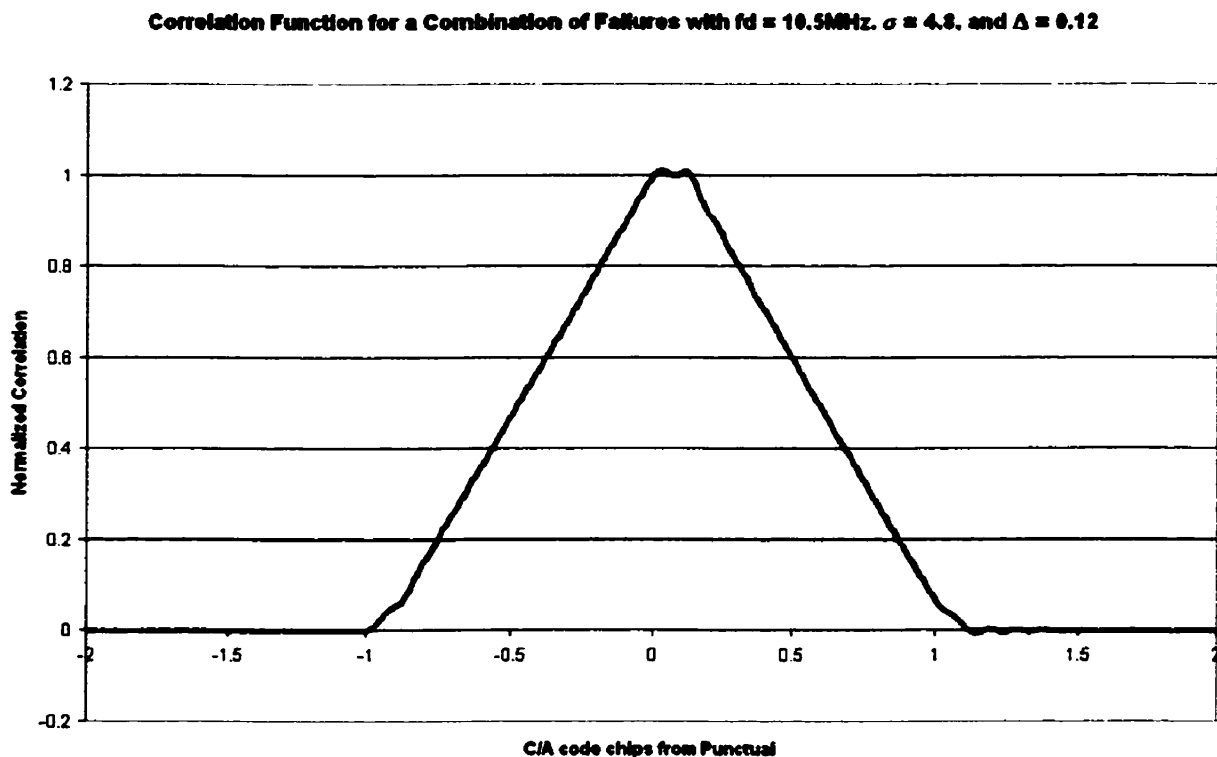


**Figure 3-8: Effect on the Correlation Function for a Combination of Failures**

### 3.1.4 Failure Impact on Tracking

All GPS receiver manufacturers enjoy the flexibility of designing their own RF hardware and applying their own code correlation tracking techniques. As a result, each receiver manufacturers' receiver will be affected differently by any anomalous signal that is present. Filtering effects from the RF componentry will skew anomalous satellite signals (as shown in Chapter 4) such that when the code correlation takes place, there are varying impacts on the tracking loops of the receiver software. As well, when multiple peaks are present as shown in Figure 3-8, or even highly distorted peaks as in Figure 3-4, the position of the correlators relative to the punctual correlator can adversely affect the tracking loops.

When multi-correlator tracking techniques are used, there can be even more distortion introduced into the estimate of the pseudorange when anomalous satellite signal are present, especially when using E-L slope techniques. This is evident by the reduced parameter values for allowable receivers using this type of DLL tracking technique as shown in [28] and [43]. The parameter space has been reduced in order to limit the impact of satellite signal failures on the measured pseudorange of the receiver.

The true problem begins when one receiver (from manufacturer A, using RF bandwidth B, correlator spacing C, and DLL tracking technique D) sends code differential corrections to another receiver (from manufacturer W, using RF bandwidth X, correlator spacing Y, and DLL tracking technique Z). With so many different variables affecting the correlation function and receiver operation, there is no way of suitably determining every possible impact of the anomalous signal on every possible receiver design. It will also be shown in Chapter 4 that part-to-part variations in the RF section of a receiver will create differences in the measured correlation function. It is these underlying variations that can lead to differential positioning errors causing safety concerns.

**However, in the unlikely event that all GPS receivers used for safety critical systems were from the same manufacturer, using the same RF design, correlator spacing and DLL tracking technique, this entire problem of anomalous satellite signals would be minimized and almost certainly disappear. This has been the approach with the Microwave Landing System (MLS). This system has standardized the equipment that must be used in order to limit the impact of potential design differences.**

### ***3.2 Additional Possible Failure Modes***

Although the previously mentioned failure modes are all directly related to the PRN 19 event, additional failures of satellites have been observed in the past [10]. These failure modes are not directly traceable to the correlation domain, as with an anomalous satellite signal being broadcast, but have more to do with component degradation or human error at the satellite control stations. The GPS satellite control segment is that portion of the system that uploads messages to the satellites for re-broadcast and monitors the satellites themselves. This process is therefore susceptible to human error.

Failures of this type can be referred to as sudden but non-catastrophic in nature, whereas failures of the PRN 19 type are both sudden and catastrophic. For example, the US Air Force, on one occasion on the 16<sup>th</sup> of January 1998, accidentally commenced maintenance on satellite 16 before setting the appropriate health flag in the satellite message. Usually both scheduled and unscheduled satellite outages are announced via the Notice Advisory to Navigation Users (NANU) and GPS maintenance activities are well organized.

Slower failures causing performance degradation over a longer time scale can be attributed to problems with oscillators on the satellites. A typical example is the effect of aging on crystal oscillators. "The time constant on the GPS satellites' VCO frequency control loop in a Caesium<sic> frequency standard can degrade from 12 seconds to 90 seconds or more over a period of three to four years of sustained operation" [4].

In addition to satellite-based failures, there are propagation-based failures such as electromagnetic and atmospheric disturbances that can severely undermine receiver integrity. Examples of this are interference, multipath, and ionospheric disturbances, such as scintillation. Ionospheric scintillations can result in random-like variations in both

amplitude and phase of the signal. As such, they will affect the operation of both code and carrier tracking loops, causing loss of lock, particularly in the carrier loop due to increased sensitivity to cycle slips in periods of high ionospheric activity. L2 codeless and semi-codeless tracking is also susceptible to substantial periods of loss of lock during high ionospheric activity. Unannounced increases in measurement noise are also common under conditions of high ionospheric activity. Loss of carrier lock is catastrophic to carrier phase processing which requires phase continuity.

[4], [3], and [7] identify many specific cases of erroneous satellite signal behaviour, a few of which are discussed below along with possible methods of detection.

### 3.2.1 SV 27 Clock Anomaly

There was a clock anomaly on SV 27 that resulted in discontinuities of the satellites' broadcast signal for 5 seconds in March 1998. This type of failure would have been readily detected by inspection of the receiver's wideband code range corrections. As previously mentioned, these measurements provide information related to the error experienced in the code tracking loop. If the estimate of the signal phase is varying significantly from the broadcast phase (in this case due to a clock error) the wideband corrections will show the error. It could also be possible to examine wide band phase corrections (from the Phase Locked Loop, PLL) to observe the phenomenon more directly, rather than through the noisier carrier-aided code tracking loop.

### 3.2.2 SV 20 Erratic Clock

Erratic clock behaviour, in the case of SV 20, could also have been detected using the wideband code range corrections if the drift magnitude were high enough to be detectable. It is unfortunate that the

wideband code range corrections make a better multipath indicator than interference/clock error indicator, as demonstrated in Chapter 6. Otherwise, this type of error would be more readily observable. As a result, such satellite clock errors or anomalies would have to be at a consistently higher level than the ambient noise of the natural environment. However, lower magnitude drifts would have similar effects to Selective Availability (SA). SA was recently removed from the broadcast GPS signal [33], which would make these types of errors more easily detectable.

### 3.2.3 SV 21 Miss-Modelling by GPS Master Control Station

Miss-modelling of the orbital parameters of a satellite by the GPS master control station would manifest themselves as SA type errors. The orbital errors should be detectable by increased residual values from the position time solution for the range to the failed satellite. With the recent removal of SA from the broadcast signal, these types of errors would be easily identifiable by performing a technique of Receiver Autonomous Integrity Monitoring (RAIM) [18].

### 3.2.4 SV 16 Vehicle Instability

Similar to the SV 21 miss-modelling anomaly, satellite orbital instability would manifest itself as an orbital error, similar to SA.

### ***3.3 Possible Threats***

In addition to the specific events that have been previously identified, there are a number of possible satellite signal failures that have not yet occurred but have still been identified as a possible threat in [4]. Only some of the feared events described therein are discussed below, along with their impact on a receivers' ability to track the signal and provide reliable outputs.

#### **3.3.1 Incorrect or Invalid Broadcast PRN Code**

Part of the GPS satellite message that is broadcast from all satellites is known as an almanac. The almanac gives information related to the position of all of the GPS satellites in the constellation. With an almanac and the receivers' position, calculations can be done to determine when a certain satellite will become visible above the local horizon, and the receiver can get an approximate position of each satellite already in view. From this information, the receiver will also be able to tell what the doppler of the satellite will be, i.e. how fast it is moving relative to the user position.

If a satellite were to broadcast an incorrect or invalid PRN code, it is unlikely that misleading information would be output from the receiver. Aligning the expected PRN code sequence with a different PRN code sequence will not provide significant inphase power to result in the acquisition of the satellite signal. The signal power would be significantly suppressed. However, if an almanac is not available in the receiver and the receiver must search for each satellite in succession (instead of knowing exactly which satellites are visible and where in the sky they are) there may be a problem with acquiring an erroneous PRN. To alleviate the problem, the satellites' doppler should be validated with one calculated

from an almanac. The almanac would either have to be stored internally or be decoded from a satellite.

### **3.3.2 Excessive or Insufficient Signal Power**

If a satellite were to broadcast insufficient power, the satellite signal may not be acquired. The same may be true if too much power were broadcast where the receiver will become saturated by the incoming signal. However, if acquisition were to take place, the C/No would be different than expected. By using information in the almanac or ephemeris to determine the position of the satellite, along with information relating the elevation of a satellite to a specific C/No, the measured C/No can be compared to the expected C/No. Through this comparison this type of situation could be determined.

Transmitted power fluctuations may also result in similar non-acquisitions. Alternately, the receiver may acquire the signal with an incorrect doppler. This phenomenon is known as tracking on a sidelobe. Sidelobes are a part of the broadcast signal and are the result of the spread spectrum signal characteristics of GPS. If the signal power fluctuates significantly, acquisition of a sidelobe is not out of the question. When tracking on a sidelobe, the receiver will fail to synchronize with the navigation data message bit edges causing data parity errors and ultimately the loss of lock of the signal.

### **3.3.3 Spectrum Corruption**

Most cases where the frequency content of the received signal is corrupted will result in a corresponding change in the shape of the correlation curve. The C/No would also drop as a result of spectrum corruption. The correlation function changes could be detected by examining MDEs and MDRs, as well as additional Multipath Meter outputs discussed in Chapter 5.

### **3.3.4 Erroneous Navigation Data**

**This is unlikely to cause a problem since protection mechanisms (parity checks) are built into the navigation message. In the event that these fail, faults in the navigation message should be detectable by checking the validity, by setting a valid range of expected values for each field, of the fields within the broadcast message.**

## CHAPTER 4

### SIGNAL QUALITY MONITORING

For signal testing of SQM measurements, NovAtel OEM3 hardware was used. A special software version was created by the author, which uses all available correlators of the receiver to monitor the correlation function of a single tracked satellite. Tracking is done using NovAtel Narrow Correlator® Tracking Technology. This 48-correlator software version is called 4.47S16. It places the correlators in a symmetrical pattern with the majority of the correlators near the peak of the correlation function at positions closer than 0.2 chips from the punctual C/A code sample. This version was used in order to ascertain the stability and repeatability of correlation function measurements near the peak (used for Satellite Failure Detection, SFD) as well as the consistency between receivers and between resets of the same receiver.

The tests examined the normalized correlation values, all values normalized by the punctual code correlation sample, from each of the receivers.

The 48-correlator values used in version 4.47S16 are as follows (with all spacing relative to the punctual code correlation value):

Correlator #	Spacing	Correlator #	Spacing
1	-0.99455	25	0.01250
2	-0.88205	26	0.02500
3	-0.74225	27	0.03750
4	-0.63765	28	0.05115
5	-0.49670	29	0.06250
6	-0.45805	30	0.07500
7	-0.39555	31	0.08750
8	-0.34670	32	0.10000
9	-0.30345	33	0.12500
10	-0.25115	34	0.15000
11	-0.22615	35	0.17500
12	-0.20000	36	0.20000
13	-0.17500	37	0.22615
14	-0.15000	38	0.25115
15	-0.12500	39	0.30345
16	-0.10000	40	0.34670
17	-0.08750	41	0.39555
18	-0.07500	42	0.45805
19	-0.06250	43	0.49670
20	-0.05115	44	0.51150
21	-0.03750	45	0.63765
22	-0.02500	46	0.74225
23	-0.01250	47	0.88205
24	0.00000	48	0.99455

Table 4-1: List of Measured Correlator Spacings in 4.47S16 in C/A Code Chips

#### ***4.1 Test Setup***

The testing was conducted using 8 different OEM3 receivers (Units Under Test, UUT) simultaneously, using PRN 18 generated from a Stanford Telecom (STEL) 7220 GPS Signal Simulator. The signal power used for the testing measured at the receiver, was 37 dB-Hz and remained constant for the duration of the test. Setting the value to 37 dB-Hz will give good results for satellites that would be near the horizon and have similar C/No values.

The satellite was stationary with a doppler of zero. This was done in order to provide a consistent signal to which inter-receiver and inter-reset measurements could be compared without having to account for measurement variations due to elevation (i.e. received signal power) and allow for fast re-acquisition of the signal after a reset.

Data was collected on each receiver over a 3600-second interval at which time all receivers underwent a software reset. This scheme was used over 16 iterations in order to accumulate more accurate statistical information. This resulted in 16 hours of data from each of the 8 receivers.

Data recorded from the receivers consisted of the raw correlator measurements from all channels. This data from each of the 3600-second test runs was normalized (to ensure inter-receiver and inter-reset comparability), averaged, and tabulated.

All receivers were at a stable temperature before beginning the testing, unless mentioned otherwise.

## 4.2 Test Results

The receiver serial numbers used in the testing are included below in Table 4-2.

Receiver Number	Serial Number
UUT1	SGL99250035
UUT2	SGL99250014
UUT3	SGL99360041
UUT4	SGL99250022
UUT5	SGL98400028
UUT6	SGL98320172
UUT7	CGL97030085
UUT8	CGL97030075

Table 4-2: List of Hardware Serial Numbers Used in Testing

The serial numbers of the receivers indicate that there is a large sample space that has been chosen. The first three letters of the code indicate the build facility of the receiver and the first two numbers the build year. With receiver manufactured in two different facilities during three different years, a good variety of receivers have been tested.

It should be noted that since all of the data presented here has been normalized, statistical information at the punctual code sample (the value used for the normalization) is unavailable.

### 4.2.1 Consistency Within Sample Periods

During each of the 3600-second sample periods, the normalized correlation function values were calculated for each observation, for each receiver. These normalized correlation function measurements were then

averaged over the entire 3600-second period providing a mean and standard deviation for that test run. For the entire test run, there were 16 3600-second samples.

Consistency of the measurements during these 16-sample periods, for UUT5, is summarized below in Figure 4-1. This figure shows results without the use of an external oscillator. Other receivers showed results that were marginally less favourable (showing slightly more deviation between successive receiver resets). UUT5 is still an accurate portrayal of the entire sample space.

The consistency of the measurements is not related to the general shape of the curve in Figure 4-1. Even with the use of an external oscillator, the overall shape of the curve will remain the same since all measurements are relative to the punctual correlator and are not to an absolute reference. It is because of this relative nature that the use of an external oscillator would show little to no advantage over the use of the lower quality on-board oscillator of the receiver. The consistency of the measurements is related to the repeatability of the measurements and the overlap of the curves in Figure 4-1.

We can see that for the entire region the consistency of the measurement standard deviations are quite good between software resets. The lines from successive resets overlaps the line from the previous reset quite well. Over all 16 resets of the receiver, the standard deviation of the measurements lies almost directly on top of one another, except near the ends of the lines (which are nearly 1-chip away from the peak measurement). Since the main focus of SFD involves looking at correlation values near the correlation peak (within  $\pm 0.2$  chips of punctual), these deviations at the fringes are less important and not included in the plot. Also, the scale of this plot will remain the same when smoothed correlator results are shown, so that comparisons can be easily made.

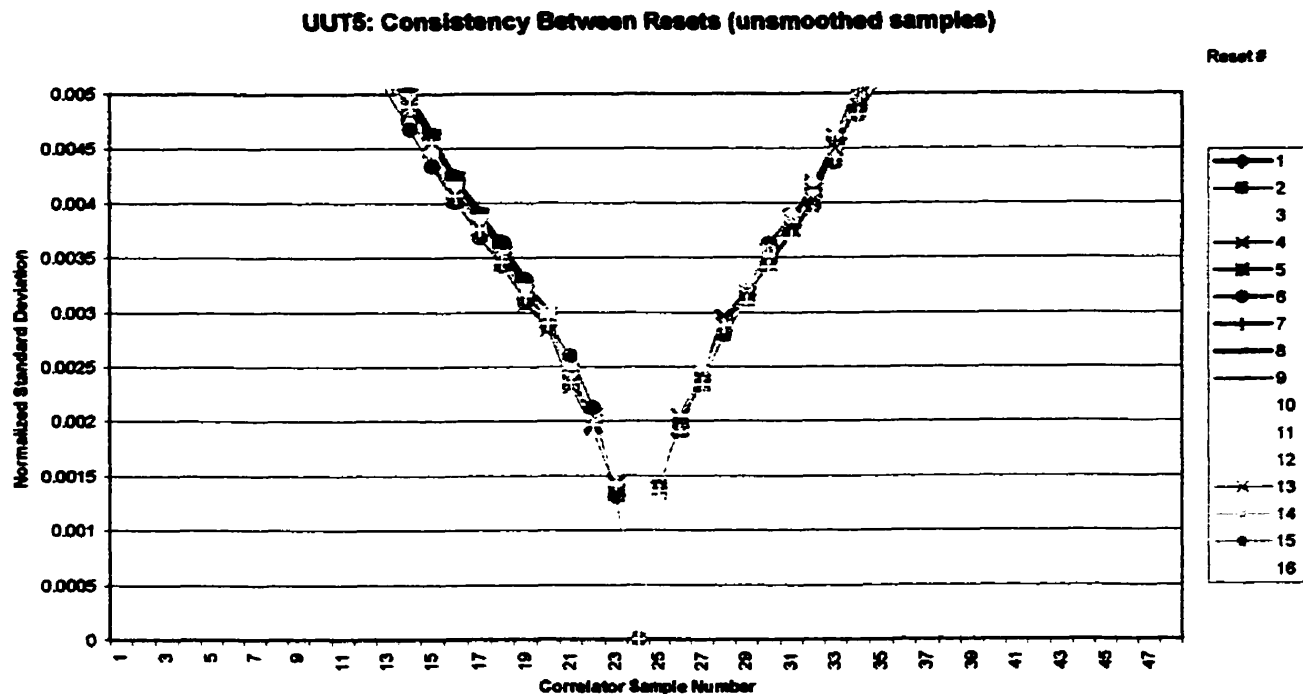


**Figure 4-1: Correlation Function Measurement Consistency Between Resets, UUT5**

From Table 4-1, we can see the points corresponding to  $-0.10$  (point 16),  $-0.075$  (18),  $-0.05115$  (20),  $0$  (24),  $+0.05115$  (28),  $+0.075$  (30), and  $+0.10$  (32) in Figure 4-1. The maximum variation due to noise is on the order of 0.4% correlation function variation, for spacings less than 0.10 chips.

#### 4.2.2 Consistency Between Resets

To further validate the value of correlation function measurement due to noise, we can look at the relative variation in the measured correlation function between receiver resets. To calculate these numbers we need to assume that one of the data sets is the “truth” data, for differencing. For simplicity, the first data set (of each receiver) was taken as truth and all

remaining 15 sample runs (from the same receiver) were differenced from it. This differencing was done for all 8 receivers.

For UUT5, the difference between sample 1 and each of the successive 15 samples is presented in Table 4-3. This data shows the normalized differences in terms of mean and standard deviation averaged across all correlation samples. The variation can be visualized as the difference between each successive averaged sample period in Figure 4-1.

Test Run Number	Normalized Difference in Means	Normalized Difference in Std Dev
1	31.3292E-05	11.44497E-04
2	28.0792E-05	7.47934E-04
3	33.8146E-05	8.44411E-04
4	43.3292E-05	13.51731E-04
5	29.3771E-05	9.55007E-04
6	4.8542E-05	4.31027E-04
7	56.9250E-05	8.72412E-04
8	34.9833E-05	9.26114E-04
9	55.5708E-05	8.59353E-04
10	27.2021E-05	8.43687E-04
11	6.6958E-05	2.74253E-04
12	44.6167E-05	8.27137E-04
13	35.0604E-05	10.33690E-04
14	37.1021E-05	6.21764E-04
15	21.0708E-05	5.14521E-04

Table 4-3: Normalized Difference in correlation function measurements between receiver resets, UUT5

From Table 4-3, we can see that the mean difference is on the order of 0.03% with a standard deviation of approximately 0.08%. These numbers are also representative of the other units under test.

The results of combining all of this differencing information together across all 8 receivers and averaging across all 15 differences are found in Table 4-4.

UUT#	Normalized Difference in Means	Normalized Difference in Std Dev
1	42.2403E-05	12.90411E-04
2	35.1871E-05	9.83990E-04
3	28.6385E-05	9.51393E-04
4	26.6424E-05	15.29734E-04
5	32.6674E-05	8.61995E-04
6	7.9829E-05	16.53144E-04
7	36.5785E-05	14.35658E-04
8	8.2050E-05	11.35743E-04
Average of all UUT	27.2677E-05	12.30259E-04

Table 4-4: Normalized Difference in correlation function measurements between receiver resets for all receivers combined

With an average normalized difference between resets on the same receiver of less than 0.03%, there is no concern of a bias resulting from resetting the receiver. A standard deviation of 0.123% also indicates that there is significant stability of correlation function measurements between resets of the receivers.

### 4.2.3 Consistency Between Receivers

The main concern is the variation of the measured correlation function between different receivers. Unit-to-unit variations are the topic of scrutiny here. The variation as a result of different RF componentry on the board is of utmost importance since we need to detect very small variations in the correlation function in order for our SFD algorithm to be effective.

Card to card variations were calculated from the average normalized correlation values across all 16-resets of the receiver. This average normalized correlation measurement for each receiver was then differenced with each of the other receivers' value to produce the plots shown in Figure 4-2 below.

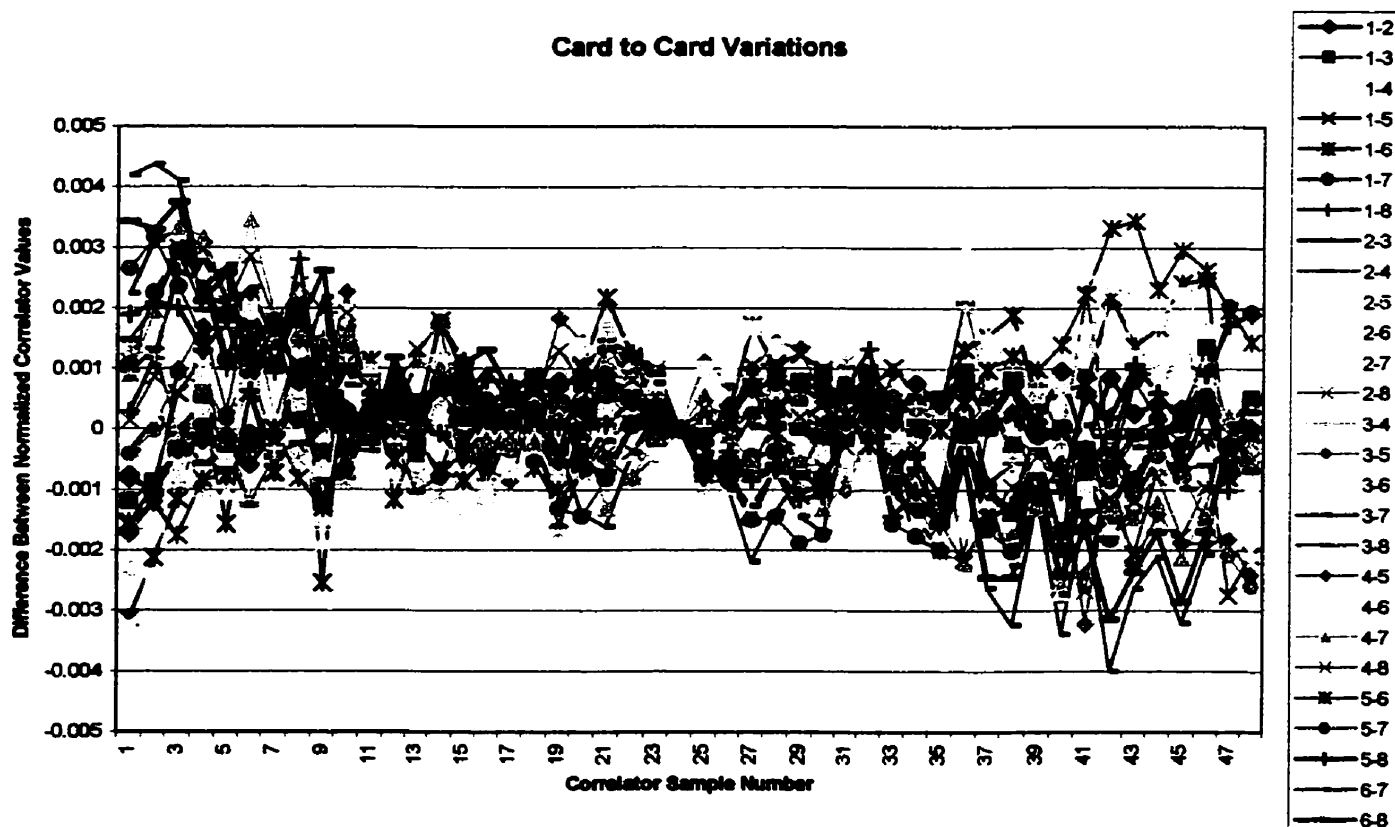


**Figure 4-2: Mean Normalized Card-to-Card Variations Between Correlation Function Measurements**

For correlators within  $\pm 0.10$  chips from punctual, the inter-receiver difference does not exceed 0.22% (with a mean value of 0.01%) with a maximum standard deviation of 0.101%.

#### 4.2.4 Temperature Variations

A GPS receiver used for SQM would most likely be in a controlled indoor environment. In this environment, it would not be uncommon for the temperature to fluctuate between  $+22^{\circ}\text{C}$  and  $+27^{\circ}\text{C}$ , as in the laboratory where the previous testing was conducted. However, in order to get a good grasp of temperature variations on the correlation function measurement, an experiment was conducted where the temperature of the receiver was varied between  $-25^{\circ}\text{C}$  and  $+80^{\circ}\text{C}$ . The test used a single OEM3 receiver with software version 4.47S16. PRN 18 was used again for consistency, at the same C/No of 37 dB-Hz. The temperature was ramped up at a rate of  $1^{\circ}\text{C}$  per 5 minutes. The temperature profile for the testing is shown in Figure 4-3 below.

Results showing the normalized correlation values (after applying a 100-second smoother to the raw correlation data) are shown in Figure 4-4. Smoothing was applied in order to assess the underlying trend of the data, while removing some of the noise. Figure 4-4 shows the normalized correlation values for those correlators on the early side of the correlation peak, with spacings less than 0.1 chips from punctual. We can see that there is a slight upwards curve to all correlator values, as the temperature gets hotter. All correlators are affected equally by the temperature variation, regardless of position from the punctual code sample.

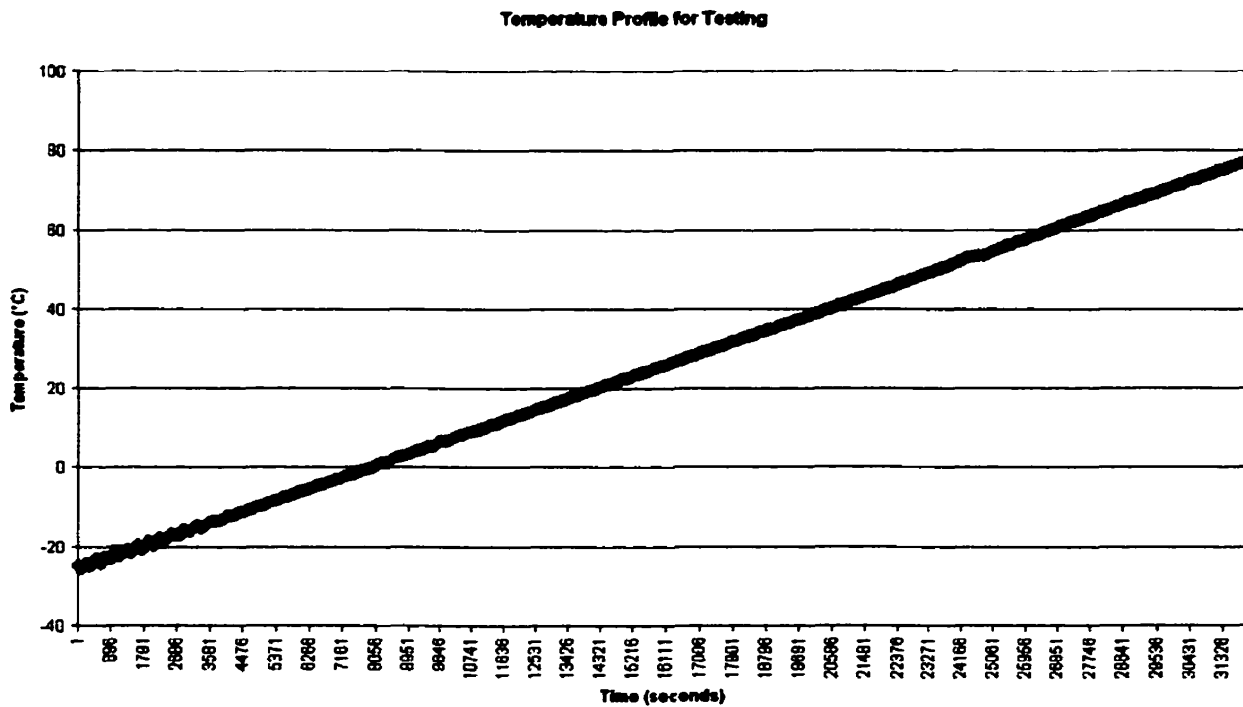


**Figure 4-3: Temperature Profile for the Temperature Variation Testing**

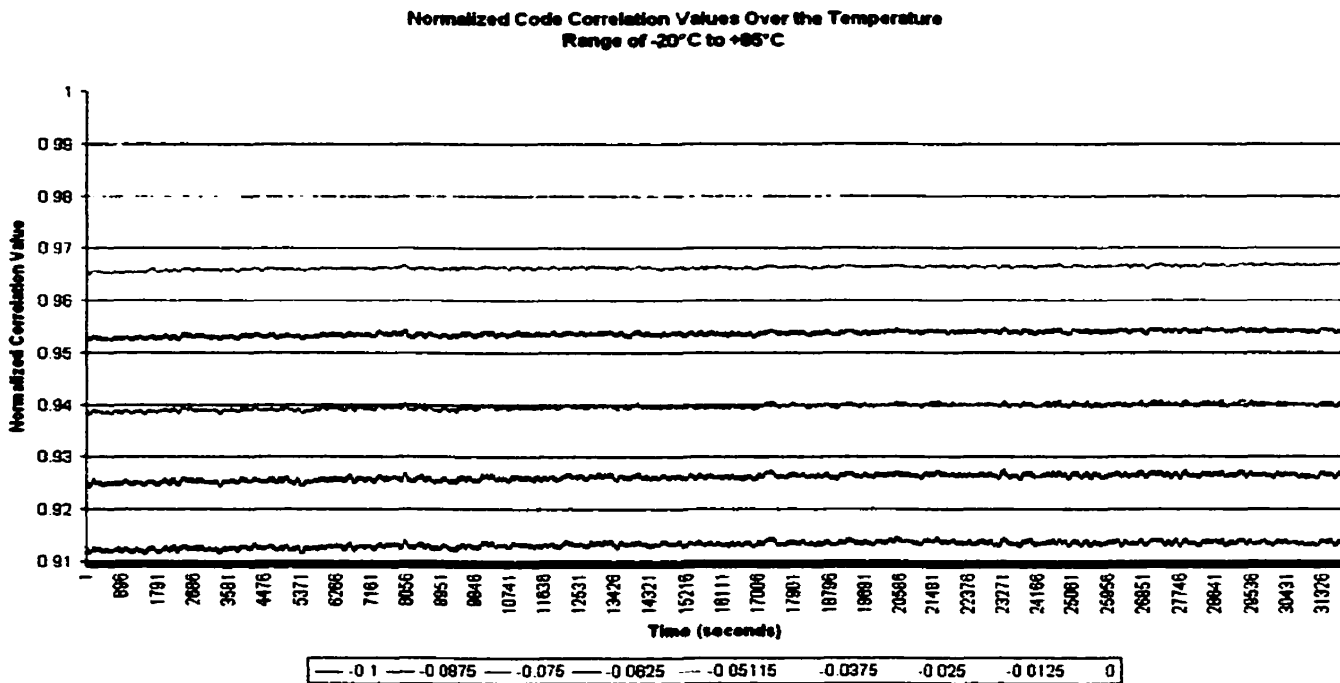


**Figure 4-4: Multiple Normalized Code Correlation Values During Temperature Variations (100-second smoothed)**

Zooming in on the single normalized correlator value of  $-0.05115$ , we can see that the temperature effects are quite significant over the tested range in Figure 4-5. This specific correlator value was chosen since it is used as part of the E-L correlation value in the DLL.

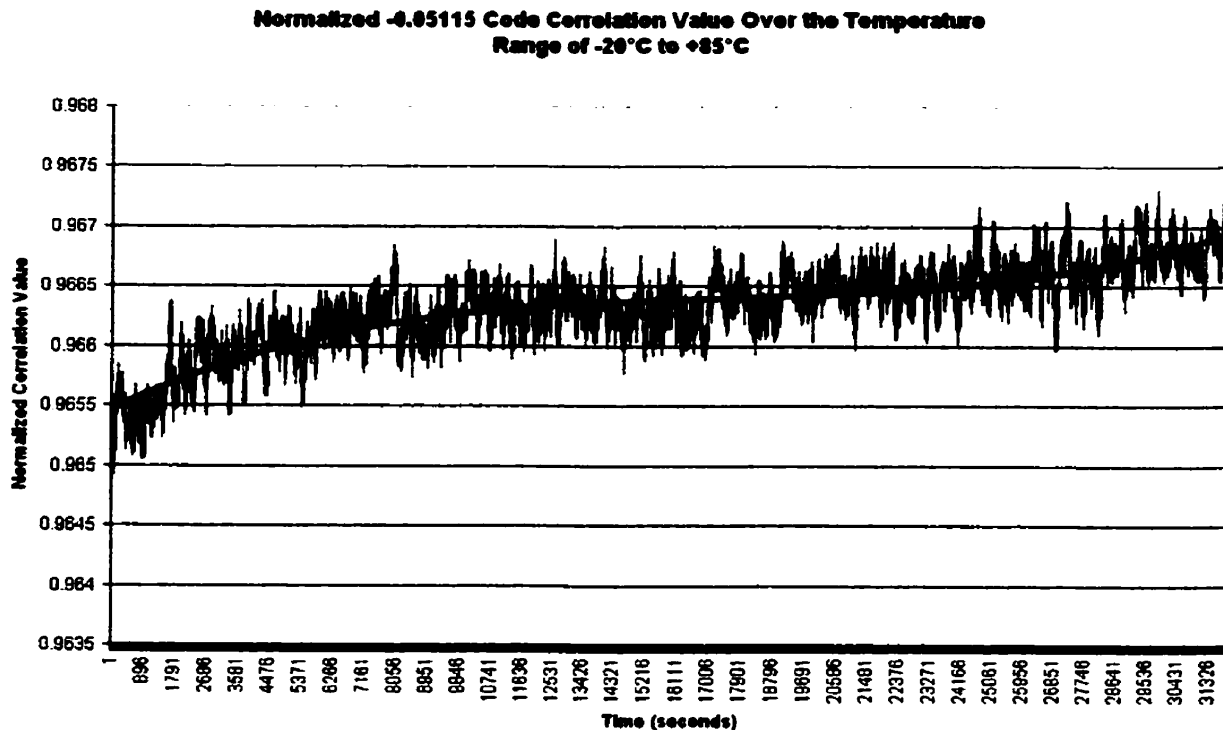


**Figure 4-5: Normalized  $-0.05115$  Code Correlation Values During Temperature Variations (100-second smoothed)**

Figure 4-5 shows a third order black trend line plotted along with the 100-second smoothed, normalized values. For the range of  $-25^{\circ}\text{C}$  to  $+80^{\circ}\text{C}$ , there are variations on the order of 1.5%. This is a very significant change that could drastically affect the MDE values. MDE values use only a single normalized correlator value, which will be affected by the temperature variations. However, MDR values will not be affected since they are using correlators from both sides of the correlation peak, and measuring the normalized difference between them. Since both the early

and late correlator values are affected equally, temperature variations on the MDR values are of no consequence.

There is a linear range of temperature change between approximately +15°C to +45°C. The linear change in the normalized correlation value across this region is approximately 0.0073% per °C.

#### 4.2.5 Componentry Differences

Inter-receiver differences in measurements due to varying componentry (i.e. componentry tolerances of items used in the RF) on the boards can also be theoretically examined.

Let us take as an example the Intermediate Frequency (IF) filter for the NovAtel OEM3 receiver. The IF filter is a Sawtek 70MHz low-loss filter with a 16MHz bandwidth [30]. The data sheet for this component specifies a minimum 3dB bandwidth of 16MHz, with a typical value of 16.5MHz. There is no maximum value specified, but it is assumed that the variation between minimum and typical would likely also exist between maximum and typical. Taking this into account, we can expect component variations of the IF filter of 1MHz, or values anywhere between 16 and 17MHz. RF component tolerances of other RF designs may have more or less variation in the bandwidth.

In order to simulate these bandwidths and the underlying filtered correlation function, a 200-pole Finite-Impulse-Response (FIR) filter was used to replicate the Sawtek filter. The bandpass ripple using a 200-pole FIR filter closely mimics the ripple presented on the IF component data sheet using both 16 and 17MHz bandwidths. A Matlab simulation was done to filter an ideal normalized correlation function using the above mentioned filters. Equations 2-3, 2-4, and 2-5 describe this ideal normalized correlation function.

These equations give a perfectly triangular correlation function, which was filtered with both the 16 and 17MHz bandwidth FIR filters in Matlab. The resulting difference in the correlation function due to the difference in IF filter is seen in Figure 4-6. Both curves were normalized by the punctual code sample therefore giving each curve a maximum value of unity. The x-axis in the graph represents the code correlation value, with zero being the punctual code value. The y-axis is the magnitude of the variation between the 16 and 17MHz correlation functions, relative to the normalized values.

From that figure, we can see that there is a maximum variation of 0.5% due to componentry differences. Our live data analysis using 8 different receivers (section 4.2.3) shows variations of the same magnitude, but slightly less pronounced. Due to the nature of the filtering done by Matlab, Figure 4-6 is slightly asymmetrical.

It should be noted that the IF filter is not the only component that contributes to the bandwidth variation of the receivers. There are a number of components that can influence this value, however the IF filter bandwidth and characteristics will be the dominant factors in the bandpass region of the RF/IF filters. Other RF component elements that may influence the shape of the correlation function also include (but are not limited to) the A/D converter and RF filter bandwidth and characteristics.

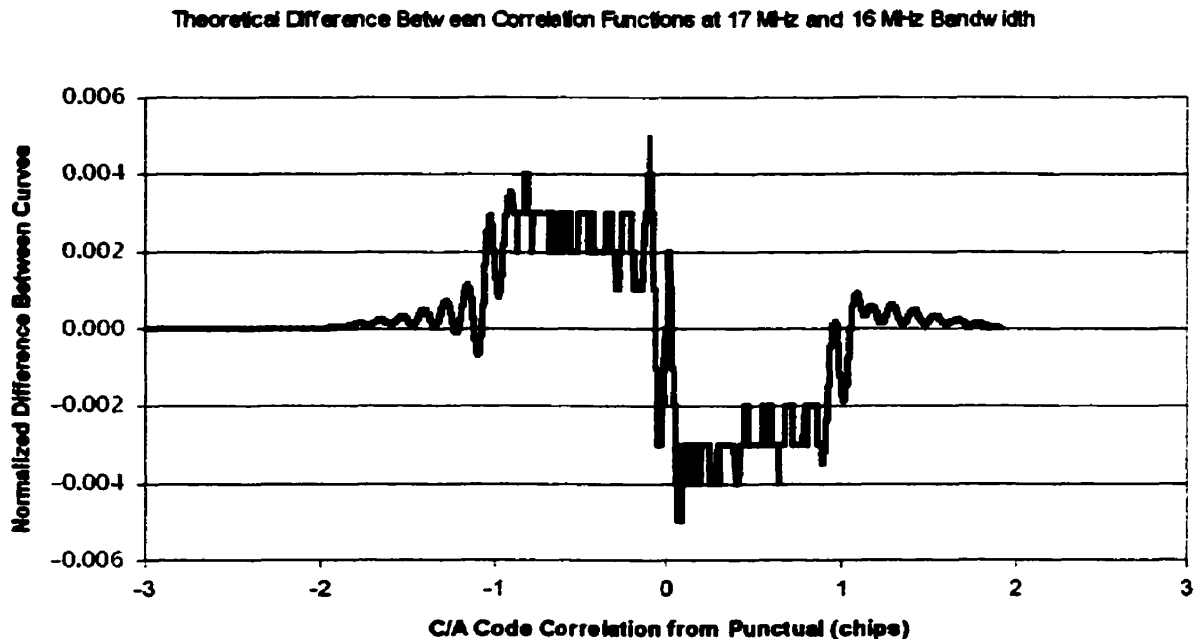


**Figure 4-6: Difference between Normalized Correlation Functions using 16 and 17MHz bandwidth filters**

#### 4.2.6 Overall Accuracy

From the analysis of receiver measurement consistency (Figure 4-1), inter-reset consistency (Table 4-3), and inter-receiver consistency (Figure 4-2), we can see that the measurement noise and component variations can cause differences in the measured correlation function.

Measurement consistency after a reset is very good, with variations significantly lower than the measurement noise.

Measurement noise and componentry differences, due to componentry tolerances, account for the majority of the correlation function measurement variations. From sections 4.2.1 and 4.2.3, the variation due to noise and componentry are 0.4% and 0.3% respectively, in terms of standard deviation. Both error terms are additive (i.e. statistically independent) and may result in variations on of up to 0.7% in the

normalized correlation function measurement. Simulation results validate this amount of variation.

#### 4.2.7 Thresholds of Detection

Minimum detectable errors and ratio values have been defined in [31] in an environment with nominal multipath.

With no smoothing on the measured correlation function (as in Figure 4-1), the error on correlation values below 0.10 chip spacing can be as much as 0.4% with additional variations due to componentry bringing the variation up to 0.7%. Values in [31] for an elevation angle of 5° indicate that the MDR values should deviate by more than 0.00337 or 0.337% of the expected value in order to indicate the presence of an anomalous satellite signal. Clearly, we would have significant problems related to false alarms if no smoothing of the data was done or this bias were not removed.

However, the Minimum Operational Performance Standards (MOPS) for WAAS airborne equipment [29] requires that airborne users implement a 100-second smoothing filter on its raw measurement data, before using it in any position solution. As a result, any implementation of a monitoring scheme can take advantage of this and smooth the raw correlation data for the same period. However, if a shorter smoothing time could be used it would be advantageous in order to warn users in a more timely manner.

Figure 4-7, below, shows the same data as in Figure 4-1, but with a 100-second smoother applied to the data before calculating any of the standard deviation values. Figures 4-1 and 4-7 have the same scale, for ease of comparisons. Results with the smoother are significantly improved, reducing the standard deviation for correlator values less than 0.10 from 0.4% to 0.04%. This is as expected with a filter of this length.

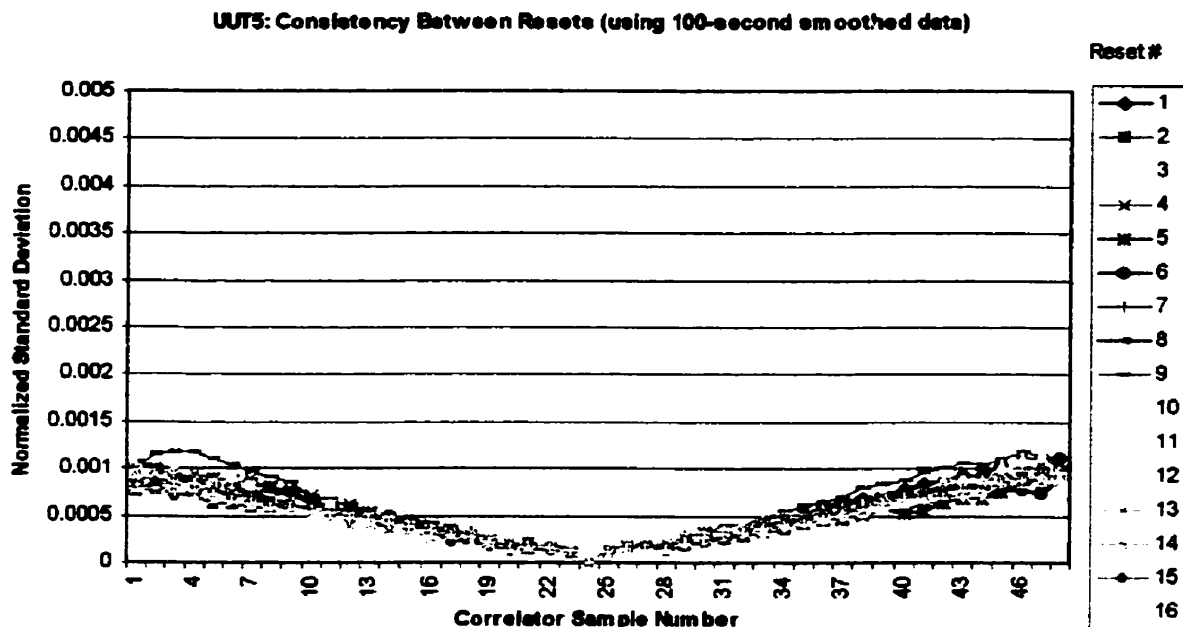


**Figure 4-7: Correlation Function Measurement Consistency Between Resets (Using a 100-second smoother), UUT5**

However, using a smoother on the raw correlation data does not alleviate the problem of a bias due to unit-to-unit variations. An additional step must be completed in order to remove this bias.

#### 4.2.8 RF Componentry Bias Removal

With the 100-second smoother applied to the data, the dominant error source shifts to the componentry differences between receiver boards. At a level of 0.3% (1 sigma), this will significantly mask all of the MDE errors that we are attempting to detect. In order to remove the effects of inter-receiver differences, a calibration routine needs to be determined that will exemplify these differences so that they can be removed.

Since all channels are equally affected by the RF componentry variations, collecting data from all tracked satellites above a certain elevation cutoff angle will provide good statistical certainty in the bias value. Removing

**this bias from the measured metric values will return their statistical mean to zero. In order for the routine to remove temperature effects and any slow degradation of the receiver components, the calibration should be continually run with either a low-pass or moving average filter.**

**Using a continuous filter with a time constant of 10 times the smoothing time will adequately remove inter-receiver biases while maintaining the ability of the SQM scheme to detect satellite failures. Lumping data from all visible satellite into the calculations of a bias term for each MDE value is necessary to avoid miss-detection of a failure. The 1000-second smoothing time used to calculate the receiver bias should use all satellites above a mask angle of at least 15°, in order to limit the skewing of the calculations due to multipath from low elevation satellites.**

**Only bias terms for the MDE values need to be calculated since both the E and L side of the correlation function are equally affected by the componentry variations. With equal effects to the E and L sides, MDR values will be unaffected by componentry variations. By doing these calculations, we ensure that each of the MDE metrics is properly aligned to a zero mean with inter-receiver independence. The removal of the componentry variations returns the metrics to a zero mean and effectively removes the bias.**

**The reason we would like to remove the bias is to allow for identical SQM algorithms to run in parallel using different receivers, without the need for receiver dependent algorithms or thresholds for SFD. These calculations allow the generalization of the SQM scheme. In addition, temperature and degradation effects will be removed so that false alarms are minimized.**

### ***4.3 Automatic Gain Control Operation***

**Automatic Gain Control (AGC) is performed using data input from the A/D converter. The A/D can provide a range of resolutions, from the simpler 1 bit variety, to the more complex variations using multiple bits. The multi-bit A/D case will be discussed here, but can be simplified to the single bit case.**

**Each of the bits of the A/D gets accumulated in bins. Each bin representing one or more bits of the A/D input depending on the implementation. Bin values are the ratios of the number of “counts” in a particular bin with respect to the sum of the “counts” in all bins. Receiver performance is optimised when the ratios of the bin values follow a Gaussian curve, with Gaussian noise input conditions. The AGC, as the name implies, offers a means to adjust the input signal gain so that the bin histograms can be optimally configured. However, component variation is significant enough that each receiver will have a slightly different histogram.**

**For this reason, a calibration routine is required at receiver start-up to maintain the optimal configuration of the AGC. Without this calibration, there is the potential for a bias in the measurements, much like for the SFD correlator measurements. Once calibrated, the AGC gain value used to reach the optimal configuration should be continually verified in order for the configuration to remain optimal.**

**This calibrated value (determined at receiver start-up) can be stored for later comparisons to the actual calibration value. This can be used for interference detection as shown in Chapter 6.**

#### 4.4 Carrier to Noise Calculation

The calculation of the carrier to noise ratio (C/No) can be done in a number of different ways [18]. Once such way is presented here, that relates code correlation measurements to the signal to noise ratio (S/No). The S/No is related to the C/No by the following equation:

$$C/No = 10 \log_{10} (S/No) \quad (4-1)$$

The S/No can be calculated from equation 4-2 below:

$$S/No = \frac{1000}{2T} * \frac{S - (2 * NF * T)}{NF * T} \quad (4-2)$$

Where:

NF = 1 millisecond noise floor estimate,

S = I<sup>2</sup> + Q<sup>2</sup>, where I and Q are code correlation accumulations, and

T = accumulation time of the I and Q data

The noise floor can be computed by two separate means. The first is from the input signal level from the A/D. This value represents the level of noise being input to the system, before any code correlations are done. The second method is a post-correlation noise floor estimate where a channel on the GPS receiver is searching for a specific satellite, but has not yet acquired it. The correlation values from this searching channel will be representative of the noise from attempting code correlation with the specified C/A code sequence with no input C/A code. The channel is attempting to correlate its C/A code with the input noise. The post-correlation noise floor estimate tends to be noisier than the pre-correlation estimate. However, the post-correlation estimate is also more indicative of the true noise floor of the input signal. Using a post-correlation noise floor value for each satellite will provide a closer estimate to the true C/No than using a pre-correlation value.

#### ***4.5 Multipath Meter Parameters***

**As previously touched on, the multipath meter concept involves taking the signal parameters output from the MEDLL algorithms and using them for quality monitoring of the GPS signal. These parameters are the delay, relative amplitude, and phase of the multipath signal along with the residual values for each correlator from the multipath estimation process. Also available are multipath corrected and uncorrected correlator measurement values for use in SFD.**

**All of these multipath meter outputs, in conjunction with one another, can be used for real-time signal quality monitoring. They can also be used for reference station site surveys to determine if a location is suitable for a GPS reference station [17]. However, the focus of their use for this thesis is their inherent ability to provide SQM.**

**Of the multipath signal parameters output, the amplitude of the multipath is of additional interest because it will indicate the presence of multipath even if it is not causing any pseudorange error. This would be the case if the phase of the multipath were 90 or 270 degrees, relative to the direct path phase.**

**Results shown in this section are for an implementation of the MEDLL algorithms on a GPS receiver with a 16MHz RF bandwidth. This wider RF bandwidth is required for the detection of correlation function distortions of the types described in sections 3.1.1, 3.1.2, and 3.1.3. Previously, the MEDLL algorithms were used on an 8MHz RF bandwidth receiver. The wider 16MHz bandwidth allows for the detection of higher frequency ringing effects on the C/A code chips. With a narrow RF bandwidth, these ringing effects are filtered out and not as easily detectable in the correlation domain.**

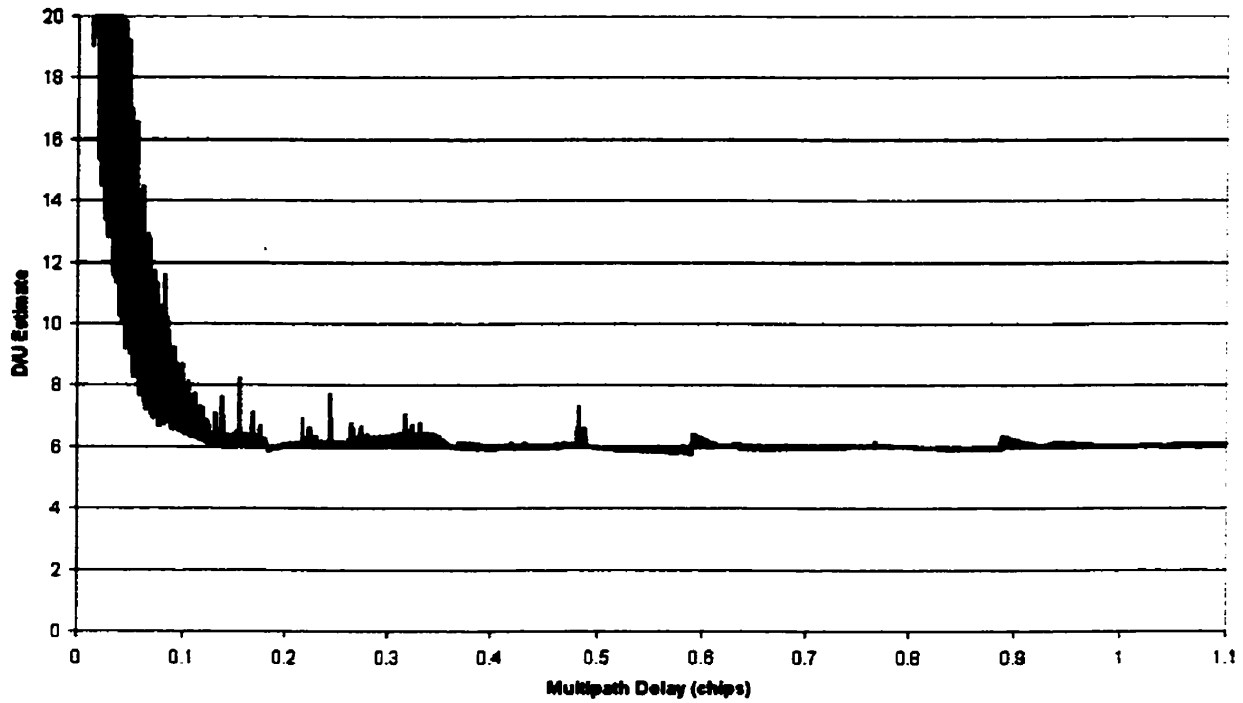
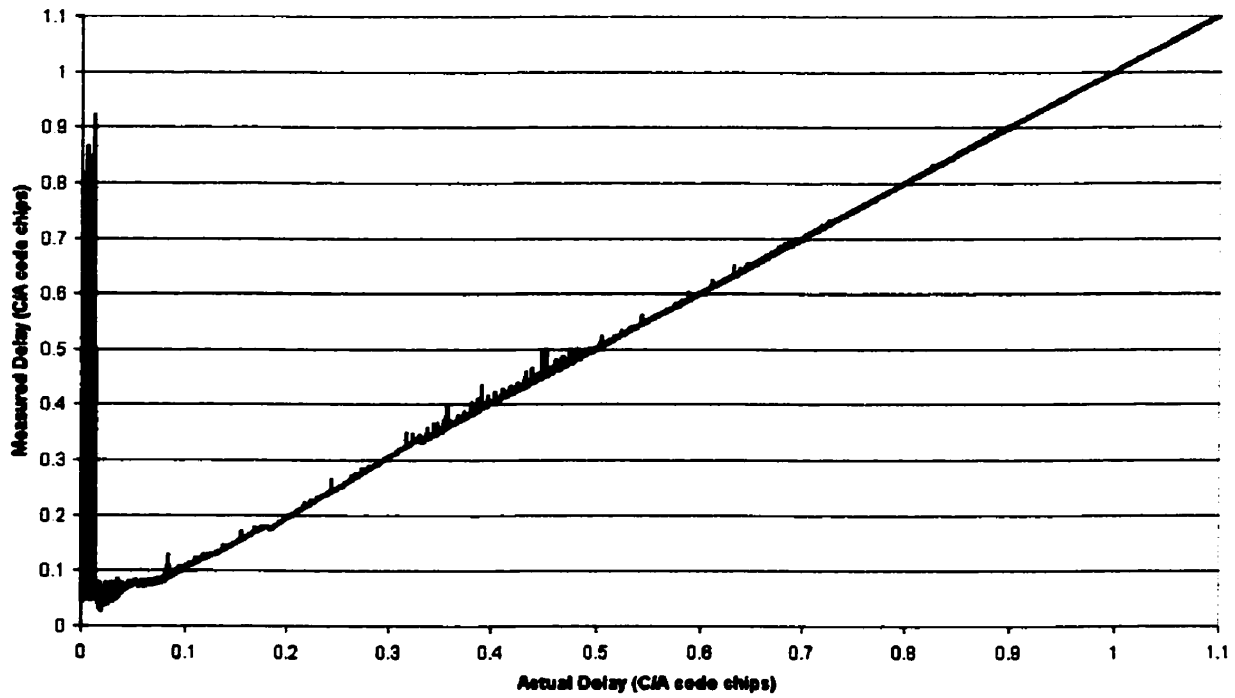
### 4.5.1 Multipath Meter Outputs

In order to show the ability of the Multipath Meter to estimate the desired to undesired signal ratio, a simulation was run that used a multipath signal with an amplitude ( $a_m$ ) of 0.5 relative to the direct path signal. The delay of this multipath signal was varied from 0 to 1.1 chips.

The multipath power is plotted in D/U (desired signal power over undesired signal power) in decibels (dB). The D/U is calculated using equation (2-11) and the results are shown in Figure 4-8.

The plot shows that the D/U converges to 6 dB as the delay of the multipath is increased. 6 dB corresponds to a relative multipath amplitude of 0.5. For delays less than 0.125 chips from punctual the D/U estimate becomes less accurate. With very short delay multipath, it is difficult to estimate the amplitude of the multipath, due to the RF filtering effects on the correlation function. As the multipath delay becomes longer, the D/U converges quite quickly to the correct solution.

The estimated delay of the multipath signal can also be seen in Figure 4-9. We can see the same effects of the close in multipath in this figure, although not as pronounced as with the amplitude estimation for the D/U. There still remains a slight difficulty in estimating the delay of very close in multipath, with delays less than 0.025 chips, but longer delay multipath poses no such problem.

**S/W Simulation: Estimate of D/U for 16MHz MEDLL Implementation****Figure 4-8: Simulation of D/U Estimate****S/W Simulation: Estimate of Multipath Delay for 16MHz MEDLL Implementation****Figure 4-9: Simulation of Delay Estimate**

As an aside to the multipath meter outputs, is the resulting pseudorange error from removing the measured multipath from the offending satellite range. We can see in Figure 4–10 the pseudorange error due to a half amplitude multipath signal with delays between 0 and 1.1 chips for both a Narrow Correlator and the 16MHz MEDLL implementation.

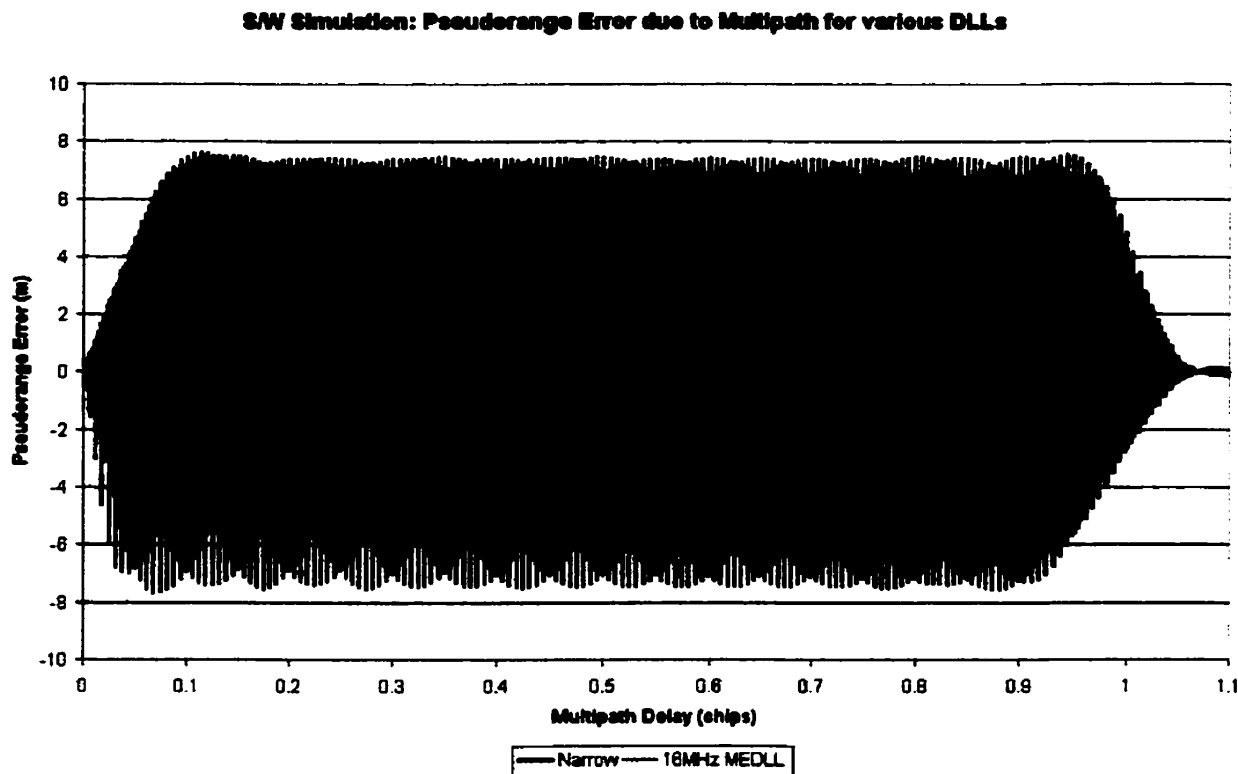


**Figure 4–10: Simulation of Pseudorange Error**

The light coloured (green) line represents the pseudorange error for the MEDLL, while the darker (blue) line represents the Narrow Correlator. We can see a significant increase in pseudorange accuracy for multipath delays greater than 0.05 chips, with negligible multipath effects for delays greater than 0.125 chips. The MEDLL also does not have additional pseudorange errors at long delay multipath signals such as those multi-correlator techniques described in sections 2.3.3 [14], [37]. With the MEDLL algorithms, we also get the added advantage of the Multipath Meter outputs for real-time SQM.

#### 4.5.2 Residuals from the Multipath Estimation Process

The residuals from the multipath estimation process are also important to examine. They tell us how well the estimation of the multipath signal has been completed. The sum of the squares of all correlator residuals is shown for the same half amplitude multipath scenario in Figure 4–11.

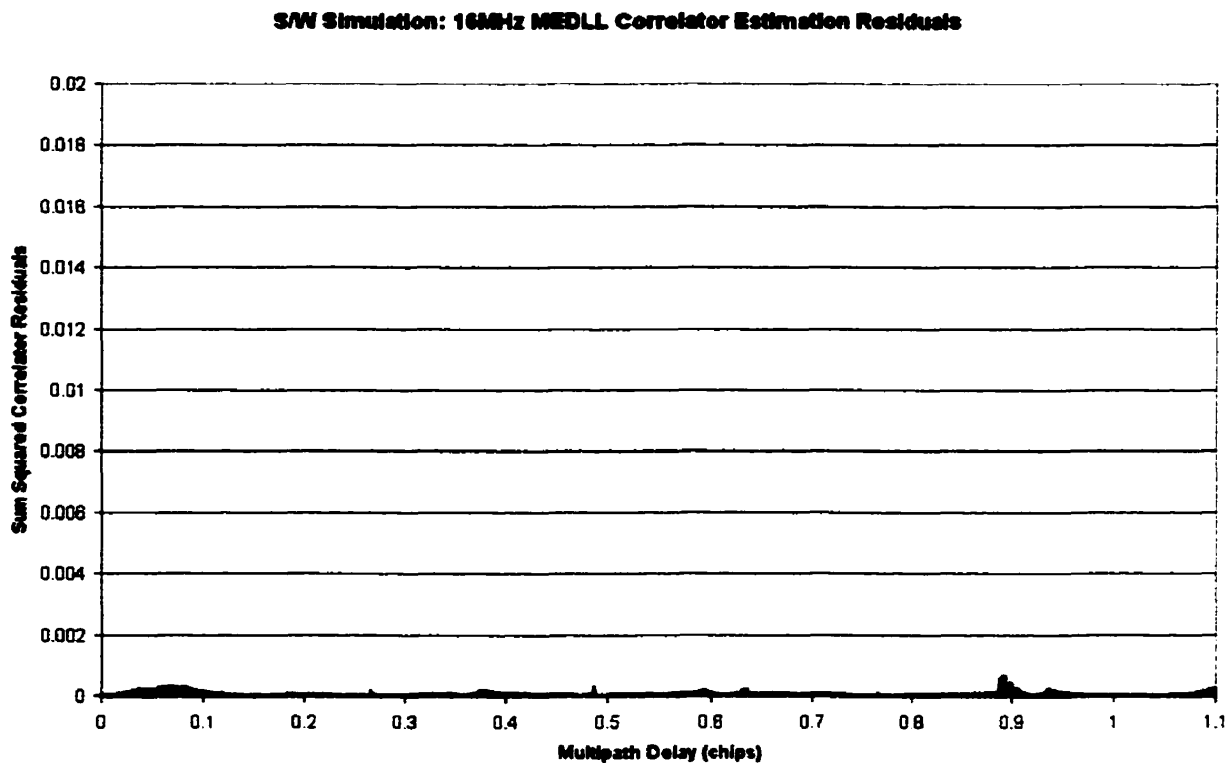


**Figure 4–11: Simulation of Estimation Residuals**

We can see that even for the very short delay multipath signals, there are no significant residuals. There is a slight increase in the curve at a multipath delay of approximately 0.05 chips, which corresponds to the point at which the delay estimate becomes more accurate. The scale of the figure may seem to be in error, but has been chosen to ease further comparisons of residual values found in Chapter 5. It has also been shown that for multiple multipath signals, the residual values will increase [16].

This is primarily due to the MEDLL only estimating and removing a single multipath signal.

### 4.5.3 Multipath Corrected Correlator Values

As discussed in section 2.6.4, multipath corrected correlator values are calculated from the measured correlator values, minus the estimated multipath component. It can also be thought of as the a-priori correlation function plus the estimation residual values.

By removing the multipath signal from the observed correlation function, we will increase the availability of the SQM scheme by reducing the amount of false alarms due to multipath. After removing inter-receiver biases and applying a 100 second smoother to all of the correlation measurements (section 4.2.8) our main source of false alarms of the SQM scheme is multipath [31]. Below in Figures 4-12, 4-13, and 4-14 are plots of the MDE correlator at +0.10 (PRN1), +0.10 (PRN3), and +0.30 (PRN3) respectively, binned by elevation. The plots show all available data based on elevation for a single satellite. Therefore, for PRN1 seen in Figure 4-12 we only see the elevations go up to 70° since the satellite never rises above that position in the sky. For PRN3, seen in Figures 4-13 and 4-14 data is available up to 85°. Data used for the plots was collected from live data on the NovAtel rooftop using a WAAS Subsystem receiver that was modified to output both multipath corrected and raw correlation measurements. This receiver implements the MEDLL algorithms on an 8MHz RF bandwidth receiver.

The data is for one complete pass of each satellite from local horizon to horizon. Each data set represents approximately 8 hours of data with at least 900 samples in each 5° elevation bin. In Figures 4-12, 4-13, and 4-14 we see the multipath corrected and uncorrected MDE value as well as the line representing the expected correlator value, with each bin value being smoothed for a minimum of 900 seconds. For all figures we see that

the multipath corrected correlator value brings the mean correlator value for that elevation closer to the expected value. In no case does it ever distort the correlation value to something that is farther away from the expected value. The result of correcting for multipath will only bring the correlation values closer to the expected value. Even for the correlation value at +0.30 C/A code chips from punctual, we see an improvement. With this technique, we could potentially use correlator values that are farther from the peak to detect signal anomalies and improve the robustness of our SQM scheme.

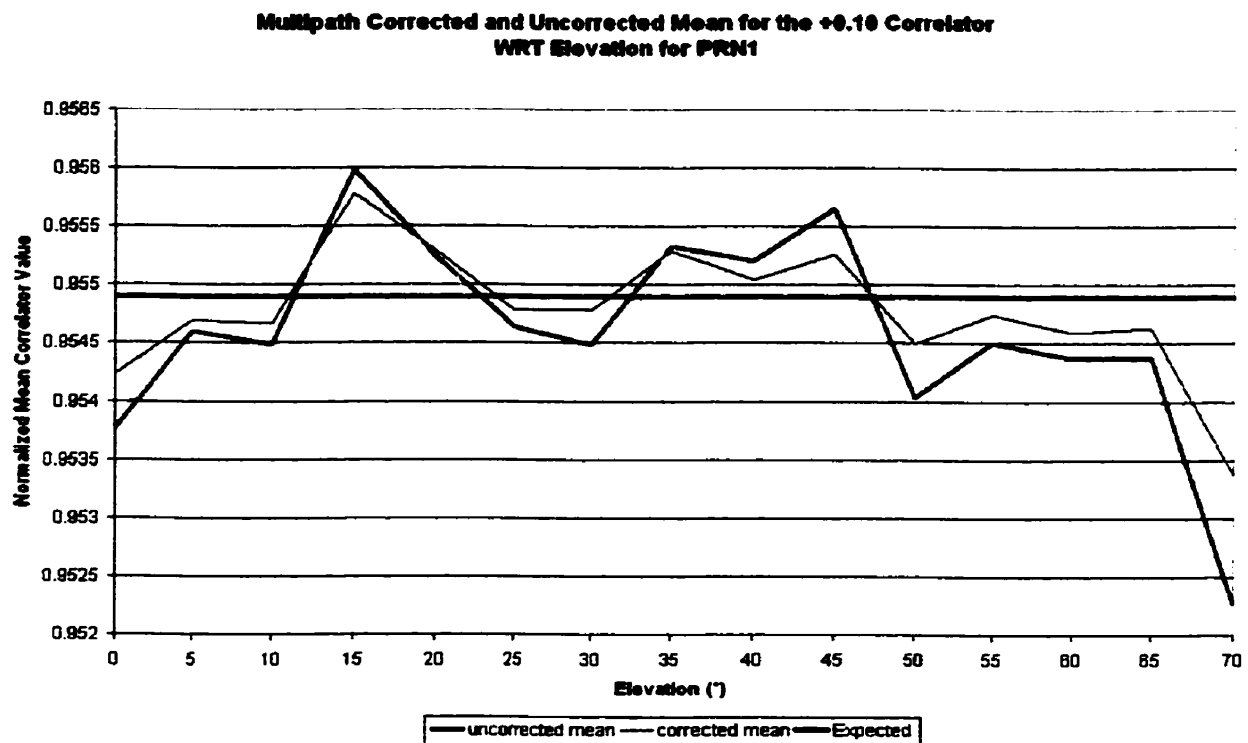


**Figure 4-12: +0.10 Mean Correlator Value for PRN1**

**Multipath Corrected and Uncorrected Mean for the +0.10 Correlator  
WRT Elevation for PRN3**

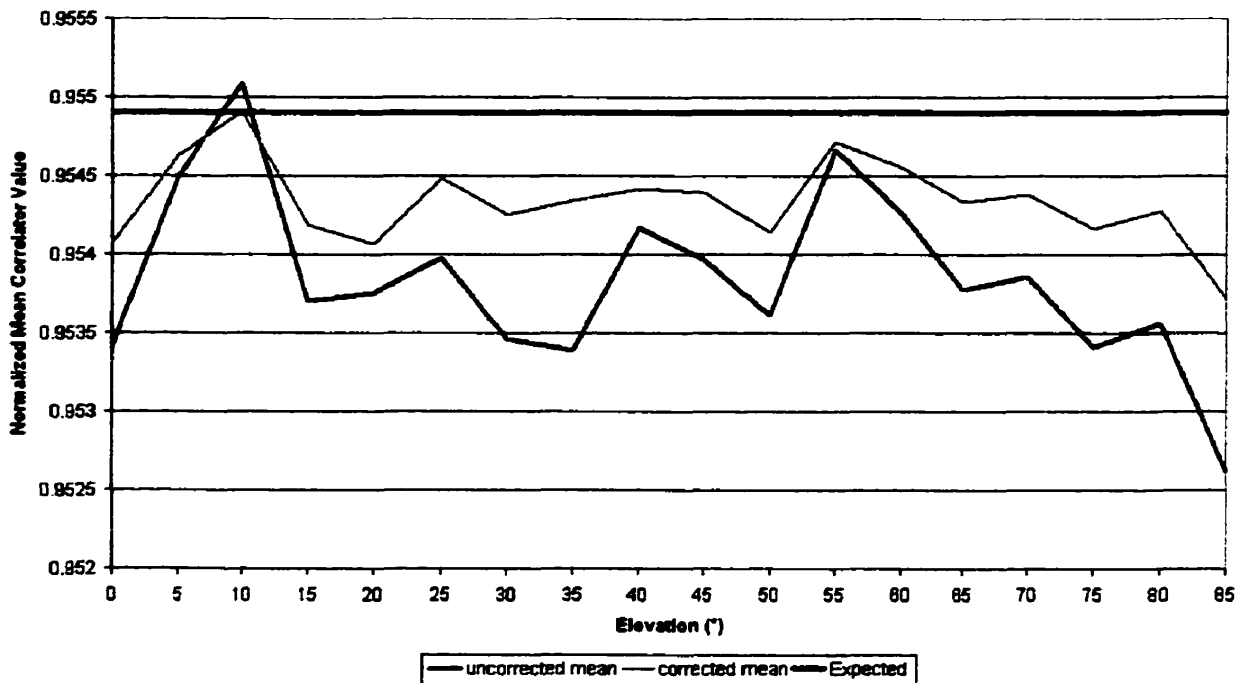


**Figure 4-13: +0.10 Mean Correlator Value for PRN3**

**Multipath Corrected and Uncorrected Mean for the +0.30 Correlator  
WRT Elevation for PRN3**

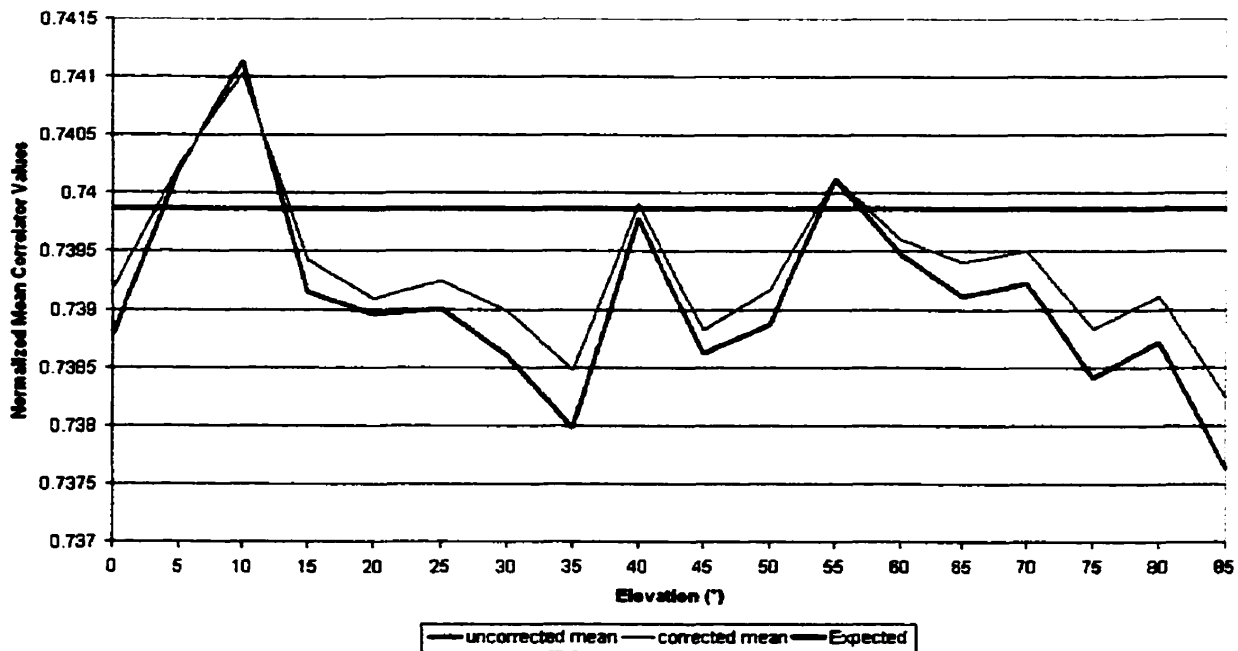


**Figure 4-14: +0.30 Mean Correlator Value for PRN3**

By removing the observed multipath from the correlation values, we can see that improvements in the mean value from Figures 4-12 through 4-14 can reach as much as 10% from the uncorrected values and 0.07% with respect to the expected value. From 4.2.7, deviations on the order of 0.337% for a 5° elevation would indicate an anomalous signal. Clearly, reducing the effects of multipath can only improve the availability of the SQM scheme.

From Figures 4-8 and 4-9 we can see that removing the effects of very close in multipath signals is difficult. Given the inherently low multipath environment in which the data was collected, the remaining deviations from the expected value can be partially attributed to close in multipath in addition to MEDLL algorithm and receiver measurement noise. Implementing the algorithms on a 16MHz RF bandwidth receiver will also help with the removal of multipath, since the wider bandwidth allows for a more accurate determination of close in multipath [16]. Also, for antennas sited in higher multipath environments there will be greater improvements in the multipath corrected correlator values. These improvements could be sufficient to use sites where multipath may be significant as a reference station and an SQM monitor station.

The standard deviation of the measurement is also dramatically improved by removing the effects of multipath. We can see this effect in Figures 4-15, 4-16, and 4-17. These figures correspond to the same measurements seen in Figures 4-12, 4-13, and 4-14 respectively.

From these figures we can see that there are specific elevations where multipath is a dominant factor, as at 45° for PRN1 and 20° and 30° for PRN3. Correcting the measurements for multipath reduces the standard deviation of the measurements by as much as 50%. This significant improvement naturally smoothes the measurements, meaning less smoothing is required in any SQM filter algorithm. This will also improve the time to alarm since the smoothing time is reduced.

**Multipath Corrected and Uncorrected Standard Deviations for the +0.10 Correlator  
WRT Elevation for PRN1**

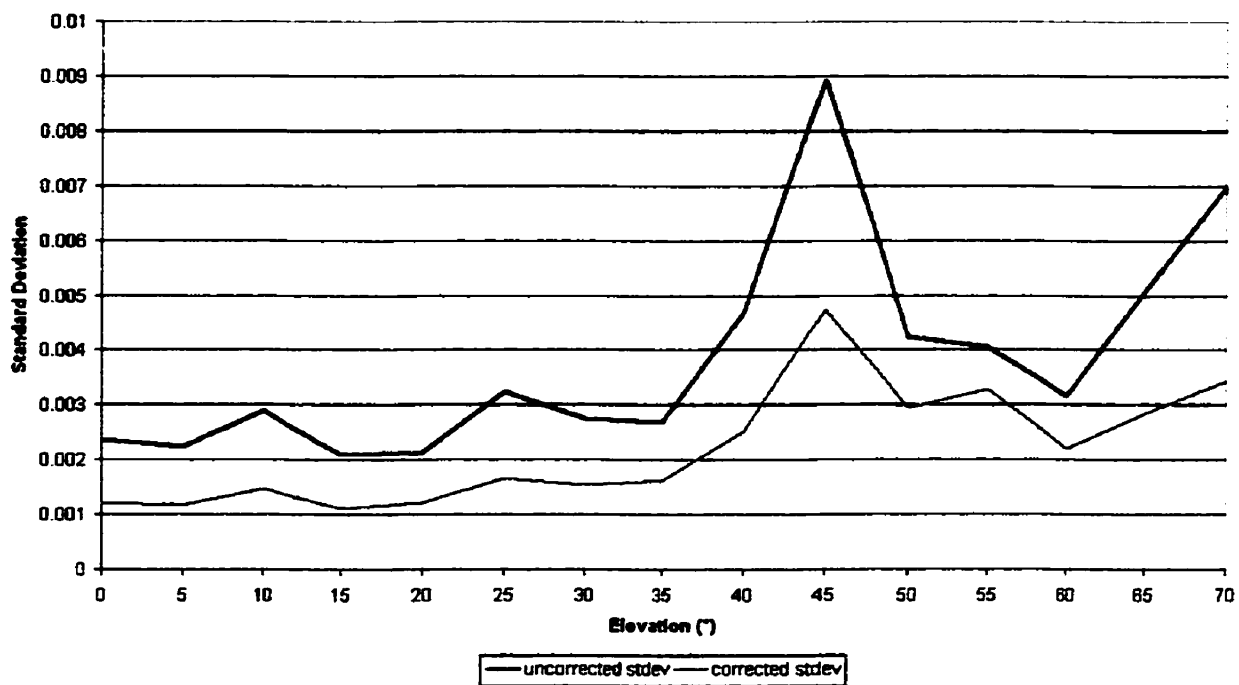


**Figure 4-15: +0.10 Correlator Standard Deviation for PRN1**

**Multipath Corrected and Uncorrected Standard Deviations for the +0.10 Correlator  
WRT Elevation for PRN3**

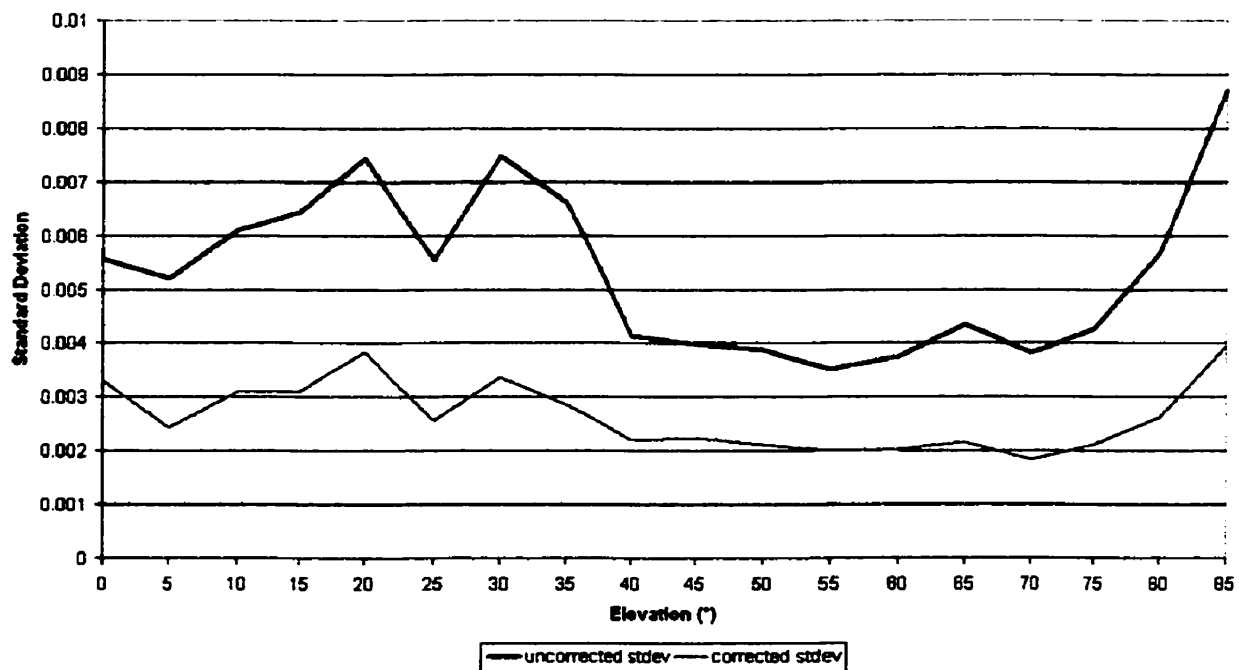


**Figure 4-16: +0.10 Correlator Standard Deviation for PRN3**

**Multipath Corrected and Uncorrected Standard Deviations for the +0.30 Correlator  
WRT Elevation for PRN3**

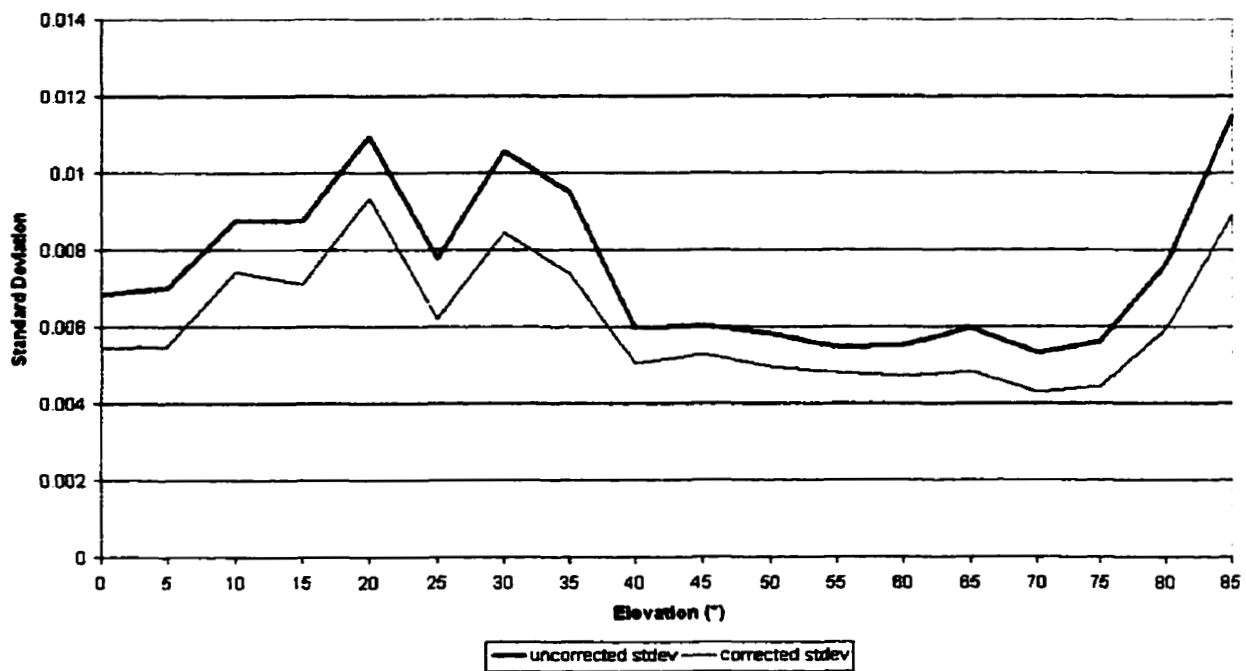


**Figure 4-17: +0.30 Correlator Standard Deviation for PRN3**

## CHAPTER 5

### MALEVOLENT SIGNAL TESTING

The next step in our analysis is to generate these satellite signal failures for use in simulation with the Multipath Meter. This chapter will prove that by removing the effects of a multipath signal we do not mask the underlying satellite signal failure that we are trying to detect. The line-of-sight signal availability is assumed.

#### *5.1 Simulation Setup for Code Correlation Failure Generation*

After generating the anomalous satellite signals (also referred to as evil waveforms) for all points in the threat space (see section 3.1) using Matlab with the previously discussed 16MHz 200 pole FIR filter, the distorted correlation functions were used to create multipath signals. All multipath testing is for a multipath signal with amplitude  $a_m = 0.5$  with variations in delay between 0 and 1.1 chips. When the delay of the multipath signal is zero, it can be interpreted as the condition when no multipath is present, since the only effect of the multipath signal will be to increase the relative amplitude of the signal. These evil multipath signals were then used as input into the MEDLL algorithms. The MEDLL still attempts to remove multipath effects using a nominal reference correlation function (i.e. a reference without any evil waveforms) when there is evil present.

Five specific points were examined in the threat space and are presented here, shown in Table 5-1. Each of the cases shows the boundary conditions of each of the threat models A through C (section 3.1) and were chosen to show both the most and least distortions possible given the pre-defined threat space.

For evaluation of the Multipath Meter, the D/U estimate, correlator residuals, and multipath corrected correlator values are examined for their abilities to detect the evil waveforms. Both MDE and MDR values are examined.

Simulation #	$\lambda$	$\mu$	$\beta$
1	0.12	0	0
2	0.01	0	0
3	0	0.8	4.0
4	0	8.8	17
5	0.12	0.8	7.3

Table 5-1: Signal Simulation Parameters

## 5.2 Detection Using MDE and MDR Values

As previously discussed, detection of anomalous satellite signals can be done by examining the MDE of a single normalized correlator value (normalized by the punctual value) or by looking at the MDR of correlator values across the peak of the correlation function. In the presence of multipath, but not in the presence of evil waveforms, MDE and MDR values of the multipath corrected and uncorrected correlator values are shown in Figures 5-1 through 5-3.

MDR1 is the ratio of the tracking error between the correlators at  $\pm 0.025$  chips (tracking pair) to the correlators at  $\pm 0.075$  chips (non-tracking pair), normalized by the punctual correlation value. MDR2 is the ratio of the tracking error between the correlators at  $\pm 0.025$  (tracking pair) chips to the correlators at  $\pm 0.125$  chips (non-tracking pair), normalized by the punctual correlation value. The expected value for all of the MDR values is zero since we expect the correlation function to be symmetrical.

MDE1 is the correlator value at +0.025 chips normalized by the punctual correlator value. MDE2 is the correlator value at +0.125 chips normalized by the punctual correlator value. The expected value for the correlator at +0.025 chips would nominally be 0.975 but is shown in Figure 5-3 to be closer to 0.989. This is due to the rounding of the correlation peak from the receivers' RF filters. The expected value for the +0.125 correlator is 0.885, slightly higher due to rounding of the correlation function than the nominal value of 0.875.

With the MEDLL implementation, there are at least 4 MDR values and 10 MDE values that can be checked. Only those mentioned above have been chosen in order to limit the size of the analysis to a manageable level.

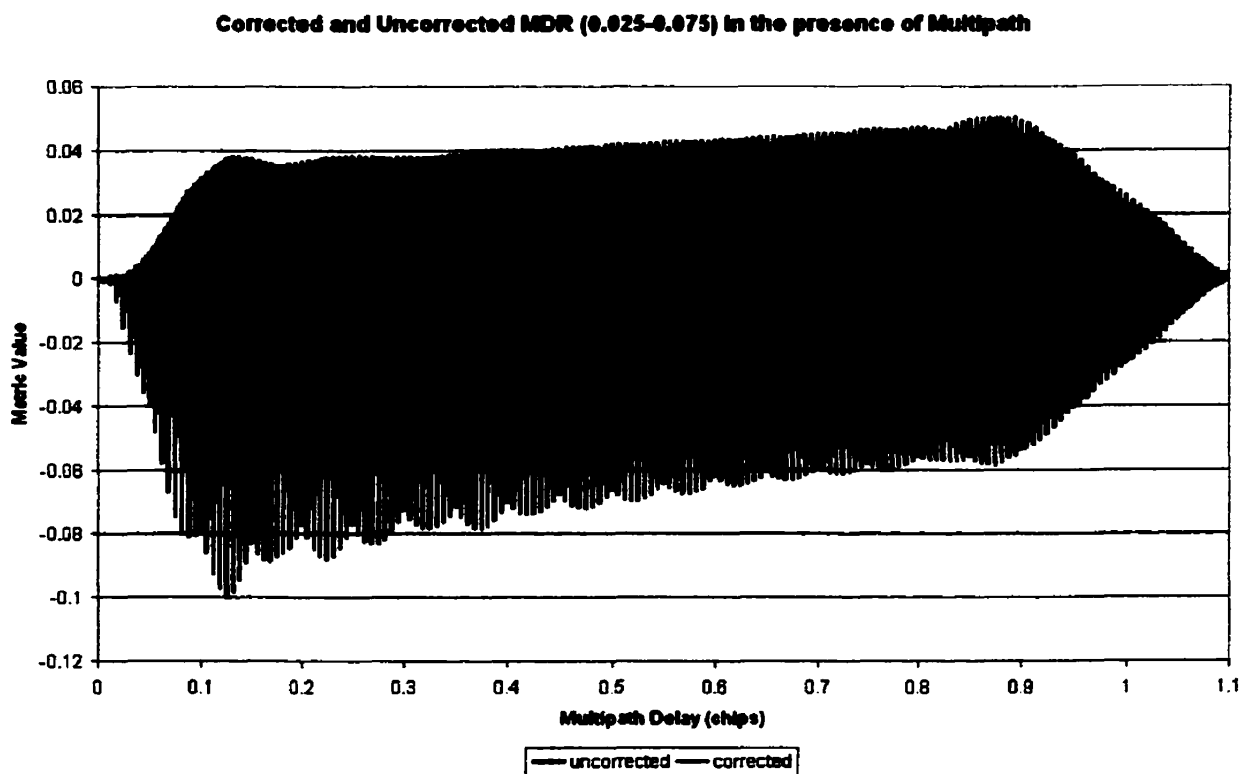


**Figure 5-1: MDR1 (0.025-0.075), No Evil**

Corrected and Uncorrected MDR (0.025-0.125) in the presence of Multipath

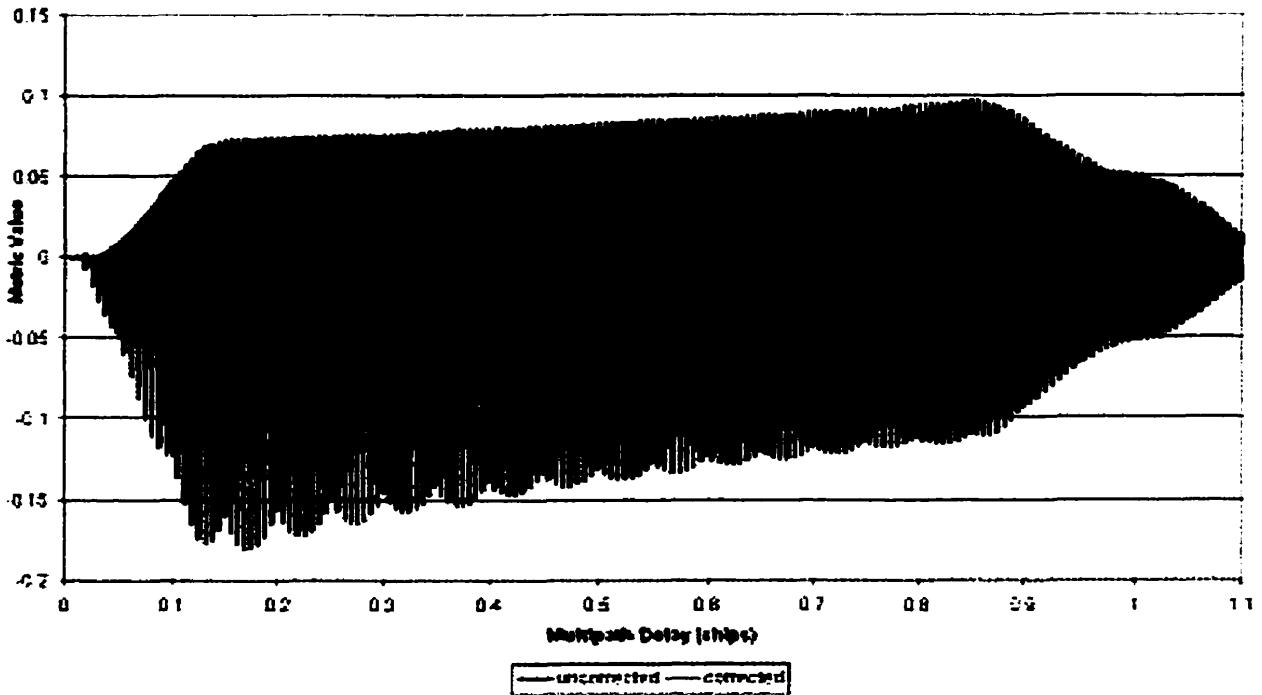


Figure 5-2: MDR2 (0.025-0.125), No Evil

Corrected and Uncorrected MDE (+0.025) in the presence of Multipath

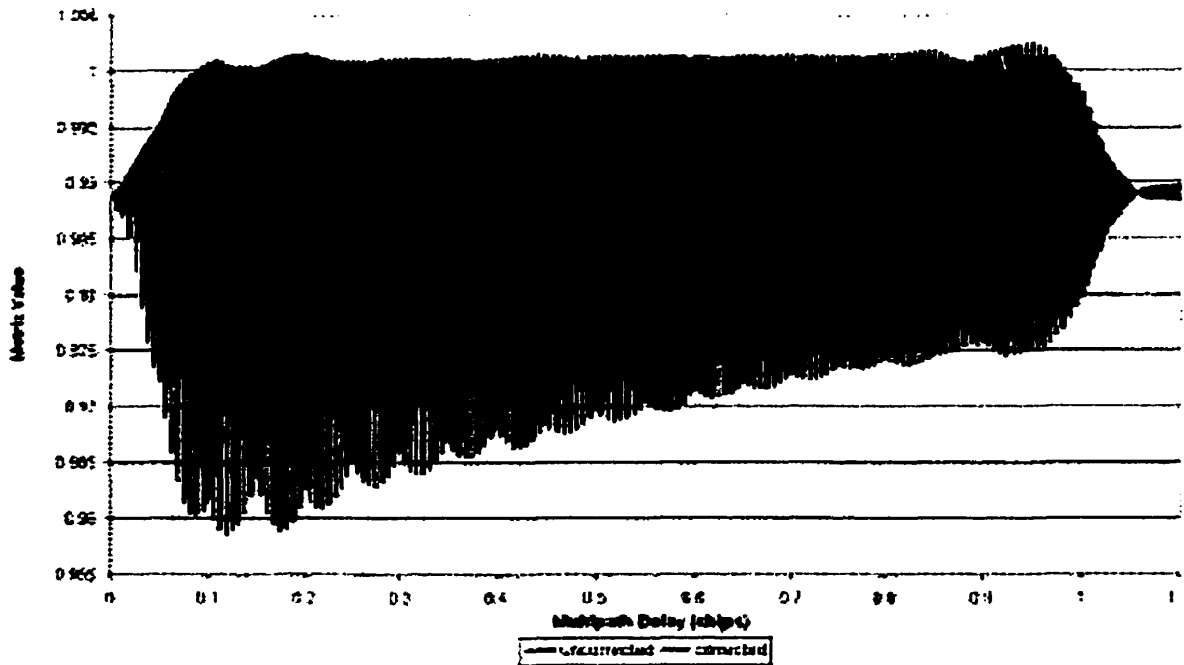
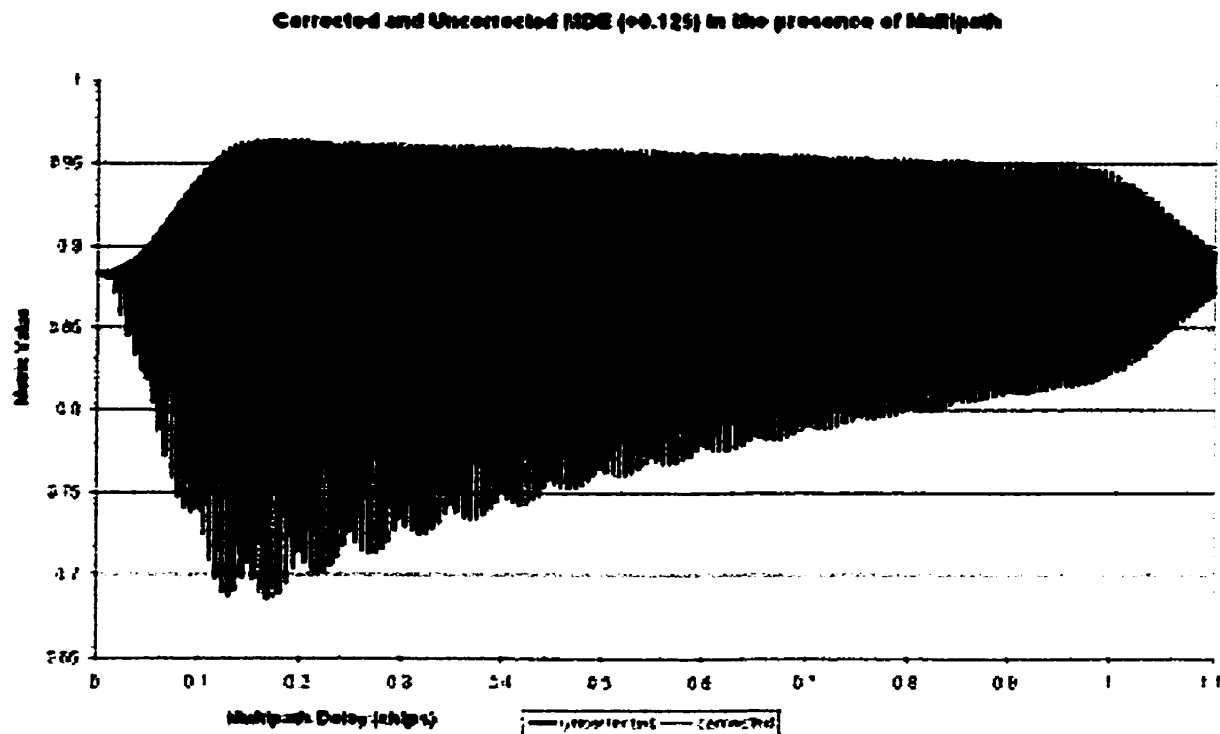


Figure 5-3: MDE1 (+0.025), No Evil



**Figure 5-4: MDE2 (+0.125), No Evil**

From Figures 5-1 through 5-4, we can see that the corrected correlator values represented by the lightly shaded line (pink) are significantly more consistent than the uncorrected values represented by the dark shaded line (blue). By reducing the noise and impact of the multipath signal on the MDE and MDR value, the threshold for detection can be significantly lowered. This will improve the ability to detect evil waveforms when multipath is present thereby reducing the false alarm rate. Another advantage is that there is little need for smoothing of the correlator values to reduce the influence of multipath, since the multipath effects have been removed by the MEDLL. This in turn will reduce the time to alarm for detecting evil waveforms.

What is of most interest now is how the multipath corrected correlator values behave in the presence of evil waveforms, and the ability of the Multipath Meter to detect their presence even with the multipath corrected correlator values.

### 5.3 Impact of Multipath on the Correlation Function

Before presenting the analysis of the multipath impacts on the correlation function, and its measurements, it would be beneficial to visualize the effects. These effects are shown when both satellite signal anomalies are present and not present.

Recalling what the nominal correlation function looks like, from Figure 2-4, we can see the effects of a multipath signal with delay of 0.5 chips, directly in phase, with amplitude  $a_m=0.5$  on the correlation function in Figure 5-5.

In the presence of an anomalous satellite signal, such as that used in simulation #5, with  $\Delta=0.12$ ,  $\sigma=0.8$ , and  $f_d=7.3$  the impact is markedly different. We can see the correlation function with no multipath and the previously mentioned satellite signal failure in Figure 5-6.

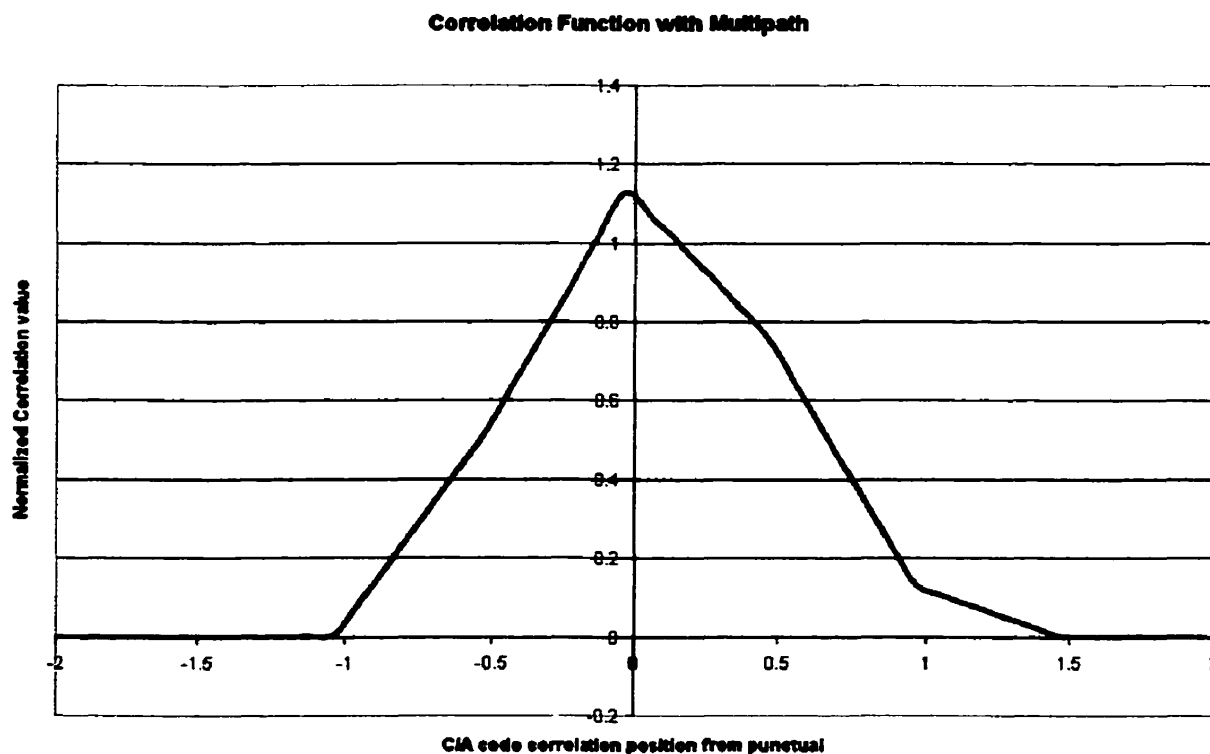
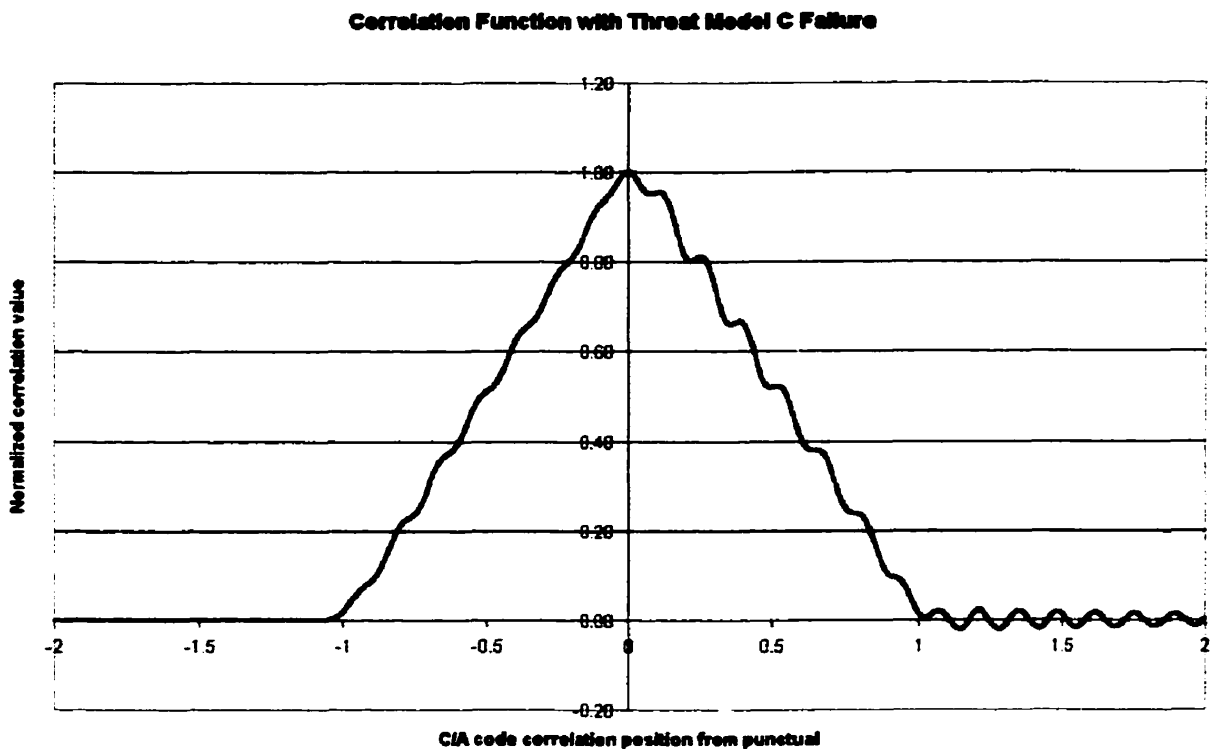
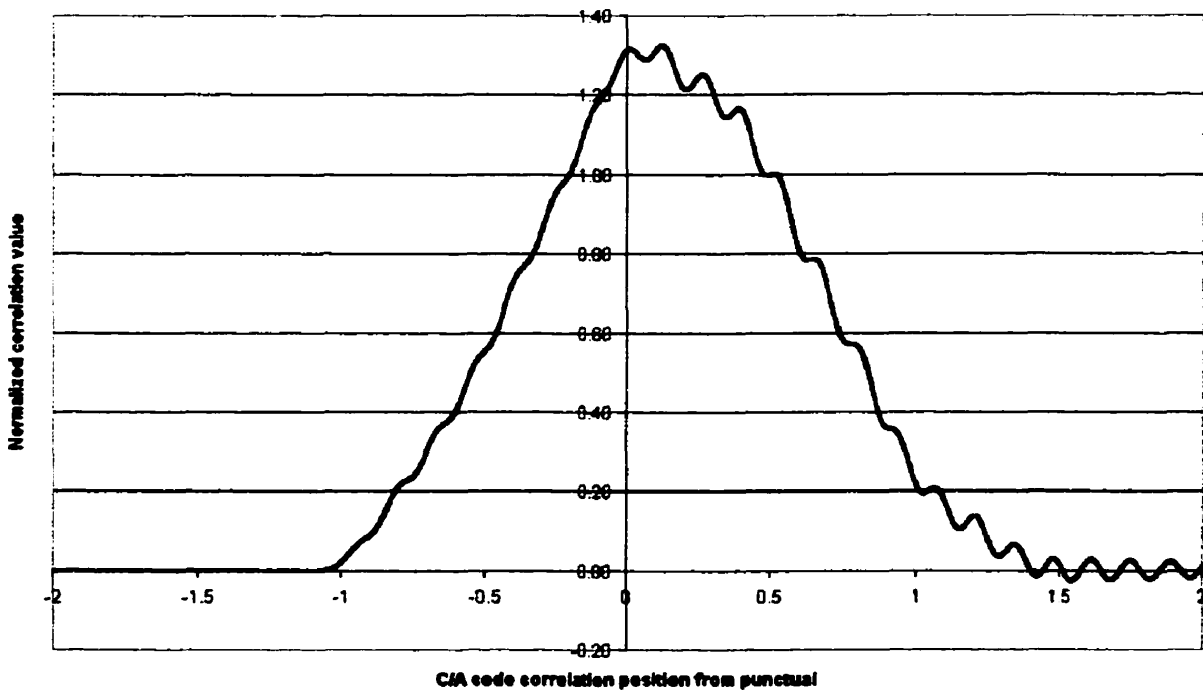


Figure 5-5: Correlation Function with Multipath



**Figure 5-6: Correlation Function with Threat Model C**  
**Correlation Function with Threat Model C Failure and Multipath**



**Figure 5-7: Correlation Function with Threat Model C and Multipath**

With the addition of the same multipath as used to generate Figure 5-5, we can see that the fluctuations of the correlation peak are significantly increased in Figure 5-7.

The tracking position of the correlators in Figure 5-7 has not been adjusted to an appropriate tracking location by computing a new Dot-Product Power discriminator value. The position of the punctual correlator has been left in the same position as in Figure 5-6. Figure 5-7 further exemplifies the concept that depending on the tracking technology and correlator spacings of the receiver, the position of the punctual correlator can be quite different.

#### *5.4 Analysis on Threat Model A in the Presence of Multipath*

Threat model A (see section 3.1.1) results are shown for a maximum  $\Delta$  value of 0.12, with  $a_m = 0.5$ . Figures 5-8 through 5-11 show the multipath corrected and uncorrected MDE and MDR values. An additional solid black line has been added to the figures to show the metric value under the no-fault condition (no multipath and no satellite failure) that corresponds to the expected values stated in the previous section.

With the uncorrected correlator values, we can see that there are certain multipath conditions that would render the detection of the evil waveform impossible when using uncorrected correlator values. The MDE and MDR metric cross the no-fault line numerous times for the uncorrected metrics. For the multipath corrected metrics, we can see that from Figure 5-11 that no multipath will ever create this undetectable condition on the MEDLL since the metric is always above the no fault line. Furthermore, Figure 5-11 seems to show better detectability results when compared to Figure 5-10 seeing as the metric crosses the no-fault line at short delay multipath in Figure 5-10 and not in Figure 5-11. This indicates that the

correlators that are further away from the peak are better suited for MDE type fault detection for threat model A type failures.

MDR values, as seen in Figures 5-8 and 5-9 seem to have difficulty detecting threat model A type failures when very short delay multipath or very long delay multipath are present. This is evident in the oscillations of the metric value around the no-fault line when short delay or long delay multipath is present.

We can also examine the D/U plot for threat model A in the presence of multipath. Figure 5-12 shows these results. We can see that threat model A type failures result in the estimation of a very strong multipath signal when in fact there is no multipath present. This condition is shown as the first data point on the graph when there is a multipath delay of zero.

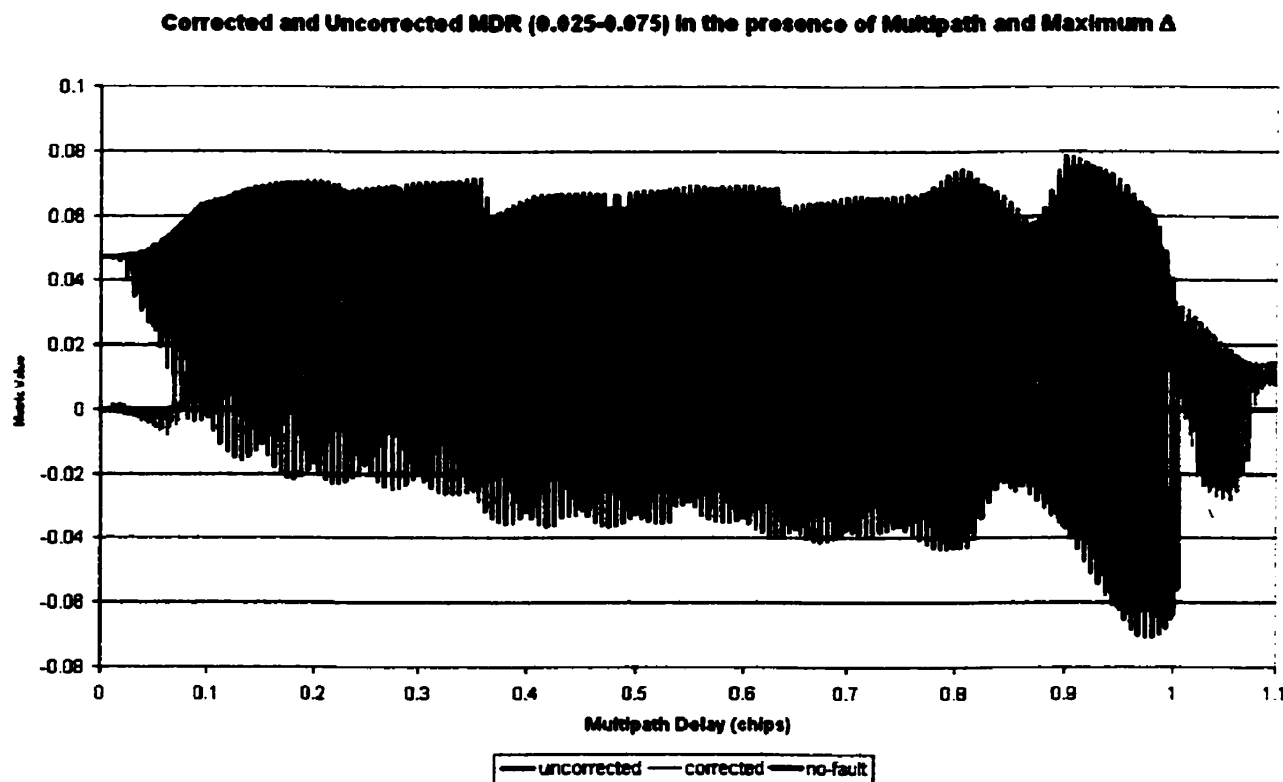


**Figure 5-8: MDR1 (0.025-0.075), Maximum Threat Model A**

**Corrected and Uncorrected MDR (0.075-0.125) in the presence of Multipath and Maximum  $\Delta$**

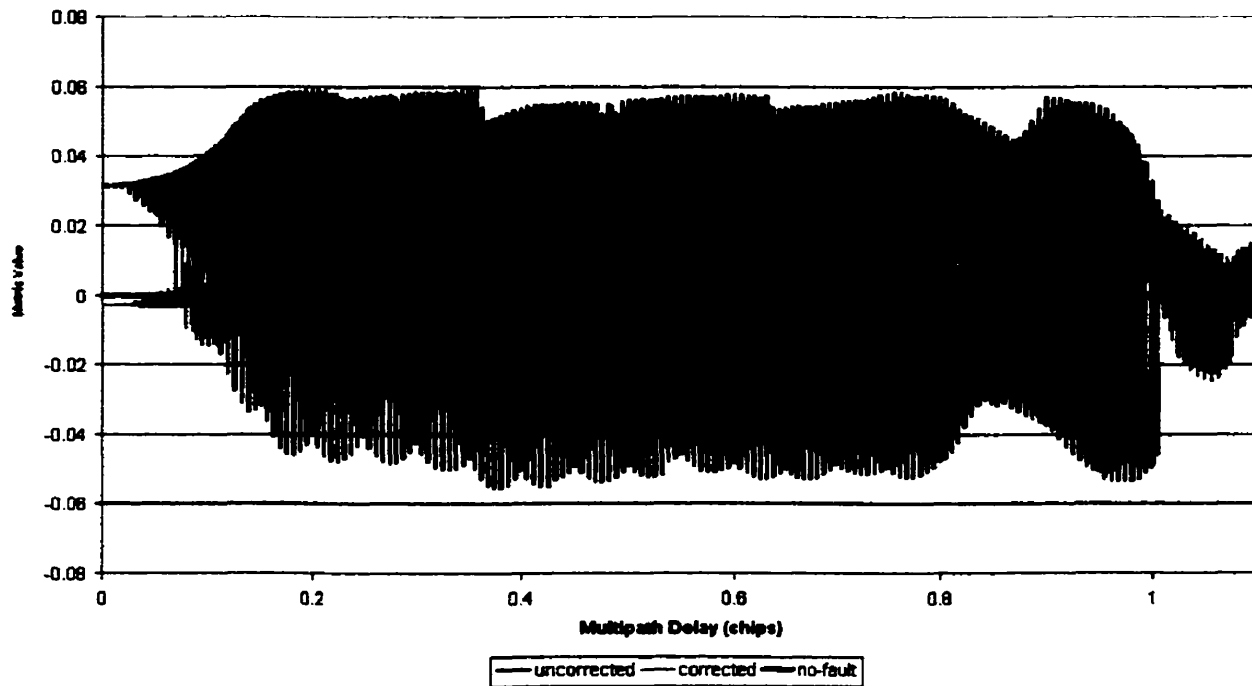


**Figure 5-9: MDR2 (0.025-0.125), Maximum Threat Model A**  
**Corrected and Uncorrected MDE (+0.025) in the presence of Multipath and Maximum  $\Delta$**

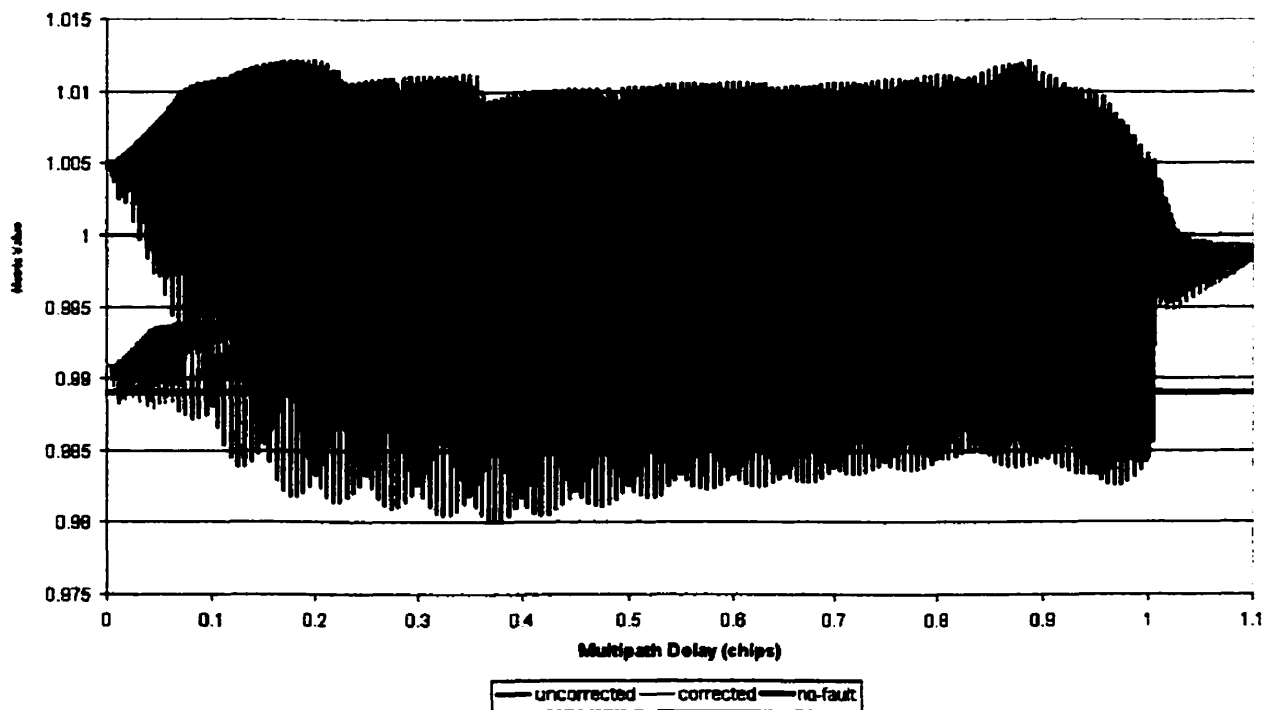


**Figure 5-10: MDE1 (+0.025), Maximum Threat Model A**

**Corrected and Uncorrected MDE (+0.125) in the presence of Multipath and Maximum  $\Delta$**

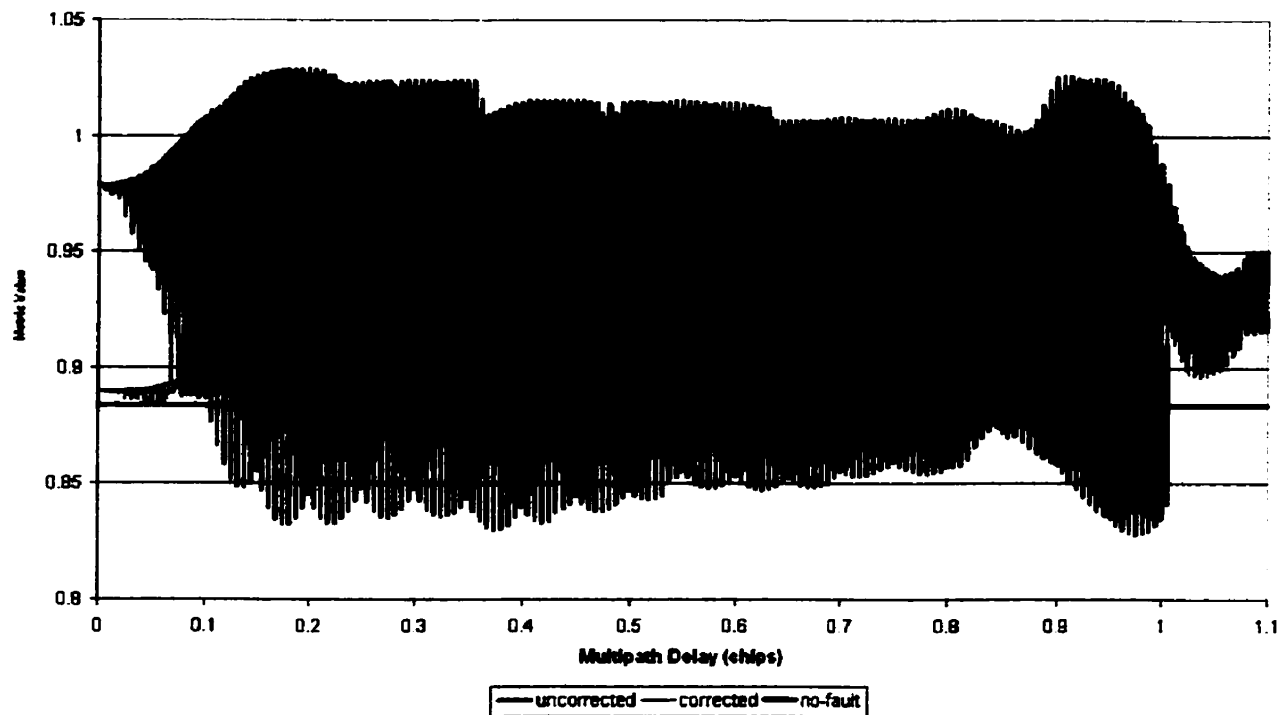


**Figure 5-11: MDE2 (+0.125), Maximum Threat Model A**

We can also see from Figure 5-12 that there are some multipath conditions with threat model A that produce a secondary peak which is more powerful than the direct path signal! As stated previously, it is always assumed that any multipath signal is of lower power than the direct path. With evil waveforms, this is no longer the case. We can see this by the estimate of a negative D/U between 0.1 and 0.2-chip multipath delay. Should a receiver lock onto this signal instead of the direct path, hazardous misleading information would most certainly be output. A 0.10 C/A code chip tracking error would result in a pseudorange error of approximately 30 meters.

The sum-squared residuals from the estimation process also show that there is significant residual error after removing the estimate of the multipath. These residuals are seen in Figure 5-13. Comparing Figures 4-11 to 5-13, we can see the precise magnitude of the difference.

Increased residual values from the estimation can be attributed to one of two things: 1) the inability of the MEDLL to properly estimate the multipath signal, or 2) the signal itself is shaped such that proper estimation is difficult or impossible. This difficulty can arise from either multiple multipath signals [46] or the presence of an evil waveform.

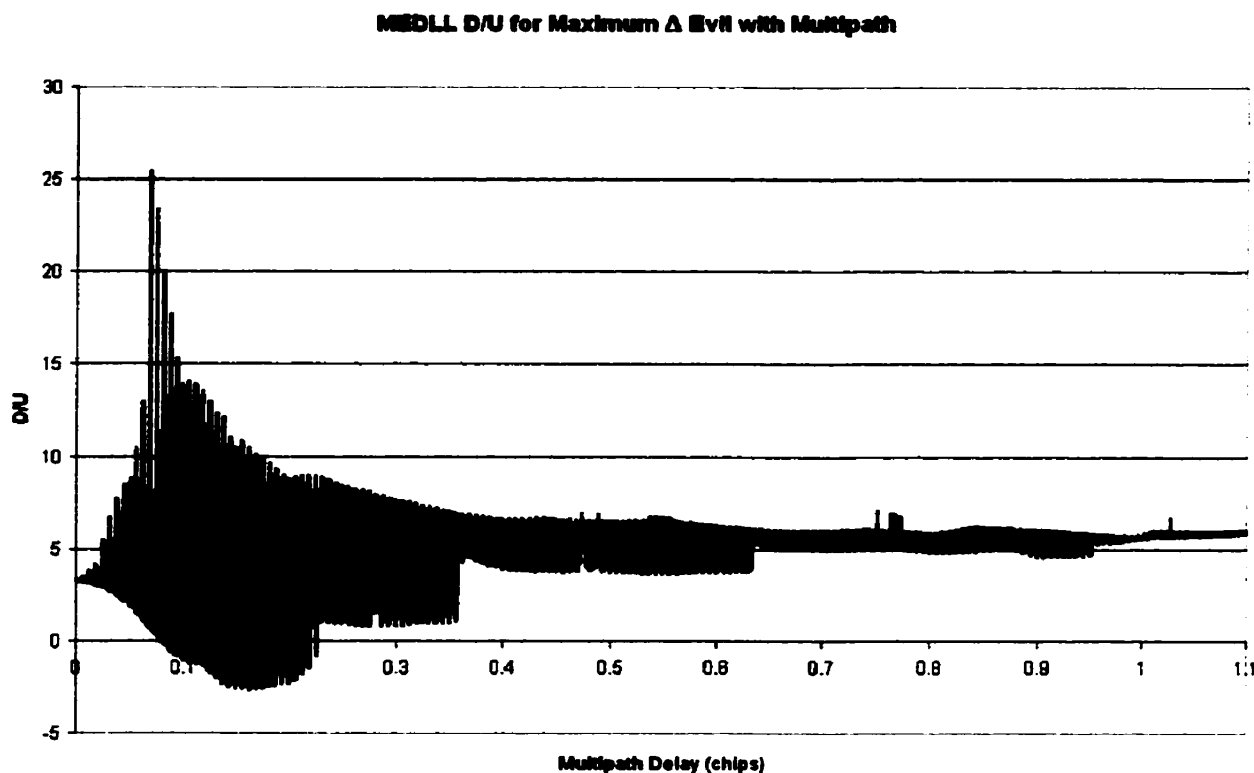


**Figure 5-12: D/U for Maximum Threat Model A with Multipath**

Figures 5-8 through 5-11 show the effects of a maximum threat model A distortion. Figures 5-14 through 5-17 show the effects for a minimum threat model A distortion.

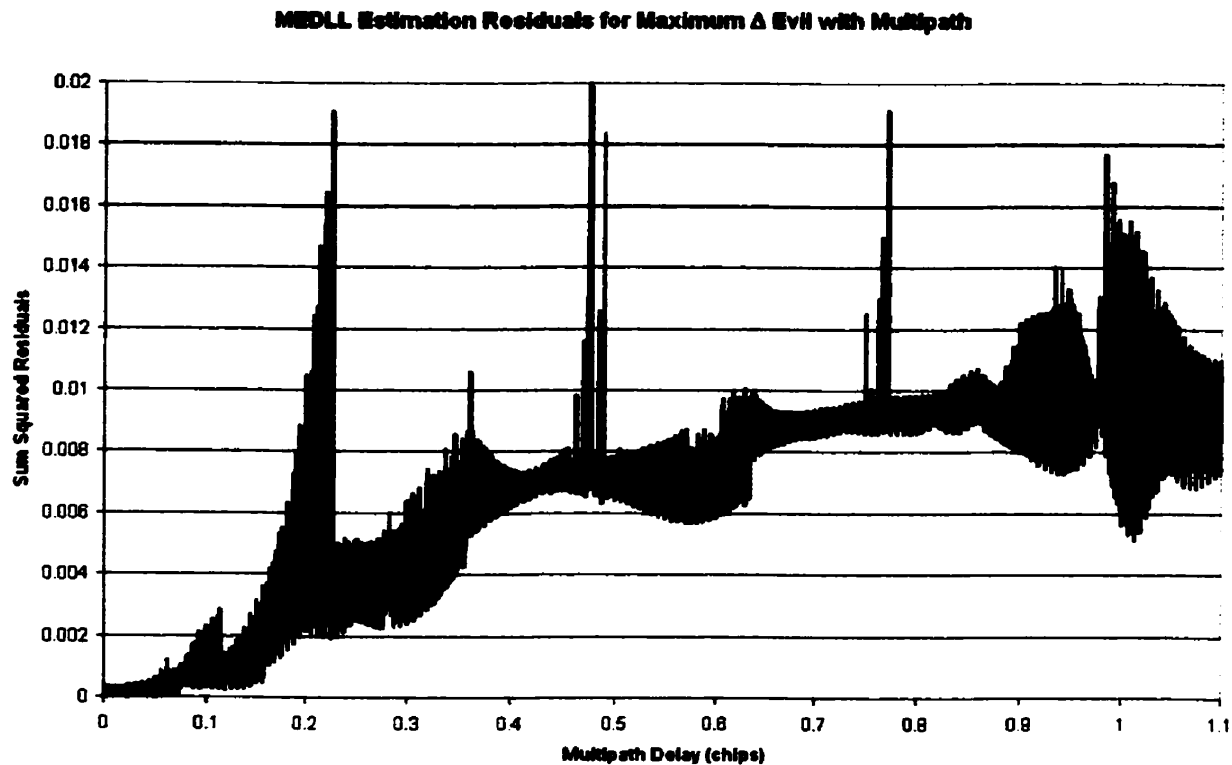


**Figure 5-13: Sum squared correlator residuals, Maximum Threat Model A**

As can be seen from the figures, having a minimal distortion of  $\Delta=0.01$  imposes greater difficulty in the detection of the failure. All of the multipath corrected correlator values still do show some deviation from the no-fault line. Given the small standard deviation values presented for multipath corrected correlator values in Chapter 4, these deviations would be sufficient to result in the satellite failure detection. Even for the condition when multipath is not present, but estimated and removed from the MEDLL, there is still a deviation from the no-fault line.

The MDRs show consistent values below that expected for all multipath delays. There are some slight deviations at short delay multipath, but these MDR values are significantly better at detecting small threat model A type failures than the MDE values since we are looking at the ratio of multiple correlator values rather than a single correlator value.

**Corrected and Uncorrected MDR (0.025-0.075) in the presence of Multipath and Minimum  $\Delta$**

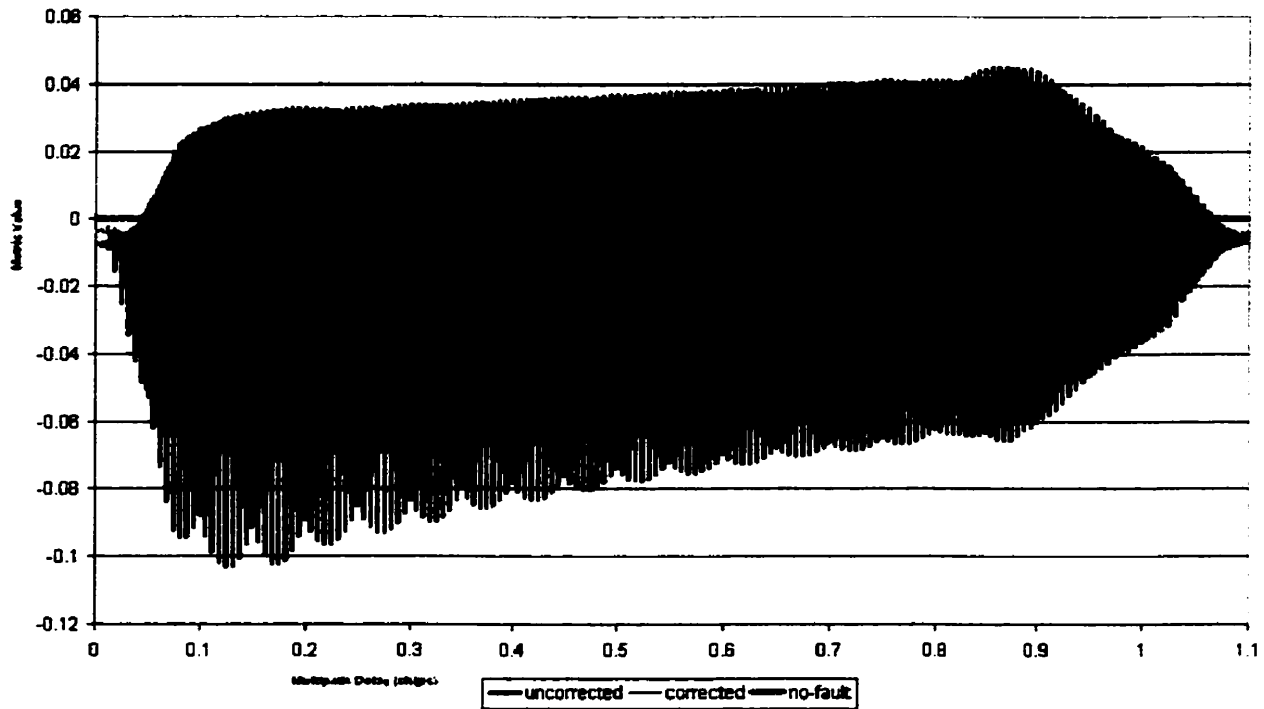


**Figure 5-14: MDR1 (0.025-0.075), Minimum Threat Model A**  
**Corrected and Uncorrected MDR (0.025-0.125) in the presence of Multipath and Minimum  $\Delta$**

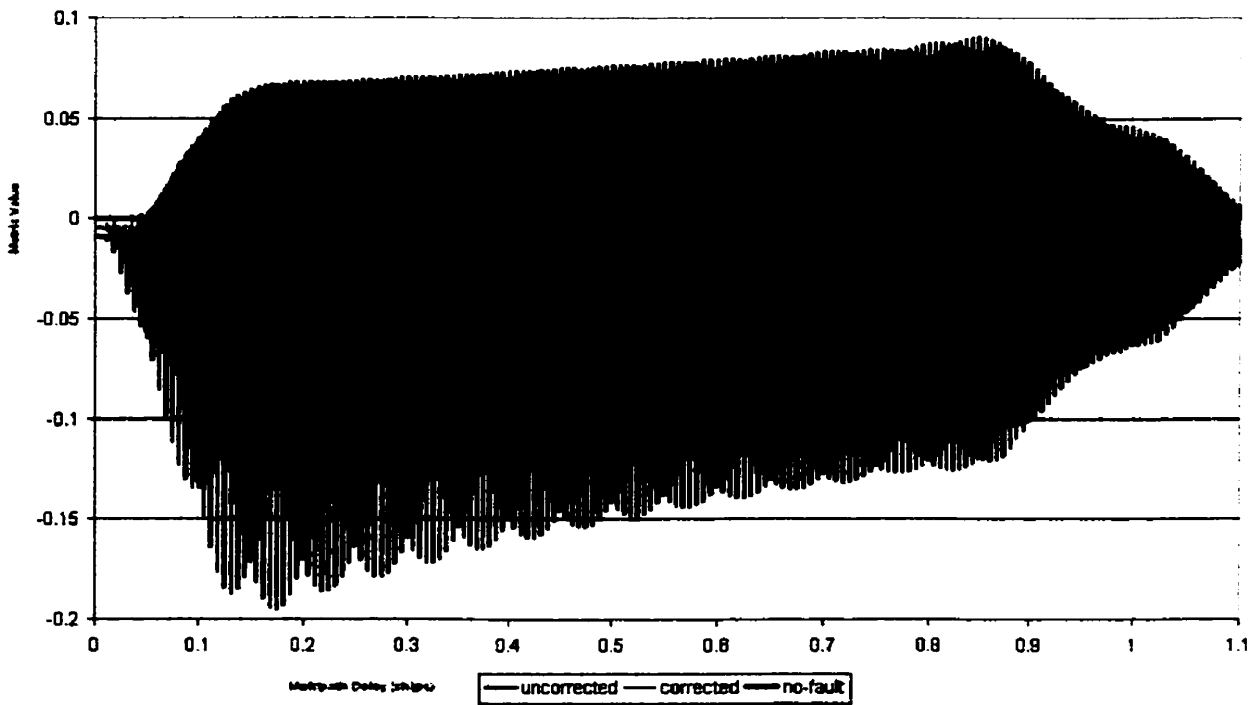


**Figure 5-15: MDR2 (0.025-0.125), Minimum Threat Model A**

Corrected and Uncorrected MDE (-0.025) in the presence of Multipath and Minimum  $\Delta$

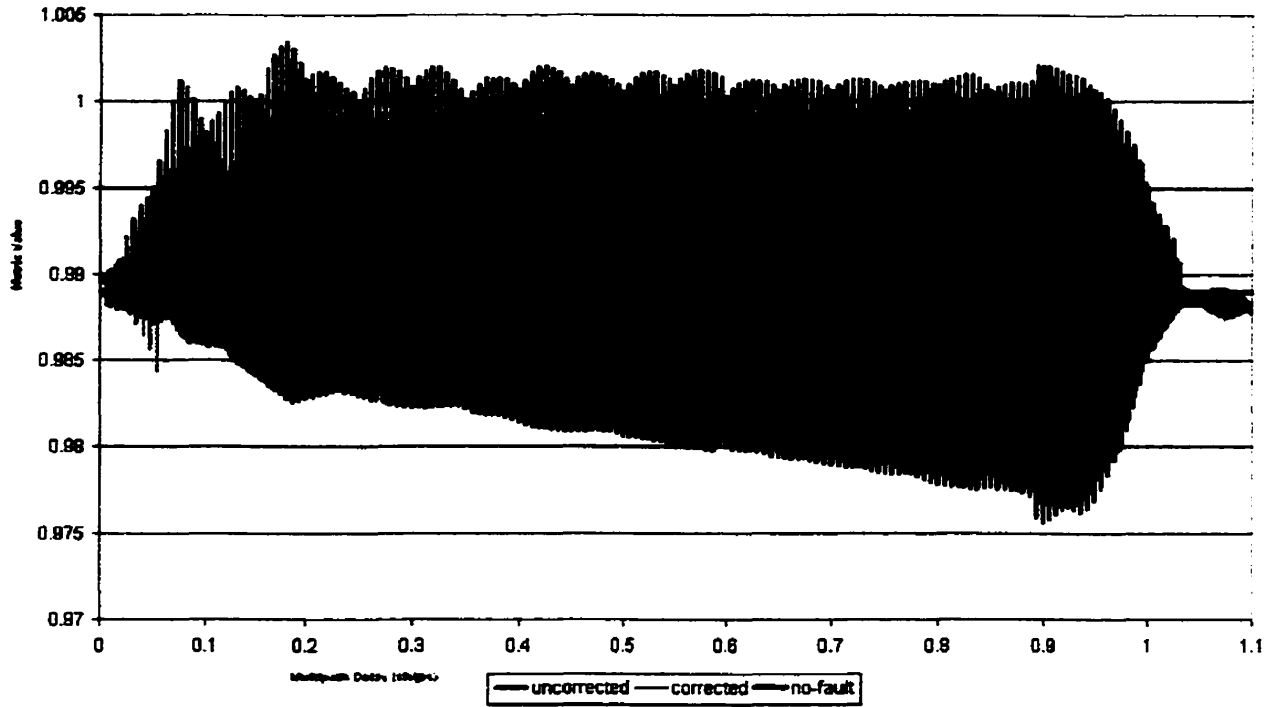


Figure 5-16: MDE1 (+0.025), Minimum Threat Model A  
Corrected and Uncorrected MDE (+0.125) in the presence of Multipath and Minimum  $\Delta$

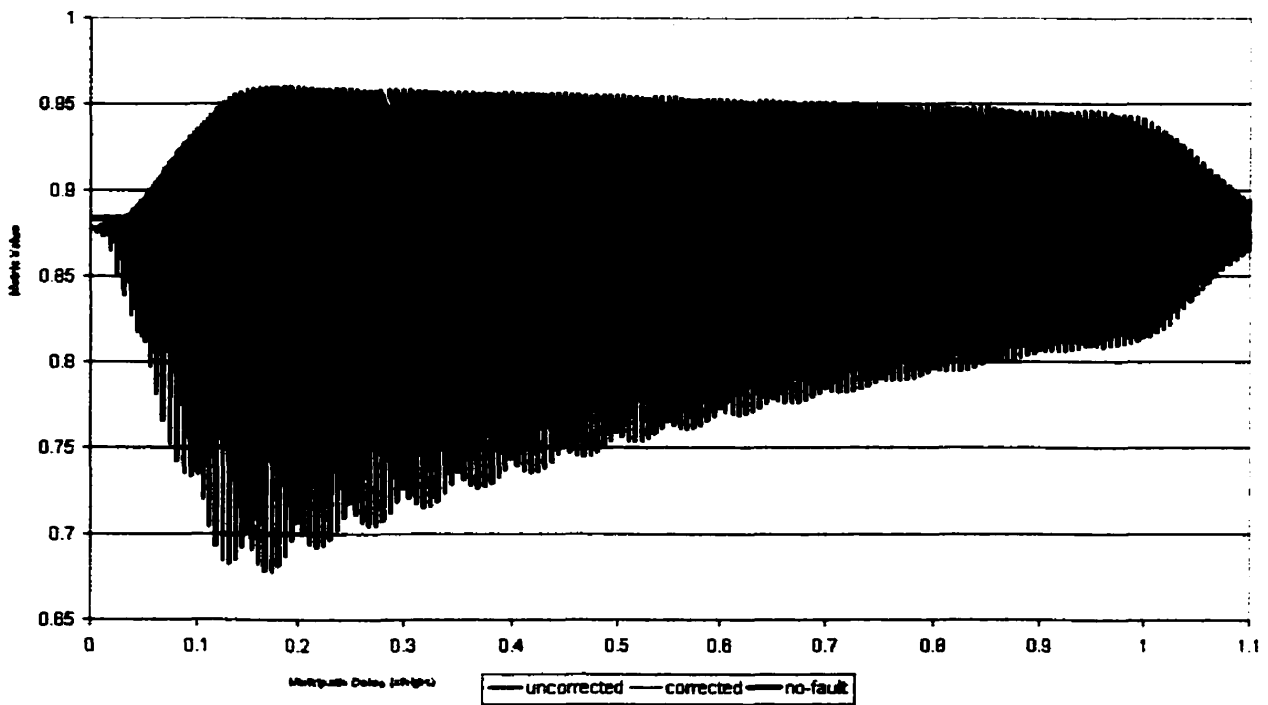


Figure 5-17: MDE2 (+0.125), Minimum Threat Model A

### ***5.5 Analysis of Threat Model B in the Presence of Multipath***

The threat model B (see section 3.1.2) parameters used for testing were  $\sigma=0.8$  and  $f_d=4$ . MDE and MDR results showing the uncorrected correlator values, the multipath corrected correlator values, and the no-fault line are in Figures 5-18 through 5-21.

We can see from the figures that again, there are certain multipath conditions that will cause the satellite failure to go undetected using standard, non-multipath corrected correlator measurements for MDE and MDR values. The combinations of the MDR values shown in Figures 5-18 and 5-19 along with the MDE values in Figure 5-20 will detect all occurrences of this threat model B failure, regardless of multipath on the signal. Results in Figure 5-21 show that the multipath corrected MDE value will not detect the failure when there is less than 0.2 chips of multipath. This only reinforces the need for multiple monitoring points on the correlation function using both MDE and MDR values in order to detect all failures in the threat space.

Residuals from the multipath estimation process further exemplify the presence of an anomalous signal. The residuals in Figure 5-22 are again significantly greater than those present in Figure 4-11, for the nominal input signal condition.

We can see that the frequency of the ringing presents itself as the multipath increases in delay. The 4MHz ringing on the satellite signal shows up as four distinct zones of the uncorrected correlator values. For the multipath corrected correlator values, there appears to be a correlation between signal ringing and zones of correlation values. However, upon further inspection, the null values of the multipath corrected correlator values directly coincide with the correlator positions used for the estimation in the MEDLL.

**Corrected and Uncorrected MDR (0.025-0.075) in the presence of Multipath and Threat B**

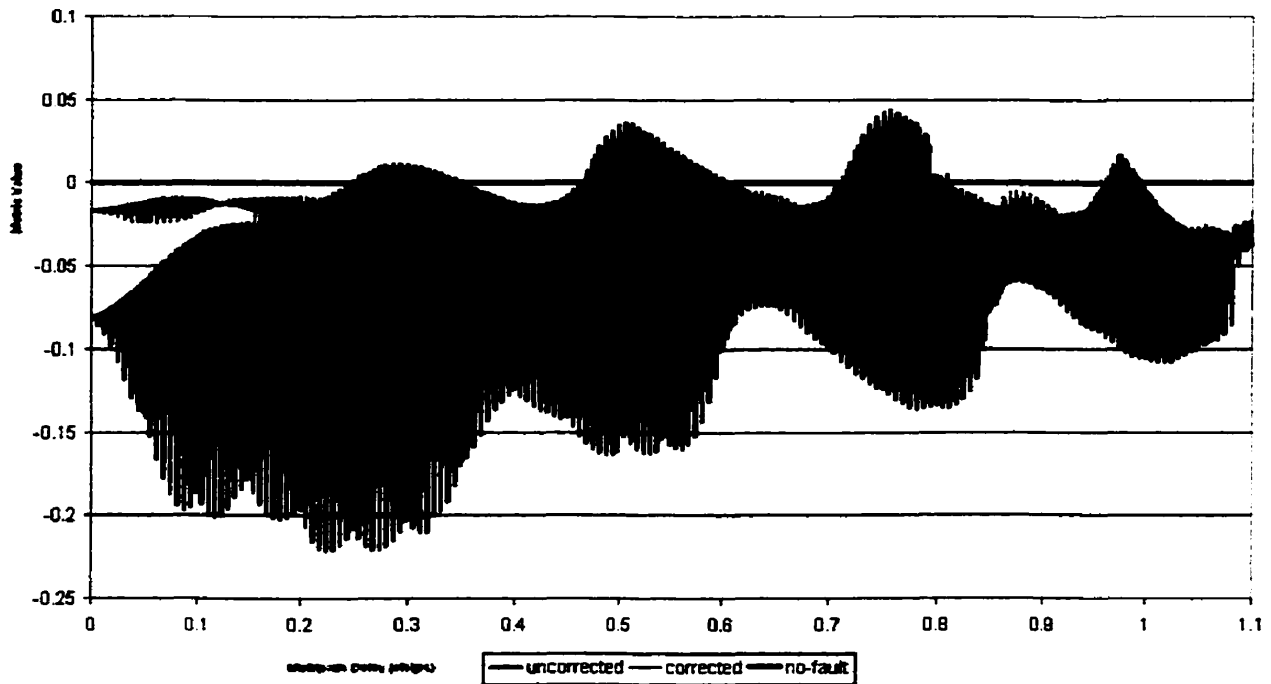


**Figure 5-18: MDR1 (0.025-0.075), Minimum Threat Model B**  
**Corrected and Uncorrected MDR (0.025-0.125) in the presence of Multipath and Threat B**

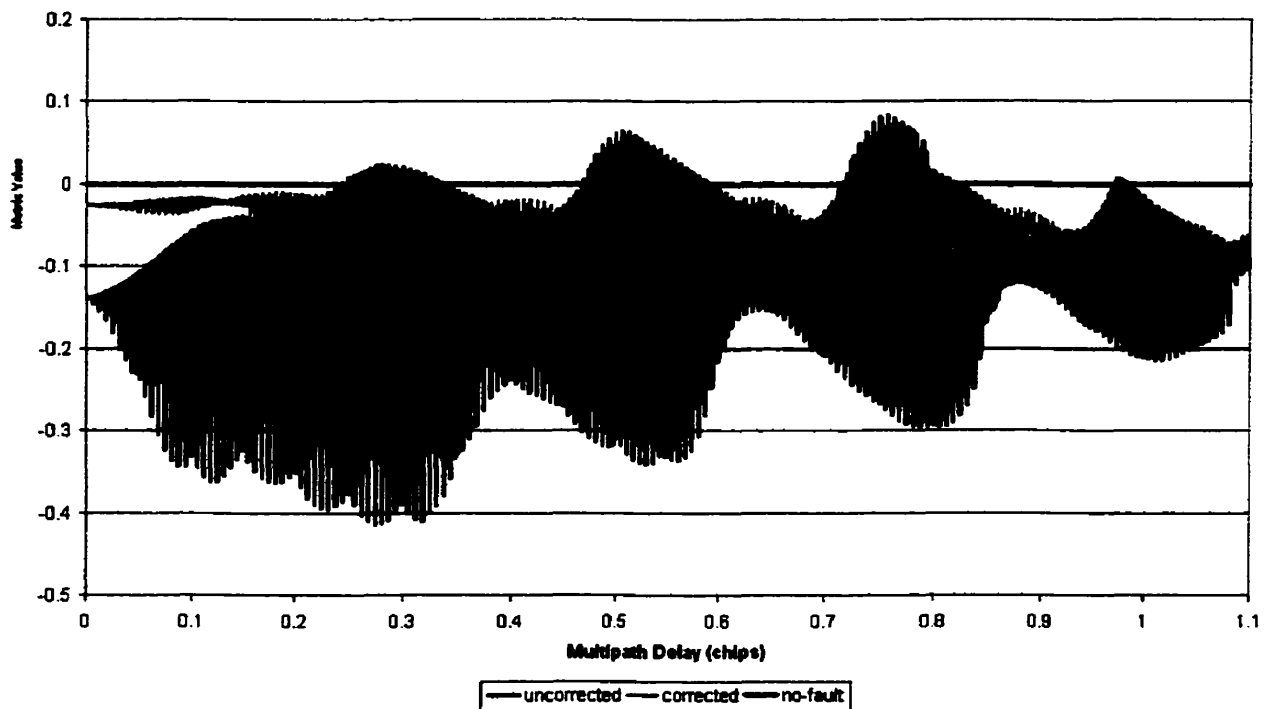


**Figure 5-19: MDR2 (0.025-0.125), Minimum Threat Model B**

**Corrected and Uncorrected MDE (+0.025) in the presence of Multipath and Threat B**

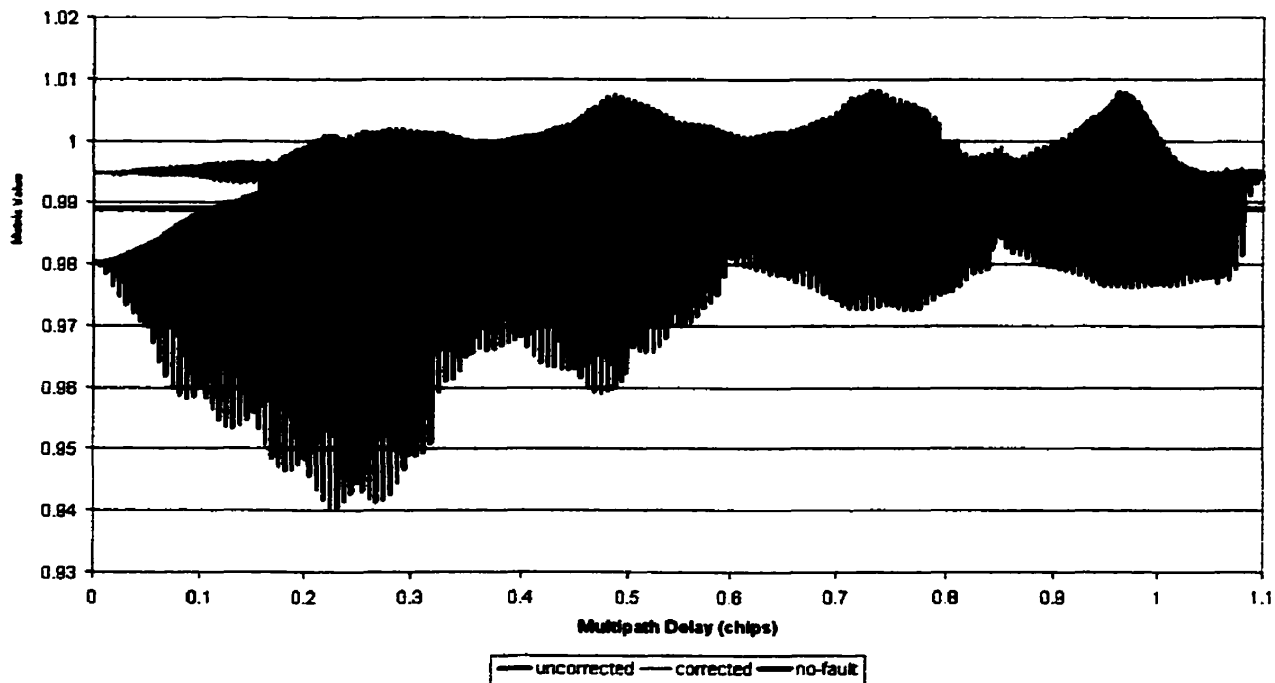


**Figure 5-20: MDE1 (+0.025), Minimum Threat Model B**

**Corrected and Uncorrected MDE (+0.125) in the presence of Multipath and Threat B**

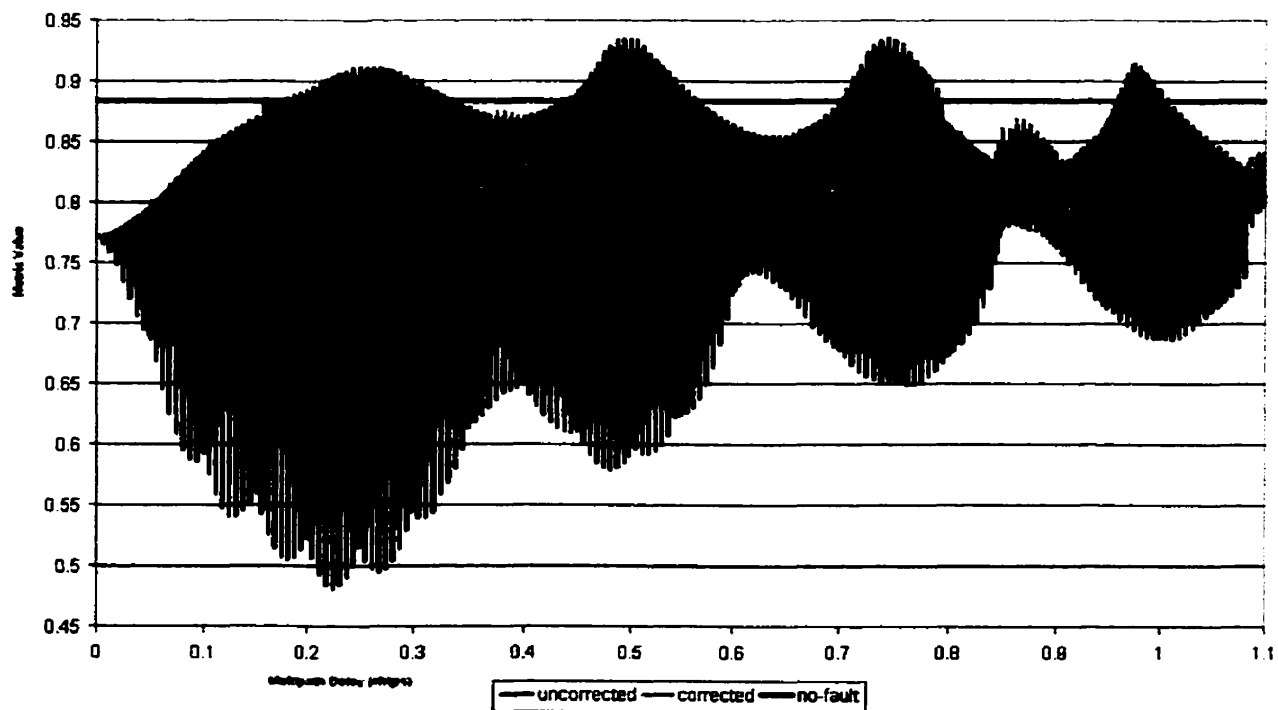


**Figure 5-21: MDE2 (+0.125), Minimum Threat Model B**

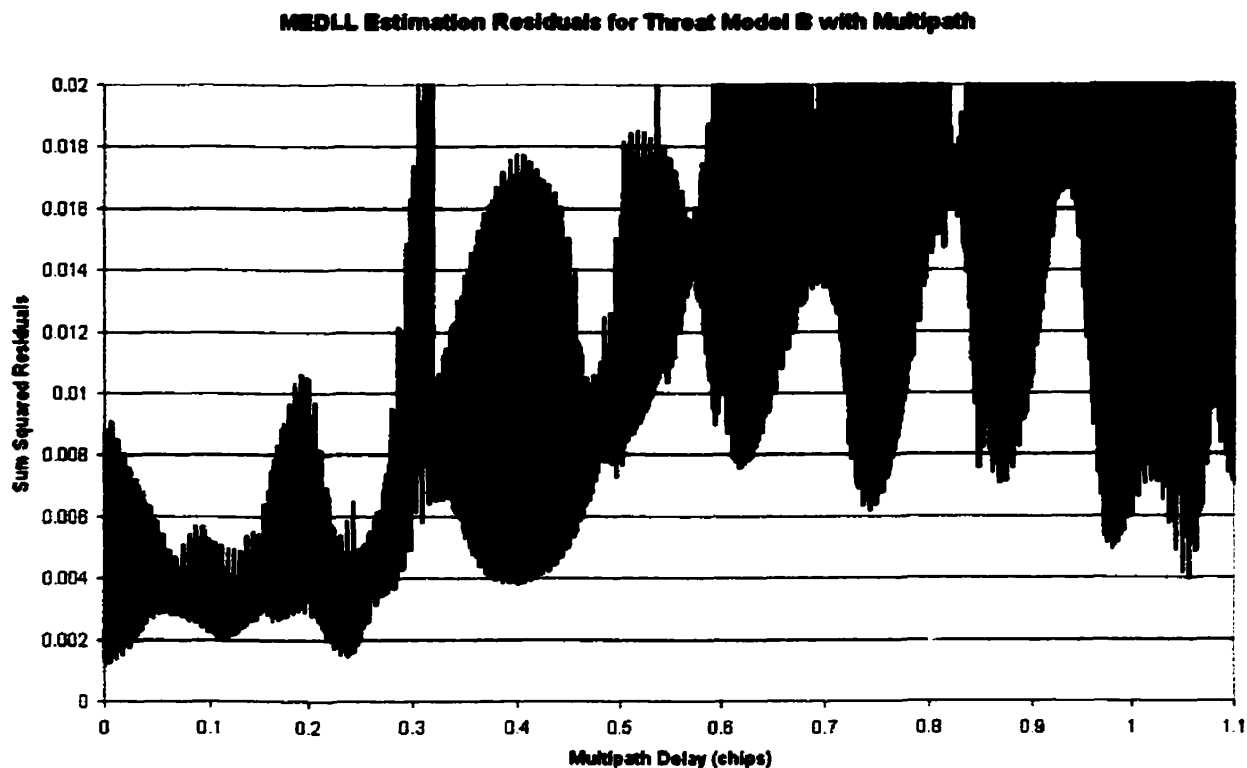


**Figure 5-22: Sum squared correlator residuals, Minimum Threat B**

Also of importance is when the ringing effects of Threat Model B are at their maximum, coupled with maximum dampening. This type of failure will produce a very slight ripple along the sides of the correlation function. We can see the effects of this type of failure when  $f_d=17$  and  $\sigma=8.8$  in Figures 5-23 through 5-26.

We can see that for very short delay multipath signals, the multipath corrected and the uncorrected correlator values follow a very similar trend. It will be difficult to detect such high frequency ringing effects using either method of detection. However, there are some spurious events in Figures 5-23 and 5-25. During these periods in Figure 5-25, the multipath corrected correlator value returns to a nominal value, very close to the expected value. This is due to the multipath signal combining with the direct path signal to produce a signal, which masks the effects of the signal failure. Nevertheless, the MDR values, as well as MDE values for

correlators at spacings further from punctual, do not return to their expected values when the failure is present.

It is also interesting to note that for the MDE1 value, with multipath delays between 0.15 and 0.9 chips, there would be no masking of the failure with multipath. The MDE value remains below the expected value. This has generally not been the case for all other points in the threat space that have been tested.

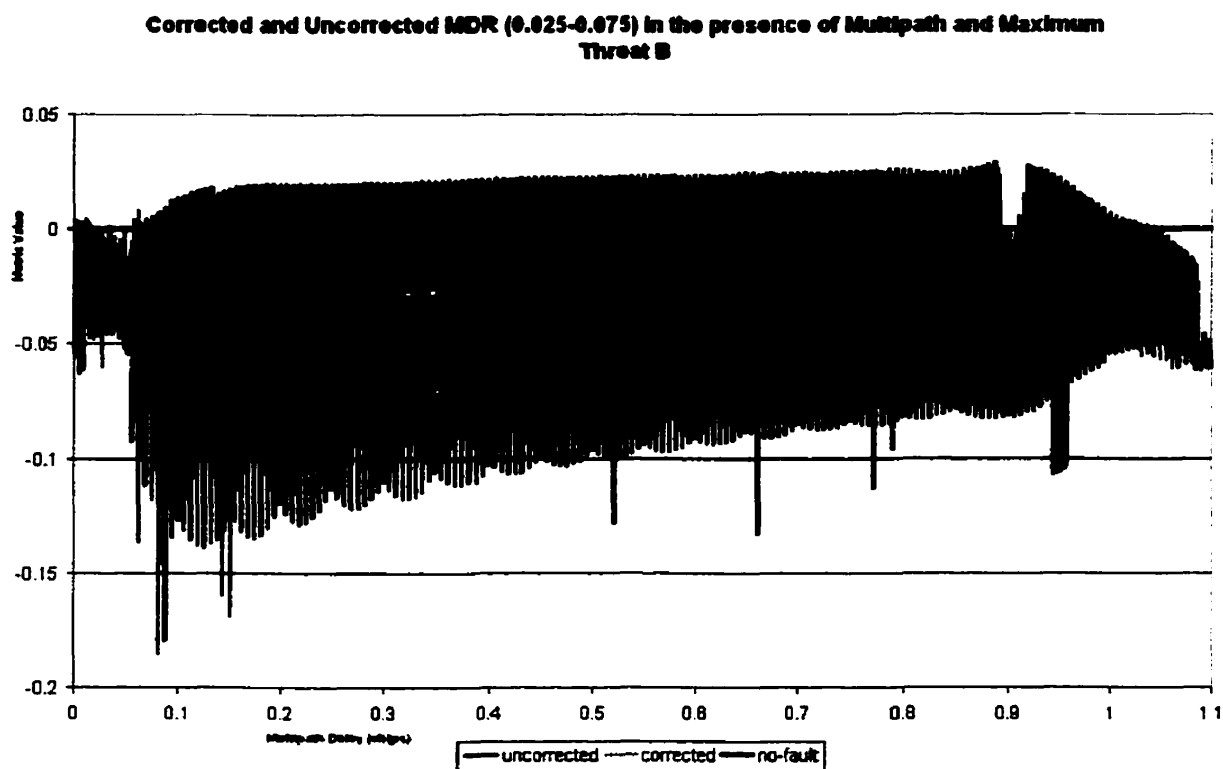


**Figure 5-23: MDR1 (0.025-0.075), Maximum Threat Model B**

**Corrected and Uncorrected MDR (0.025-0.125) in the presence of Multipath and Maximum Threat B**

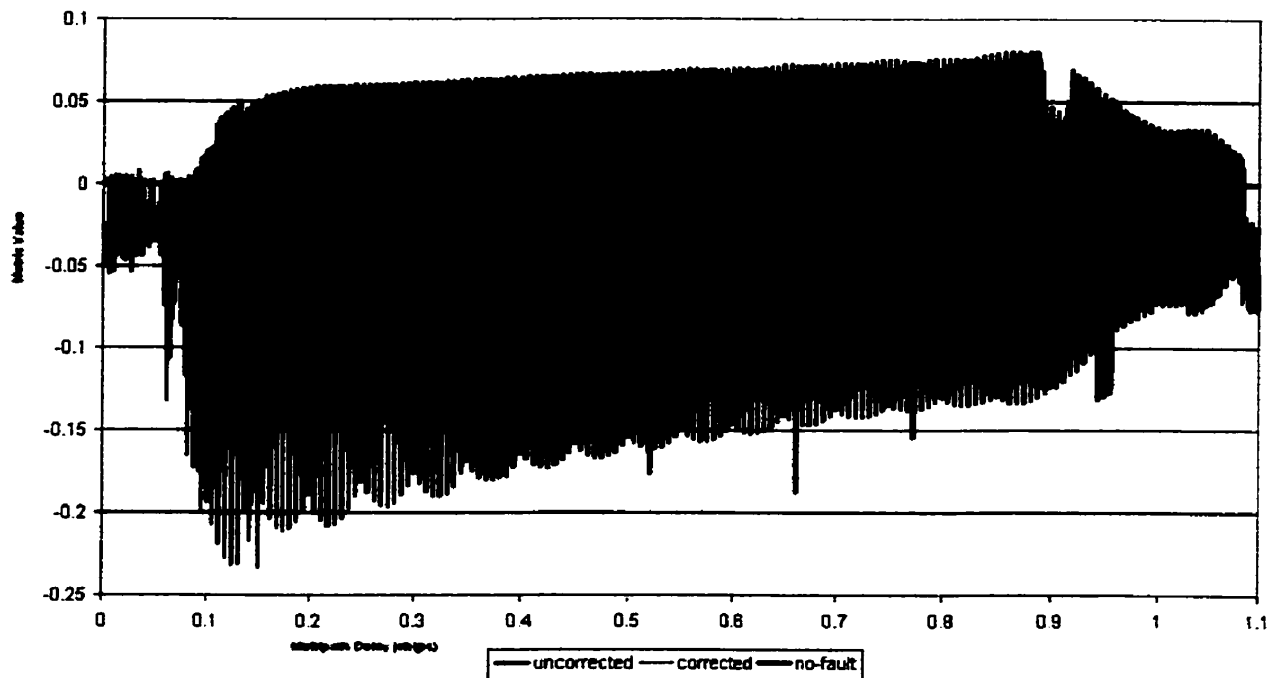


**Figure 5-24: MDR2 (0.025-0.125), Maximum Threat Model B**  
**Corrected and Uncorrected MDE (+0.025) in the presence of Multipath and Maximum Threat B**

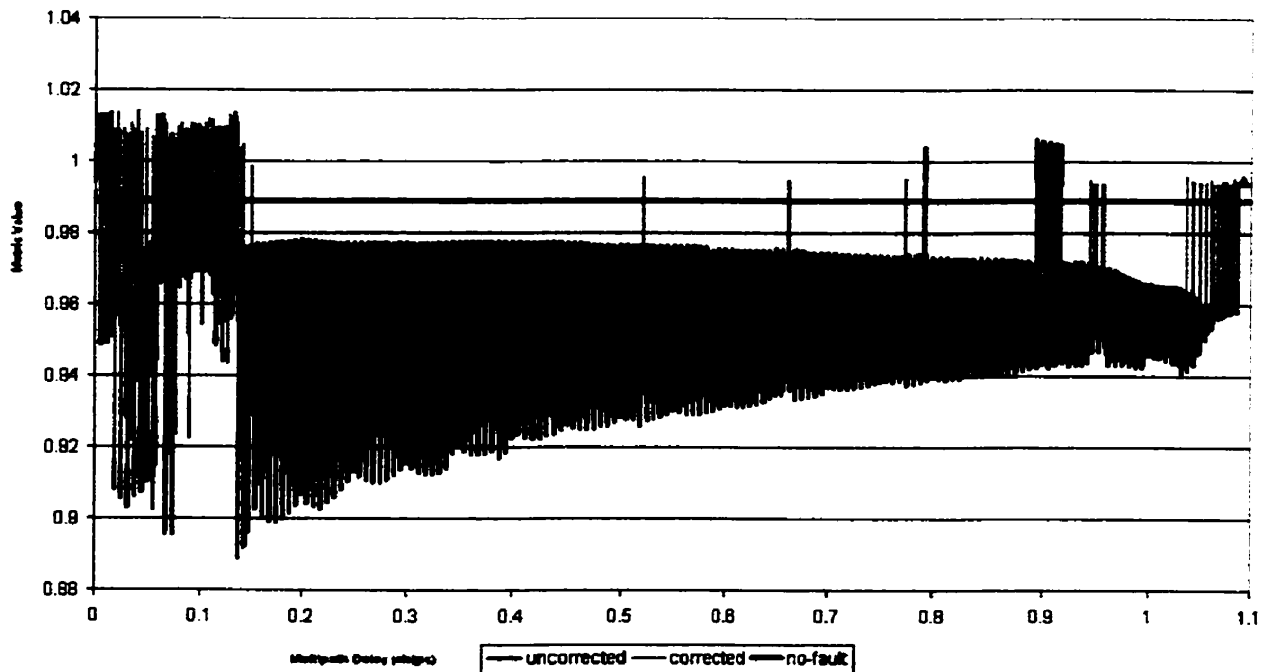


**Figure 5-25: MDE1 (+0.025), Maximum Threat Model B**

Corrected and Uncorrected MDE (+0.125) in the presence of Multipath and Maximum Threat B

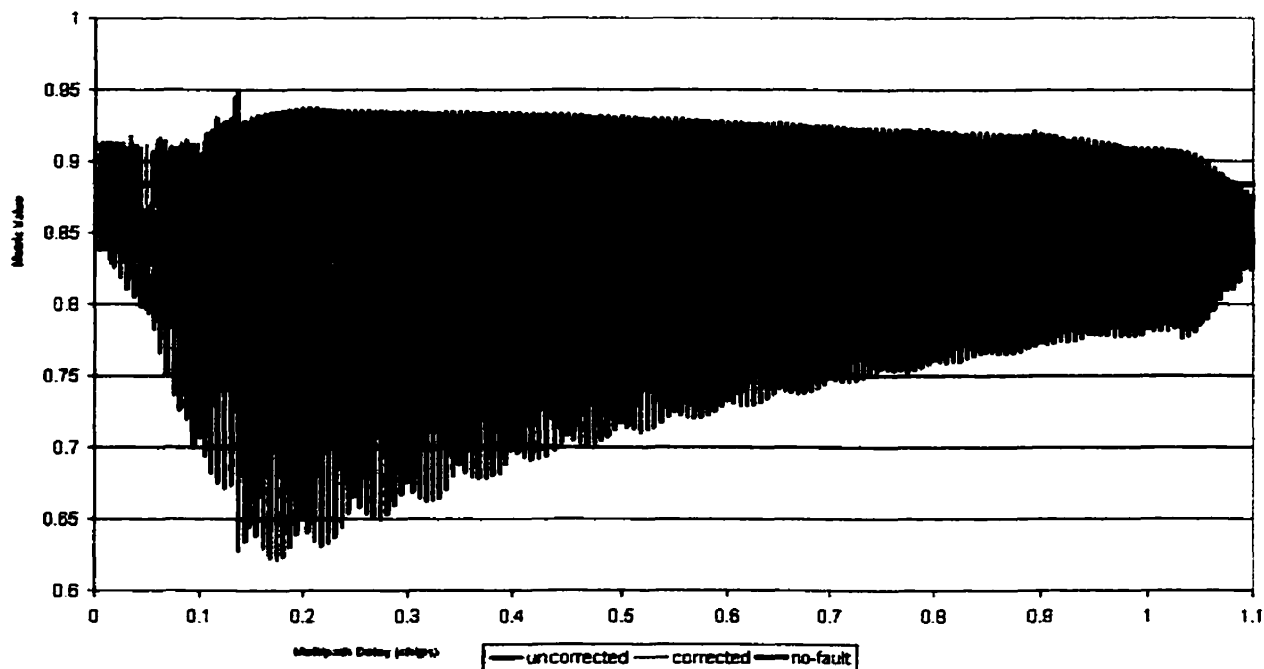


Figure 5-26: MDE2 (+0.125), Maximum Threat Model B

### 5.6 Analysis of Threat Model C in the Presence of Multipath

Threat model C (see section 3.1.3) has the potential to introduce the most distortion of any of the three models, since we are combining all three parameters of distortion. With  $\Delta=0.12$ ,  $\sigma=0.8$ , and  $f_d=7.3$ , the correlation function is quite devious and is as described by Figure 5-6. Increasing the complexity of the correlation function with multipath, as in Figure 5-7, poses real problems for detection using non-multipath corrected correlator values.

Figures 5-27 through 5-30 show the uncorrected, corrected, and no-fault lines for the MDE and MDR values. We can see from these figures that certain multipath scenarios even prove to be difficult to detect using the multipath corrected correlator values, especially with very short delay

multipath. Figure 5-29 showing the very close in correlator at +0.025 chips indicates many crossings of the no-fault line.

However, we also have additional parameters from the Multipath Meter that we can examine for satellite failures. If we look at the sum squared of the residual error from the estimation process, we can see that the residuals indicate that the MEDLL is not estimating the multipath very well. This is the case for instances of evil waveforms, which has also been shown in Figures 5-13 and 5-22. For the threat model C testing, the residuals from the MEDLL can be seen in Figure 5-31. Comparing the residuals from Figure 4-11 to Figure 5-31, we can see that there is a significant change in the magnitude of the residuals over all multipath delays.

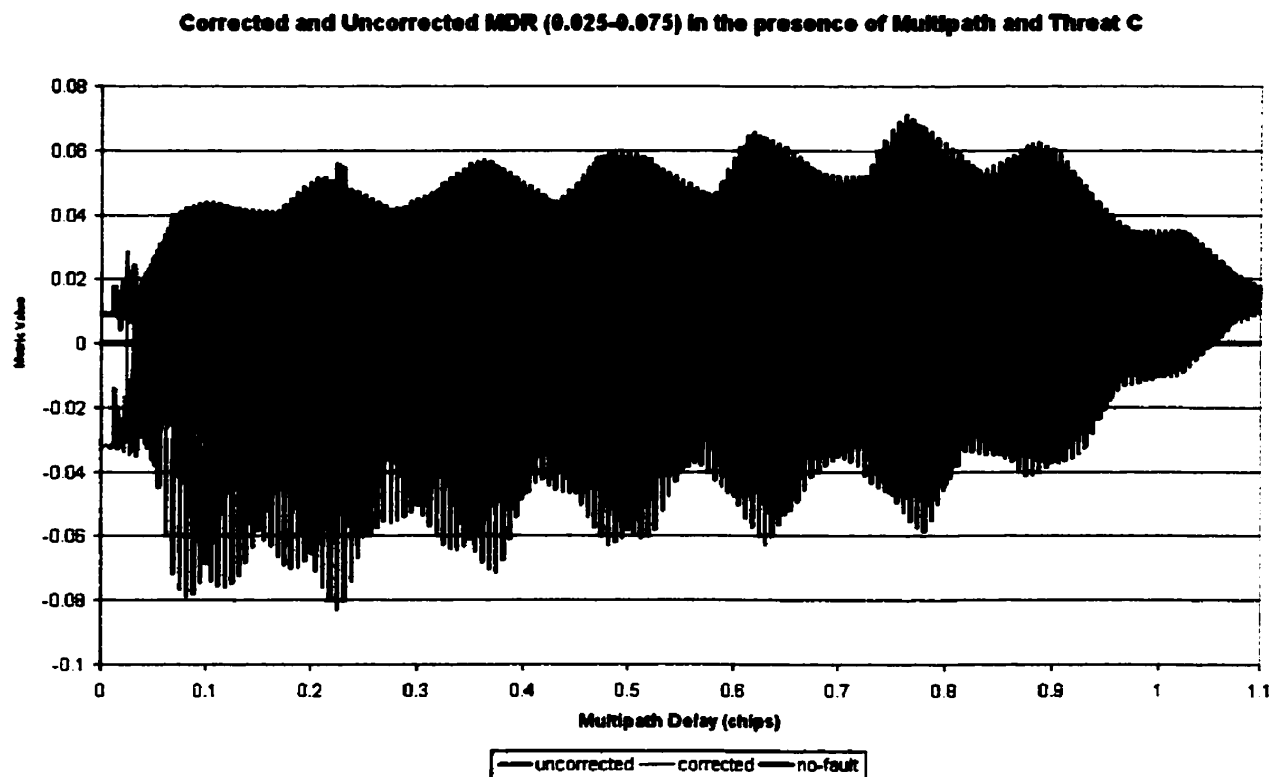


**Figure 5-27: MDR1 (0.025-0.075), Threat Model C**

Corrected and Uncorrected MDR (0.025-0.125) in the presence of Multipath and Threat C

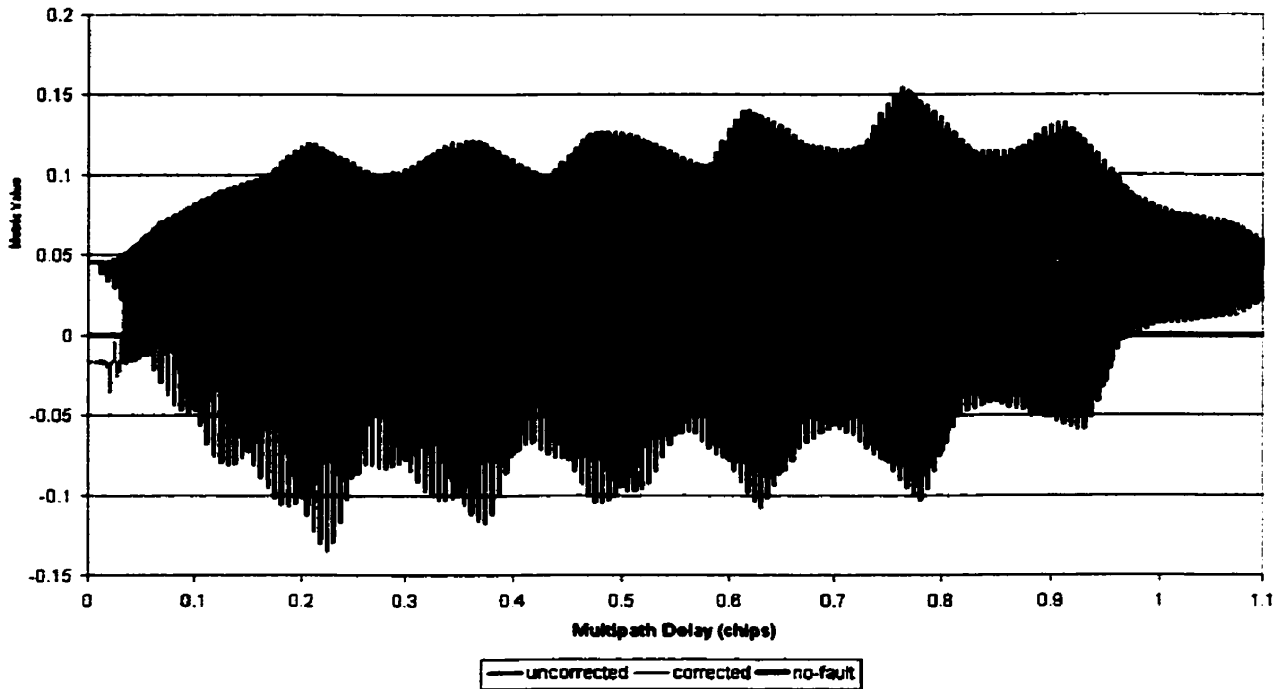


Figure 5-28: MDR2 (0.025-0.0125), Threat Model C  
Corrected and Uncorrected MDE (+0.025) in the presence of Multipath and Threat C

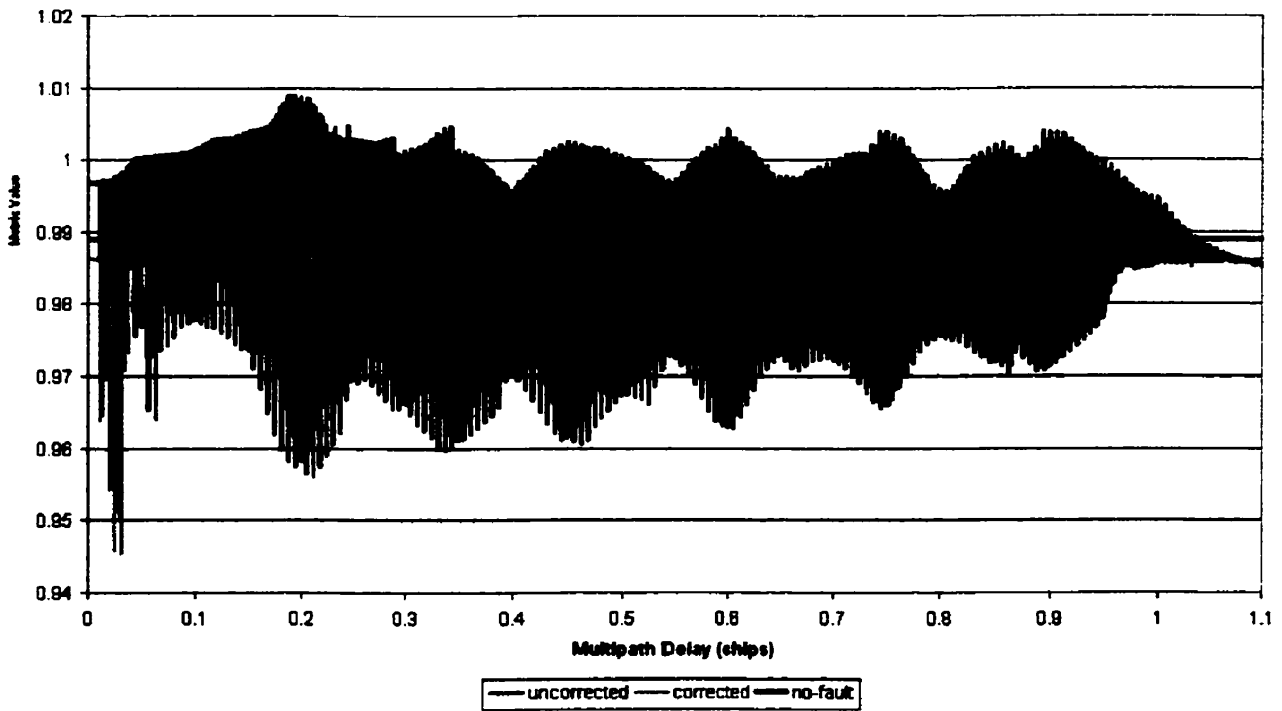
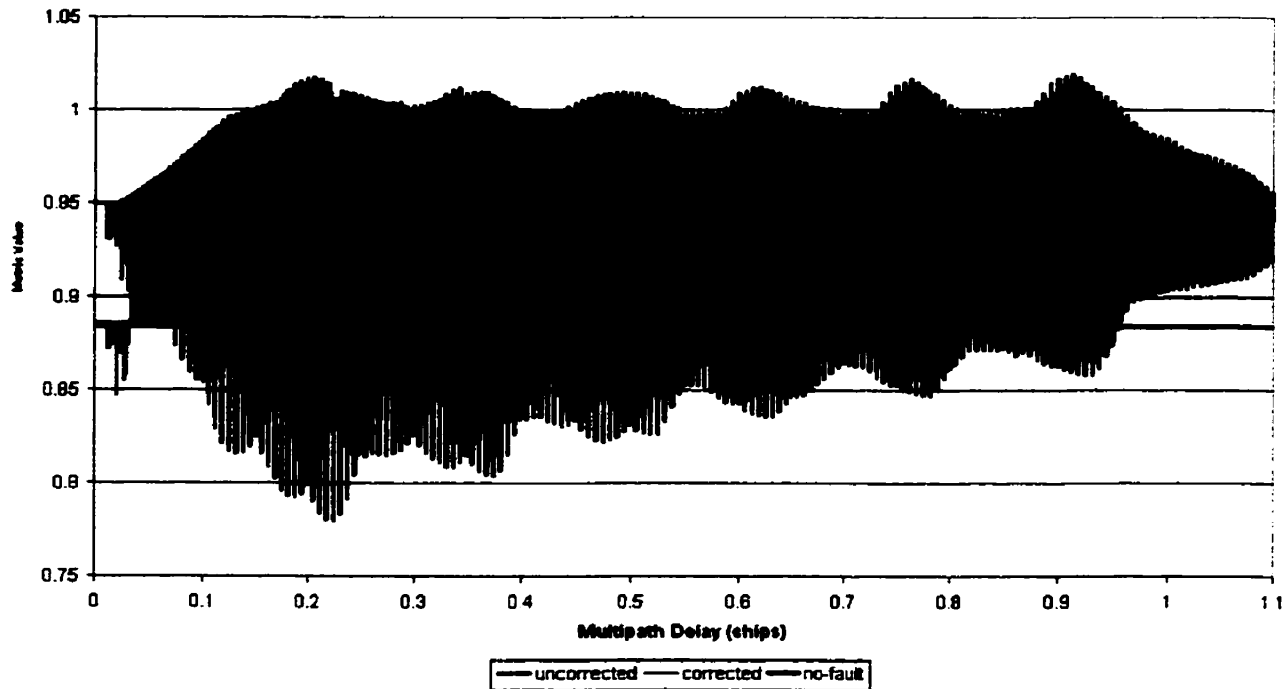


Figure 5-29: MDE1 (+0.025), Threat Model C

**Corrected and Uncorrected MDE (+0.125) in the presence of Multipath and Threat C**



**Figure 5-30: MDE2 (+0.125), Threat Model C**

**16 MHz MEDLL Correlation Estimation Residuals: Threat C**

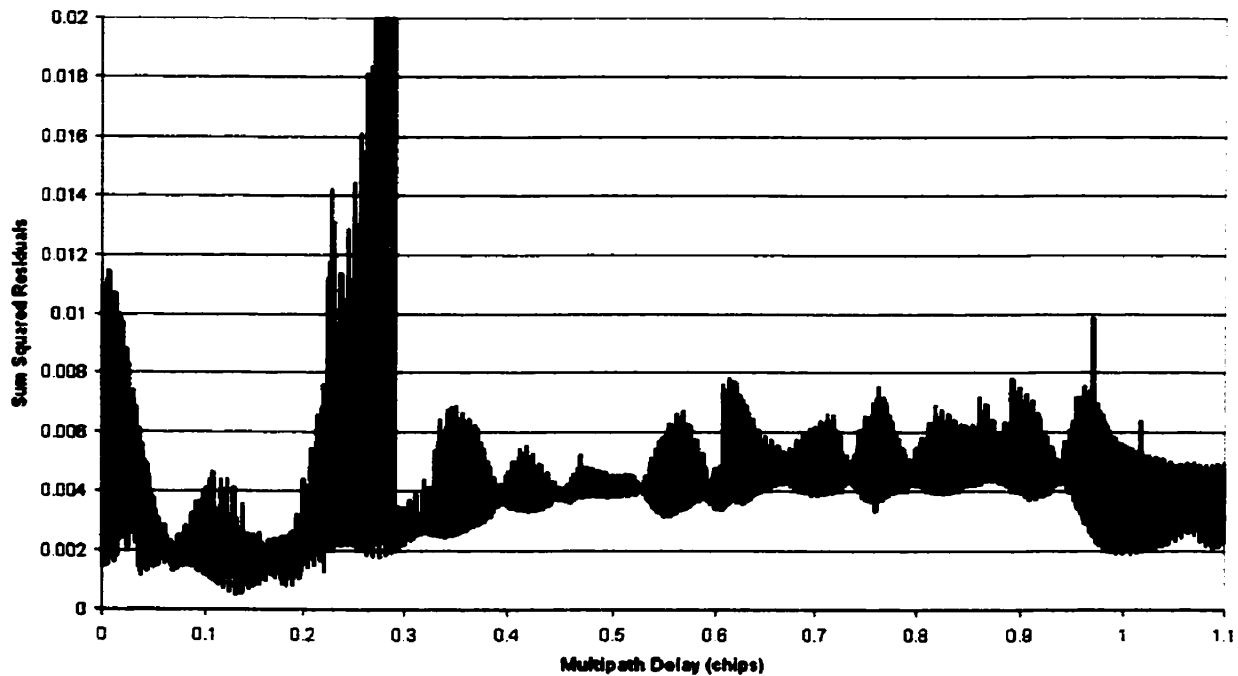


**Figure 5-31: Sum Squared Correlator Residuals, Threat Model C**

### ***5.7 Conclusions of Simulation Testing***

The results from this analysis show that the Multipath Meter is useful for signal quality monitoring. For SQM the D/U, residuals, and multipath corrected correlator values can be used in harmony with one another to detect satellite signal failures. Using this approach provides for fewer false alarms due to multipath, since the multipath effects have been largely removed, and a shorter time to alarm, since the multipath corrected correlator measurements are less noisy. The D/U estimate can also be used to detect hazardous conditions when there is a secondary peak that is more powerful than the direct path signal.

The detection of the evil waveforms was shown to be possible even when multipath corrected correlator values were used with no multipath present. Removing the effects of multipath does not mask the effects of a satellite failure, even when there is no multipath present.

When the MEDLL is unable to adequately estimate and remove multipath effects (as seen in the large residual values), the pseudorange accuracy shown in Figure 4-10 cannot be assured. Regardless of the source of the estimation error, either from signal failure or multiple multipath signals [46], the satellite measurements should not be used when residual values are extremely large.

The overall detection technique for determining when a signal should or should not be used includes the checking of all parameters: MDEs, MDRs, D/U, and estimation residuals. By using all values together we are assured to have the most robust signal quality monitoring scheme available to us. If any of the values used in the detection scheme should indicate that a failure has occurred, the signal should not be used.

## CHAPTER 6

### INTERFERENCE ENVIRONMENTS

There are a number of methods that can be used for the detection of in-band RF interference, including variations in C/No, AGC, Wide Band Code Range Corrections, and even directly in the correlation domain [6]. When the interfering frequency is within  $\pm 10\text{MHz}$  of the central frequency of the signal, either L1 or L2, the interferer is said to be "in-band". This 20MHz range is specified since there are practical limitations imposed on the GPS receiver to mitigate the effects of out-of-band interferers (beyond the 20MHz range) in the LAAS MOPS [28]. It is assumed that the out-of-band interferers are mitigated by the RF filters of the GPS receiver.

By using the C/No and AGC methods together, we will be able to detect the presence of various types and intensities of interferers. These two methods will complement one another in the detection of interferer, and add to the overall effectiveness of our SQM scheme.

It was initially theorized that the use of the standard deviation of the Wide Band Code Range Corrections could be used as a means of detecting interference. It will be shown in section 6.4 that this method is inadequate for detecting interferers when used in conjunction with the C/No and AGC jammer detection methods.

#### *6.1 Test Setup for Interference Generation*

Interference testing has been conducted for interferers with double-sided bandwidths of 100kHz, 50kHz, 25kHz, 10kHz, 5kHz, 2.5kHz, 1kHz, and 0.6kHz. When the interferer had a bandwidth greater or equal to 1kHz, the central frequency of the interferer was offset by 100Hz from L1 or L2 in order to avoid spectral lines of the input signal. When a very narrow

interferer is present directly on a spectral line of the input signal, it can result in a complete denial of the signal to the receiver.

All of these interferer bandwidths were tested for both L1 and L2. Data was collected using all interference detection mechanisms so that the data could be easily compared between interference detection methods. The interferer is turned off at the beginning of each test in order to observe a constant state before introducing the interferer. The interferer to signal ratio, I/S, is increased in 1dB steps every 250 seconds after the interferer is initially turned on. A single satellite was used in order to simplify the testing at minimum signal power inputs (40dB L1, 34dB L2). These minimum levels correspond to a satellite at approximately 10° elevation.

PRN18 was chosen as the test satellite to show the interference results. If the power of the interferer is not high enough, or the interferer is too far out of band, there may be very little to no variation in interference detection metrics. These situations will likely not impact the performance of the receiver and their non-detection is of no consequence. The non-detection will not result in misleading information being output from the receiver.

Data was collected on a NovAtel OEM3 receiver with special firmware version 4.444S29, which allows for the tracking of satellites to very low C/No values.

## ***6.2 C/No Interference Detection***

The presence of interference can have a large effect on the C/No measurement output by the receiver. For a low I/S, C/No is negligibly affected but as the I/S increases the C/No will start decreasing until there is a one-to-one relationship. Meaning a 1 dB increase in I/S will cause a

1 dB decrease in C/No above a certain I/S threshold. This threshold is dependent on the central frequency of the interferer.

The interferer effects on an individual satellites' C/No will depend on its PRN code as well as the bandwidth and frequency of the interferer. This makes the C/No measurement a good indication if a satellite measurement is being affected by interference. The indicator used will be a simple threshold test as shown in the following equation:

$$(C/No_{\text{expected}} - C/No_{\text{measured}}) > C/No \text{ threshold} \quad (6-1)$$

Where,

$C/No_{\text{measured}}$  is the measured C/No reported by the receiver, and  
 $C/No_{\text{expected}}$  is the expected C/No based on the signal strength specifications in the GPS ICD [2] and the elevation of the satellite.

If equation 6-1 is true, the interference is present and if false interference is not present.

In Figure 6-1, taken from live data on the NovAtel rooftop, we can see that for different PRNs there can be a difference in the expected C/No values for satellites at the same elevation of approximately 1.5dB, when the elevation is greater than 30° and multipath effects are minimal. The event at approximately 18° elevation is the result of multipath from known reflectors near the antenna location. When selecting a C/No threshold for the detection of interference, it must be adequately large in order to account for variations due to acceptable levels of multipath while balancing the probability of missed detection. The probability of missed detection should be assessed based on requirements of the ground station implementing the SQM scheme. As seen in Figure 6-1, the variation due to multipath approaches 4dB at 18°. The rooftop where the data was collected is a very low multipath environment, and (in the absence of interference) the deviation of C/No from the expected value is directly proportional to the level of multipath at the antenna.

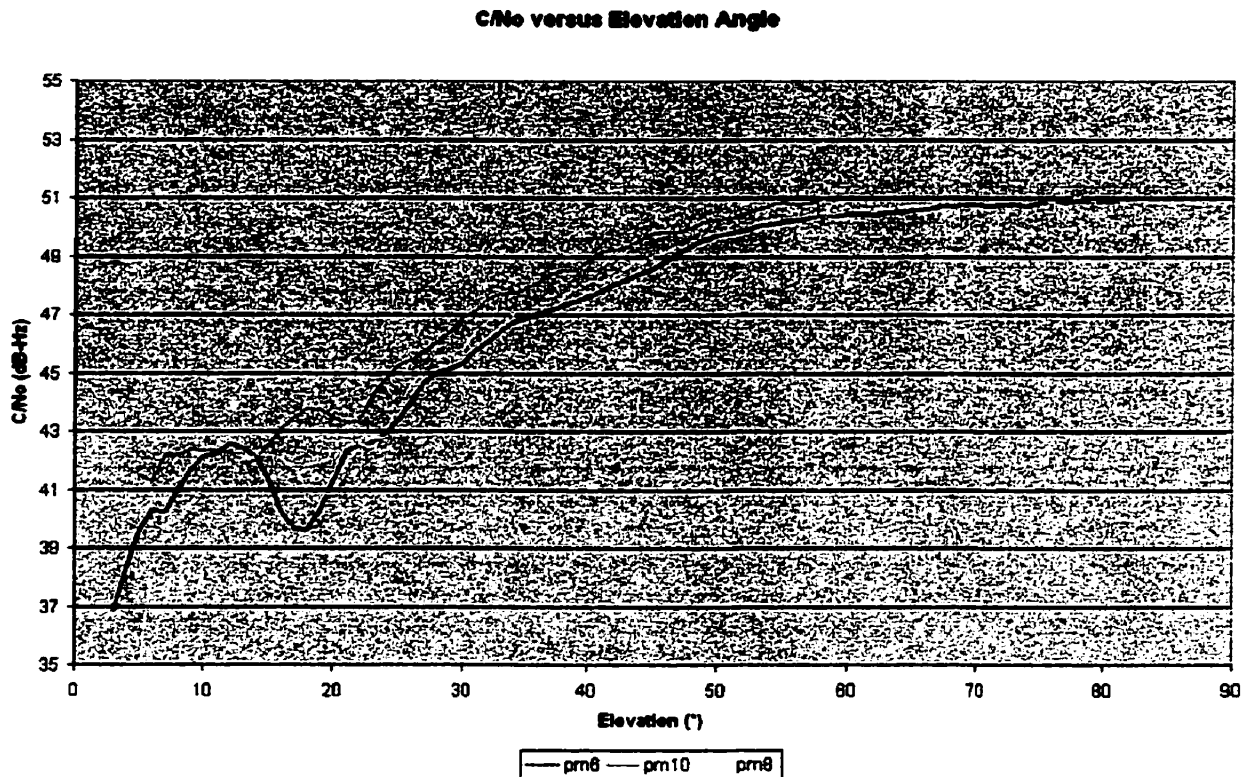


**Figure 6-1: C/No versus Elevation Angle**

When a channel initially acquires the signal, the C/No may fluctuate during the first few seconds of code lock due to initialization parameters used in the receiver. Therefore, the algorithm used began when the satellite code lock time was greater than 5 seconds. Smoothing of the measured C/No was done for 20 seconds to reduce variations due to ambient noise. The smoother used was a moving average of the form:

$$\overline{C/No}_{measured} = \frac{\sum_{i=1}^{20} (C/No)_i}{20} \quad (6-2)$$

When the satellite is not being tracked and while the filter has not reached the total sample size, no interference detection can begin. Smoothing for longer periods of time will reduce the noise on the measurements. However, the C/No measurements of the NovAtel receiver

are not inherently noisy and therefore do not require long smoothing periods.

### 6.2.1 C/No Testing Results

Figures 6-2 through 6-9 show the results of the C/No interference detection algorithm for a 100kHz, 50kHz, 25kHz, 10kHz, 5kHz, 2.5kHz, 1kHz, and 0.6kHz interferer signal respectively. The I/S is plotted along with the C/No in order to determine an adequate interference detection level. Both L1 and L2 C/No are plotted as their deviation from the expected C/No values of 40dB for L1 and 34dB for L2. The intensity and spectral characteristics of the interferer dictate the amount of the C/No drop.

We can see from Figures 6-2 to 6-9 that as the interferers' bandwidth becomes smaller, the impact on the C/No also becomes smaller. There is less deviation from the expected C/No for the narrow band interferer of 600Hz in Figure 6-9 than for the wide band interferer of 100kHz in Figure 6-2.

For interferers wider than 1kHz, the impact of the interferer on the C/No is very similar. Only when the interferer bandwidth is less than 1kHz does the impact on the C/No begin to change. In addition, depending on the exact spectral characteristics of the very narrow band interferer, a complete loss of lock on the satellite is possible if the central frequency of the interferer lies directly on a spectral line and it has a high enough I/S.

We can also note from Figure 6-2 through 6-9 that the L2 C/No is largely unaffected by the interferers centered at L1. There is only marginal variation of the L2 C/No for the 600Hz interferer at higher I/S values. As a result, interferers centered at L1 will not cause false alarms of the L2 interference detection through the use of the C/No detection method.

The same can be said about the impact of L2 interferers on the L1 C/No, as seen from Figures 6-10 through 6-15.

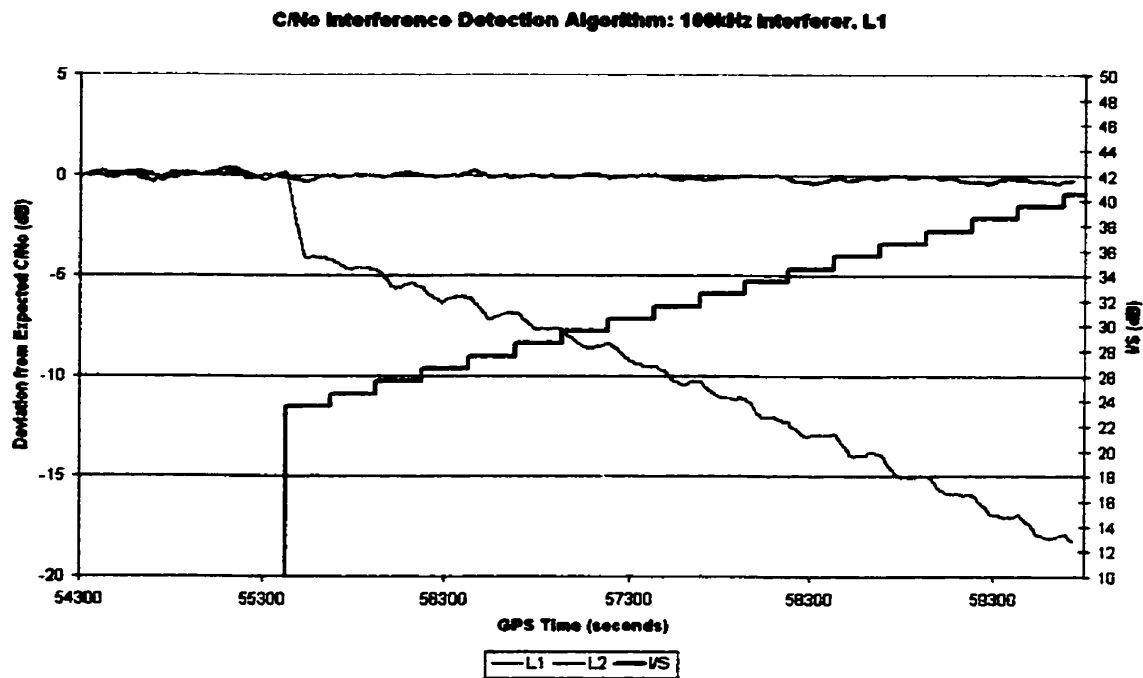


**Figure 6-2: C/No for 100kHz Interferer, centered at L1**

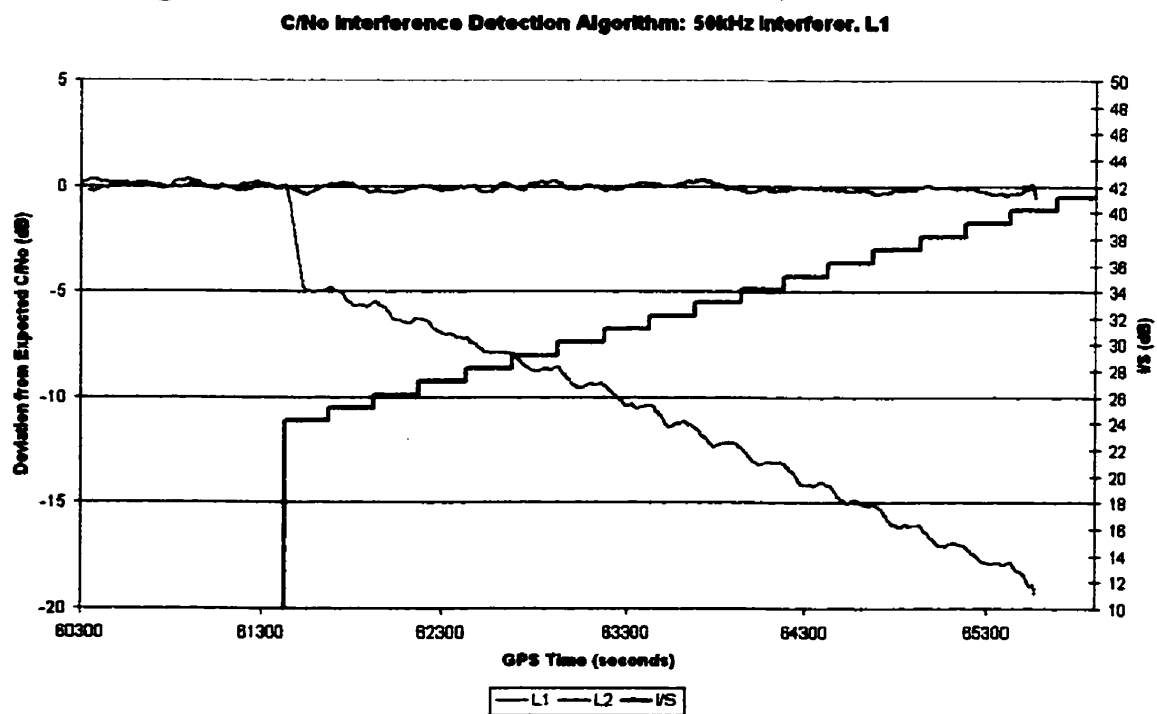


**Figure 6-3: C/No for 50kHz Interferer, centered at L1**

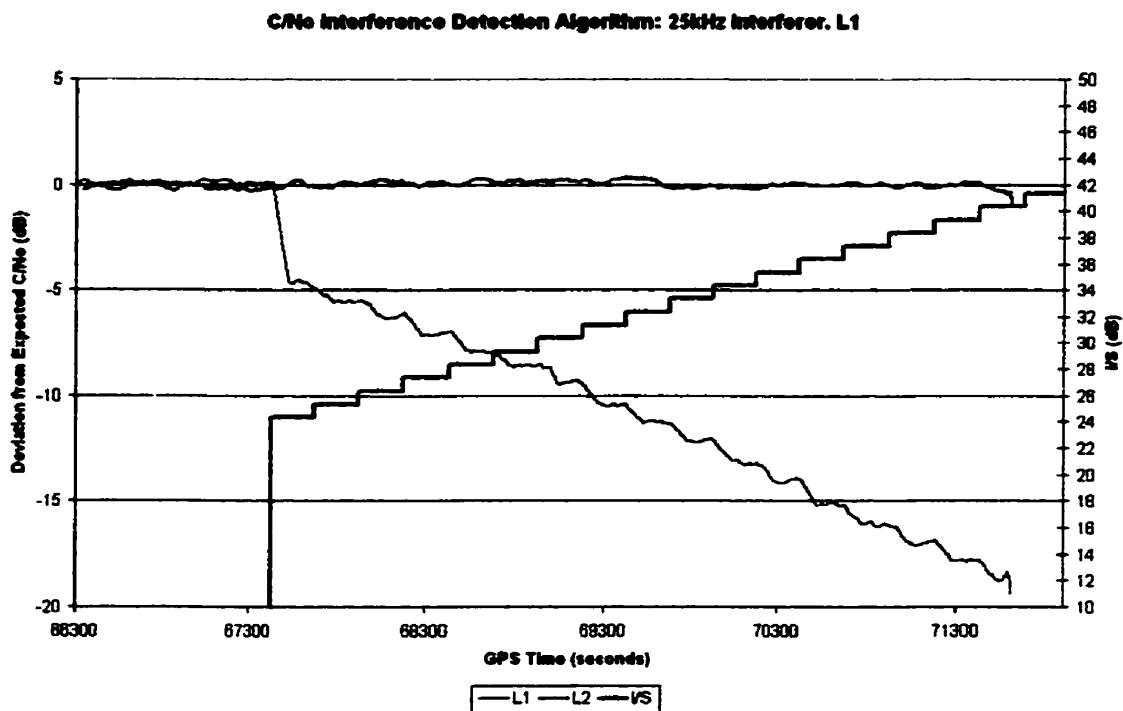


**Figure 6-4: C/N<sub>0</sub> for 25kHz Interferer, centered at L1**

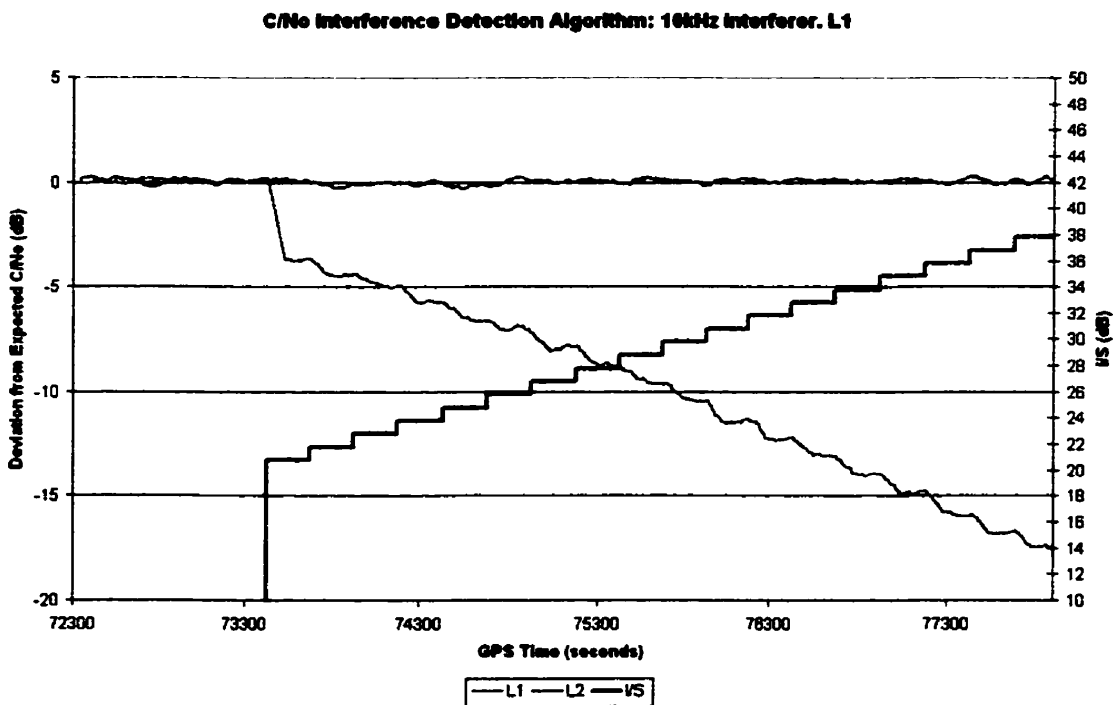


**Figure 6-5: C/N<sub>0</sub> for 10kHz Interferer, centered at L1**

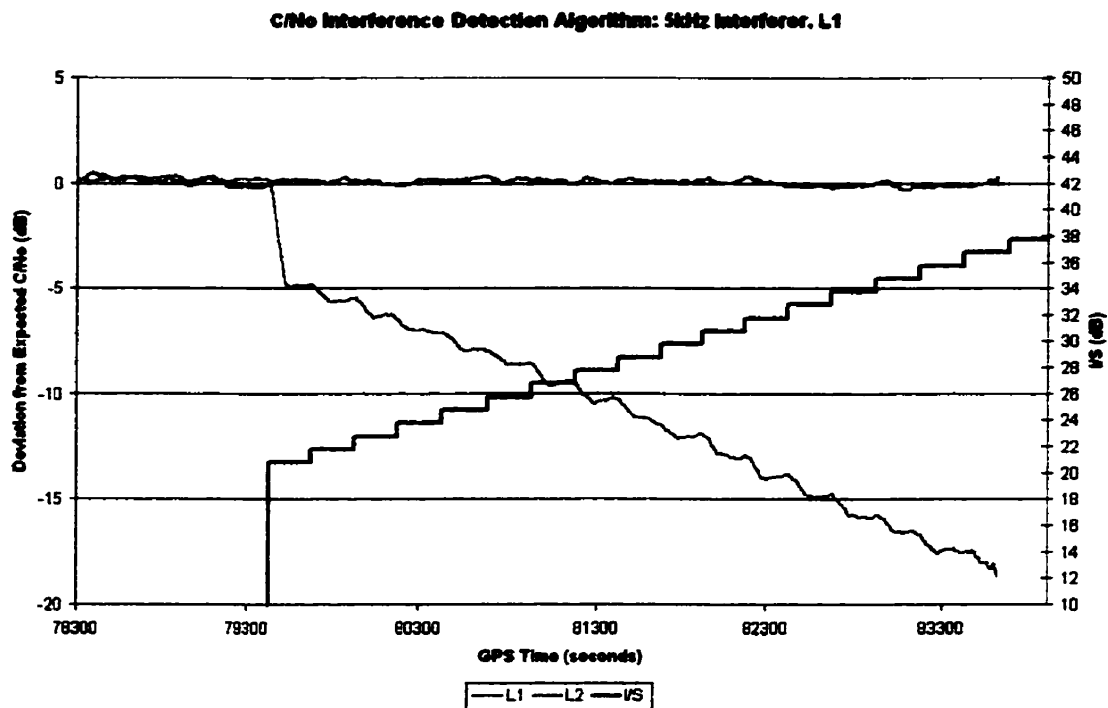


**Figure 6-6: C/N<sub>0</sub> for 5kHz Interferer, centered at L1**

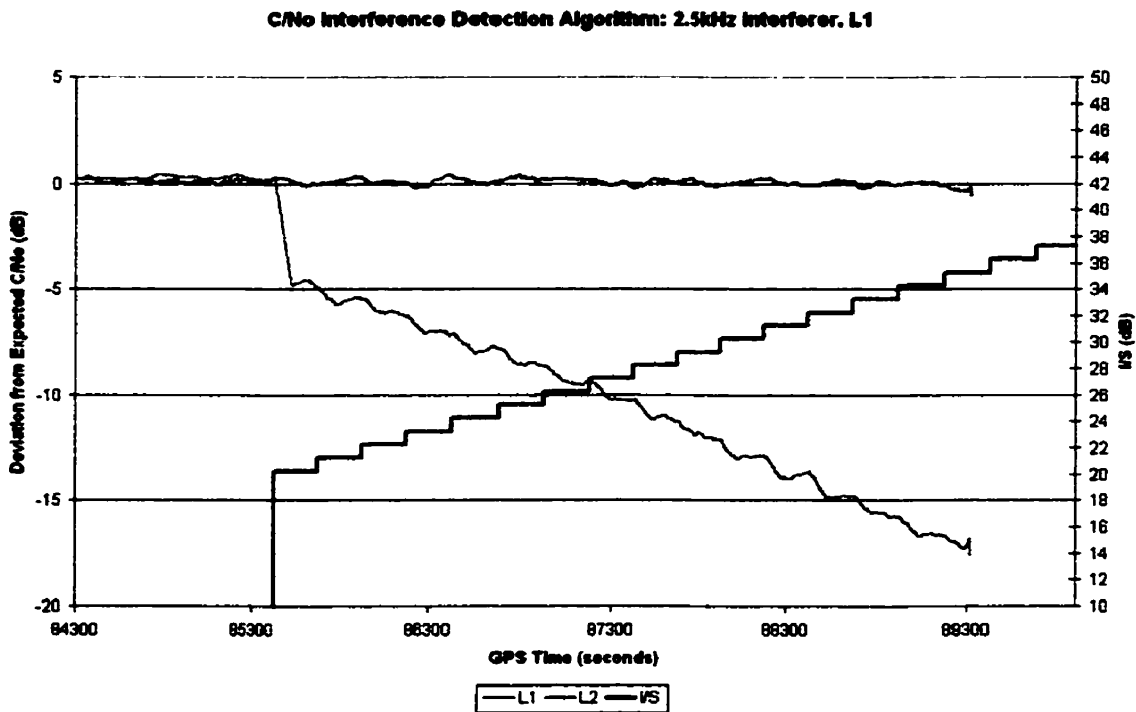


**Figure 6-7: C/N<sub>0</sub> for 2.5kHz Interferer, centered at L1**

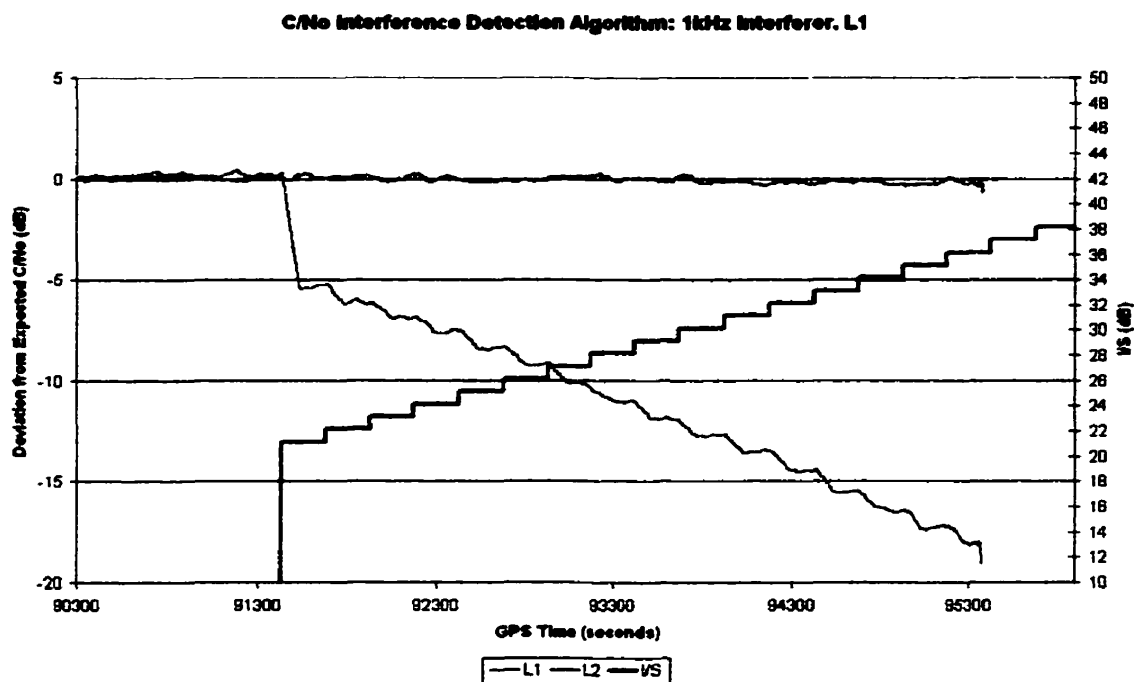


**Figure 6-8: C/No for 1kHz Interferer, centered at L1**  
**C/No Interference Detection Algorithm: 0.6kHz Interferer, L1**

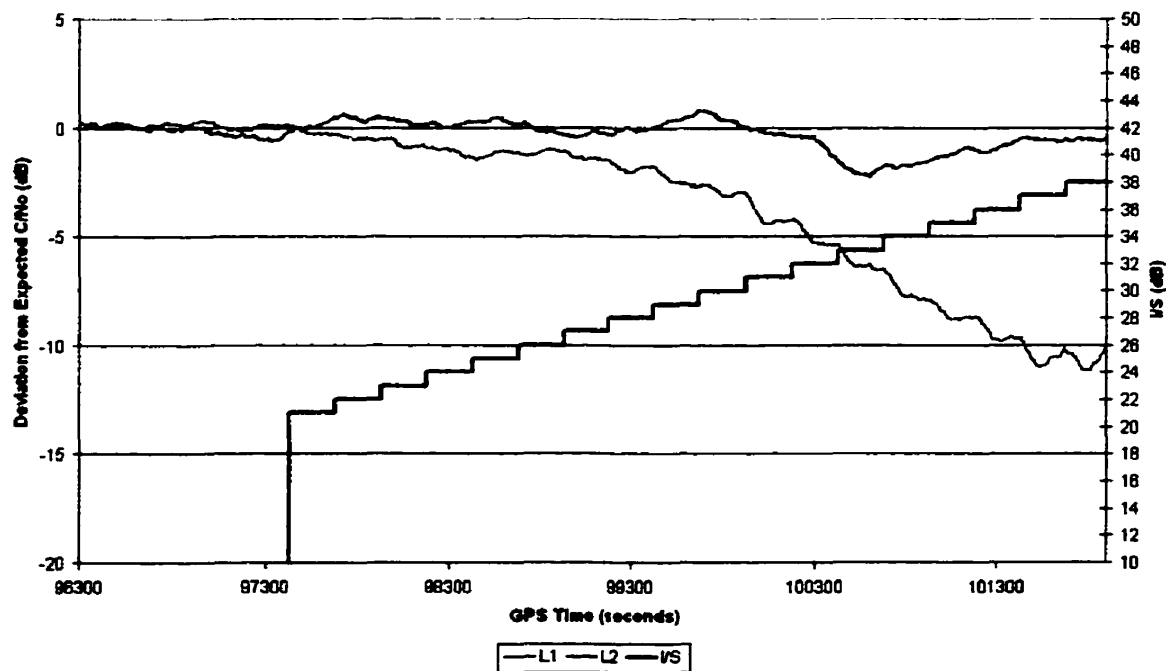


**Figure 6-9: C/No for 0.6kHz Interferer, centered at L1**

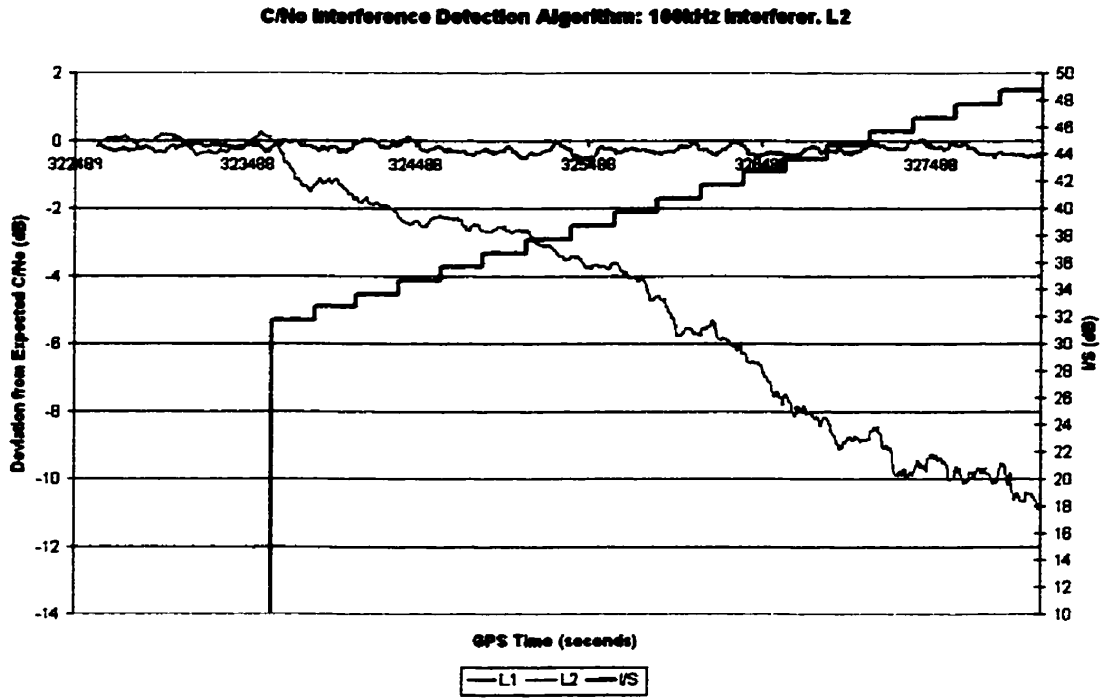


**Figure 6-10: C/No for 100kHz Interferer, centered at L2**

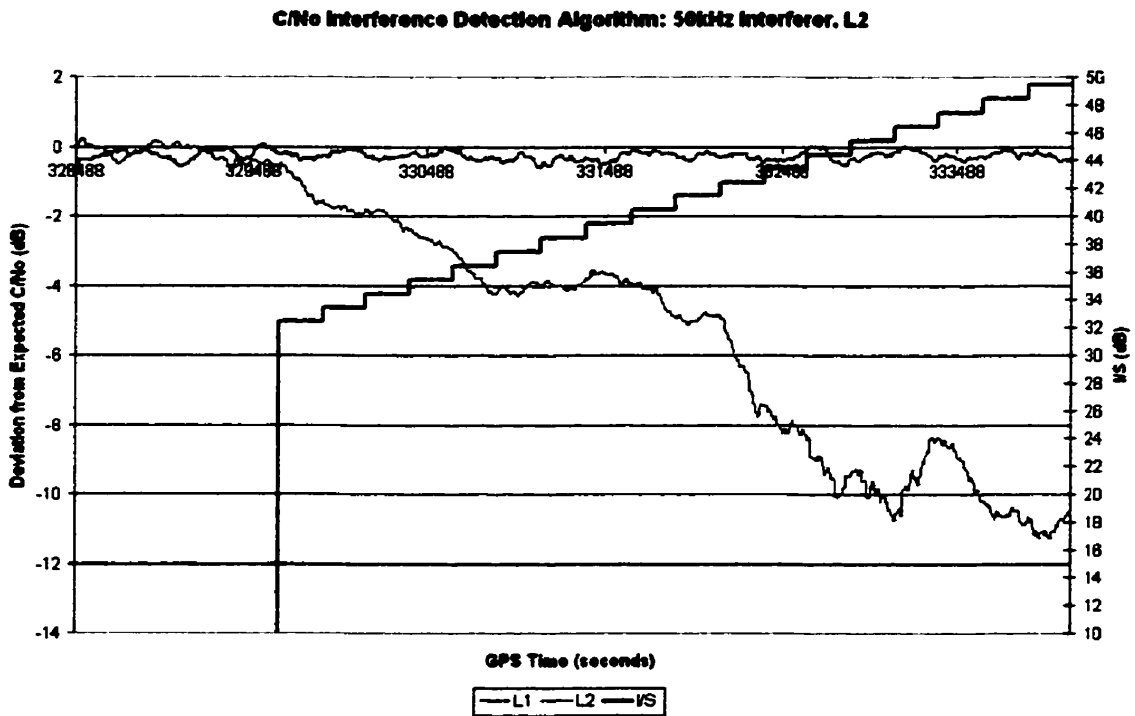


**Figure 6-11: C/No for 50kHz Interferer, centered at L2**

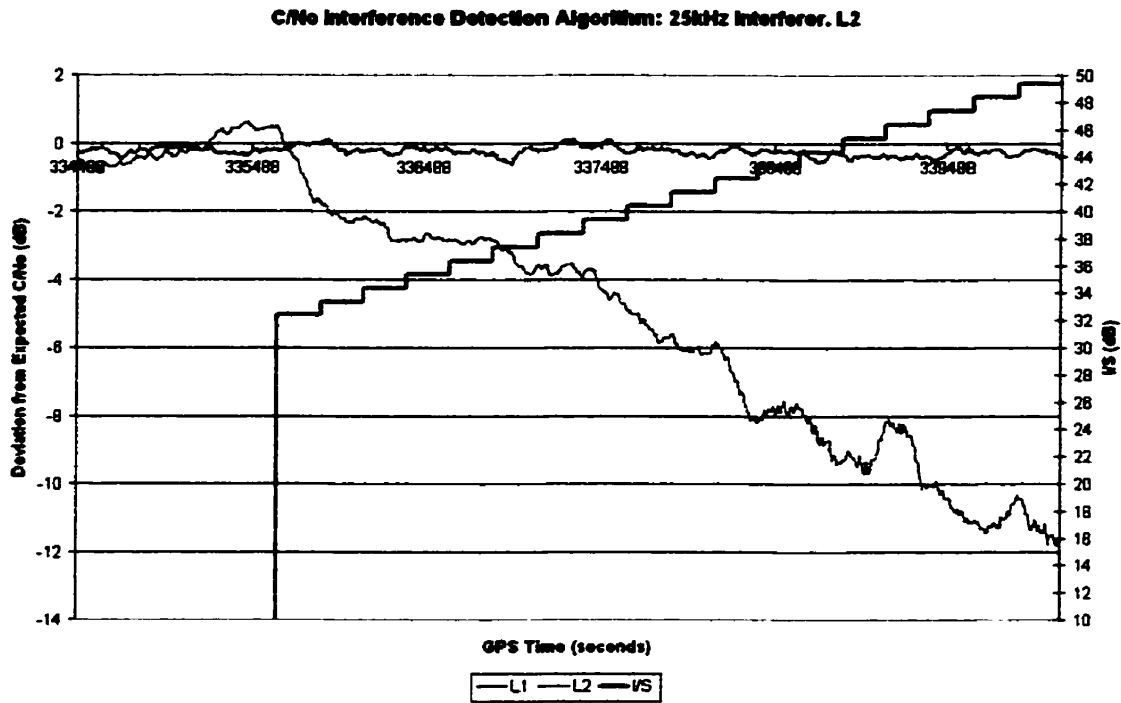


**Figure 6-12: C/No for 25kHz Interferer, centered at L2**

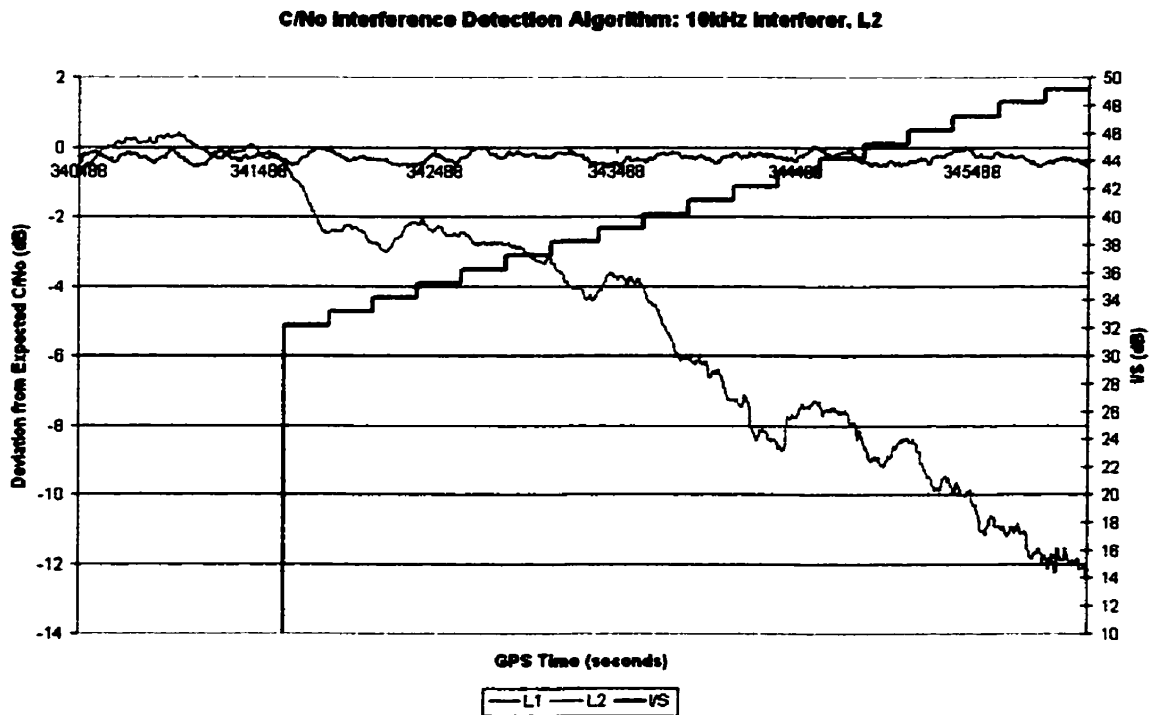


**Figure 6-13: C/No for 10kHz Interferer, centered at L2**

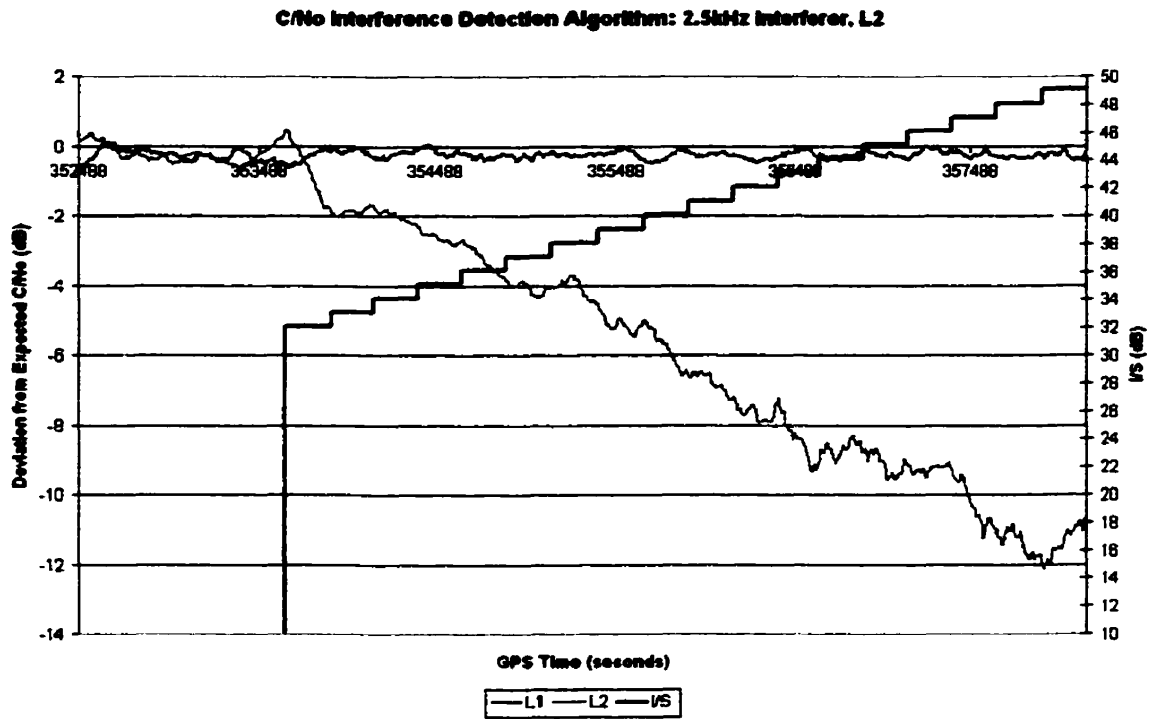


**Figure 6-14: C/No for 5kHz Interferer, centered at L2**

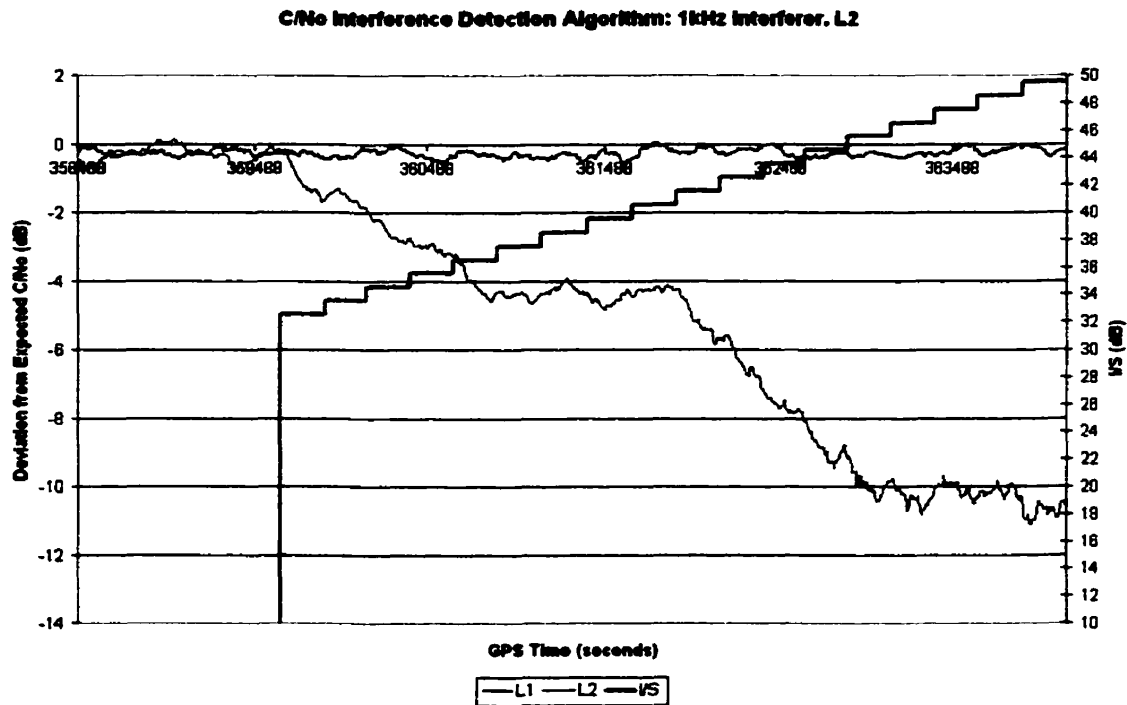


**Figure 6-15: C/No for 1kHz Interferer, centered at L2**

### 6.2.2 C/No Interference Detection Threshold

From Figures 6-2 through 6-8 we can confidently detect L1 interferers who cause a C/No deviation greater than 5dB. This level serves as a good point to limit the amount of false alarms due to multipath, as seen in Figure 6-1. A variation of 4dB for L2 would serve as good point to alarm at since the L2 C/No drops slightly less with the same intensity of interferer as L1, as seen in Figures 6-10 through 6-15 and is less susceptible to multipath because of the higher chipping rate of the P-code.

Generally, interferers with bandwidths less than 1 kHz do not affect all satellites in view while interferers with bandwidths wider than 1 kHz will affect all satellites. We can use this information as a means of further reducing the false alarms due to wider bandwidth interferer. It can be used to distinguish interference from multipath.

Using a different method of interference detection, other than the C/No method, will enable us to detect narrower bandwidth interferers that are undetectable, or not easily detectable, by this method.

### 6.3 AGC Interference Detection

As discussed in section 4.3, the AGC is based on A/D converter distribution and is therefore PRN independent. As a result, the receiver need not be tracking any satellites for the detection algorithm to be carried out.

At receiver startup, the actual bin values are adjusted to accommodate for the RF componentry on the board and will not necessarily be identical to the nominal, expected values. These calibrated bin values are then used to determine the presence of the interferer by comparing them to the current bin values using the following equation:

$$AGC\ Statistic = \sum_{i=1}^n \frac{(calibrated[i] - measured[i])^2}{calibrated[i]} \quad (6-3)$$

Where  $i$  = bin number

calibrated[ $i$ ] = calibrated AGC bin value for bin  $i$

measured[ $i$ ] = current measured AGC bin value for bin  $i$

$n$  = last bin number used for the AGC

The AGC Statistic value is not smoothed since variations due to noise will be significantly masked by the presence of interferers, as shown below.

#### 6.3.1 AGC Testing Results

Figures 6-16 through 6-23 show the AGC Statistic value (Equation 6-3) for various interferer bandwidths with increasing I/S. The AGC Statistic will indicate the presence of narrow band and CW interferers, while wide band interferers are more difficult to detect. We can see this effect as we look in succession at Figures 6-16 through 6-23. As the bandwidth of the interferer becomes smaller, our ability to detect it with the AGC becomes greater. This is the opposite effect of the C/No detection

method. As a result, both methods are complementary to each other and allow for the detection of all interferers tested.

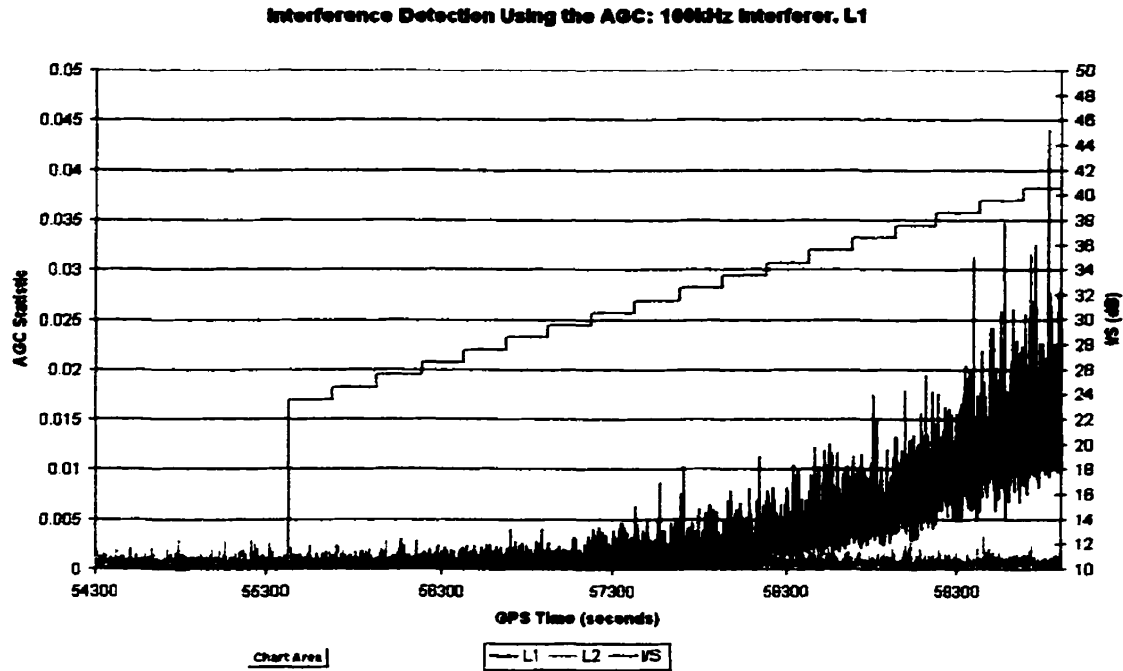


**Figure 6-16: AGC Statistic for 100kHz Interferer, centered at L1**

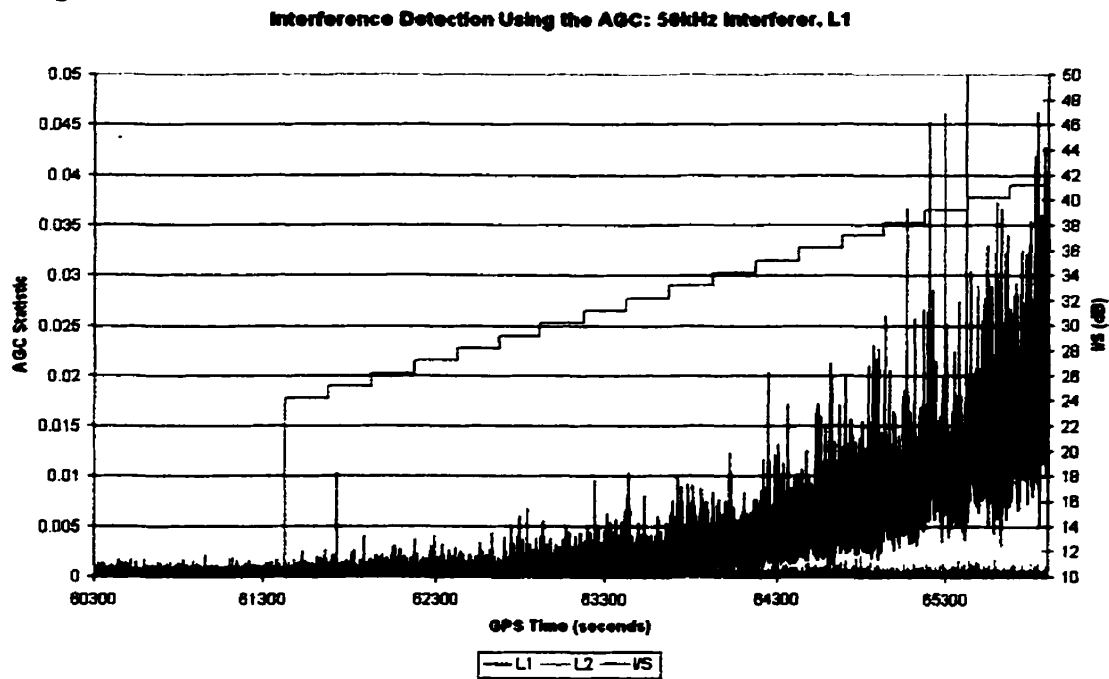


**Figure 6-17: AGC Statistic for 50kHz Interferer, centered at L1**

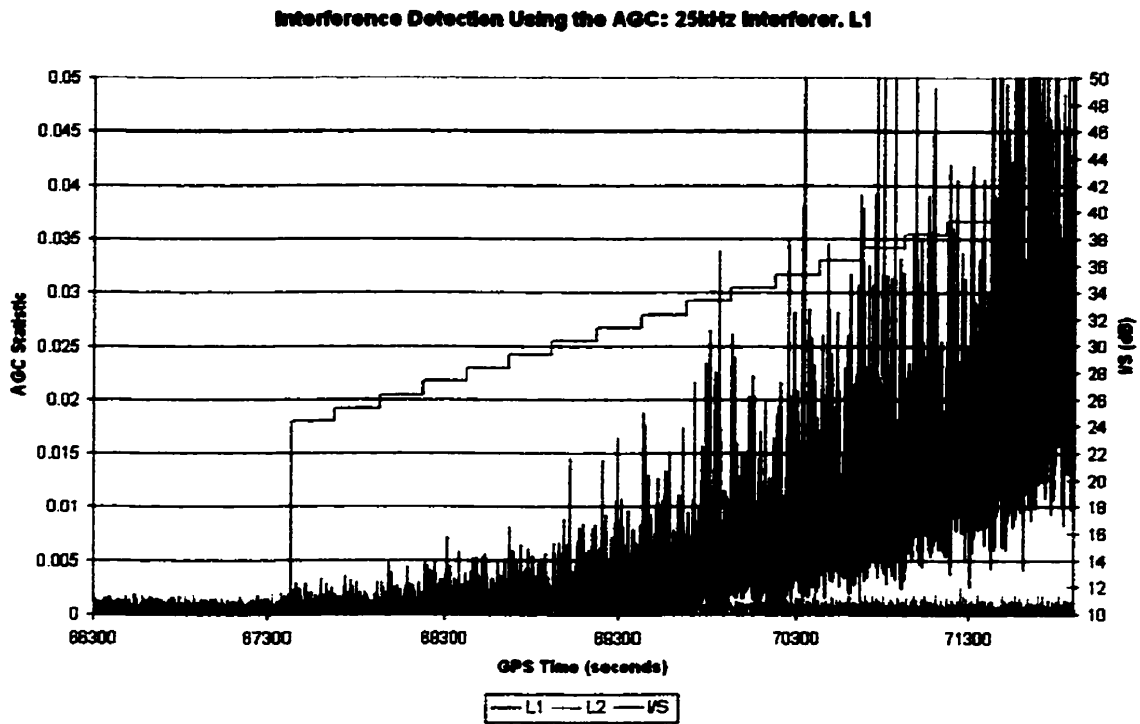


**Figure 6-18: AGC Statistic for 25kHz Interference, centered at L1**

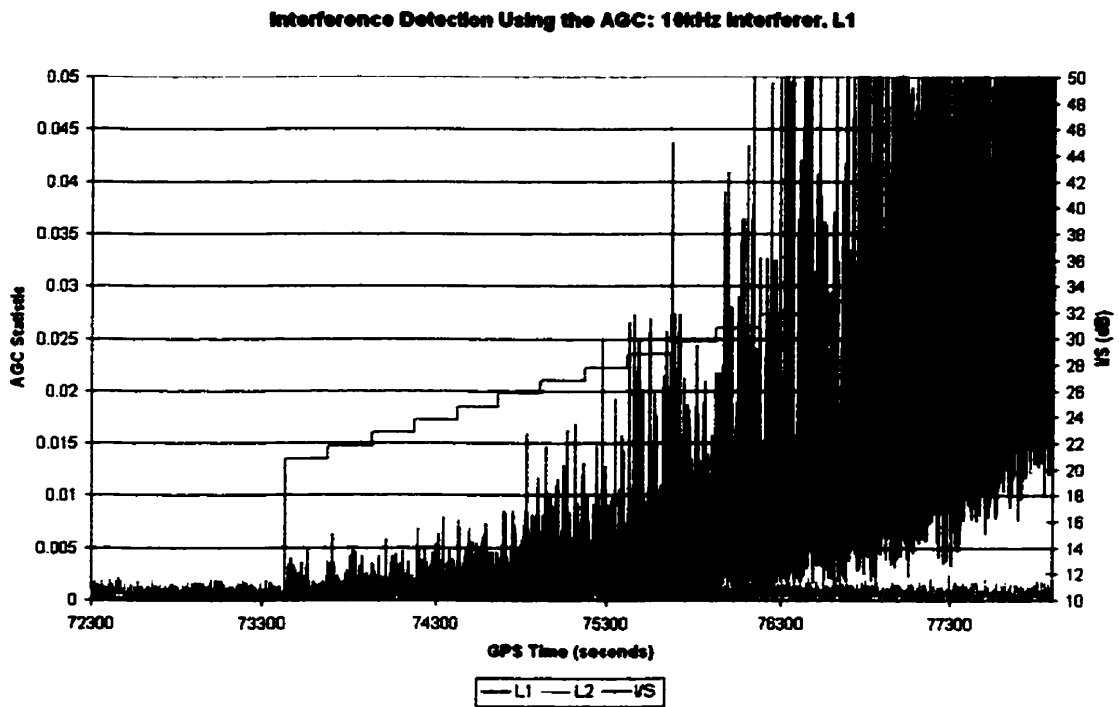


**Figure 6-19: AGC Statistic for 10kHz Interferer, centered at L1**

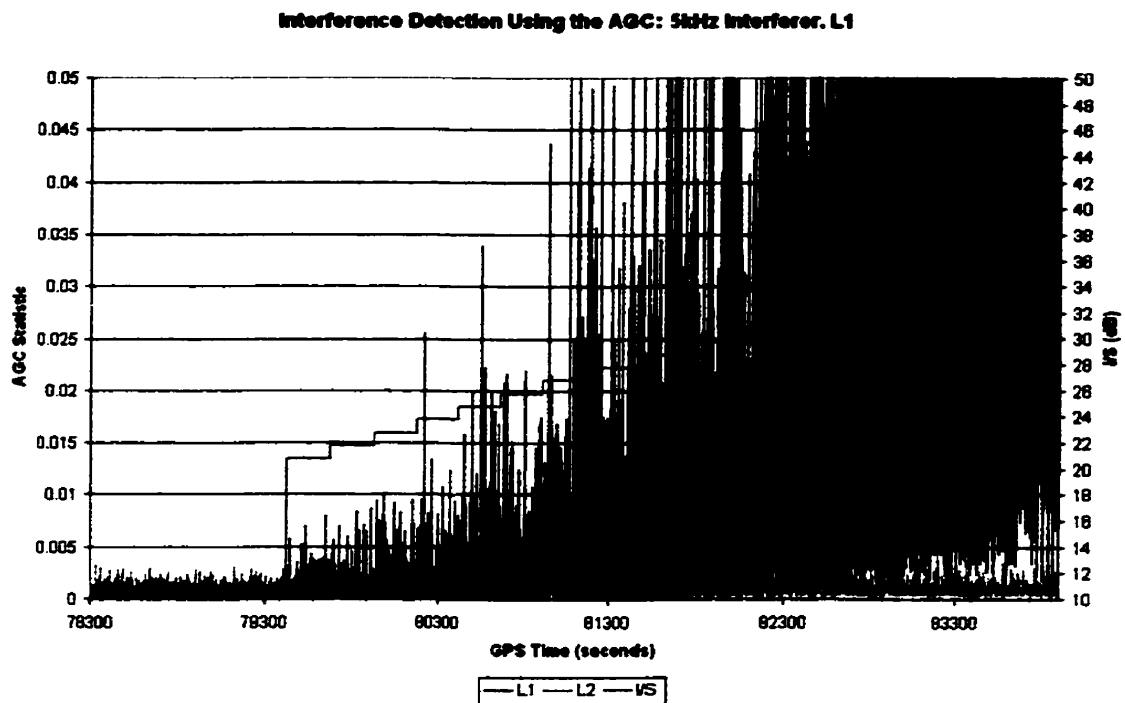


**Figure 6-20: AGC Statistic for 5kHz Interferer, centered at L1**  
**Interference Detection Using the AGC: 2.5kHz Interferer. L1**

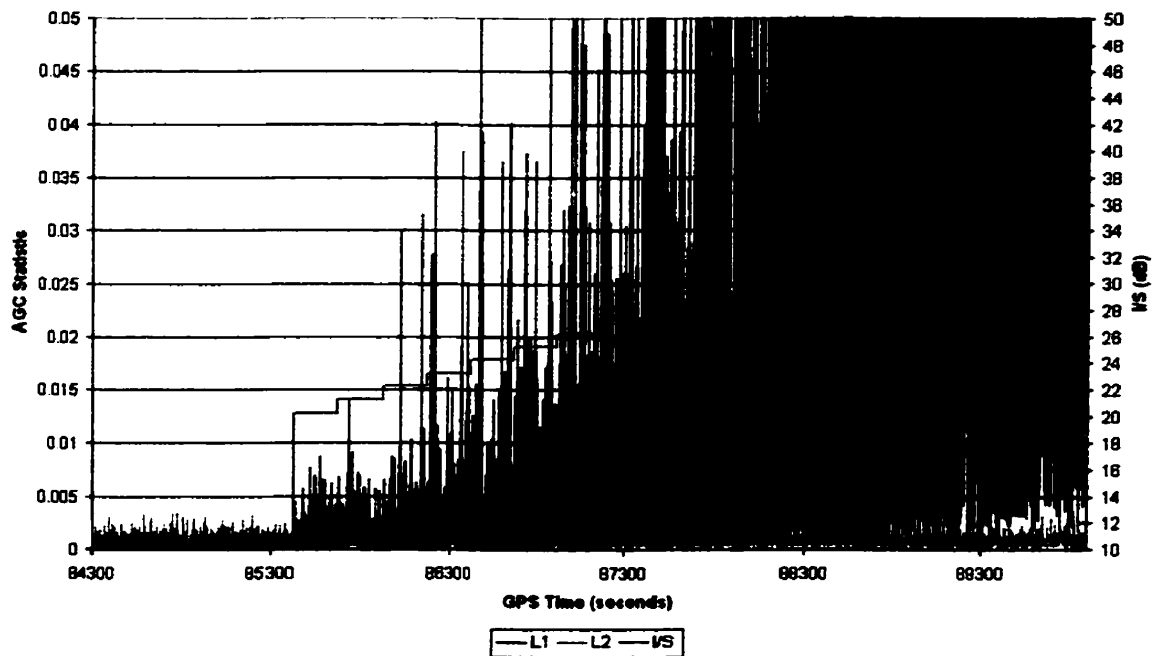


**Figure 6-21: AGC Statistic for 2.5kHz Interferer, centered at L1**

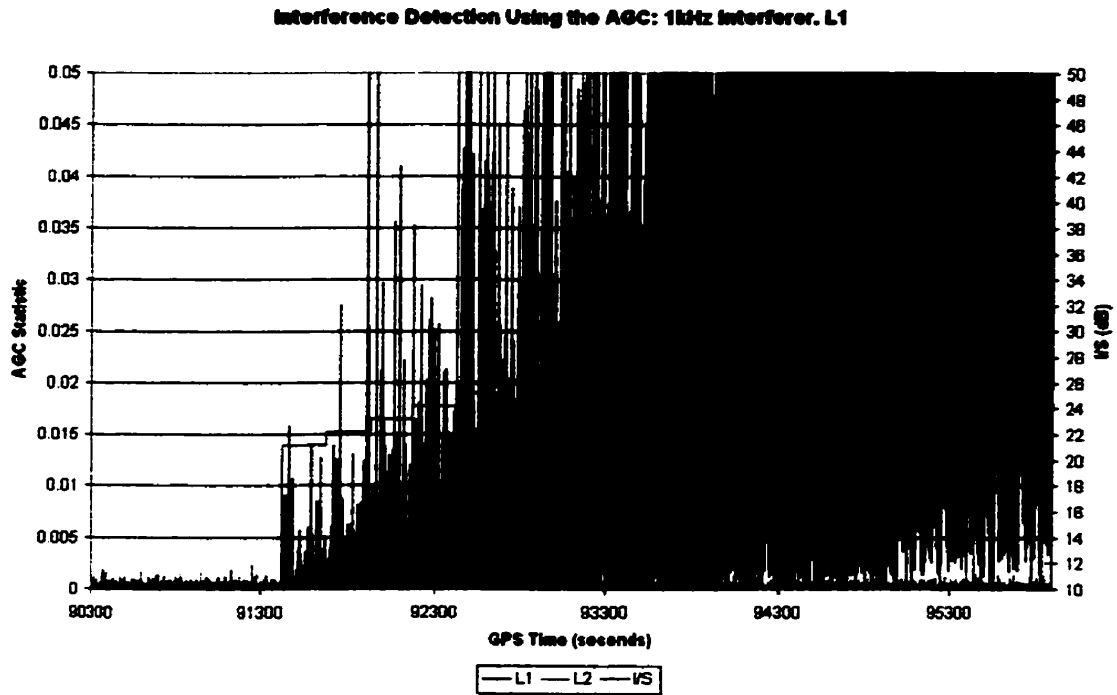


**Figure 6-22: AGC Statistic for 1kHz Interferer, centered at L1**  
**Interference Detection Using the AGC: 0.6kHz Interferer. L1**

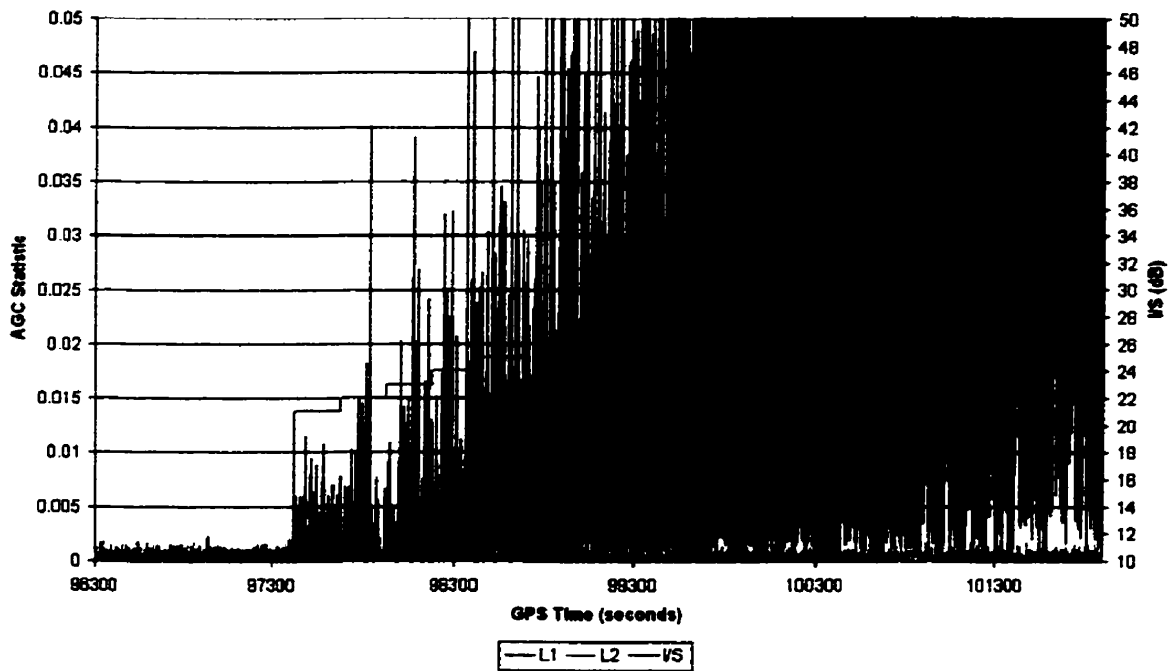


**Figure 6-23: AGC Statistic for 0.6kHz Interferer, centered at L1**

Figures 6-24 through 6-30 show the AGC Statistic value for interferers centered at L2.

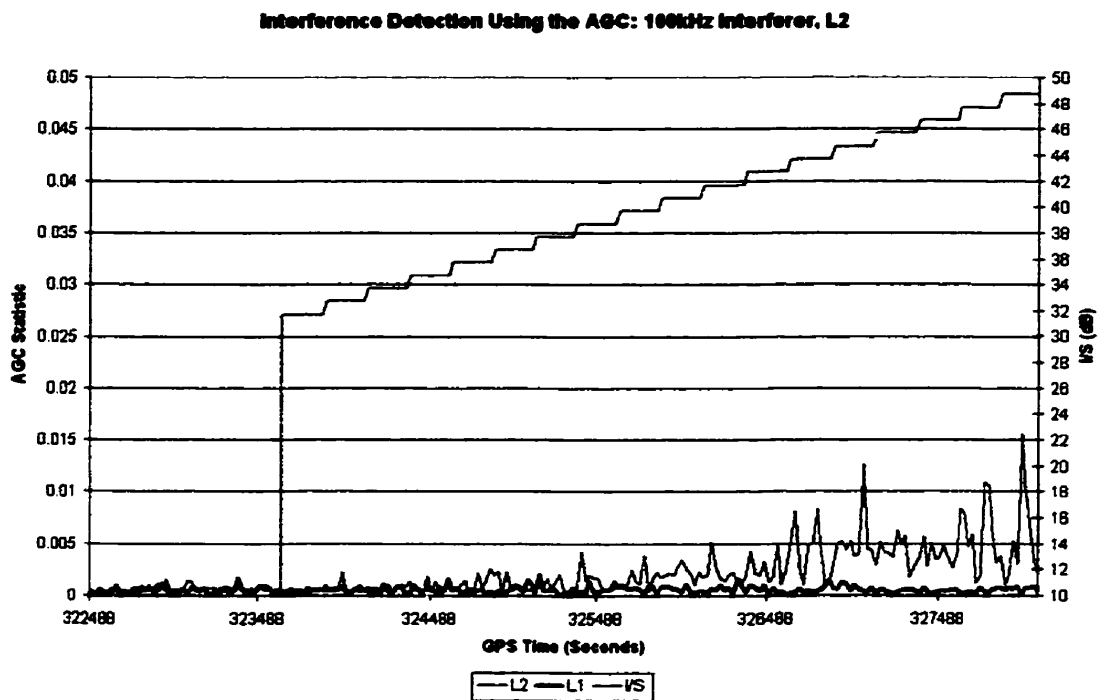


**Figure 6-24: AGC Statistic for 100kHz Interferer, centered at L2**

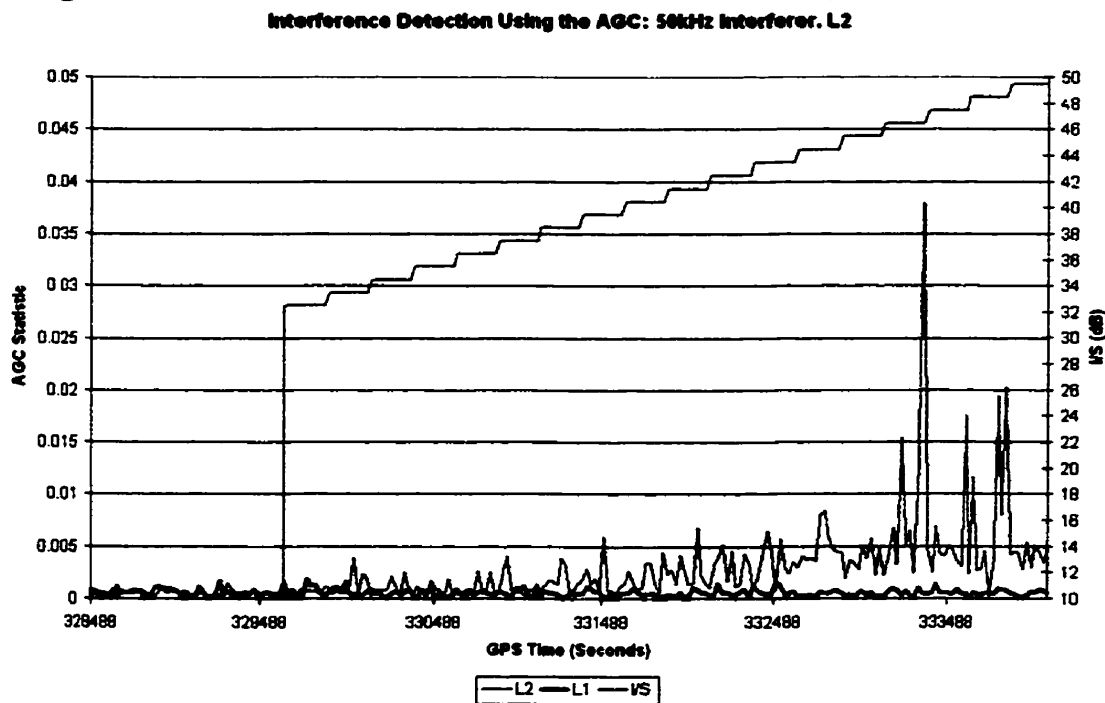


**Figure 6-25: AGC Statistic for 50kHz Interferer, centered at L2**

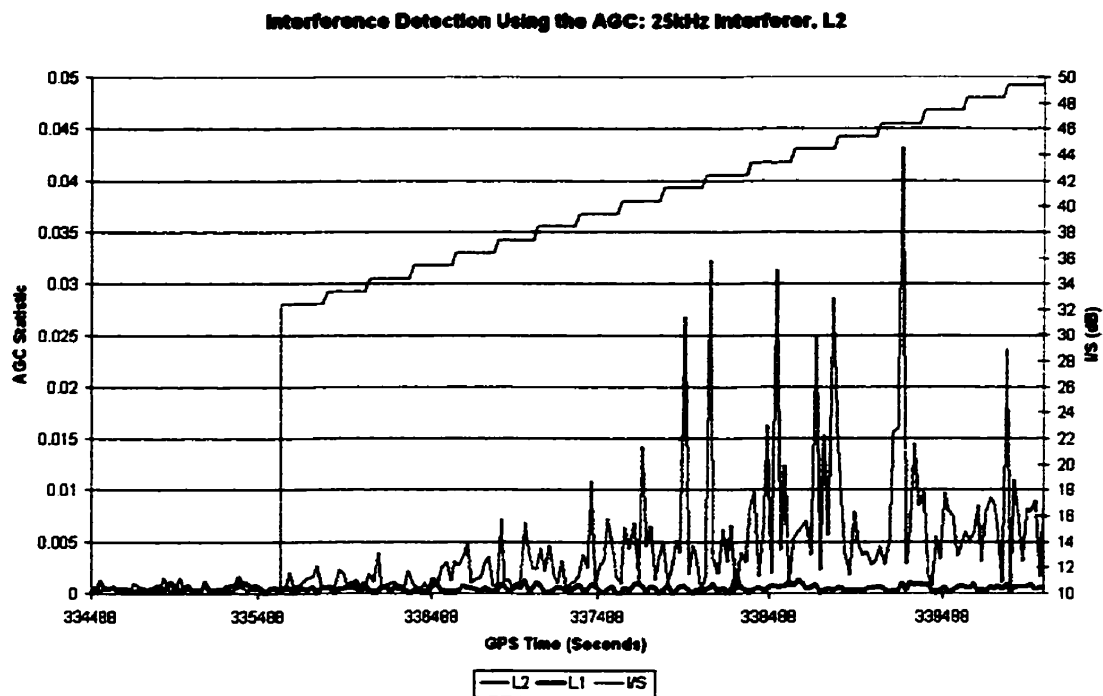


**Figure 6-26: AGC Statistic for 25kHz Interferer, centered at L2**

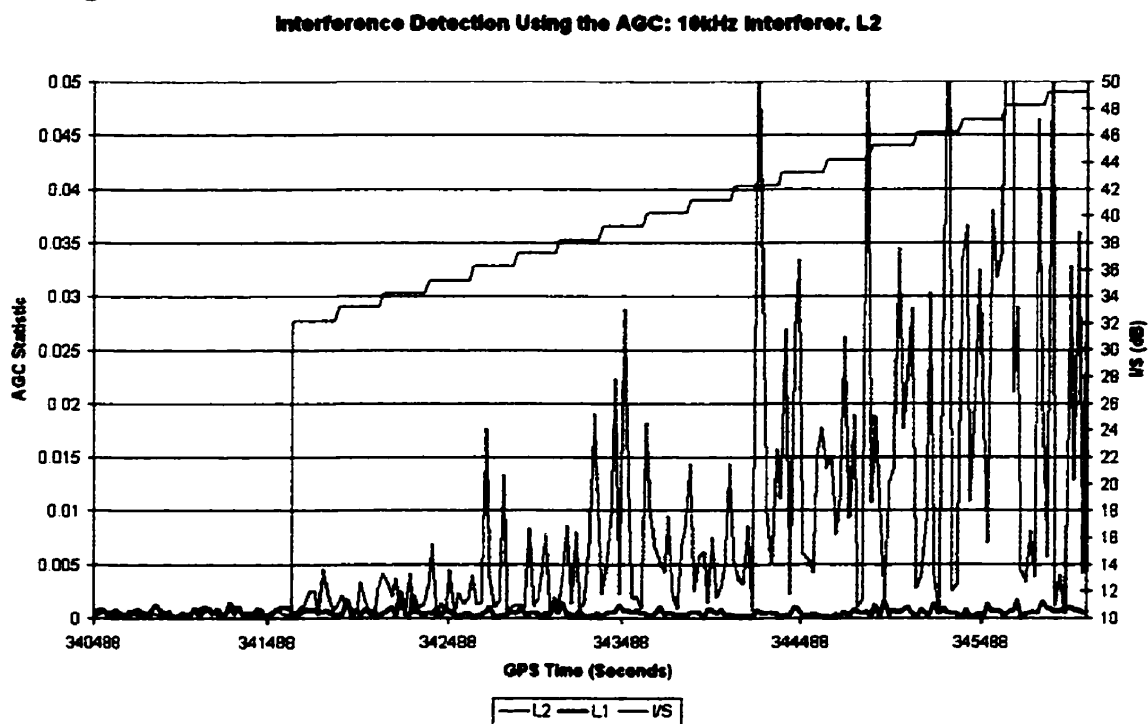


**Figure 6-27: AGC Statistic for 10kHz Interferer, centered at L2**

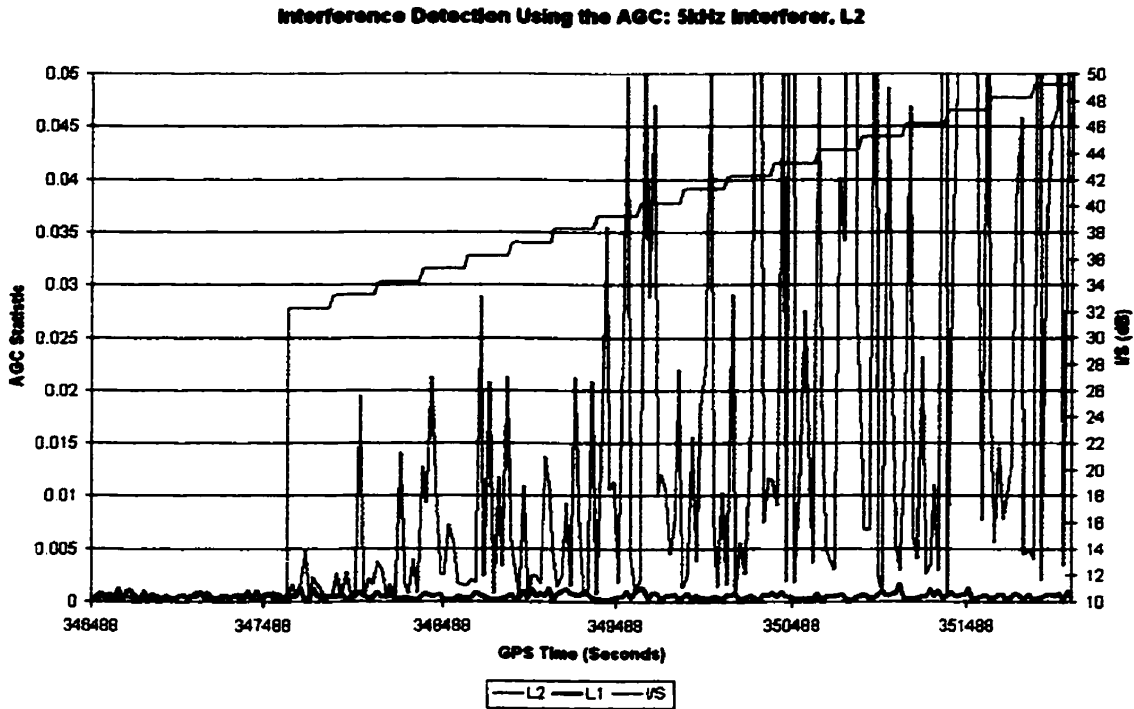


**Figure 6-28: AGC Statistic for 5kHz Interferer, centered at L2**

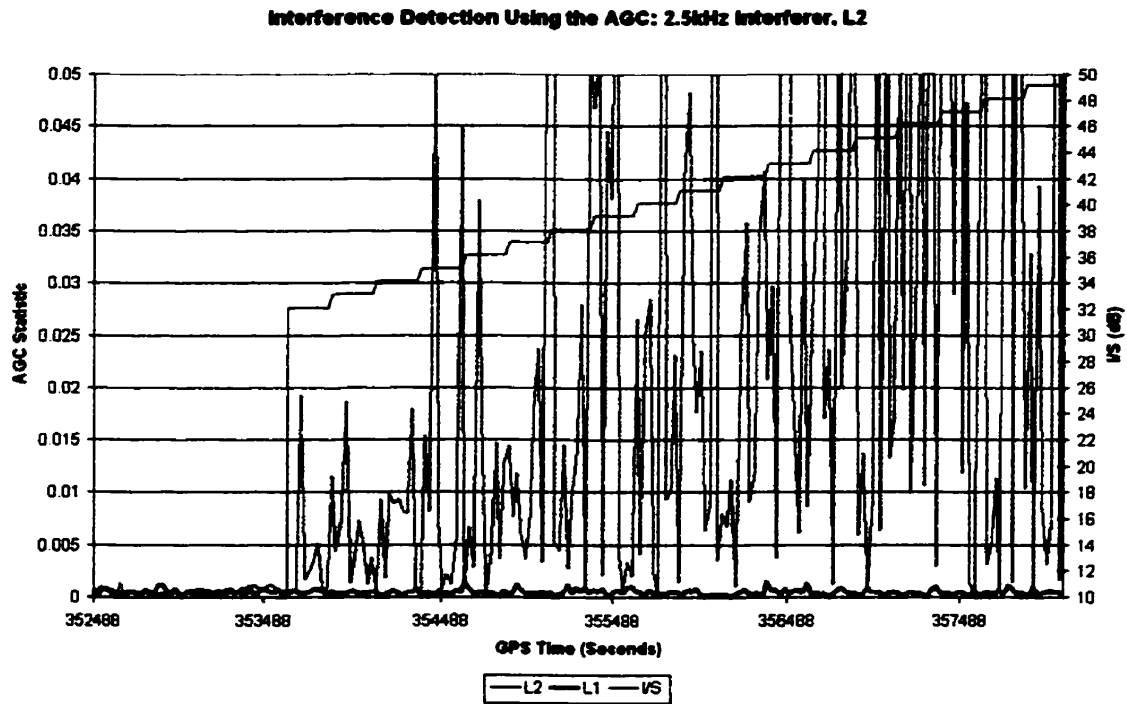


**Figure 6-29: AGC Statistic for 2.5kHz Interferer, centered at L2**

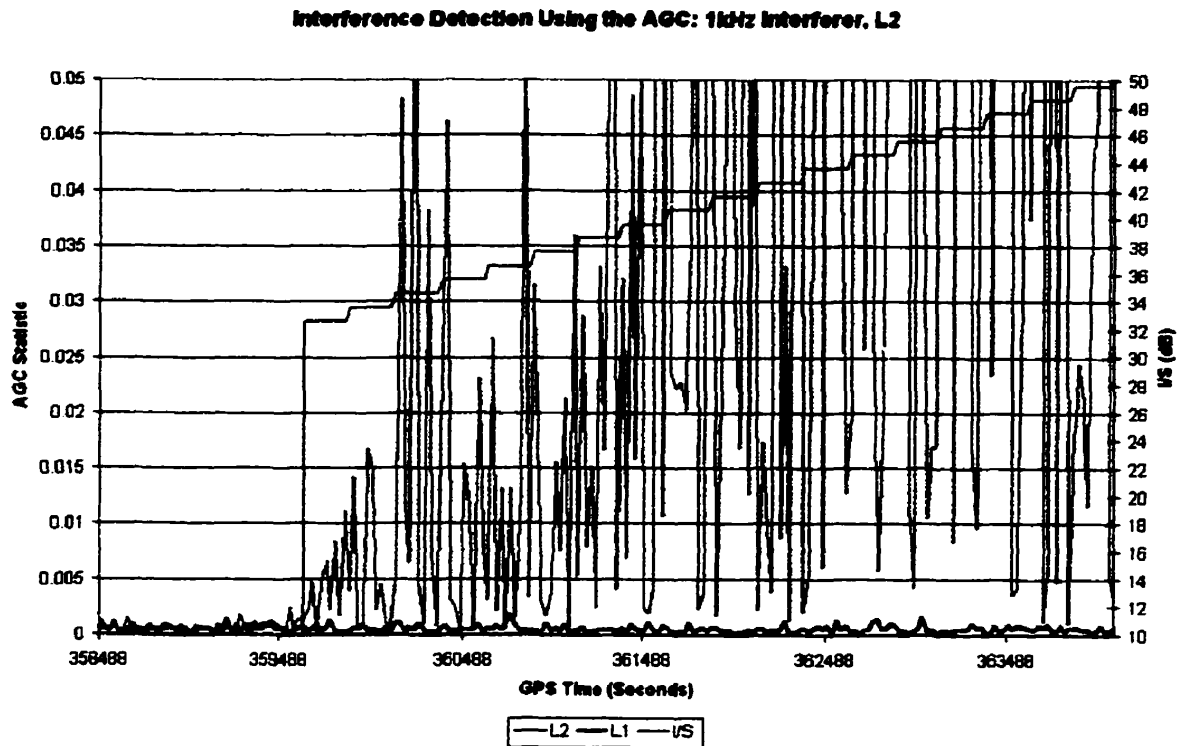


**Figure 6–30: AGC Statistic for 1kHz Interferer, centered at L2**

### 6.3.2 AGC Interference Detection Threshold

Using thresholds of 0.005 for L1 and 0.005 for L2 allow for the detection of narrow bandwidth interferer. Typically, the AGC statistic for both is approximately half the detection threshold. Using the chosen values for the indication will provide for adequate detection of narrow band interferers. Also, since the AGC statistic is PRN independent, it does not suffer from false alarms due to multipath or similar signal distortions. As the C/No method does.

From Figures 6–24 through 6–30, we can see that the variation in the AGC Statistic is just as pronounced with the L2 interferers as with the L1 interferers.

Using detection thresholds of 0.005 for both L1 and L2 will allow for the immediate detection of interferers with bandwidths less than 5kHz (when centered at L1) when the I/S is greater than 21dB for L1 and 32dB for L2. The I/S must be slightly higher to detect wider bandwidth interferers. However, the C/No detection method will detect these wider bandwidth interferers more readily. Using both methods together, wider bandwidth interferers will be detected by the C/No method and narrower bandwidths by the AGC.

#### **6.4 Standard Deviation of the WBC**

In addition to examining the C/No and AGC Statistic, it was theorized that by examining the standard deviation of the wide band code range corrections ( $\sigma$ WBC), we could detect interference. The  $\sigma$ WBC could potential add information to our SQM scheme.

##### **6.4.1 Background $\sigma$ WBC Information**

Under nominal conditions,  $\sigma$ WBC will follow the equation:

$$\sigma WBC = \sqrt{\frac{T * D}{2 * S / No}} * codeLength \quad (6-4)$$

**Where**      **T = accumulation time of the I and Q samples for the WBC; 1 second**  
                  **D = correlator spacing of the receiver;**  
                  **S/No = Signal to Noise ratio**  
                  **codeLength = 293.052256 for C/A code on L1 and 29.3052256 for P code on L2**

The S/No is related to the C/No by equation 4-1 and is calculated from equation 4-2. Since the  $\sigma$ WBC uses the S/No in its theoretical calculation and the S/No will be affected by any interference source (as seen in section 6.2), the above equation is used for theoretical calculations. For this same reason, in the algorithm for interference detection we need to have a lookup table for the expected S/No with respect to elevation angle.

For the detection of excessive interference using the WBC, we will be checking the following ratio:

$$\left[ \sum_{i=0}^k \left[ \sqrt{\frac{\sum_{n=0}^m (\overline{WBC} - WBC_n)^2}{m-1}} \right] \right] / \sqrt{\frac{T * D}{2 * S / N_o}} * 293.052256 > \text{threshold} \quad (6-5)$$

Where

- $n$  = wide band correction sample number
- $m$  = size of the WBC sample space used in the calculation of the standard deviation
- $i$  = standard deviation smoothing sample number
- $k$  = length of smoothing
- $\overline{WBC}$  = mean wide band correction value over the sample space  $m$
- $WBC_n$  = wide band correction sample  $n$
- $T$  = accumulation time of the I and Q samples for the WBC
- $D$  = correlator spacing of the receiver
- $S/No$  = Signal to Noise ratio, from lookup table

Using a sample space of  $m=100$  will give sufficient statistical information from the sample space to provide accurate results. This means that the  $m^{\text{th}}$  measurement will be the most recent measurement from the receiver, and the samples from  $n=0$  to  $n=m$  will be from past measurements. For every second after the initial sample size has been collected, the oldest sample will be removed from the calculation of the mean and replaced with the newest sample (i.e. a moving average). This moving average is used in the calculation of the standard deviation. The rationale for using a moving average,  $\overline{WBC}$ , is in order to detect any short-term jumps in the mean.

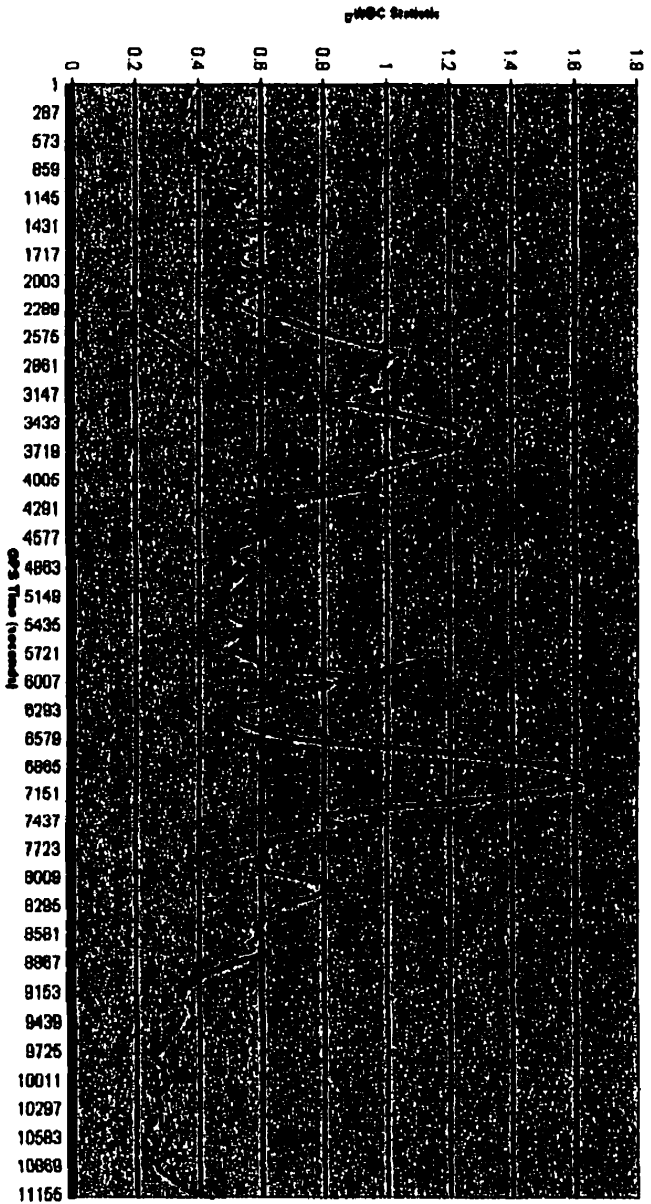
The calculated standard deviations are then smoothed over the period  $i=0$  to  $i=k$  to reduce the overall algorithm noise. A smoothing time of  $k=100$  seconds was found to sufficiently reduce the noise. By calculating a moving average of the standard deviation we will detect any changes that would have otherwise been missed by using a much larger sample space with no smoothing.

Figure 6–31 and 6–32 below show the justification for the chosen sample space and smoother values, using two different data sets. Figure 6–31 shows the impact of a different sample space while keeping the smoothing value constant at 100 seconds. We can see that at a sample size of 10, there are significantly fewer distortions observed since we do have sufficient statistical information to observe the underlying trend. As well, variations between a 100 second and 200 second sample space are negligible. This negligible change suggests that the 100 second sample space will be a better choice since it will reduce the filter startup time by 100 seconds (as compared to the 200 second smoother) without impacting the results.

Figure 6–32 shows the impact of a different smoothing length while keeping the same standard deviation sample space of 100 seconds. We can see that the 100 second smoother adequately removes the jumps visible in the 10 second smoother curve. The 200 second smoother offers no visible advantage over the 100 second smoother. In fact, it may smooth through some of the variations that we are intending to observe and identify, if short bursts of interference are present.

Data used to generate Figures 6–31 and 6–32 was taken from live data collected from the NovAtel rooftop. In order to observe changes in the trends over short periods, data was used from a low elevation satellite as it was setting near the horizon. Both figures show different periods of time during the setting of the satellite.

**$\sigma$ WBC Ratio for Interference Detection, PRTM, EGNOSSTD  
(for different  $\sigma$  sample size and a 100 second smoother)**



**Figure 6-31 :  $\sigma$ WBC Ratio for different standard deviation sample sizes**

**$\sigma$ WBC Ratio for Interference Detection, PRTM, EGNOSSTD  
(for different smoothing times and a sample space of 100)**

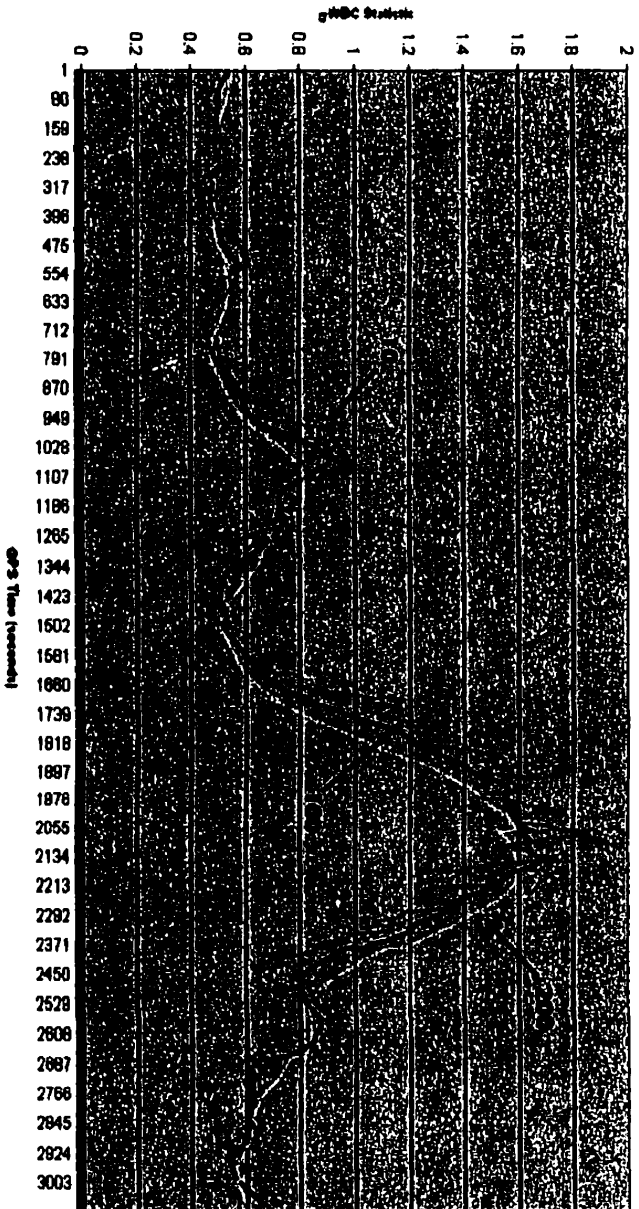


**Figure 6-32:  $\sigma$ WBC Ratio for different smoothing lengths**

### 6.4.2 WBC Testing Results

With data used from the same interference testing, as done in sections 6.2 and 6.3, the  $\sigma$ WBC interference detection results are shown below. The data was plotted using a standard deviation sample space of 100 seconds. The output standard deviations were then smoothed over a period of 100 seconds.

The expected value for each of the  $\sigma$ WBC ratios is 1.0. At that value, the metric value exactly matches the predicted value. The metric needs to grow well above a value of 1.0 for the ratio to indicate the presence of interference. When the metric is below 1, the measured  $\sigma$ WBC is less than the expected value and does not indicate a failure of interference of any sort.

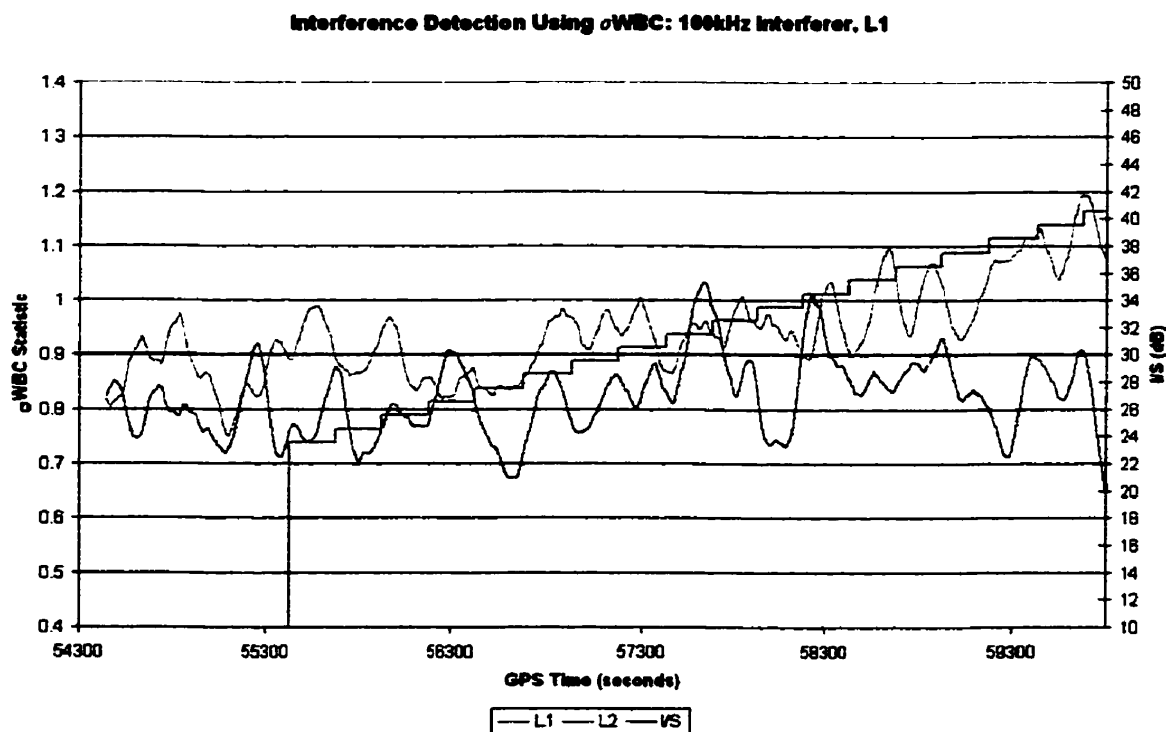


**Figure 6-33:  $\sigma$ WBC for 100kHz Interferer, centered at L1**

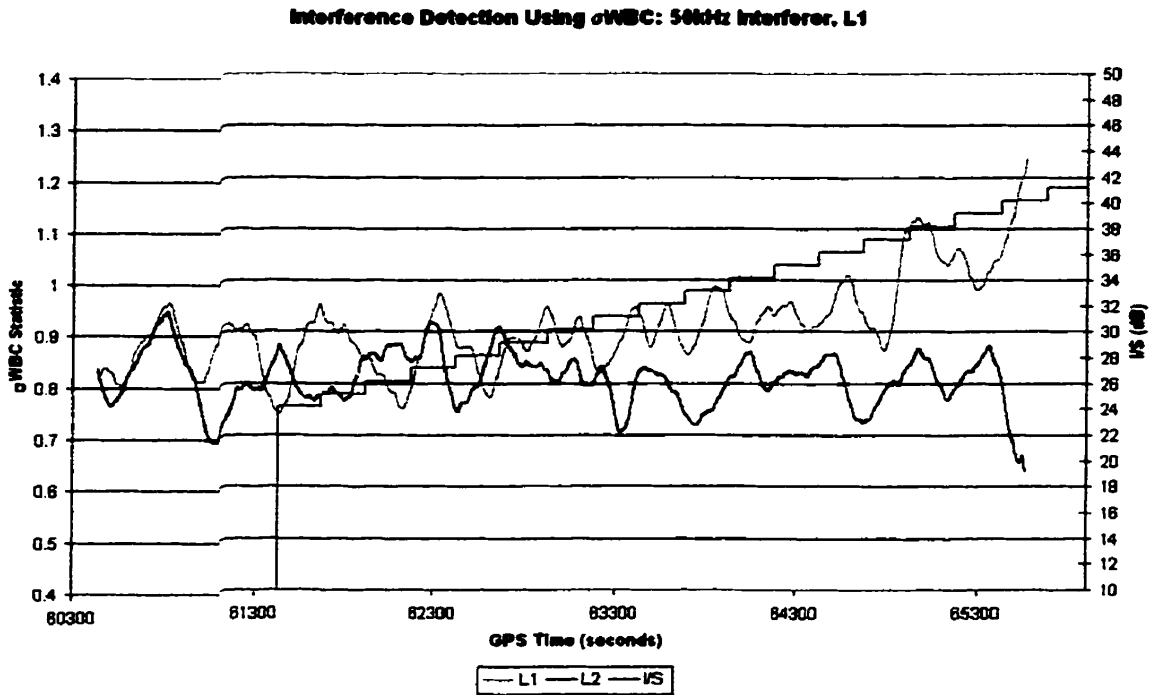


**Figure 6-34:  $\sigma$ WBC for 50kHz Interferer, centered at L1**  
Interference Detection Using  $\sigma$ WBC: 25kHz Interferer, L1

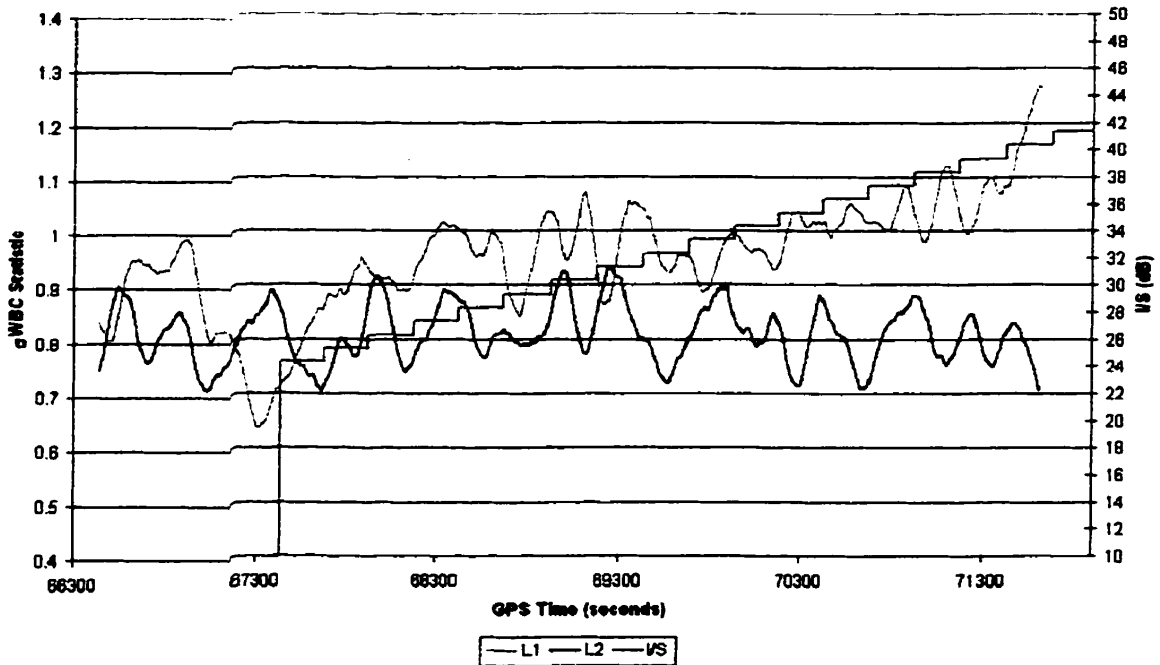


**Figure 6-35:  $\sigma$ WBC for 25kHz Interferer, centered at L1**

Interference Detection Using  $\sigma$ WBC: 10kHz Interferer. L1

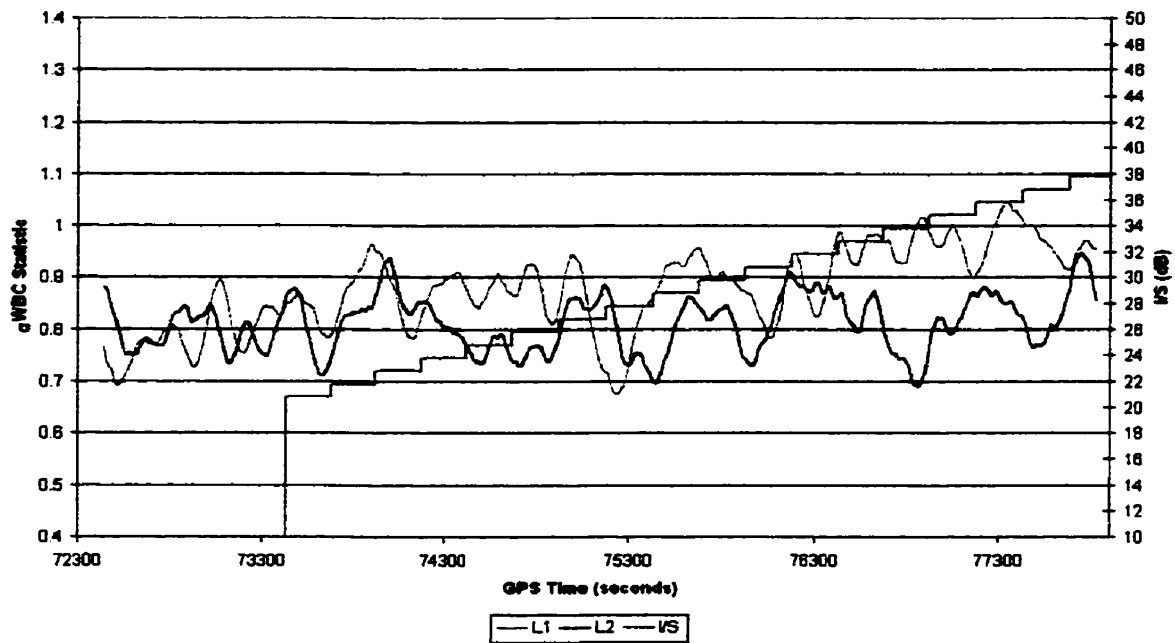


Figure 6-36:  $\sigma$ WBC for 10kHz Interferer, centered at L1

Interference Detection Using  $\sigma$ WBC: 5kHz Interferer. L1

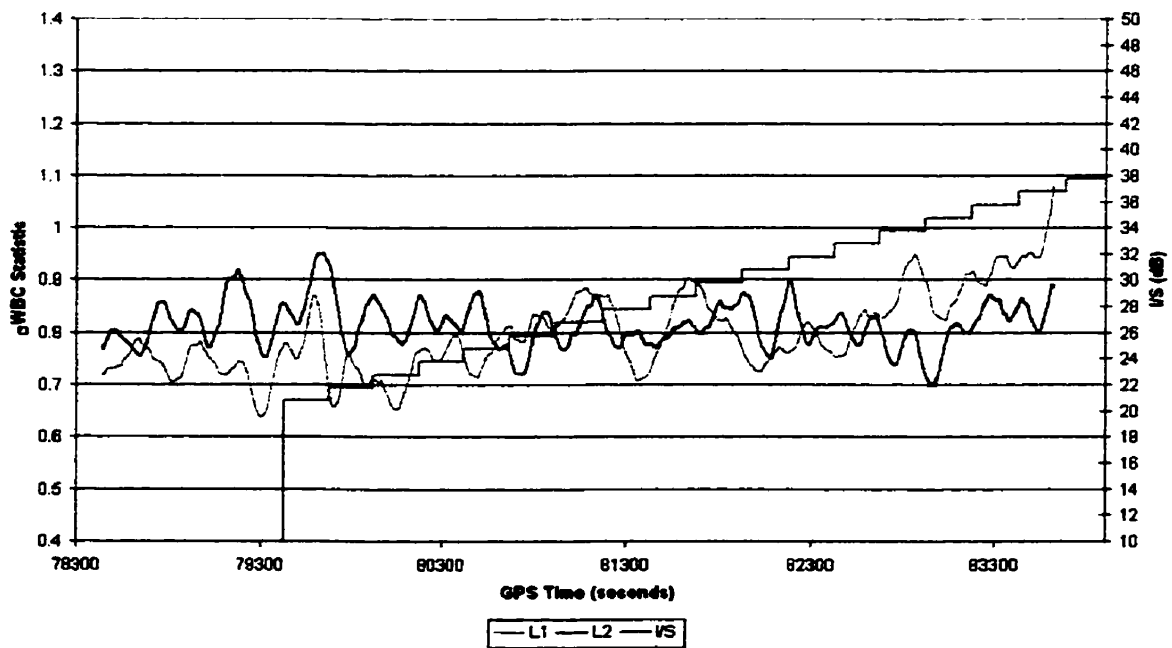
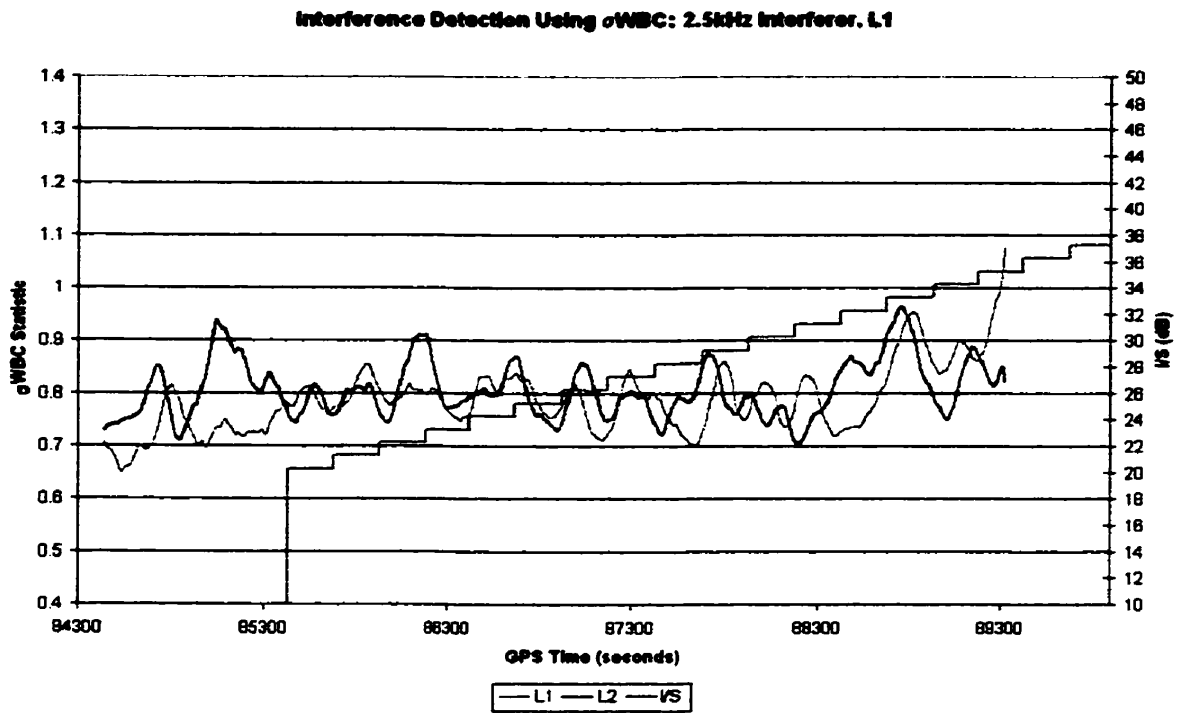
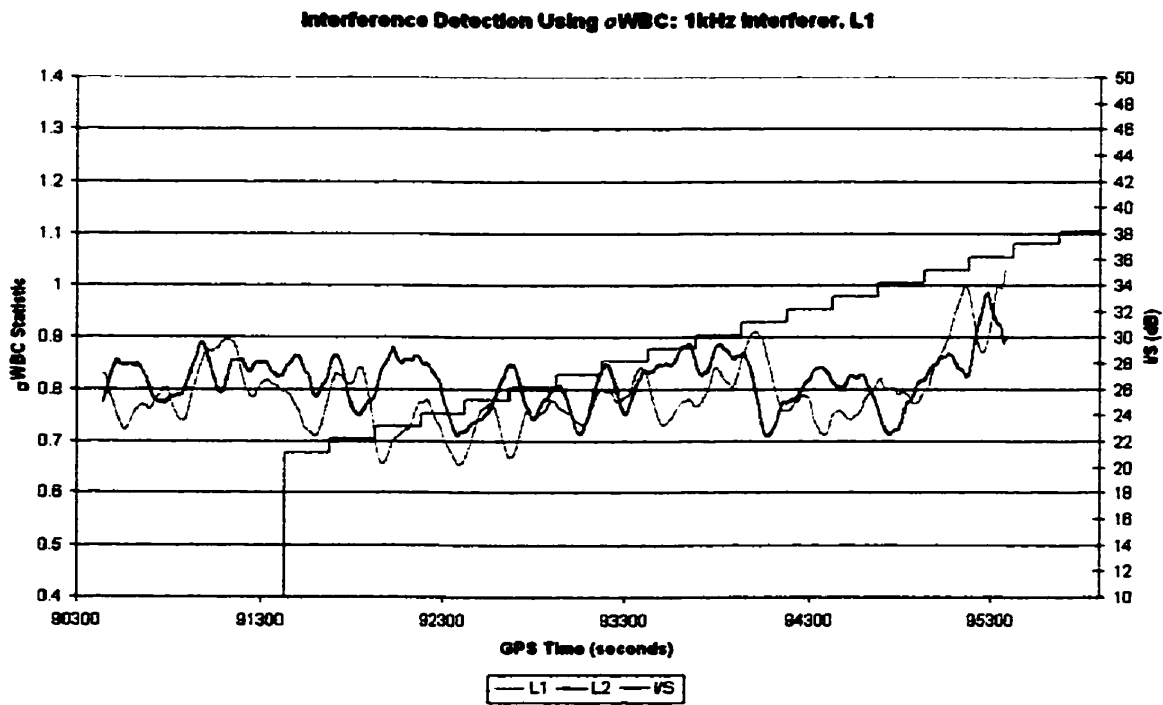


Figure 6-37:  $\sigma$ WBC for 5kHz Interferer, centered at L1



**Figure 6-38:  $\sigma$ WBC for 2.5kHz Interferer, centered at L1**



**Figure 6-39:  $\sigma$ WBC for 1kHz Interferer, centered at L1**

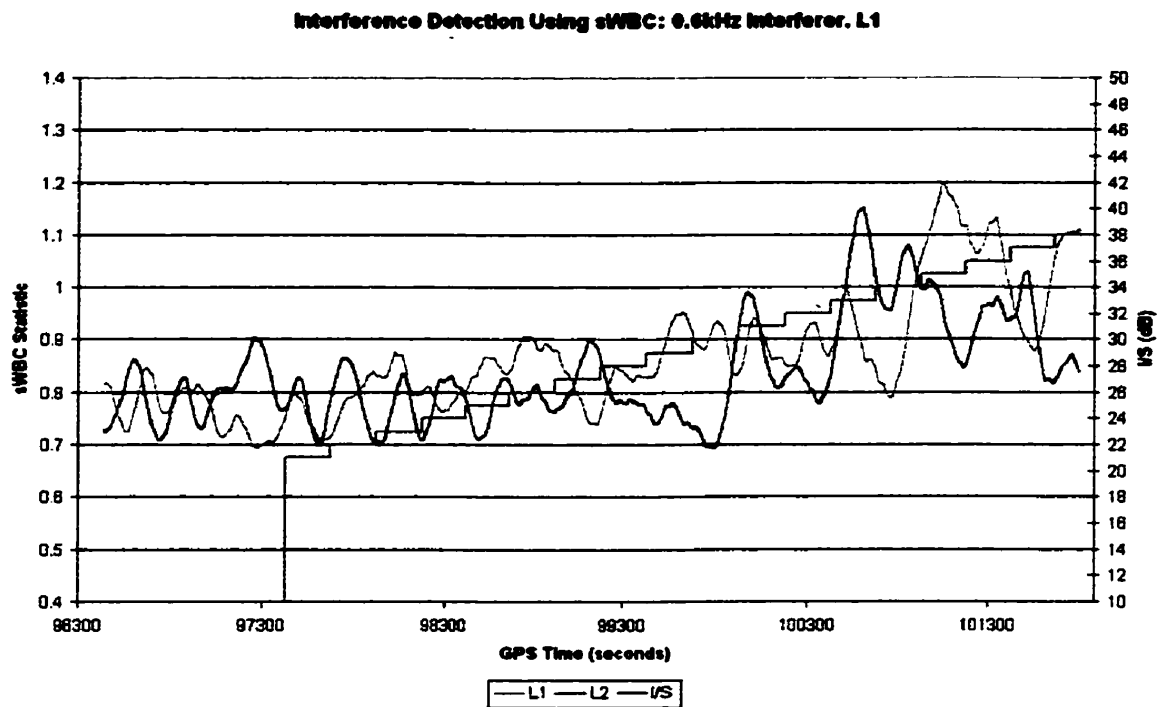


**Figure 6-40:  $\sigma$ WBC for 0.6kHz Interferer, centered at L1**  
**Interference Detection Using  $\sigma$ WBC: 100kHz Interferer. L2**

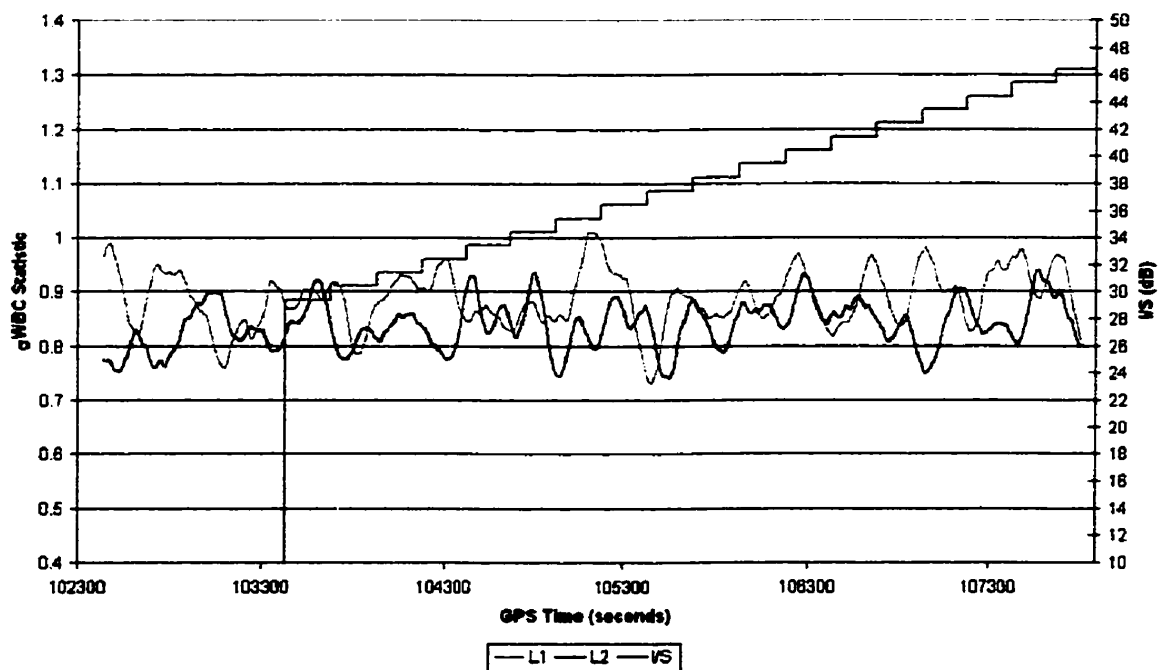


**Figure 6-41:  $\sigma$ WBC for 100kHz Interferer, centered at L2**

Interference Detection Using  $\sigma$ WBC: 50kHz Interferer. L2

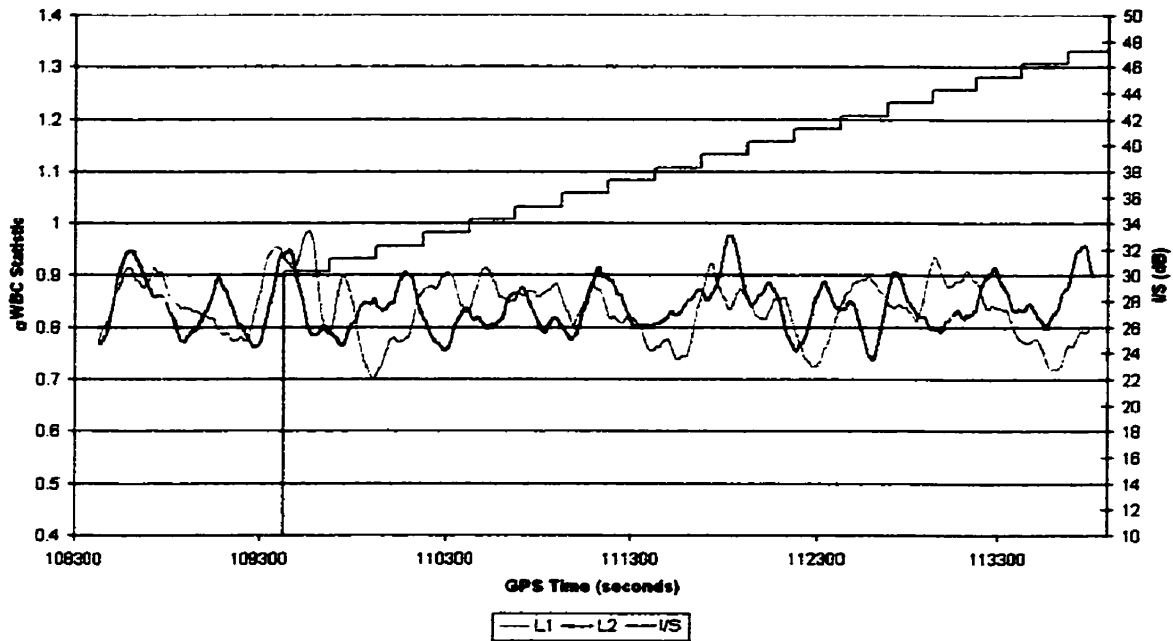


Figure 6-42:  $\sigma$ WBC for 50kHz Interferer, centered at L2

Interference Detection Using  $\sigma$ WBC: 25kHz Interferer. L2

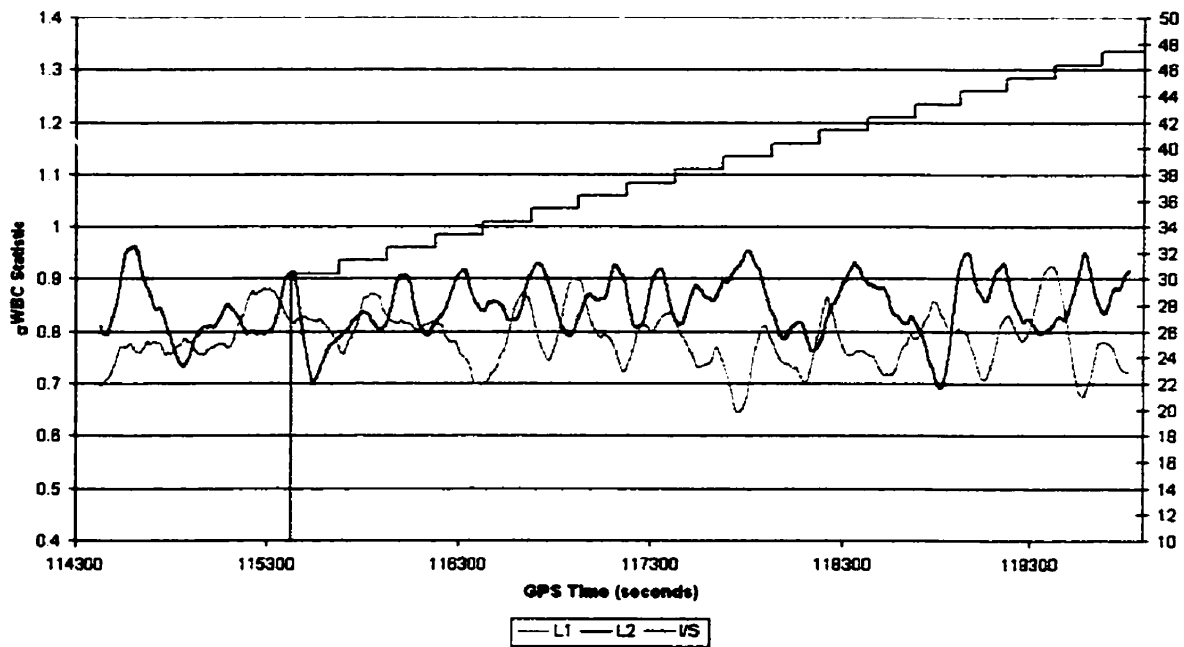
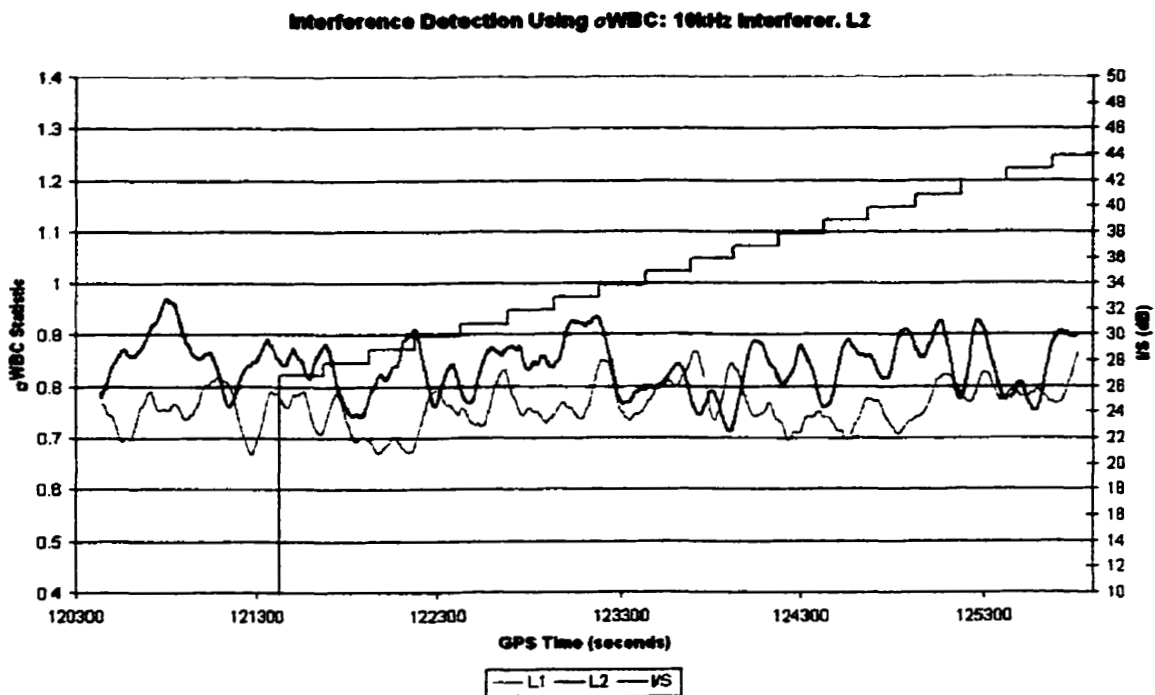
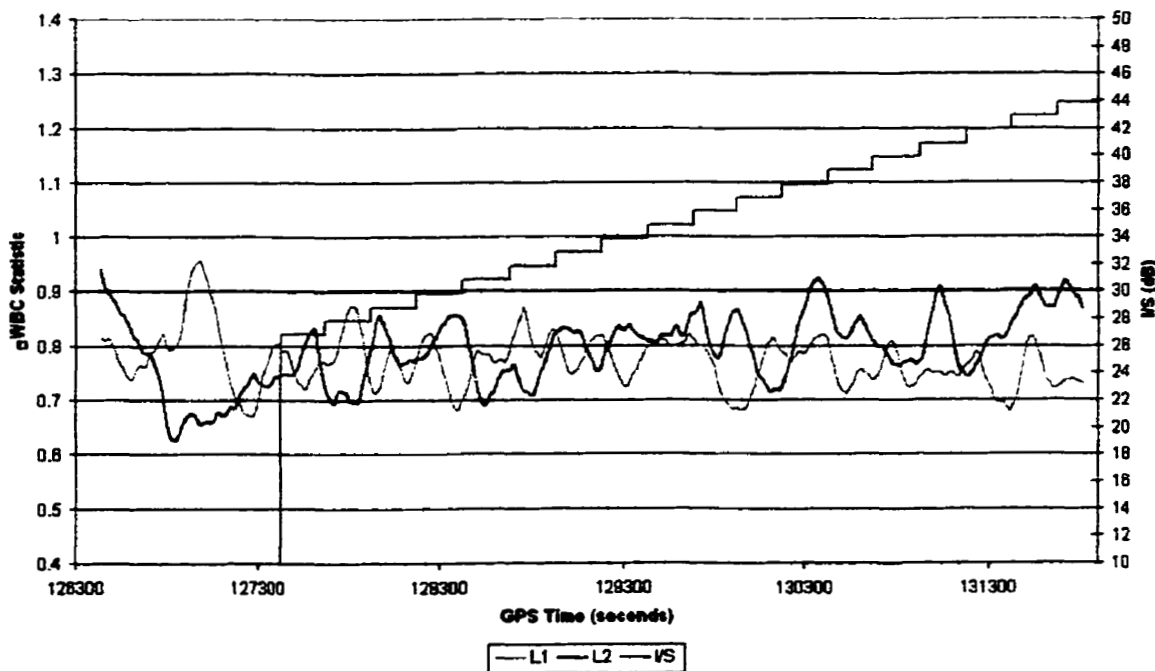


Figure 6-43:  $\sigma$ WBC for 25kHz Interferer, centered at L2



**Figure 6-44:  $\sigma$ WBC for 10kHz Interferer, centered at L2**  
**Interference Detection Using  $\sigma$ WBC: 5kHz Interferer. L2**



**Figure 6-45:  $\sigma$ WBC for 5kHz Interferer, centered at L2**

Interference Detection Using  $\sigma$ WBC: 2.5kHz Interferer. L2

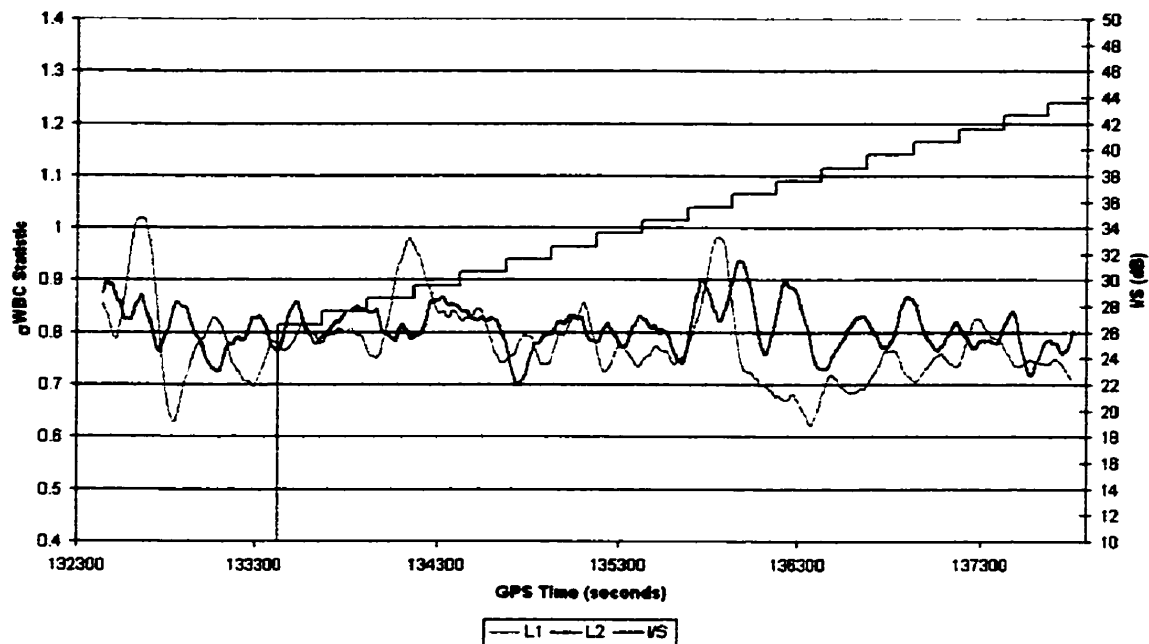


Figure 6-46:  $\sigma$ WBC for 2.5kHz Interferer, centered at L2

Interference Detection Using  $\sigma$ WBC: 1kHz Interferer. L2

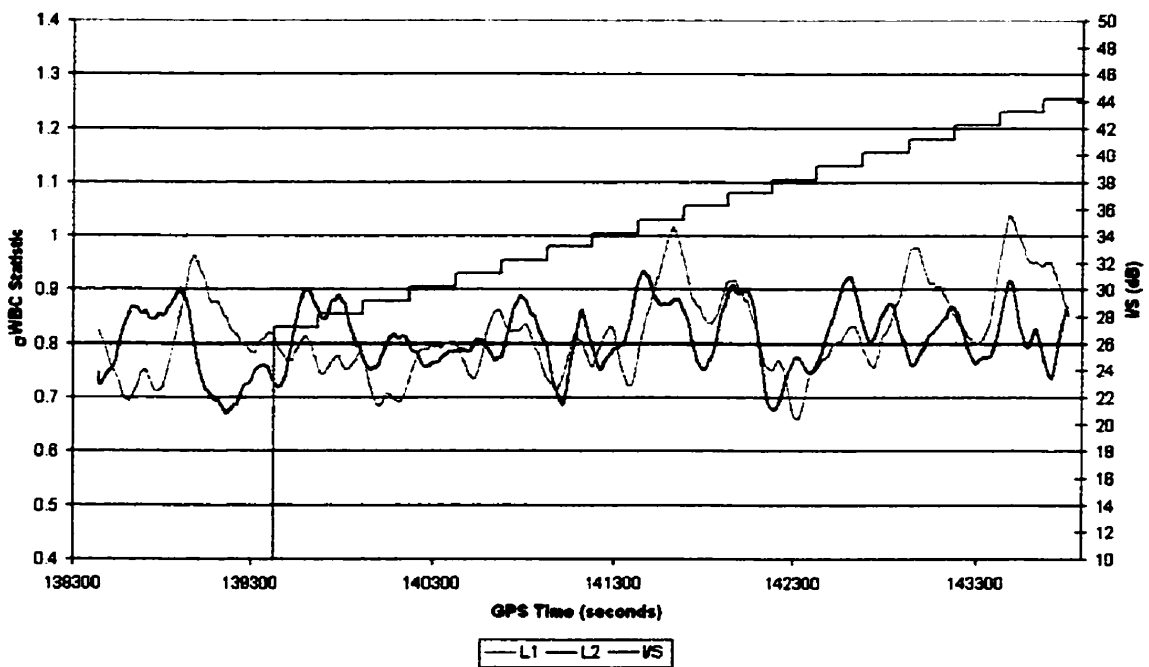
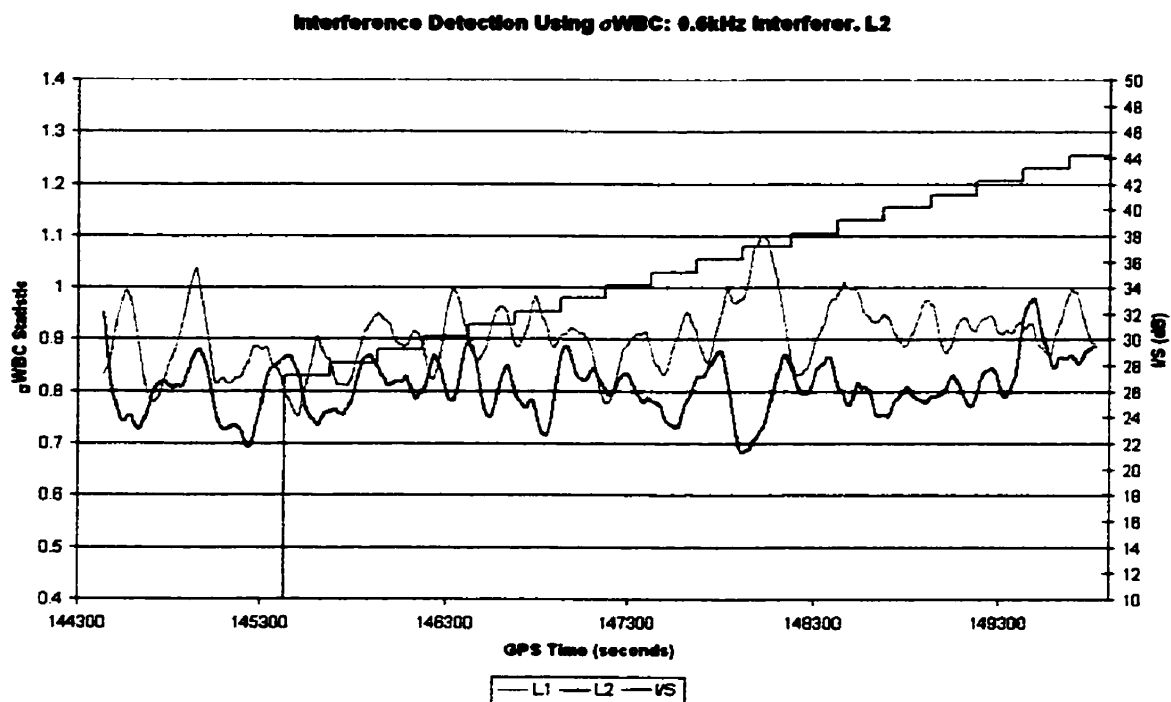


Figure 6-47:  $\sigma$ WBC for 1 kHz Interferer, centered at L2



**Figure 6-48:  $\sigma$ WBC for 0.6kHz Interferer, centered at L2**

### 6.4.3 WBC Testing Conclusions

As can be seen from all plots of L1 (Figures 6-33 to 6-40) and L2 (Figures 6-41 to 6-48) interferers over all tested bandwidths, the  $\sigma$ WBC correction testing does not follow any trend associated with the interferer and in fact shows more variation due to noise than the actual interferer.

Given this lack of an identifiable trend in the  $\sigma$ WBC statistics for the interference data and the presence of variation in Figures 6-31 and 6-32 for the live data close to the horizon, the  $\sigma$ WBC detection method is better suited to detect multipath than interference. Also, with large variations due to multipath at low elevations, this interference detection method would be problematic, in terms of false alarms, for higher multipath environments.

However, the  $\sigma$ WBC method is not without merit. We can see that as the bandwidth of the interferer gets to be large, at 100kHz for L1 (Figure 6-34), a noticeable change in the metric begins to occur at an I/S of 37dB. However, this type of interferer would be more readily detectable by the C/No deviation method as seen in Figure 6-2 when the I/S is at 26dB (significantly weaker).

There is also slight variation in the  $\sigma$ WBC metric for very narrow bandwidth interferers. For L1, as seen in Figure 6-40, we see some detectable variation at an I/S of 32dB. However, we will more easily detect the interferer with the AGC test at an I/S of less than 21dB, as seen in Figure 6-23.

Even the L2  $\sigma$ WBC values do not show any appreciable variation that could be used to determine that there is the presence of an interferer.

As a result of the testing, it has been determined that the complex use of the  $\sigma$ WBC method for interference detection is not as useful as the combination of C/No and AGC measurements, and is therefore not encouraged for an SQM scheme.

## CHAPTER 7

### SUMMARY AND CONCLUSIONS

The invention of the Multipath Meter [38] has proven to be a useful tool in the signal quality monitoring of GPS satellite signals. The outputs of the Meter, namely the multipath corrected correlator measurements, can substantially improve the consistency of the correlator measurements by as much as 10% from uncorrected values and 0.7% absolute, in addition to reducing the standard deviation of the measurements by a factor of 2. Once inter-receiver biases are removed from MDE and MDR values and temperature variations are compensated for, multipath remains the dominant error source in attempting to detect satellite signal anomalies. With multipath corrected correlator measurements the multipath influences can be minimized, significantly reducing false alarms due to multipath and improving reliability and availability of the SQM scheme.

It was also shown that in conjunction with additional Multipath Meters outputs such as the delay, relative amplitude, and phase of the multipath signal, desired to undesired signal ratio, and estimation residuals, MDE and MDR values using the multipath corrected correlator values will still be able to detect all possible failure modes within the specified threat space for LAAS [28], [43].

As part of the SQM scheme, interference detection was also shown to be achievable using GPS receiver AGC and C/No measurements. In tandem, these methods will allow the detection of inband RF interferers not mitigated by the receivers' antenna. Also, the complex use of the WBC as an interference detector was proven ineffective.

It should finally be noted that both the proposed interference detection scheme and the Multipath Meter are being used in the development of a signal quality monitoring system for the European Geostationary Navigation Overlay System.

## REFERENCES

1. Akos, D.M., Phelts, R.E., Pullen, W., Enge, P., Signal Quality Monitoring: Test Results, Proceedings for the Institute of Navigation, January 2000.
2. ARINC Research Corporation, NAVSTAR ICD-GPS-200b, July 1991.
3. Bower, R.E., Dieter, G.L., GPS Navigation Payload Scheduled Maintenance: An Explanation of Satellite Outage Time, Proceeding of the Institute of Navigation, September 1996.
4. Brocard, D., Raizonville, P., Technical Note: GPS/GLONASS/GEO Satellite Signal Anomalies, European Space Agency, E-TN-SYS-E-002-ESA, Issue 1, July 27, 1998.
5. Brown, R.G., Receiver Autonomous Integrity Monitoring, Global Positioning Systems: Theory and Applications, Volume II, American Institute of Aeronautics and Astronautics Inc., 1996.
6. Chatre, E., Bastide, F., Macabiau, C., Site Survey: A New Criterion for Characterization of Multipath Environment, Proceedings of the Institute of Navigation, January 2001.
7. Cobb, H.S., et al., Observed GPS Signal Continuity Interruptions, Proceedings for the Institute of Navigation, September 1995.
8. Cox, D.T., Shallberg, K.W., Manz, A., Definition and Analysis of WAAS Receiver Multipath Error Envelopes, NAVIGATION, Journal of the Institute of Navigation, Vol.46, No.4, Winter 1999-2000, pp.271-282.
9. Enge, P., Evil Waveforms, presented at RTCA SC159 WG4 meeting, Washington D.C., June 9, 1999.

10. Enge, P., Phelts, E., Mitelman, A., Detecting Anomalous Signals from GPS Satellites, Draft Stanford University Report, October 12, 1999.
11. Enge, P., Mitelman, A., SQM Performance Versus Aircraft Correlator Spacing & Precorrelator Bandwidth, For RTCA WG4, April 29, 1999.
12. Falkenberg, T. Ford, K. Ng, Van Dierendonck, A.J., NovAtel's GPS Receiver: The High Performance OEM Sensor of the Future, Proceeding's of the 4th International Technical Meeting the Institute of Navigation 1991, Albuquerque, NM, USA.
13. Fenton, P.C., United States Patent Number 5414729: Pseudorandom noise ranging receiver which compensates for multipath distortion by making use of multiple correlator time delay spacing, May 1995.
14. Hansen, A., Walter, T., Enge, P., Lawrence, D., GPS Satellite Clock Event on SVN 27 and its Impact on Augmented Navigation Systems, Proceedings for the Institute of Navigation, September 1998.
15. Jakab, A.J., An Approach to GPS Satellite Failure Detection, Proceeding for the Institute of Navigation, September 1999.
16. Jakab, A.J., Townsend, B.R., Analysis of the Multipath Meter Performance in the Presence of Anomalous Satellite Signals, Proceedings for the Institute of Navigation, January 2001.
17. Jaksic, J., GPS Multipath Assessment Tool, GPS World Magazine, February 2001.
18. Kaplan, E.D. (editor), Understanding GPS Principles and Applications, Artech House Publishers, 1996.

19. Lachapelle, G., GPS Theory and Applications, NovAtel Inc., University of Calgary Press, February 1998.
20. Macabiau, C., Chatre, E., Signal Quality Monitoring for Protection of GBAS Users Against Evil Waveforms, Proceedings for the Institute of Navigation, September 2000.
21. Mitleman, A.M., Jung, J., Enge, P., LAAS Monitoring for a Most Evil Satellite Failure, Proceedings for the Institute of Navigation, January 1999.
22. Mitleman, A.M., Phelts, R.E., Akos, D.M., Pullen, S.P., Enge, P.K, A Real-Time Signal Quality Monitor For GPS Augmentation Systems, Proceedings for the Institute of Navigation, September 2000.
23. Murphy, J., Rooney, J., MINOS3 L1/L2 Interface and Control Document, NovAtel Internal Document D00390, November 1995.
24. Parkinson, B.W., Spilker Jr., J.J., Global Positioning System: Theory and Applications, Volume 1, American Institute of Aeronautics and Astronautics, 1996.
25. Phelts, R.E., Akos, D., Enge, P., Signal Quality Monitoring Validation, Presented to the International Civil Aviation Organization, GNSSP WG-B, WP/29, Seattle WA, USA, 2000.
26. Phelts, R.E., Akos, D.M., Enge, P., Robust Signal Quality Monitoring and Detection of Evil Waveforms, Proceedings for the Institute of Navigation, September 2000.
27. Renard, A., Fouilland, B., US Patent Number 5781152: Method and circuit for the reception of signals for positioning by satellite with elimination of multiple-path errors, July 1998.

28. RTCA, Minimum Operational Performance Standards for GPS Local Area Augmentation System Airborne Equipment, D0-253, Prepared by SC-159, January 2000.
29. RTCA, Minimum Operational Performance Standards for GPS Wide Area Augmentation System Airborne Equipment, D0-229B, Prepared by SC-159, October 1999.
30. Sawtech Incorporated, 16MHz Bandwidth Low-Loss Filter Data Sheet, Sawtech Part #854668, November 1999.
31. Schuster-Bruce, A., Van Dierendonck, A.J., Jakab, A., Wiebe, J., Townsend, B. Detection of GPS Satellite Signal Failures in Satellite Based Augmentation Systems, Proceedings for the Institute of Navigation, September 2000.
32. Shively, C., Brenner, M., Kline, P., Multiple Ground Tests Protecting Against Satellite Correlation Symmetry Faults in LAAS, Revision 5, presentation for RTCA SC159 WG4, September 13, 1999.
33. Stansell, T., GPS After Selective Availability, United States Department of Transportation, Volpe Centre, Information Session, June 2000.
34. Townsend, B.R., van Nee, D.J.R., Van Dierendonck, K., Fenton, P., L1 Carrier Phase Multipath Error Reduction Using MEDLL Technology, Proceedings of the 8th International Technical Meeting of the Satellite Division of the Institute of Navigation 1995, Palm Springs, CA, USA.
35. Townsend, B.R., van Nee, D.J.R., Van Dierendonck, K., Fenton, P., Performance Evaluation of the Multipath Estimating Delay Lock Loop, Proceedings the Institute of Navigation National Technical Meeting 1995, Anaheim, CA, USA.

36. Townsend, B.R., Fenton, P., A Practical Approach to the Reduction of Pseudorange Multipath Errors in a L1 GPS Receiver, Proceedings of the 7th International Technical Meeting of the Satellite Division of the Institute of Navigation 1994, Salt Lake City, UT, USA.
37. Townsend, B.R., Performance Evaluation of the Multipath Estimating Delay Lock Loop, Proceedings for the Institute of Navigation, January 1995.
38. Townsend, B.R., Jakab, A.J., Wiebe, J., United States Patent for a Multipath Meter, Provisional Patent and Final Patent Applications, January 2000-2001.
39. Townsend, B.R., Jakab, A.J., Wiebe, J., Results and Analysis of using the MEDLL as a Multipath Meter, Proceedings of the Institute of Navigation, National Technical Meeting, 2000.
40. Townsend, B.R., Jakab, A.J., Wiebe, J., Analysis of the Multipath Meter Performance in Environments with Multiple Interferers, Proceedings of the Institute of Navigation, Salt Lake City, September 2000.
41. United States Air Force Space Command Center, Press Release: Global Positioning System Fully Operation, July 17, 1995.
42. United States Department of Transportation and Department of Defense, Federal Radionavigation Plan, Washington, DC, February 2000.
43. United States Department of Transportation, Federal Aviation Administration, Specification for Performance Type One Local Area Augmentation System Ground Facility, FAA-E-2937, September 21, 1999.

44. Van Dierendonck, A.J., Akos, D., Pullen, S., Phelts, E., Enge, P., Practical Implementation Considerations in the Detection of GPS Satellite Signal Failure, Proceedings for the Institute of Navigation, June 2000.
45. Van Dierendonck, A.J., Fenton, P. and Ford, T. Theory and Performance of Narrow Correlator Spacing in a GPS Receiver, NAVIGATION, Journal of the Institute of Navigation, USA, Vol. 39, No. 3, Fall 1993, pp. 265–283.
46. van Nee, D.J.R., et al., The Multipath Estimating Delay Lock Loop: Approaching Theoretical Accuracy Limits, Proceedings of the IEEE, Position, Location, and Navigation Symposium, Las Vegas, 1994.
47. van Nee, D.J.R., US Patent Number 5615232: Method of estimating a line of sight signal propagation time using a reduced-multipath correlation function, March 1997.
48. van Nee, D.J.R., Optimum DGPS Receiver Structures, Proceedings of the 2nd International Symposium on Differential Satellite Navigation Systems, Amsterdam, The Netherlands, 1993.
49. Walpole, R.E., Myers, R.H., Probability and Statistics for Engineers and Scientists, Macmillan Publishing, Fifth Edition, 1993.
50. Zhodzicshsky, M., et. al; United States Patent Number 5953367: Spread spectrum receiver using a pseudo-random noise code for ranging applications in a way that reduces errors when a multipath signal is present, September 1999.